# *Molecular architecture and functional group effects on segregation in polymers*

Helen Louise Thompson

# Molecular Architecture and Functional Group Effects on Segregation in Polymers

1998

Helen Louise Thompson

Chemistry Department

University of Durham

Supervisor: R. W. Richards

University of Durham

A thesis submitted to the University of Durham in partial fulfilment of the regulations for the degree of Doctor of Philosophy.

# Abstract

## Molecular Architecture and Functional Group Effects on Segregation in Polymers

**Helen Louise Thompson**

**PhD Thesis 1998**

The properties of a polymer surface can be manipulated by the addition of a small quantity of surface active functionalised polymer to the bulk. On annealing above the glass transition these low surface energy functional groups attach to the air/polymer interface forming a brush like layer. To quantify this effect perdeuterated polystyrenes with fluoroalkane groups at specific locations in the polymer have been blended with unmodified polystyrene. Three key areas have been studied; effect of molecular architecture; effect of the molecular weight of the matrix polymer; and the rate of formation of the segregating layer. The complementary techniques of neutron reflectometry and nuclear reaction analysis have been used to determine the near surface depth profile of the deuterated polymer.

Architectures studied were linear polystyrene with functional groups at both ends of the polymer chain, a 3-armed star with a functional core and linear polystyrene with functional groups evenly spaced along the chain. The architecture affected the shape of the composition profile but had little effect on the surface volume fraction and surface excess values obtained for the same bulk volume fraction. Self-consistent field theory simulations were carried out to determine the 'sticking energy' of the functional groups and good comparisons were obtained between the experimental volume fraction profiles and those predicted. Some segregation of functional polymer was observed during sample preparation and equilibrium segregation was obtained in less than one hour for 50000 $M_w$ linear polymer up to eight hours for the 3-armed star after annealing under vacuum at 413K. For the difunctional polystyrene the functional groups did not have a significant affect on the rate of diffusion compared to non-functional polystyrene and diffusion coefficients obtained ranged from $6\times10^{-16}$ to $9\times10^{-15}$ $cm^2s^{-1}$. The 3-armed star had the lowest diffusion coefficient value of $2\times10^{-16}cm^2s^{-1}$ because of the inability for branched molecules to diffuse by reptation.

## Acknowledgements

I would like to thank Prof. Randal Richards for his enthusiasm and persistence and for giving me the opportunity to carry out this work. There are many other people at the University of Durham whose assistance has been essential: Tom Kiff for his excellent synthesis of the polymers used in this work; Gordon Forrest who carried out GPC and DSC measurements; Gordon and Ray, 'the glassblowers' for providing the diamond tipped glass knife used during sample preparation; Terry Harrison for his computer expertise and Jean and Helene for arranging transport to the many locations visited during this work.

David Bucknall, John Webster and Jeff Penfold the instrument scientists for CRISP and SURF the neutron reflectometers used, and Steve King the instrument scientist for LOQ are thanked for their patient assistance, along with the many other staff involved in the running of the ISIS facility at the Rutherford Appleton Laboratory. Devinder Sivia is also thanked for his permission and help in using his maximum entropy fitting program, VOLFMEM. Whilst at the University of Surrey I have been well looked after by Tony Clough, his postdocs and postgrads and the other staff of the D. R. Chick Laboratory. At this point Prof. Ken Shull should also be mentioned for his generosity in providing his self-consistent field theory programs along with some advice on their use.

A very special thanks is given to all the people who have helped in carrying out the neutron reflectivity experiments, from doing the driving to working the nightshift: Helen Varley, Andrew Brown, Stella Peace, Antonio Brunacci and Mike Watson – your help was appreciated. Rob Staples deserves an award for sharing a

house throughout our time at Durham and all other members of the IRC, past and present, are thanked for making it an excellent place to work.

Last, but not least, I would like to thank my Parents and Andrew for supporting me throughout my studies and for always being there for me, even if they haven't quite understood what I have been doing.

## Declaration

The work reported in this thesis has been carried out at the Durham site of the Interdisciplinary Research Centre in Polymer Science and Technology, Rutherford Appleton Laboratory, Chilton, Oxon. and the University of Surrey, Guildford between October 1994 and September 1997. This work has not been submitted for any other degree either in Durham or elsewhere and is the original work of the author except where otherwise stated.

## Statement of Copyright



## Financial Support

I gratefully acknowledge the provision of a CASE award from the Engineering and Physical Sciences Research Council and Courtaulds Plc to support the work described herein.

## Contents

# CHAPTER 1

# Introduction

The surface composition of a polymer mixture influences the properties of the mixture, in particular properties such as adhesion, wetting and friction. In some cases it is desirable to have a surface which does not interact with other materials, e.g. for non-stick coatings[1] and lubrication in moving parts. Alternatively it is sometimes desirable to have a surface that will adhere strongly to different materials. Mixtures of materials are often blended carefully to obtain the right bulk properties; however, a small excess of a different component can drastically alter the properties at the surface compared with the bulk. If the factors that influence segregation and the rate at which it is attained can be understood and controlled, this could be used industrially to balance useful properties against production costs by designing materials with the correct, combined bulk and surface properties.

## 1.1 Surface Segregation in Polymer Blends

In a blend of two components the surface is usually enriched in the component of lower surface energy in an attempt to reduce the total free energy of the system. The amount of enrichment is favoured by a large difference in surface energy, but reduced by the free energy loss in maintaining a composition gradient. In polymers, where the entropy of mixing is small, a small difference in surface energy can cause considerable segregation in a blend.

There are two key processes whereby segregation can occur:

***Surface Enrichment.*** Whereby the component with the lower surface energy forms a wetting layer at the surface, it is assumed that all segments of the segregating polymer chain have equal attraction to the surface. This has been studied extensively

for hydrogenous polystyrene (hPS) / perdeuterated polystyrene (dPS) blends[2-7]. Figure 1.1 shows a schematic diagram of surface enrichment.

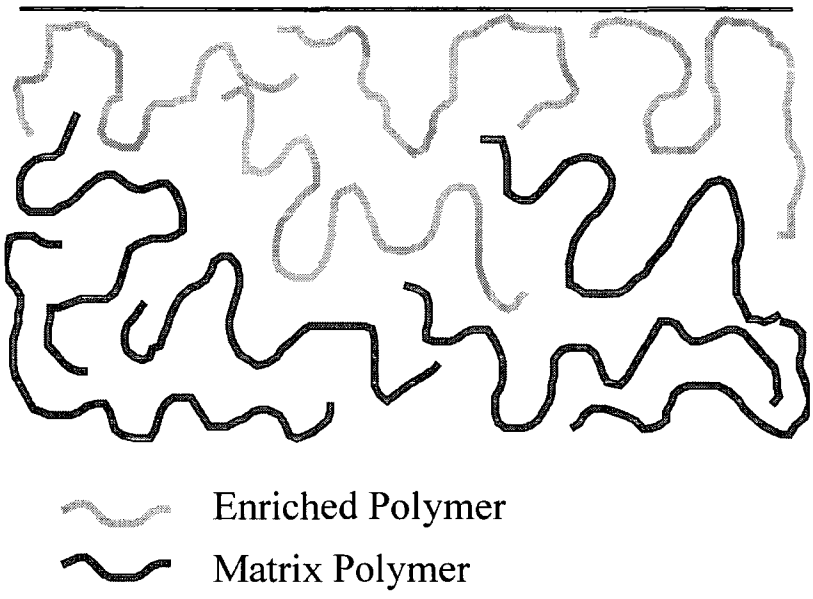


**Figure 1.1 Diagram to show the surface composition when a polymer has enriched to the surface of a blend.**

***Brush Formation.*** A group of lower surface energy within the polymer chain 'attaches' itself to an interface forming a brush. Two types of brush behaviour are encountered, wet brush when the matrix is a solvent and dry brush when the matrix is another polymer of equal or greater molecular weight. Figure 1.2 shows a schematic diagram for a polymer brush with a surface-active group at one end of the polymer chain in a polymeric matrix.

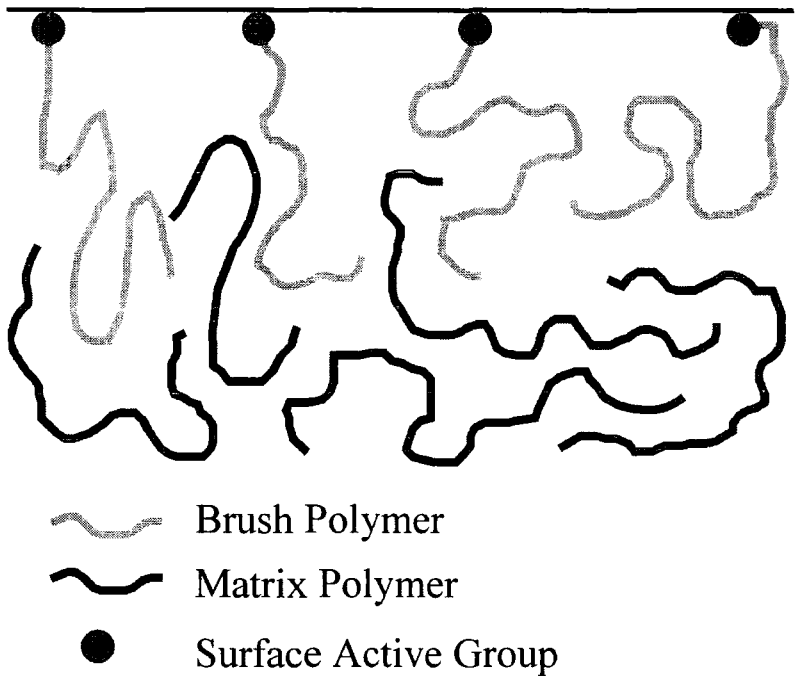


**Figure 1.2 Diagram to show the composition profile when a polymer has end attached to an interface to form a polymer brush.**

To characterise the composition profile the surface volume fraction, $\phi_s$; bulk volume fraction, $\phi_b$; surface excess, $z^*$ of the segregating polymer and the shape of the composition profile are required. L is a measure of the extent of the segregated layer (cf. brush height) and w is the width of the interface between the segregated layer and the bulk polymer. Figure 1.3 shows the relationship between these parameters on a model composition profile. The surface excess is defined as the integrated area under the composition profile after subtracting the bulk volume fraction (eqn 1.1). A further parameter determined is the dimensionless surface grafting denity, $\sigma=z^*/aN_D$, of D chains of degree of polymerisation N grafted at the surface, where a is the statistical segment length of the polymer chain.

$$z^* = \int(\phi(z) - \phi_b)dz \qquad \text{eqn 1.1}$$

$$L = \frac{1}{z^*}\int z(\phi(z) - \phi_b)dz \qquad \text{eqn 1.2}$$

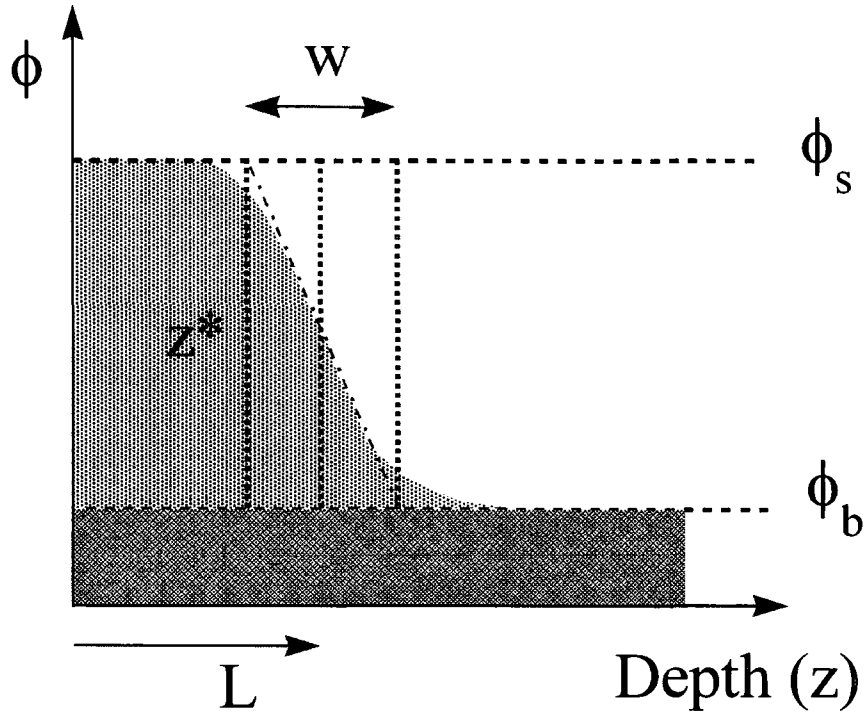


**Figure 1.3 Diagram to show a typical volume fraction profile when a polymer has segregated to the surface showing the parameters that are determined from the profile as described in the text.**

### 1.1.1 Surface Enrichment

Cahn[8] introduced the theory of surface enrichment or wetting by one component of a blend. Nakanishi and Pincus[9] and Schmidt and Binder[10] developed this for polymer blends. This theory was then simplified by Jones and Kramer[11] to approximate the surface volume fraction and surface excess for blends where the degree of polymerisation of the two components (A and B) is the same, i.e. $N_A = N_B$. They predicted that the surface excess would depend more strongly on the Flory - Huggins interaction parameter between segments of the two polymers, than the

difference in surface energy. Due to the small entropy of mixing, a small surface energy difference will allow a large surface segregation.

Initial experimental work on hPS ($M_w$ $1.8\times10^6$) and dPS ($M_w$ $1.03\times10^6$) was carried out by Jones et al using forward recoil spectroscopy (FRES)[2], and neutron reflectometry (NR) and secondary ion mass spectroscopy (SIMS)[3]. This showed good agreement with mean field theory predictions. The effect of annealing time was studied using FRES[4] and SIMS and time of flight forward recoil spectroscopy (TOF-FRES)[5], with diffusion limiting the rate of formation of the enrichment layer.

For non-equilibrium systems, a depletion zone just below the surface layer was found which was in local equilibrium with the surface layer[4]. Figure 1.4 shows the shape of the composition profile for this situation. It was suggested that as the enriched layer is formed, there is depletion in the region immediately behind where the material segregating to the surface has originated. Further material from the bulk diffuses down the concentration gradient to replenish the depleted area and allow continued surface enrichment. The size of the depletion zone is controlled by the diffusion distance $(Dt)^{1/2}$ where D is the mutual diffusion coefficient and t the annealing time. If the size of the depletion zone is greater than the characteristic length of the enriched layer ($\sim R_g$), then the rate of diffusion from the bulk to the depletion zone will be the limiting step in the formation of the enriched layer.

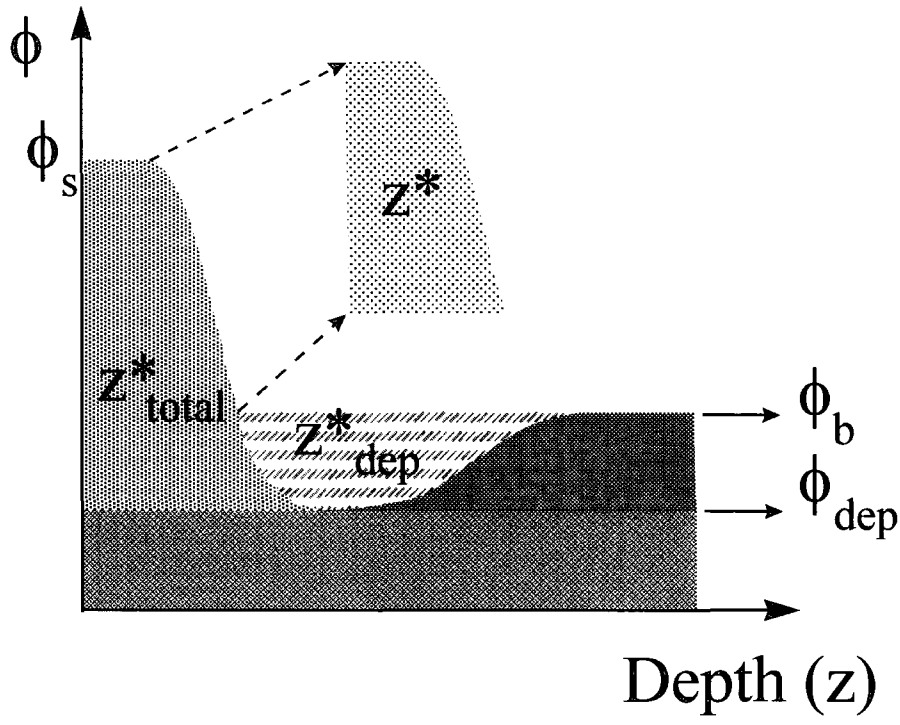


**Figure 1.4 Diagram to show a volume fraction profile when there is a depletion zone ($z^*_{dep}$) following the surface segregated layer. $\phi_{dep}$ is the volume fraction at the lowest point in the profile and $z^*_{total}$ is calculated assuming the surface segregated layer is in equilibrium with $\phi_{dep}$.**

In all these systems dPS was seen at the air - polymer interface. Hariharan[6] et al have shown using neutron reflectometry (NR) that the molecular weight of the polymers plays an important role. In asymmetric blends where the molecular weight of the hPS is lower than that of the dPS, the hPS can segregate to the air surface. The entropy effects of placing a shorter chain at the surface outweighing the energy gain of having the deuterated segments at the surface. These results were supported by Hong et al using surface enhanced raman spectroscopy (SERS)[7].

### 1.1.2 Polymer Brushes

The type of interface to which a polymer brush can attach is varied - solid / liquid; solid / substrate; solid / air; liquid / liquid interfaces, etc. Hence they have many applications, e.g. the stabilisation of colloidal dispersions and the compatibilisation of the interface between immiscible polymers.

The molecular weight of the adsorbing species, the molecular weight of the matrix and the areal density of adsorbed polymer chains at the interface determine the characteristics of the brush. At high coverage, the unattached end of a polymer brush stretches away from the surface to prevent overlapping. This distance can be much greater than the unperturbed size of the polymer chain.

If the matrix is very low molecular weight, i.e. solvent, the chains stretch away from the surface due to excluded volume effects and affinity for the solvent. The concentration of matrix in the brush is quite high. This is referred to as a wet brush, and much of the theoretical and experimental work has concentrated on this situation. Milner[12] presents a general review with a more in depth theoretical and experimental background in the book 'Polymers at Interfaces'[13].

The concentration of matrix in the brush decreases as the matrix molecular weight increases, until a limiting form is reached when the molecular weights of the brush and matrix are the same. This is known as a dry brush. The volume fraction of matrix within the brush no longer changes with increasing molecular weight but is not necessarily totally excluded because of the high cost this would have on the free energy of the system.

The systems studied here have been in the dry brush regime, with the brush polymer and matrix having approximately the same molecular weight.

Shull[14] has developed a self-consistent field theory to determine the properties of dry polymer brushes with particular respect to a brush-forming polymer with one surface-active end. This end group has a different free energy of interaction with the surface than with the bulk. The theory was developed for the case of strong adsorption i.e. when the volume fraction of the brush forming polymer in the bulk is zero, but can be applied to weak adsorption.

The brush characteristics are not strongly affected by $N_A$ / $N_B$, and Shull suggests a limiting form when $N_A$ / $N_B$ = 8. The shape of the composition profile can be described by a hyperbolic tangent function (eqn 1.3), where $\phi(z)$ is the volume fraction at depth z, $\phi_a$ and $\phi_b$ are the volume fractions at the surface and in the bulk respectively. $z_{off}$ is the height of the brush and w is the width of the overlap region between the brush and the bulk. The volume fraction profiles can be described by the ratio $z^*/R_g$ where $R_g$ is the unperturbed radius of gyration of the brush forming polymer chain.

$$\phi(z) = \phi_b + \frac{\phi_a - \phi_b}{2}\left[1 + \tanh\left(\frac{2(z_{off} - z)}{w}\right)\right] \quad \text{eqn 1.3}$$

There are also scaling theories applied to polymer brushes. De Gennes[15] discussed the case for brushes in solvent or polymer solution. Aubouy and Raphaël[16] have adjusted this for polymeric matrices. Shull[17] further extended his self-consistent field theory predictions to the crossover between wet and dry brushes and obtained good agreement in the profiles produced with scaling theory predictions.

Scaling analysis defines a number of regimes for a grafting chain of degree of polymerisation N depending upon the grafting density, $\sigma$, and the degree of polymerisation of the surrounding matrix, P. The different types of behaviour predicted are given below with the corresponding expected layer thickeness, L, and the different regimes are shown on figure 1.5.

(i) $0 < \sigma \leq N^{-6/5}$:

Swollen Mushroom ($P<N^{1/2}$)

$L \sim aN^{3/5}P^{-1/5}$

Ideal Mushroom ($P>N^{1/2}$)

$L \sim aN^{1/2}$

(ii) $N^{-6/5} < \sigma < 1$:

Stretched Wet Brush ($P<N^{1/2}$)

$L \sim aNP^{-1/3}\sigma^{1/3}$

(iii) $N^{-1} \leq \sigma \leq N^{-1/2}$

Unstretched Brush ($P>N^{1/2}$)

$L \sim aN^{1/2}$

(iv) $N^{-1/2} \leq \sigma \leq 1$

Stretched Dry Brush ($P>N^{1/2}$)

$L \sim aN\sigma$

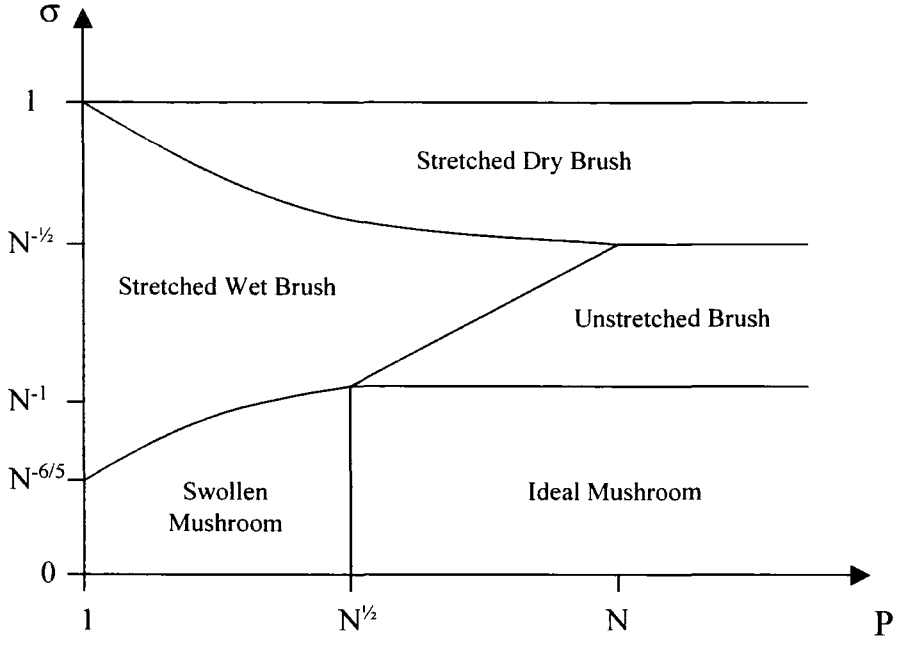


**Figure 1.5 Diagram to show the scaling regimes predicted for a polymer brush in a matrix of degree of polymerisation P.**

## 1.2 Depth Profiling Techniques.

Variation of the volume fraction of the segregating polymer occurs over distances of the order of the radius of gyration, $R_g$ of the segregating polymer (50 - 500Å). To obtain information about the composition of a polymer film there are a variety of experimental techniques that can be used. Suitable techniques need to be able to distinguish between the components of the sample and give compositional data on the immediate surface or preferably probe depths of the order of 2000Å with good resolution. Some of the techniques that have been used to analyse polymeric samples include reflectivity[18-20] (X-ray and neutron reflection), ion beam[21] (Rutherford back scattering, forward recoil spectroscopy, nuclear reaction analysis and secondary ion mass spectroscopy), other spectroscopic techniques[22] (X-ray photoelectron spectroscopy, attenuated total reflection Fourier transform infra red spectroscopy) and microscopic methods (scanning electron microscopy and atomic

force microscopy) to name but a few. Some of the key advantages and disadvantages of the more commonly used methods are given below, references are provided to give examples of experimental results for polymeric systems. Two or more of these techniques are often used together to gain information on the experimental system under consideration. More detailed information on the two techniques used in this work, neutron reflectometry (NR) and nuclear reaction analysis (NRA) is given in sections 1.2.1 and 1.2.2.

X-ray Reflection

Determines the reflectivity of the sample based on the electron density profile of the sample. Contrast needs to be present in the sample, usually high atomic mass elements, and therefore is not commonly used for polymers, however, polystyrene / polybromostyrene interfaces can be studied using X-ray reflectivity[23, 24]. Information on surface roughness and interface widths can be obtained with ~1nm resolution.

Neutron Reflection (NR)

A similar technique to X-ray reflectivity, however contrast is provided by variation in scattering length density of the sample, isotopic substitution of hydrogen by deuterium provides suitable contrast for polymer studies in both liquid and solid state[25-29]. Resolution of ~1nm is possible however the technique is insensitive to broad interfaces and the optical transform is obtained so the experimental data need to be fitted by model reflectivity profiles to obtain the volume fraction profile.

Rutherford Back Scattering (RBS)

Back scattered ions from the sample are detected with little sample damage. High atomic number elements are required to achieve good depth resolution (~30nm) which is limited by overlapping signals due to mass and depth.

Forward Recoil Spectroscopy (FRES)

Detects forward recoiling nuclei produced from collisions with He ions, the energy of the nuclei are dependent upon the mass of the target nuclei and the distance from the surface. Hence FRES is sensitive to different elements and different isotopes of the same element, so deuterium substitution allows a particular species in a sample to be studied detecting both hydrogen and deuterium[30-32]. The depth resolution of FRES is ~80nm, however this can be improved to around 30nm using time of flight geometry.

Nuclear Reaction Analysis (NRA)

A similar technique to FRES with improved resolution of ~15nm at the surface but with decreasing resolution with depth into the sample. The element determined is dependent upon the particular nuclear reaction used. Commonly, deuterium is detected using a $^{3}He^{+}$ beam[33-35].

Secondary Ion Mass Spectroscopy (SIMS)

Sample is bombarded with primary ions and the sputtered secondary ions of differing mass are detected allowing ions of different isotopes to be distinguished[36-

[38]. Static SIMS probes the top 10Å of the sample, dynamic SIMS can provide a depth profile but sample damage limits the resolution to ~13nm.

X-ray Photoelectron Spectroscopy (XPS)

A near surface technique with a typical sampling depth of ~50Å, though angle dependent experiments can probe depths from 10 – 200Å. Chemical constitution is determined so functional groups can be distinguished[38-41].

ATR-FTIR

This technique has been used to study diffusion in polymer films[42-46]. Whilst it is not possible to obtain a depth profile, the $e^{-1}$ reduction in the strength of the evanescent wave away from the crystal means that it is possible to observe the increase or decrease in a component at the polymer/crystal interface from the change in the area of the ir peak with time. The components of the sample need to have ir distinguishable absorption bands.

A further experimental technique used in this work that is not surface specific was small angle neutron scattering (SANS). In this technique the elastically scattered neutron radiation is measured and the resulting scattering pattern can be analysed to provide information about the size, shape and orientation of some component of the sample. Neutrons are scattered by the nucleus and the scattering cross section of an atom varies randomly with atomic number. There is a significant variation in the scattering cross section of hydrogen and deuterium so isotopic substitution can be used to distinguish between molecules or parts of a molecule. Experiments were

carried out to confirm the value of radius of gyration of the polymers studied for use in theoretical calculations and no unusual behaviour was observed, therefore further information on the technique will not be provided here. Interested readers are referred to the literature with texts such as that by Higgins and Benoit[47] and that available from neutron sources such as the spallation source at the Rutherford Appleton Laboratory, Oxon. (http://www.isis.rl.ac.uk/ISISpublic/index.htm) and the reactor at the Institut Laue Langevin (http://www.ill.fr).

### 1.2.1 Theory of Neutron Reflection (NR)

The specular reflection of neutrons, i.e. the angle of reflection equal to the angle of incidence, from a surface gives information on the neutron refractive index profile perpendicular to the surface. Reflection data can therefore provide information on the composition of surfaces and interfaces.

In contrast to X-ray reflectivity, nuclear scattering lengths vary randomly across the periodic table. Hydrogen and deuterium have greatly different scattering lengths, hence isotopic substitution can be used to provide contrast in polymer blends.

The reflectivity, R(Q) provides information on the variation of nuclear scattering length density perpendicular to the surface, $\rho_N(z)$. The shape of the reflectivity profile arises from the interference of neutrons reflected from the air polymer surface, giving 'Kiessig fringes' for thin samples, and from scattering length density gradients within the sample.

The nuclear scattering length density, $\rho_N$ of a polymer is given by equation 1.4 where $\rho$ is the density of the polymer, m is the monomer mass, $N_A$ is Avogadro's

constant and $\Sigma b_i$ is the sum of the nuclear scattering lengths of all the atoms in the monomer.

$$\rho_N = \rho \frac{N_A}{m} \sum b_i \qquad \text{eqn 1.4}$$

As scattering length density is additive the composition in a blend can be determined by equation 1.5,

$$\rho_N(z) = \phi_D(z)\rho_D + \phi_H(z)\rho_H \qquad \text{eqn 1.5}$$

where $\phi_H(z) = 1 - \phi_D(z)$ and $\phi_D(z)$ and $\phi_H(z)$ are the volume fractions of the deuterated and hydrogenous components at depth z. $\rho_D$ and $\rho_H$ are the scattering length densities of the deuterated and hydrogenous polymers respectively. The scattering length densities used in this work are given in table 1.1. These were calculated using the values of nuclear scattering length quoted by Russell[48]. For the functional polymer studied the presence of the functionality was assumed to have no effect on the value of scattering length density as the functional group represented less than 1% of the total polymer molecular weight.

| **Component** | $\rho_N$ / Å$^{-2}$ $\times 10^{-6}$ |
|---|---|
| hPS | 1.41 |
| dPS | 6.41 |
| Si | 2.095 |
| $SiO_2$ | 3.676 |
| Air | 0.0 |

**Table 1.1 The scattering length densities used.**

The theory which follows is based on the reviews on neutron reflection by Russell[48], Penfold[49] and Thomas[50] and course notes from a reflectivity course attended at the Rutherford Appleton Laboratory (RAL). Further information on the facilities at RAL and results of experiments carried out can be found on the ISIS web site: http://isis.rl.ac.uk/largescale/

The refraction and reflection of neutrons involves the interference between the incident neutron wave and waves scattered in the forward direction. The refractive index, n at the boundary between two media is defined by $n = \underline{k}_2 / \underline{k}_1$ where $\underline{k}_1$ and $\underline{k}_2$ are the neutron wave vectors perpendicular to the surface inside and outside the medium. Figure 1.6 shows the relationship between the incident and refracted vector at an interface.

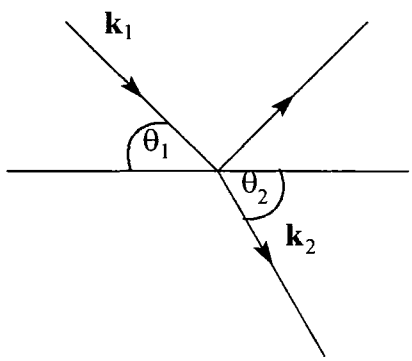


**Figure 1.6 Incident and refracted wave vectors at an interface between media**

$\underline{Q}$, the scattering vector is related to the wave vectors by equation 1.6 where $\lambda$ is the wavelength of the incident radiation.

$$\underline{Q} = \underline{k}_1 - \underline{k}_2 = \frac{4\pi}{\lambda}\sin\theta \qquad \text{eqn 1.6}$$

The refractive index can also be written as equation 1.7 where the nuclear scattering length density, $\rho_N$ is defined above. The imaginary term $i\lambda A$ takes into account incoherence and absorption effects and is important for strong absorbers, e.g. cadmium. For polymers this term is small and can be neglected.

$$n = 1 - \frac{\lambda^2 \rho_N}{2\pi} - i\lambda A \qquad \text{eqn 1.7}$$

The neutron refractive index for most materials is less than unity, 1 - n is of the order of $10^{-6}$. So at small incidence angles total external reflection is observed. From Snell's Law, the critical angle, $\theta_c$ below which total external reflection occurs is given by $\cos\theta_c = n$

For small values of $\theta$, $\cos\theta$ approximates to $1-(\theta_c^2 / 2)$, therefore the critical angle can be determined using equation 1.8. For incidence angles less than the critical angle, the reflectivity is one.

$$\theta_c = \lambda\left(\frac{\rho_N}{\pi}\right)^{\frac{1}{2}} \qquad \text{eqn 1.8}$$

Fresnels Law, equation 1.9, gives the reflectivity from a single interface.

$$R(\underline{Q}) = \frac{16\pi^2}{\underline{Q}^4}\Delta\rho_N{}^2 \qquad \text{eqn 1.9}$$

For a single thin film, as shown in figure 1.7, the reflectivity is given by equation 1.10 where $r_{ij}$ is the Fresnel coefficient (equation 1.11) at the ij interface, $n_i$ is the neutron refractive index and $d_i$ the thickness of the $i^{th}$ layer.

$$R(\underline{Q}) = \left| \frac{r_{01} + r_{12} e^{-2i\beta}}{1 + r_{01} r_{12} e^{-2i\beta}} \right|^2 \qquad \text{eqn 1.10}$$

$$r_{ij} = \frac{p_i - p_j}{p_i + p_j} \qquad \text{eqn 1.11}$$

$$p_i = n_i \sin\theta_i = (n_i^2 - n_{i-1}^2 \cos^2\theta_{i-1})^{1/2}$$

$$\beta_i = \frac{2\pi}{\lambda} n_i d_i \sin\theta_i$$

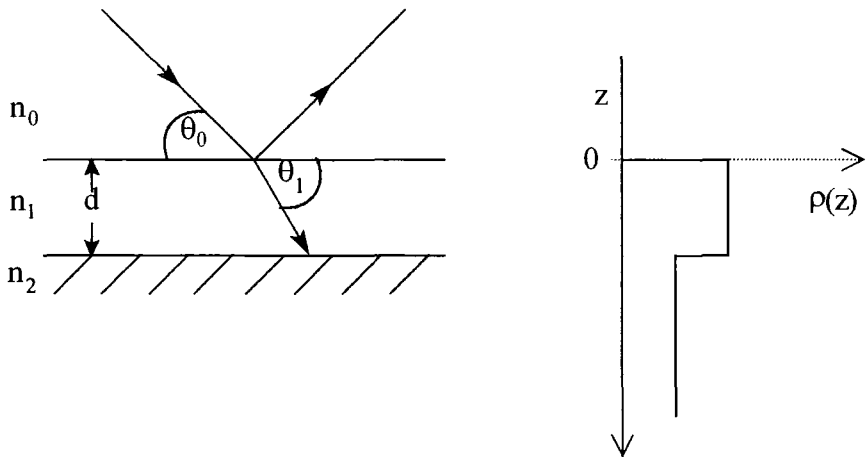


**Figure 1.7 A diagram to show the reflectivity from a single film on a substrate and the associated scattering length density profile.**

Allowing for a rough or diffuse interface, the reflected intensity is modified by a Debye - Waller like factor (equation 1.12) where R is the reflectivity with roughness, $R_o$ without surface roughness and $\sigma$ is the root mean square Gaussian roughness.

$$R = R_o \exp(-q_o q_1 \langle \sigma^2 \rangle) \qquad \text{eqn 1.12}$$

$$q_i = \frac{4\pi}{\lambda} \sin\theta_i$$

Hence, the Fresnel coefficient, allowing for air - film and film - substrate interfacial roughness becomes equation 1.13.

$$r_{ij} = \frac{(p_i - p_j)}{(p_i + p_j)} \exp -0.5(q_i q_j \langle \sigma^2 \rangle) \qquad \text{eqn 1.13}$$

For reflection from multiple layers, either discrete multilayers or a concentration gradient split into a series of discrete layers, a more general solution is needed. Figure 1.8 shows how a concentration gradient can be split into a number of layers of uniform thickness.

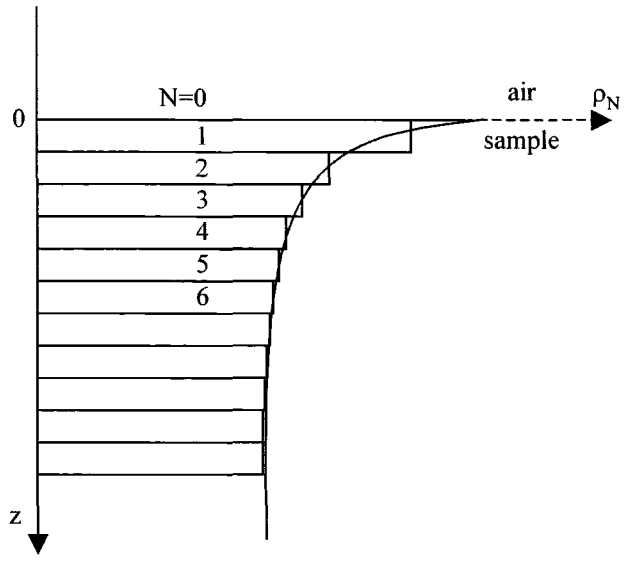


**Figure 1.8 A concentration gradient split into a number of layers.**

A commonly used method is the matrix formulism of Born and Wolf. A characteristic matrix for the Jth layer assuming the wave functions and gradients are continuous at each boundary,

$$M_j = \begin{bmatrix} \cos\beta_j & -(i/p_j)\sin\beta_j \\ -ip_j \sin\beta_j & \cos\beta_j \end{bmatrix}$$

The resultant reflectivity for n layers is obtained from the product of the characteristic matrices,

$$M_R = [M_1][M_2].....[M_n] = \prod_{j=1}^{n} M_j$$

$$R = \left[ \frac{(M_{11} + M_{12}p_s)p_a - (M_{21} + M_{22})p_s}{(M_{11} + M_{12}p_s)p_a + (M_{21} + M_{22})p_s} \right]^2$$

where a and s refer to air and substrate.

The drawback of this method is that it does not include interface imperfections and the reflectivity cannot be inverted to give the composition profile.

An alternative multilayer method using Fresnel coefficients is Abeles method. The characteristic matrix per layer is now defined,

$$M_j = \begin{bmatrix} e^{i\beta_{j-1}} & r_j e^{i\beta_{j-1}} \\ r_j e^{-i\beta_{j-1}} & e^{-i\beta_{j-1}} \end{bmatrix}$$

For n layers the matrix elements $M_{11}$, $M_{21}$ of the resultant matrix $M_R$ give the reflectivity,

$$R = \frac{M_{21} M_{21}^*}{M_{11} M_{11}^*}$$

This method can be used to calculate neutron reflectivity for non-ideal systems and can be used in least squares model fitting routines to extract the composition profile.

Due to the loss of phase information, the reflectivity is not unique to a single composition profile. Hence a range of different composition profiles may produce experimentally identical reflectivity profiles. The reflectivity profile may then be fitted to several model composition profiles, a number of which will be chemically or physically unreasonable and can be ruled out using knowledge of the system and further information gained from other techniques.

### 1.2.2 Nuclear Reaction Analysis (NRA)

Jones[51] has given a general review of the use of ion beam analysis for the investigation of thin polymer films. This work has made particular use of nuclear reaction analysis.

For collisions between light ions, nuclear forces are important and scattering cross sections become non-Rutherford. Collisions can be inelastic, producing energy. Nuclear reaction analysis as used in this work utilises the following nuclear reaction, where Q = 18.352 MeV:

$$^{3}He^{+} + {}^{2}H \rightarrow {}^{4}He + {}^{1}H^{+} + Q$$

The kinematics of the collision are calculated by conserving momentum and energy, taking into account the energy released in reaction.

The nuclear reaction is used to gain the direct depth profile of the deuterium in the polymer film using a method developed for polymer systems by Payne et al at the University of Surrey[52]. An incident $^{3}He^{+}$ beam of 0.7 MeV is used. As this penetrates the sample it loses energy through electronic interactions. The differential energy loss with path length for the ion passing through the sample is known as the stopping power. If the stopping power of the sample is known, the depth at which the reaction occurred can be deduced from the measured energy of the emitted spectrum.

The $^{3}He^{+}$ ions react with $^{2}H$ in the sample via a $^{5}Li$ intermediate. The protons produced have an energy typically greater than 11 MeV and dependent upon the energy of the $^{3}He^{+}$ at reaction. The protons are detected at a backwards angle to the incident beam with protons from the surface having a lower energy than those produced within the sample.

The incident angle of the $^{3}He^{+}$ beam affects the depth probed and the resolution obtained. A lower angle has a greater path length for a given penetration depth, and hence greater resolution. Payne et al found a resolution of 300Å (FWHM) for samples at 15° to the incident beam and a backward detection angle of 165°. These were the general conditions used in this work, though some work was carried out at a lower incident angle.

Chaturvedi[53] et al have also developed NRA for the investigation of thin polymer films. They detected $^{4}He$ at forward angles. The energy of the emitted $^{4}He$ decreases with depth. This set up has the highest ultimate resolution, but at the cost of sensitivity.

Maldener et al[54] used nuclear reaction analysis to profile the fluorine in a blends of fluorinated and nonfluorinated polymers using the resonant nuclear reaction $^{19}F(p, \alpha\gamma)^{16}O$ and detecting the $\gamma$-rays. The polymers studied were heavily fluorinated, though, and required a different experimental set-up to that available at the University of Surrey.

## 1.3 Objectives and Aims of this Work

The aim of this work was to study surface segregation in blends of surface-active functionalised polystyrene in 'normal' hydrogenous polystyrene using the techniques of nuclear reaction analysis and neutron reflectometry. The functional polystyrene was perdeuterated; primarily to act as a label in the analytical techniques employed, with a perfluoro alkane group or groups at specific locations in the polymer. Recent work has shown that perdeuterated polystyrene with a

perfluorohexane group at one end will end attach to the air-polymer interface[55, 56]. The aim here was to study the effect of the architecture of the polymer chain, and the amount and position of surface-active functionality on brush formation. The equilibrium surface depth profiles and their rate of attainment for various blends were studied, comparing the results obtained with current theory. Chapter 2 explains the experimental methods employed and chapter 3 looks at the behaviour of a linear chain with functional groups at both ends of the chain when blended with polystyrene of the same molecular weight and in a range of different molecular weight matrices. Chapters four and five report the results for a three-armed star polymer with a functional group as the core and a linear chain with functional groups evenly spaced along the chain respectively when blended with linear polystyrene of the same total molecular weight. In chapter six the results of experiments to study the kinetics of the formation of a segregated layer from both blended samples and bilayer samples are reported. Each chapter has its own conclusions and references, however, an overall summary along with some suggestions for further work are given in chapter seven.

## 1.4 References


1 R. F. Brady, *Chemistry and Industry*, 1997, 219.

2 R. A. L. Jones, E. J. Kramer, M. H. Rafailovich, J. Sokolov, and S. A. Schwarz, *Physical Review Letters*, 1989, **62**, 280.

3 R. A. L. Jones, L. J. Norton, E. J. Kramer, R. J. Composto, R. S. Stein, T. P. Russell, A. Mansour, A. Karim, G. P. Felcher, M. H. Rafailovich, J. Sokolov, X. Zhao, and S. A. Schwarz, *Europhysics Letters*, 1990, **12**, 41.

4 R. A. L. Jones and E. J. Kramer, *Philosophical Magazine B-Physics of Condensed Matter Structural Electronic Optical and Magnetic Properties*, 1990, **62**, 129.

5 X. Zhao, W. Zhao, J. Sokolov, M. H. Rafailovich, S. A. Schwarz, B. J. Wilkens, R. A. L. Jones, and E. J. Kramer, *Macromolecules*, 1991, **24**, 5991.

6 A. Hariharan, S. K. Kumar, and T. P. Russell, *Journal of Chemical Physics*, 1993, **98**, 4163.

7 P. P. Hong, F. J. Boerio, and S. D. Smith, *Macromolecules*, 1994, **27**, 596.

8 J. W. Cahn, *Journal of Chemical Physics*, 1977, **66**, 3667.

9 H. Nakanishi and P. Pincus, *Journal of chemical Physics*, 1983, **79**, 997.

10 I. Schmidt and K. Binder, *Journal de Physique*, 1985, **46**, 1631.

11 R. A. L. Jones and E. J. Kramer, *Polymer*, 1993, **34**, 115.

12 S. T. Milner, *Science*, 1991, **251**, 905.

13 G. J. Fleer, M. A. Cohen Stuart, J. M. H. M. Scheutjens, T. Cosgrove, and B. Vincent, 'Polymers at Interfaces', Chapman and Hall, 1993.

14 K. R. Shull, *Journal of Chemical Physics*, 1991, **94**, 5723.

15 P. G. de Gennes, *Macromolecules*, 1980, **13**, 1069.

16 M. Aubouy and E. Raphael, *Journal de Physique II*, 1993, **3**, 443.

17 K. R. Shull, *Macromolecules*, 1996, **29**, 2659.

18 M. Stamm, G. Reiter, and K. Kunz, *Physica B*, 1991, **173**, 35.

19 T. P. Russell, *Physica B*, 1996, **221**, 267.

20 R. K. Thomas and J. Penfold, *Current Opinion in Colloid and Interface Science*, 1996, **1**, 23.

21 L. C. Feldman, 'Rutherford Backscattering and Nuclear Reaction Analysis', in 'Ion Spectroscopies for Surface Analysis', ed. A. W. Czanderna and D. M. Hercules, Plenum Press, 1991.

22 A. W. Czanderna and D. M. Hercules, 'Ion Spectroscopies for Surface Analysis', Plenum Press, 1991.

23 S. Huttenbach, M. Stamm, G. Reiter, and M. Foster, *Langmuir*, 1991, **7**, 2438.

24 W. Zhao, X. Zhao, M. H. Rafailovich, J. Sokolov, T. Mansfield, R. S. Stein, R. C. Composto, E. J. Kramer, R. A. L. Jones, M. Sansone, and M. Nelson, *Physica B*, 1991, **173**, 43.

25 J. B. Field, C. Toprakcioglu, R. C. Ball, H. B. Stanley, L. Dai, W. Barford, J. Penfold, G. Smith, and W. Hamilton, *Macromolecules*, 1992, **25**, 434.

26 K. Kunz and M. Stamm, *Macromolecules*, 1996, **29**, 2548.

27 C. J. Clarke, R. A. L. Jones, J. L. Edwards, K. R. Shull, and J. Penfold, *Macromolecules*, 1995, **28**, 2042.

28 H. E. Hermes, J. S. Higgins, and D. G. Bucknall, *Polymer*, 1997, **38**, 985.

29 N. N. Pellegrini, M. Sikka, S. K. Satija, and K. I. Winey, *Macromolecules*, 1997, **30**, 6640.

30 P. J. Mills, P. F. Green, C. J. Palmstrom, J. W. Mayer, and E. J. Kramer, *Applied Physics Letters*, 1984, **45**, 957.

31 W. Wu, W. E. Wallace, J. H. van Zanten, B. J. Bauer, D. Liu, and A. Wong, *Polymer*, 1997, **38**, 2583.

32 N. C. Stoffel, S. Chandra, E. J. Kramer, W. Volkson, and T. P. Russell, *Polymer*, 1997, **38**, 5073.

33 A. Budkowski, J. Klein, and L. J. Fetters, *Macromolecules*, 1995, **28**, 8571.

34 T. E. Shearmur, A. S. Clough, D. W. Drew, M. G. D. vanderGrinten, and R. A. L. Jones, *Physical Review E*, 1997, **55**, R3840.

35 F. Zink, T. Kerle, and J. Klein, *Macromolecules*, 1998, **31**, 417.

36 X. Zhao, W. Zhao, M. H. Rafailovich, J. Sokolov, T. P. Russell, S. K. Kumar, S. A. Schwarz, and B. J. Wilkens, *Europhysics Letters*, 1991, **15**, 725.

37 X. Zhao, W. Zhao, X. Zheng, M. H. Rafailovich, J. Sokolov, S. A. Schwarz, M. A. A. Pudensi, T. P. Russell, S. K. Kumar, and L. J. Fetters, *Physical Review Letters*, 1992, **69**, 776.

38 S. Affrossman, P. Bertrand, M. Hartshorne, F. T. Kiff, D. Leonard, R. A. Pethrick, and R. W. Richards, *Macromolecules*, 1996, **29**, 5432.

39 K. Kunze, M. Stamm, M. Hartshorne, and S. Affrossman, *Acta Polymer*, 1996, **47**, 234.

40 Z. H. Su, D. C. Wu, S. L. Hsu, and T. J. McCarthy, *Macromolecules*, 1997, **30**, 840.

41 P. Jannasch, *Macromolecules*, 1998, **31**, 1341.

42 J. G. Van Alsten and S. R. Lustig, *Macromolecules*, 1992, **25**, 5069.

43 E. Jabbari and N. A. Peppas, *Macromolecules*, 1993, **26**, 2175.

44 E. Jabbari and N. A. Peppas, *Journal of Materials Science*, 1994, **29**, 3969.

45 J. G. Van Alsten, S. R. Lustig, and B. Hsiao, *Macromolecules*, 1995, **28**, 3672.

46 J. G. Van Alsten, *Trends in Polymer Science*, 1995, **3**, 272.

47 J. S. Higgins and H. C. Benoit, 'Polymers and Neutron Scattering', Clarendon Press, 1994.

48 T. P. Russell, *Materials Science Reports*, 1990, **5**, 171.

49 J. Penfold, 'The adaptation of methods in multilayer optics for the calculation of specular neutron reflection', RAL-88-088, Rutherford Appleton Laboratory, 1988.

50 J. Penfold and R. K. Thomas, *Journal of Physics-Condensed Matter*, 1990, **2**, 1369.

51 R. A. L. Jones, 'Polymer Surfaces and Interfaces II', John Wiley and Sons Ltd., 1993.

52 R. S. Payne, A. S. Clough, P. Murphy, and P. J. Mills, *Nuclear Instruments and Methods in Physics Research B*, 1989, **42**, 130.

53 U. K. Chaturvedi, U. Steiner, O. Zak, G. Krausch, G. Schatz, and J. Klein, *Applied Physics Letters*, 1990, **56**, 1228.

54 J. Maldener, K.-H. GieBler, T. Becht, F. Rauch, M. Stamm, and E. Arai, *Nuclear Instruments and Methods in Physics Research B*, 1995, **99**, 444.

55 S. Affrossman, M. Hartshorne, F. T. Kiff, R. A. Pethrick, and R. W. Richards, *Macromolecules*, 1994, **27**, 1588.

56 I. Hopkinson, F. T. Kiff, R. W. Richards, D. G. Bucknall, and A. S. Clough, *Polymer*, 1997, **38**, 87.

# CHAPTER 2

# Experimental

## 2.1 Polymer Synthesis

All the polymers used were synthesised by F. T. Kiff at Durham, except for four polystyrene samples that had been purchased previously from Polymer Laboratories. The synthesis of the functional polymers was based upon a method described by Hunt[1] et al.

The polymers used were normal hydrogenous polystyrene (hPS); perdeuterated polystyrene (dPS), prepared from the fully deuterated monomer; a difunctional perdeuterated polystyrene capped at both ends with 1H,1H,2H,2H-perfluoro octyl dimethyl chlorosilane (dPSF2); perdeuterated polystyrene three-armed star with 1H,1H,2H,2H-perfluoro octyl trichlorosilane as the core (STAR) and a multiple fluorine labelled perdeuterated polystyrene with a $-CH_2CH_2(CF_2)_4CH_2CH_2-$ group at intervals along the deuterated polystyrene chain (MFL).

The hydrogenous and deuterated polystyrene and the individual perdeuterated arms of the STAR were prepared by anionic polymerisation of the purified monomer in benzene, under vacuum at room temperature. The initiator used was secondary butyl lithium. For hPS and dPS the reaction was terminated using degassed methanol. The living arms of the STAR were reacted with ~5 units of butadiene. This allowed 3 arms to react with the fluorinated core. The structure of the STAR is shown in figure 2.1.

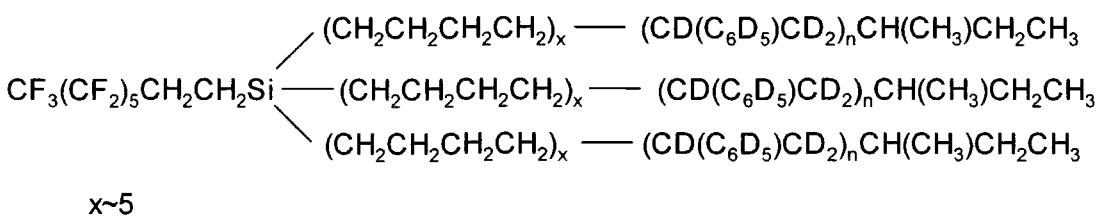


**Figure 2.1 Perdeuterated polystyrene 3 armed star (STAR).**

The difunctional polystyrene, dPSF2, also referred to as double F end capped, and multiple fluorine labelled polymers were also prepared by anionic polymerisation. A difunctional initiator, figure 2.2, was used so that both ends of the polymer chain were living.

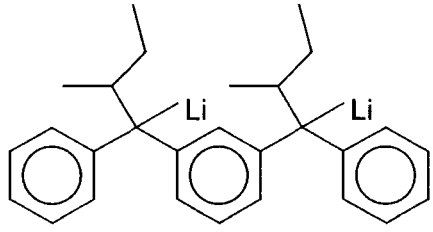


**Figure 2.2 1,3 - Phenylene bis (3-methyl-1-phenylpentylidene) dilithium.**

For dPSF2 the polymerisation was carried out in benzene with 1% v/v tetrahydrofuran added to maintain a narrow molecular weight distribution. The reaction was terminated using excess 1H,1H,2H,2H-perfluoro octyl dimethyl chloro silane. Unreacted silane was removed by redissolving the polymer in butanone and precipitating out in methanol. The structure of the difunctional polystyrene is given in figure 2.3.

To prepare the multiple fluorine labelled polymer, the reaction was carried out in tetrahydrofuran at 195K. The living perdeuterated polystyrene was reacted with 1,8 di-iodo 3,3,4,4,5,5,6,6 octafluoro octane. The aim was to have three polystyrene chains separated, and capped by the fluorinated species. The unreacted ends were capped with n-butyl lithium. The idealised structure is shown in figure 2.4.

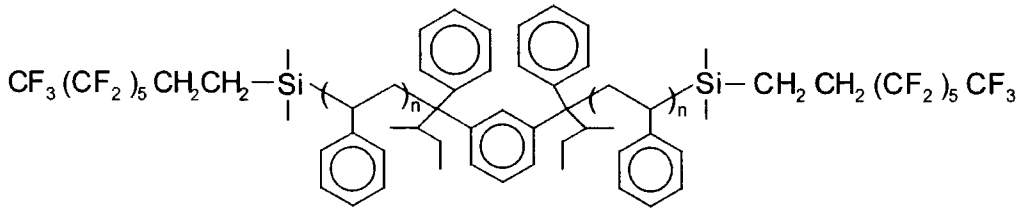

**Figure 2.3 Difunctional perdeuterated polystyrene (dPSF2).**

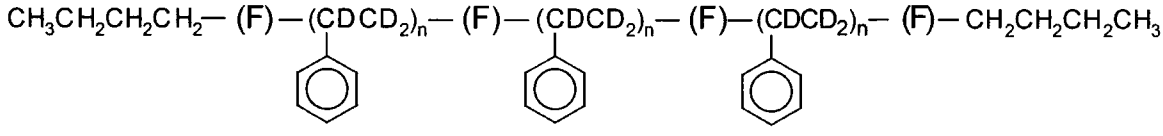

(F) = $-(CH_2)_2(CF_2)_4(CH_2)_2-$

**Figure 2.4 Multiple fluorine labelled perdeuterated polystyrene (MFL).**

In reality the difunctional living perdeuterated polystyrene chains were twice the expected molecular weight, hence on average six chains had reacted with the fluoro alkane and the total molecular was greater than that targetted.

The linear hydrogenous and perdeuterated polystyrenes were used as received. The STAR and multiple fluorine labelled polymers needed to be fractionated before use. The 3-armed star polymers were fractionated to remove the excess unreacted arm present in the polymer. The multiple fluorine labelled polymer was fractionated to obtain a narrower molecular weight fraction.

Fractionation was carried out by dissolving the polymer in butanone to give a 3% solution. The solution, in a separating funnel, was clamped in a thermostatically controlled water bath at 298K. The solution was stirred whilst methanol was added

slowly until the solution remained cloudy on further addition of methanol. The temperature of the bath was then raised slowly until the solution became clear. More methanol was added and the process was repeated until a temperature range of ~10 degrees had been covered and all the polymer was in solution. The temperature controller was turned off and the stirrer removed allowing the solution to cool slowly, overnight. On cooling the solution phase separated. The lower, high molecular weight containing layer was drawn off, a small amount of butanone was added to this to prevent the polymer precipitating out of solution.

The polymer was then precipitated out into stirring methanol, filtered off and dried under vacuum at 313K before been analysed by size exclusion chromatography. If necessary the remaining solution was fractionated further. For the STAR the first fraction gave the desired material. For the multiple fluorine labelled polymer the middle fraction was used as this had the extremes of the original molecular weight distribution removed. Unfortunately precise structure determination of the multiple fluorine labelled polymer has not been possible because of the small amount of fluorine present relative to the remainder of the polymer.

## 2.2 Polymer characterisation

### 2.2.1 Size exclusion chromatography

The polymers used have been analysed by size exclusion chromatography to determine the molecular weight and polydispersity. The eluting solvents were tetrahydrofuran or chloroform. Calibration of the instrument was carried out using hydrogenous polystyrene standards supplied by Polymer Laboratories. Table 2.1 shows the polymers used with their reference code; abbreviated description; weight

average molecular weight, $M_w$ and the polydispersity $M_w$ / $M_n$, where $M_n$ is the number average molecular weight.

| Code | Polymer | $M_w$ | $M_w$ / $M_n$ |
|---|---|---|---|
| TK 96 | hPS | 19 000 | 1.05 |
| TK 191 | hPS | 43 000 | 1.05 |
| TK 79 | hPS | 44 700 | 1.05 |
| PL 52 | hPS | 52 000 | 1.03 |
| TK 192 | hPS | 106 000 | 1.06 |
| TK 241 | hPS | 121 000 | 1.03 |
| PL 120 | hPS | 122 800 | 1.04 |
| PL 330 | hPS | 303 000 | 1.01 |
| PL 1m | hPS | 1 080 000 | 1.05 |
| TK 250 | dPS | 42 000 | 1.01 |
| TK 204 | dPS | 111 000 | 1.05 |

**Table 2.1a Non-functional polymers used and their molecular weights.**

| Code | Polymer | $M_w$ | $M_w$ / $M_n$ |
|---|---|---|---|
| TK 145 | dPSF2 (50k) | 56 000 | 1.04 |
| TK 181 | dPSF2 (100k) | 102 000 | 1.04 |
| TK 249 | dPSF2 (100k) | 98 000 | 1.04 |
| TK 200 | STAR | 65 200 | 1.25 |
| | fractionated | 88 300 | 1.05 |
| | unreacted arm | 29 800 | 1.01 |
| TK 213 | MFL | 164 000 | 2.77 |
| | fractionated | 364 000 | 1.86 |
| | unreacted 'arm' | 58 400 | 1.19 |

**Table 2.1b Functional polymers used and their molecular weights.**

### 2.2.2 Glass Transition Temperature

The glass transition temperature, $T_g$ of the polymers was required to ensure that any annealing process carried out was at a suitable temperature. Differential scanning calorimetry, (DSC) was carried out using a Perkin Elmer DSC7, on a sample of hydrogenous polystyrene and some of the perdeuterated functional polystyrenes. The results are given in table 2.2. Where the polymer had been fractionated the

analysis was carried out on the fraction used in the blends. These values are of the order expected for polystyrene[2]

| Code | $T_g$/°C |
|---|---|
| TK 79 | 104.4 |
| TK 145 | 102.2 |
| TK 181 | 104.8 |
| TK 200 | 100.4 |
| TK 213 | 104.4 |

**Table 2.2 Glass transition temperatures for hPS and dPS.**

### 2.2.3 Density

The densities of the hydrogenous and perdeuterated polystyrenes used in calculations were:

hPS 1.05 $gcm^{-3}$

dPS 1.13 $gcm^{-3}$

The value for hPS is the literature value for amorphous hydrogenous polystyrene[3]. The value for dPS was calculated assuming the volume per mole was the same and the only difference was the extra mass due to deuterium. The functionality was assumed to have no effect on the density. The values used here were also the same as those reported by Geoghegan et al[4].

To support this, the densities of hPS (PL 120) and dPS (TK 204) were also determined using a density gradient column. A column in the range 0.93 to 1.15 $gcm^{-3}$ was prepared from solutions of zinc chloride and aqueous ethanol. A sample was prepared by dissolving polymer in a small amount of butanone, which was then allowed to evaporate off. This formed a thick film, with no air bubbles, which was suitable for adding to the column. Small pieces of each sample were taken and added

to the column. These were allowed to settle for ~4 hours and the average height taken. The density was calculated by comparing the heights obtained with the height of calibrated density beads. The values obtained are given in table 2.3, and are in good agreement with the values determined above.

| Sample | Density / $gcm^{-3}$ |
|---|---|
| PL 120 | 1.046 |
| TK 204 | 1.120 |

**Table 2.3 Density values for hPS and dPS.**

## 2.3 Sample preparation

The polymer films studied in this work were prepared by the spin casting of the pure polymer or polymer blend from solution.

The polymer(s) were weighed accurately into a volumetric flask and toluene added. The solutions were allowed to stand overnight before use to ensure that the polymers were fully dissolved. For a blend the volume fraction of the functional polymer (deuterated) was calculated using equation 2.1,

$$\phi_D = \frac{m_D / 1.13}{\frac{m_D}{1.13} + \frac{m_H}{1.05}} \qquad \text{eqn 2.1}$$

where $m_D$ is the mass of perdeuterated polymer and $m_H$ the mass of hydrogenous matrix polymer. The volume fraction was determined accurately from the masses of the polymers used, but the solution concentrations quoted were only approximate as these were used only as a method to control the film thickness. The polymer molecular weight also had an affect on the thickness of the films prepared and was

taken into consideration when deciding what solution concentration to use. The same solutions were generally used to prepare samples for both NR and NRA.

### 2.3.1 Neutron Reflectometry

Films were spun onto optically flat silicon blocks using a Dynapert Precima Ltd. photoresist spinner. The silicon blocks were 50mm in diameter and 5mm thick, orientation (100) or (110). The blocks were used as received if new, or after cleaning. The cleaning process involved rinsing off the polymer with chloroform. Leaving the blocks to stand overnight in toluene and then placing them in a beaker of fresh toluene in an ultrasonic bath for 30 minutes at around 303K. The blocks were rinsed with fresh toluene and allowed to dry. No attempt was made to remove the native silicon oxide surface layer that is present and a 15Å silicon oxide layer was accounted for in the fitting of the data. The effect of this $SiO_2$ layer on the calculated profile is negligible for all but the thinnest films i.e. thickness less than circa 2500Å.

Before spinning the surface of the silicon block was wiped with optical tissue to remove any dust. An aliquot of the solution (~0.5$cm^3$) was placed in the centre of the block, and the block immediately spun at 2000 to 4000 rpm for 25 seconds. This procedure gave reproducible films of uniform thickness.

Samples that were to be left unannealed were kept in a desiccator until measurement. Annealed samples were placed in a vacuum oven at a temperature above the glass transition temperature. Samples annealed to equilibrium were left under these conditions for up to 7 days before removing to a desiccator. Samples used for kinetics studies were annealed for different lengths of time under similar

conditions. On removal from the oven they were cooled quickly by placing on a cold metal block and also kept in a desiccator.

The film thicknesses were measured using contact profilometry. A scratch was made in the polymer film using a scalpel blade, which revealed the substrate. Contact profilometry measured the displacement of a stylus drawn across this scratch. The values obtained were generally within ±50Å of the values calculated from the neutron reflectometry experiments.

### 2.3.2 Nuclear Reaction Analysis

Samples were prepared in a similar manner to those for neutron reflectometry measurements. The substrate used for these samples were silicon wafers 50mm in diameter and ~0.4mm thick and the wafers were used new, as received. After the film had been spun, the samples were cut up by scoring with a diamond tipped glass knife, each sample was around 30mm × 10mm, though the exact dimensions varied.

Equilibrium and kinetics samples were annealed above the glass transition temperature in a vacuum oven and the thickness measured by contact profilometry. These measurements were confirmed by the NRA data.

### 2.3.3 Small Angle Neutron Scattering (SANS)

For SANS, discs of polymer were required 12mm in diameter and ~1mm thick. Hence the sample preparation for SANS analysis on LOQ was different to that described above for thin films. Concentrated solutions of the polymers to be studied were prepared using butanone and left overnight to dissolve. The dissolved polymer blend was then precipitated out into stirring methanol, filtered off and dried.

Approximately 0.23g of the blended polymer was placed in the die of a heated Specac infra red press. The sample was initially pressed under hand tight pressure and vacuum applied. The temperature was raised to 418K, and when the $T_g$ was reached (375K) the pressure screw was tightened further. After 15 minutes a pressure of ~2 tonnes was applied and 5 minutes later the vacuum was turned off. The sample was left at 418K for 45-60 minutes ensuring that the pressure remained constant, and then cooled back to room temperature taking around 90 minutes. The sample was removed from the press and the thickness measured using a micrometer.

The samples were placed in brass cells between quartz windows with a PTFE spacer. The cell in an aluminium holder was placed in an oven at 413K for ~6 hours to ensure that no air bubbles were present in the sample.

## 2.4 Polymer systems studied

This work has looked at three key areas:

- blends of the functional perdeuterated polystyrene in a similar molecular weight linear hydrogenous polystyrene both annealed to equilibrium and intermediate annealing times up to equilibrium
- blends of difunctional perdeuterated polystyrene (100k dPSF2) in a range of molecular weight linear polystyrene matrices
- kinetic studies where the pure or blended difunctional perdeuterated polystyrene (100k dPSF2) has been overlaid with a layer of pure hydrogenous polystyrene.

### 2.4.1 Index to coding used to describe samples

A system of reference codes was used to describe comprehensively each blend used. This system is summarised below:

| | |
|---|---|
| H2F | Higher molecular weight double F end capped dPSF2 (100k) |
| L2F | Lower molecular weight double F end capped dPSF2 (50k) |
| STAR | Higher molecular weight 3 armed FSTAR |
| MFL | Multiple fluorine labelled polystyrene |
| DPS | Higher molecular weight unfunctionalised perdeuterated polystyrene |
| ...X... | X volume percent functional polystyrene in blend |
| .....a | Sample has been annealed to equilibrium |
| .....u | Sample as prepared, no annealing |
| .....aY | Annealing time, Y minutes or hours for kinetics samples |
| Z..... | Matrix molecular weight Z |

The term higher refers to polymer blends with a molecular weight of ~100000, and lower refers to blends with a molecular weight of ~50000.

## 2.5 Neutron Reflectometry (NR)

The neutron reflectometry experiments were carried out using the CRISP reflectometer on the ISIS pulsed spallation neutron source at the Rutherford Appleton Laboratory, Chilton. Full details of the instrument and the hardware and software used can be found in the CRISP instrument manual[5].

Neutrons are produced by bombarding a depleted uranium or tantalum target with high-energy protons (~800 MeV) from a synchrotron. For each proton striking the heavy metal target ~25 high-energy neutrons are produced. The neutrons are

moderated by passing through a hydrogenous moderator at a temperature dependant upon the energy distribution required (liquid hydrogen at 20K).

The neutron reflectivity, R(Q) is measured as a function of the scattering vector, Q over a wide range of Q.

$$R(Q) = \frac{I_R(Q)}{I_o(Q)} \qquad \text{eqn 2.2}$$

Where $I_R(Q)$ is the reflected intensity and $I_o(Q)$ the incident intensity of the neutron beam.

$$Q = \frac{4\pi}{\lambda}\sin\theta \qquad \text{eqn 2.3}$$

$\lambda$ is the neutron wavelength and $\theta$ the angle between the plane of the sample and the incident beam.

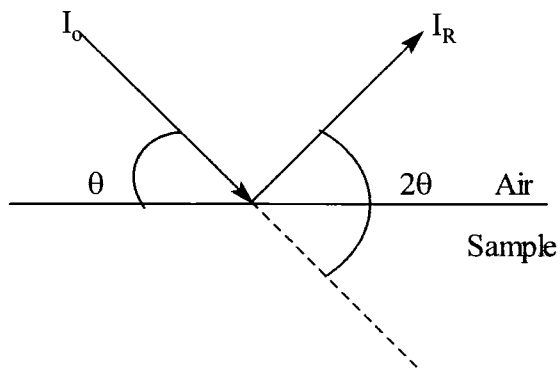


**Figure 2.5: Polymer interface showing the incident and reflected neutron beam.**

CRISP is a fixed angle, variable wavelength instrument. A schematic diagram is shown in figure 2.6. The wavelength range normally covered is 0.5 to 6.5Å at an operating frequency of 50Hz, but a supermirror can be interposed in the beam which

reduces the wavelength range to 2.0 to 6.5Å. Three incident angles have been used in this work, 0.25, 0.6 and 1.5°. These cover the following overlapping Q ranges (assuming supermirror is in place):

| Incident angle | Q range / Å |
|---|---|
| 0.25 | 0.009 - 0.027 |
| 0.60 | 0.021 - 0.065 |
| 1.50 | 0.051 - 0.150 |

The lowest Q values are below the critical edge for the silicon substrate used. Some data points in the region below the critical edge are needed to normalise the reflectivity profile.

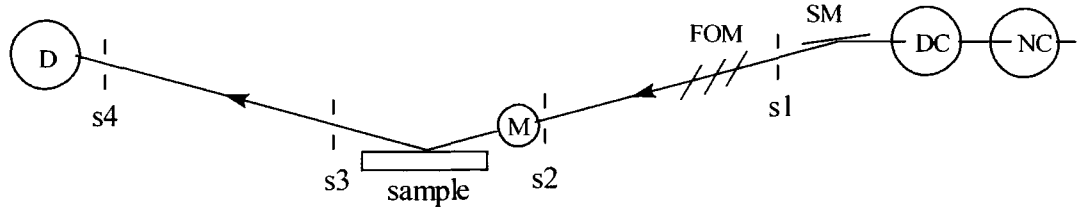


**Figure 2.6: A schematic diagram of the CRISP spectrometer. Explanation of the symbols is given in the text.**

The CRISP spectrometer views a hydrogen moderator at 20K. A nimonic chopper, NC, timed to block the view of the target during the period of the proton pulse, suppresses background noise by attenuating the 'fast' neutrons produced in the moderator at the start pulse. Background counts are produced by high-energy neutrons and $\gamma$ rays.

A double disk variable aperture chopper rotating at 50Hz defines the wavelength range. This also helps to suppress the frame overlap neutrons, i.e. the longer wavelength neutrons produced by previous pulses.

The supermirror, SM reflects neutrons of the desired wavelength but high-energy neutrons and γ rays pass straight through. Thus the sample position and detectors are not in direct line with the target, reducing background further. Nickel coated frame overlap mirrors, FOM reflect long wavelength (>13Å) slow neutrons which have passed through from previous pulses. The shorter wavelength neutrons pass straight through.

The low efficiency beam monitor, M is used to measure the incident neutron beam intensity, $I_o$. This and a further beam monitor are used to ensure neutrons are passing through the instrument and to determine the shape of the beam.

The neutron beam is reflected off the sample and the reflected intensity, $I_R$ measured using one of two detectors.

***Single detector.*** A well shielded $^3$He single scintillation detector. This has a higher sensitivity and lower intrinsic background, but needs to be carefully aligned to the specular reflection peak. The background is determined from the intensity of the beam at high Q values. The post sample slits, s3 and s4 are set to minimise background whilst ensuring all the off specular reflection reaches the detector.

***Multi detector.*** A one dimensional position sensitive multi detector. This is a $BF_3$ gas filled detector with a positional resolution of ~1mm. The sample alignment is less critical as the precise position of the specular reflection can be determined, a straight through measurement needs to be made as a reference for determining the exact angle of reflection. The background level can be measured from the signal collected away from the specular peak. When this detector is used a 'nose cone', coated with boron impregnated resin is positioned between the sample and the detector to reduce background and slit 4 is not used.

Typical beam dimensions are 40mm width and between 0.2 and 4mm height. Two cadmium collimating slits, s1 and s2 define the final beam size. The aperture of these slits determines the geometric resolution, $\Delta\theta / \theta$.

$$\Delta\theta = \tan^{-1}\left(\frac{s1 + s2}{2l}\right) \qquad \text{eqn 2.4}$$

Where s1 and s2 are the heights of the collimating slits, l is the distance from the sample to the detector and $\theta$ is the incidence angle.

The instrumental resolution, $\Delta Q / Q$ has contributions from $\Delta\theta / \theta$ and $\Delta t / t$, where t is the time of flight. For CRISP $\Delta t / t$ is small and its contribution to the resolution can be neglected. Hence the resolution is constant over the whole Q range and generally of the order of 4%. The instrumental resolution is included in calculated reflectivity profiles as a Gaussian smoothing function of width $\Delta Q$.

The samples used in this work were light reflective. This meant that the samples could be aligned using a laser coincident with the neutron beam. The detector angle was defined with respect to the sample. Data for each sample was collected for all the incident angles used, before the next sample was aligned.

Sample measurements were computer controlled by a command file, the beamline components are motor driven, so the slit heights and angle control are automated and can also be controlled by the command file. Measurements at higher incident angles have a lower reflectivity so require a longer sampling time to ensure good signal to noise levels. The amount of time that a sample required could be controlled by measuring the number of μamps of protons received at the target. During the time of these experiments ISIS was running at around 180 to 190 μamps

per hour, so samples at 0.25° waited for 40μamps to be collected, taking ~15 minutes. At 0.6°, a 100μamps were collected, taking ~40 minutes and if a higher angle was used around 150μamps were collected taking ~60 minutes. Each individual angle was a unique measurement, but the data were later combined to give one file.

Data were obtained as counts versus time for the single detector or counts versus time / position for the multi detector. Time zero is the proton pulse. The time is directly related to wavelength, the longer wavelength, longer time and lower Q.

Initial data reduction was carried out at the Rutherford Appleton Laboratory using programs in GENIE, a data manipulation package running as a sub process from VAX. The exact procedure varies slightly depending on the detector used.

Single detector data is reduced using QUICK. This corrects for detector efficiency and the incident spectral shape, as measured by the beam monitor. The program requires as input the raw data file and 2θ. Output is the reflectivity versus Q, as used in this work or versus wavelength, λ.

Multi detector data is reduced in two stages. First the centre of the specular peak is determined using 'm'. This plots counts versus position on the multi detector, x. The peak is determined using a Gaussian peak fitting routine, pk. This value, along with the straight through beam position is used to determine the exact angle of incidence. The corrected angle of incidence is used in the program @g:norm_md2. The reflectivity, R(Q) is obtained by integrating over x. The background is extracted here by interpolating the background level under the specular peak, and subtracting this value from the data.

The reduced files have data in the form:

Q R(Q) error

where the error is the statistical error in R calculated from Poisson statistics. The Q data is in histogram format. The data is rebinned into the same Q interval to match the resolution.

At this point the reflectivity is on an arbitrary scale, and the data for each incident angle may not be on the same scale. The data at the lowest angle is normalised by multiplying the data by a factor such that the reflectivity in the critical region of total reflection is one. Subsequent data sets are normalised to the previous data set using the region of overlap.

When the data sets are normalised they are combined into one data set using @g:COMBINE. This can then be saved as a binary file, which can be used in GENIE and as an ASCII file, which can be transferred to other programs for data analysis.

The second reflectometer at the Rutherford Appleton Laboratory, SURF was used during the instruments commissioning period to carry out one experiment. SURF has some differences compared to CRISP, which are mainly of benefit to the study of liquid systems[6]. For this work the use of the instrument was the same as for CRISP so the differences will not be explained here.

### 2.5.1 Data Analysis

The aim of the data analysis was to obtain the volume fraction profile of the deuterated polymer against depth into the sample. The volume fraction of deuterated polymer is directly related to the scattering length density at that point.

For the pure polymer the scattering length is given by

$$\rho_N = \rho \frac{N_A}{m} \sum b_i \qquad \text{eqn 2.5}$$

where ρ is the density of the polymer, m is the monomer mass, $N_A$ Avogadro's constant and $\sum b_i$ is the sum of the nuclear scattering lengths of all the atoms in the monomer. Table 2.4 gives the values of scattering length used in this work. There is some variation in values quoted in the literature[7-10] but the values are all of this order. For the functional polymers studied the functionality was assumed to have no effect on the scattering length density of the polymer. The possibility was investigated, but the amount of functional group at less than 1% of the total molecular weight gave no observable difference to the calculated profiles.

| Component | $\rho_N$ / $Å^{-2} \times 10^{-6}$ |
|---|---|
| hPS | 1.41 |
| dPS | 6.41 |
| Si | 2.095 |
| $SiO_2$ | 3.676 |
| Air | 0.0 |

**Table 2.4 Values of scattering length density used in NR analysis.**

In a binary blend, assuming incompressibility, the scattering length density at any is position is given by

$$\rho_N(z) = \phi_D(z)\rho_D + \phi_H(z)\rho_H \qquad \text{eqn 2.6}$$

where $\phi_H(z) = 1 - \phi_D(z)$ and $\phi_D(z)$ and $\phi_H(z)$ are the volume fractions of the deuterated and hydrogenous components at depth z, and $\rho_D$ and $\rho_H$ are the scattering length densities of the deuterated and hydrogenous polymers. Hence, from the scattering length density at any position in the sample it is possible to determine the volume fraction of deuterated polymer.

Three methods have been used to fit the experimental data to obtain composition profiles of the volume fraction of the deuterated component versus depth,

Helix3, VOLFMEM and PCMULF. Details of each program and the particular benefits are outlined below.

***Helix3.*** A FORTRAN program for the PC based on the program 'PHOENIX' written by I. Hopkinson[11]. This utilises the FITFUN[12] routine, which is based on a Marquardt - Levenberg algorithm. This program can be used to fit three types of function, a stretched exponential, a hyperbolic tangent or an error function to the data. A multilayer model can also be used, fitting up to four layers with Gaussian roughness between the layers.

For the functional forms, the profile is split into a number of layers of uniform thickness, usually 10-20Å, and the reflectivity modelled using the Abeles method. Resolution is accounted for by convoluting the model reflectivity with a Gaussian function of the appropriate width. For all the composition profiles a silicon dioxide layer of 15Å is included at the silicon polymer interface. The segregated layer can be at the air, substrate or both interfaces.

***VOLFMEM.*** The program VOLFMEM was written by D. Sivia, currently at the Rutherford Appleton Laboratory and utilises a maximum entropy algorithm[13]. A model with high entropy is favoured over a low entropy model. The entropy is calculated relative to a uniform density profile using no prior assumptions.

The composition profile is fitted with a 'free form'. The profile is divided into a maximum of 255 layers of equal thickness, and the composition of each layer allowed to vary. Hence an accurate measurement of the sample thickness is required. The fitting process often produces sharp changes in the composition profile obtained, which are physically impossible due to the polymer chain dimensions. Therefore an

internal correlation function, ICF, of ~50 Å is applied, which reduces sharp fluctuations in composition.

***PCMULF.*** This is a program for a PC based upon the program MULF at the Rutherford Appleton Laboratory. This program uses the optical matrix method to calculate the reflectivity, and fits the scattering length density of a number of layers of varying thickness with Gaussian roughness between the layers. The calculated reflectivity is fitted to the experimental data using one of two methods, the non-linear least squares routine VA05A or a SIMPLEX minimisation. The scattering length density profile is obtained, which relates directly to the volume fraction of deuterated polymer, so the volume fraction profile can be obtained.

For the majority of this work a functional form model based on an exponential profile has been fitted at the air interface. The stretched exponential is a flexible model, which has been able to fit the data well, and in good agreement with other composition profiles produced.

$$\phi(z) = (\phi_s - \phi_b)\left[\exp\left(\frac{-z}{\lambda}\right)^{\beta}\right] + \phi_b \qquad \text{eqn 2.7}$$

Where $\phi(z)$ is the volume fraction of the deuterated component as a function of depth, z from the air - polymer interface. $\phi_s$ and $\phi_b$ are the bulk and surface volume fractions of functional polymer, $\lambda$ is the characteristic decay length of the profile and $\beta$ is the exponent. The shape of the profile is dependent upon the value of $\beta$. If $\beta=1$ then the profile is a simple exponential becoming more block like as $\beta$ is increased (figure 2.7).

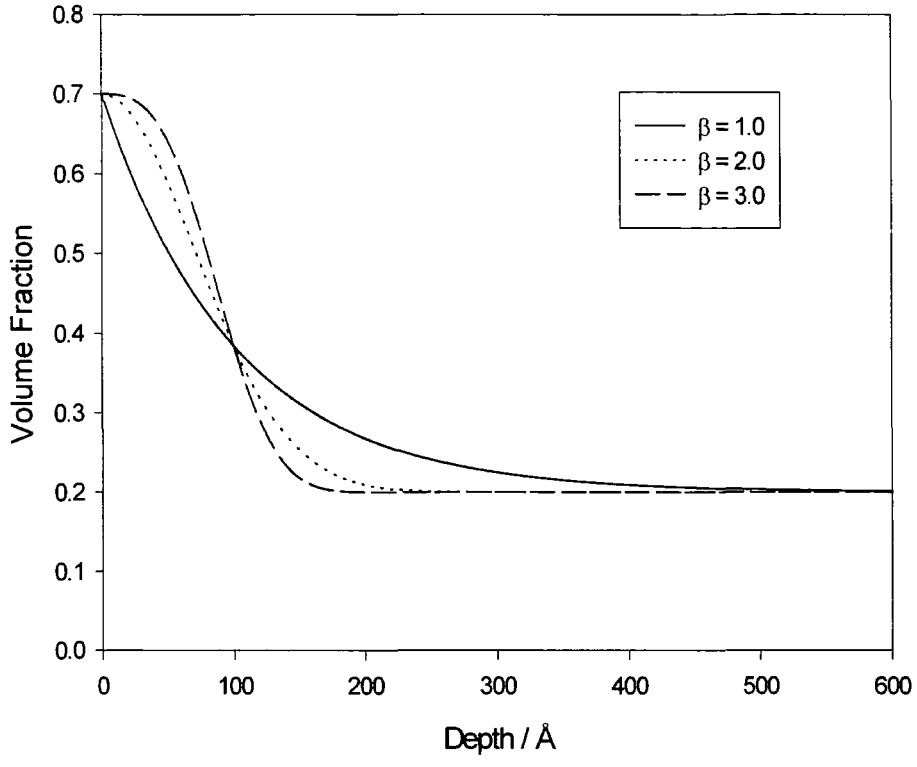


**Figure 2.7 Graph to show the effect of increasing β when $\phi_s$, $\phi_b$ and λ remain the same.**

The Tanh function as predicted by Shull[14] for dry polymer brushes, is for brushes in the strong adsorption limit that has not been reached in these systems. However, the profiles produced using this function are identical within experimental error to those produced by the stretched exponential (usually when β is circa 2).

$$\phi(z) = \phi_b + \frac{\phi_a - \phi_b}{2}\left[1 + \tanh\left(\frac{2(z_{off} - z)}{w}\right)\right] \qquad \text{eqn 2.8}$$

$\phi_a$ approximates to the surface volume fraction. $z_{off}$ is the height of the offset of the decay to bulk and w is the width of the interfacial region.

A functional form model at the air surface has been used for all the equilibrium data except for the multiple fluorine labelled polymer. Attempts to use functional forms for this system only gave poor fits to the data (see chapter 5). For

this system, unannealed samples for all systems and samples for kinetics measurements a simple layer profile was used fitting the layer thickness, volume fraction and roughness between the layers. VOLFMEM was used on all the annealed and unannealed samples as an unbiased comparison with the other composition profiles and generally gave excellent agreement. For kinetic samples from blends VOLFMEM was also very good, but only poor results were obtained for the bilayer kinetics (samples annealed less than 240 minutes) as the program struggled to fit the lower scattering length density hPS layer at the air surface. For later annealing times the comparison again was good.

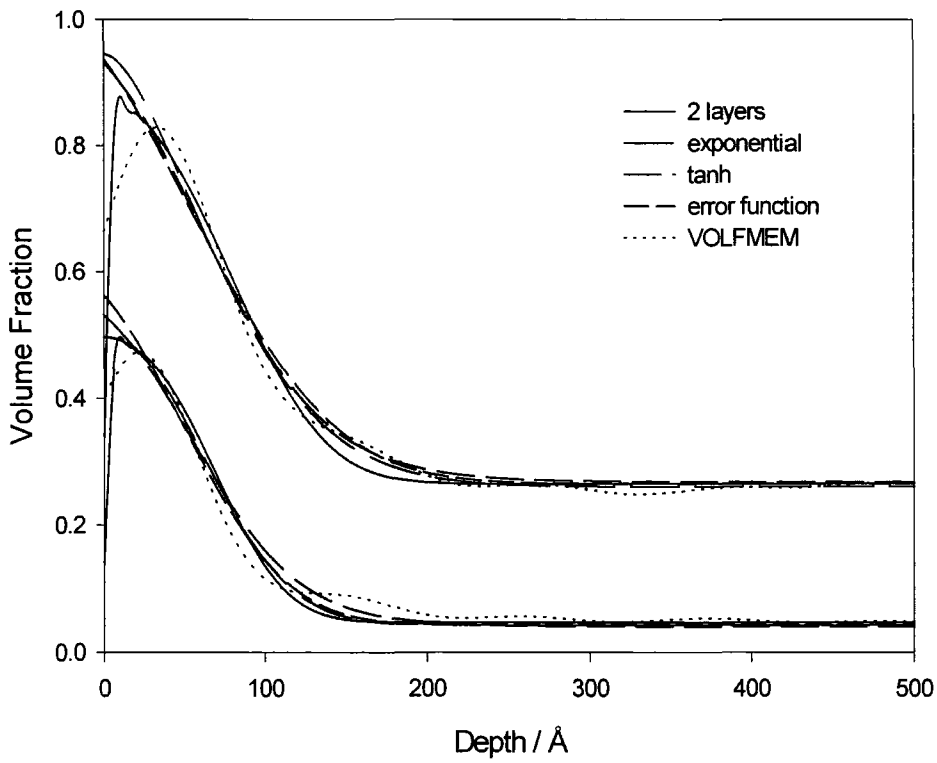


**Figure 2.8 Comparison of the various composition profiles obtained for H2F30a and H2F05a using the different fitting programs. The 2 layer profile is the solid line and the exponential profile the large dash.**

Figure 2.8 shows the comparison in the profiles obtained for H2F30a and H2F05a. The profiles are essentially the same, the main difference is the downturn in the volume fraction profile at the surface for the 2 layer and VOLFMEM profiles. VOLFMEM has no mechanism to account for surface roughness so the downturn is an artefact seen to allow for the sharp interface. The 2 layer model has a 5Å surface roughness included in the profile which causes the downturn at the surface, the other profiles used 5Å roughness in the fits but this has not been included in the profiles shown.

| | H2F05a | | | H2F30a | | |
|---|---|---|---|---|---|---|
| **Model** | $\phi_b$ | $\phi_s$ | **z*/Å** | $\phi_b$ | $\phi_s$ | **z*/Å** |
| 2 layer | 0.05 | 0.49 | 30 | 0.27 | 0.87 | 49 |
| exponential | 0.04 | 0.50 | 33 | 0.26 | 0.95 | 56 |
| tanh | 0.04 | 0.53 | 35 | 0.27 | 0.93 | 55 |
| error function | 0.04 | 0.56 | 34 | 0.26 | 0.97 | 56 |
| VOLFMEM | 0.05 | 0.47 | 30 | 0.26 | 0.83 | 52 |
| **average** | 0.05 ±0.006 | 0.51 ±0.04 | 32 ±2.5 | 0.26 ±0.005 | 0.91 ±0.06 | 53 ±3.0 |

**Table 2.5 Surface parameters obtained for different fitting models.**

The values obtained from the volume fraction profiles for the different fitting methods are given in table 2.5. The errors are determined from the standard deviations and are generally good. The worst agreement is for the surface volume fraction, which is mainly due to the surface roughness effects already mentioned.

Figure 2.9 shows a comparison of the 4 layer fit and VOLFMEM fit for MFL25a. Again the comparison is very good. There is a slight difference in the profile at the substrate interface, but with the large surface segregation the reflectivity profile

is insensitive to slight variations in the region of the substrate. The values obtained from the two methods are given in table 2.6. The agreement is very good especially at the air surface.

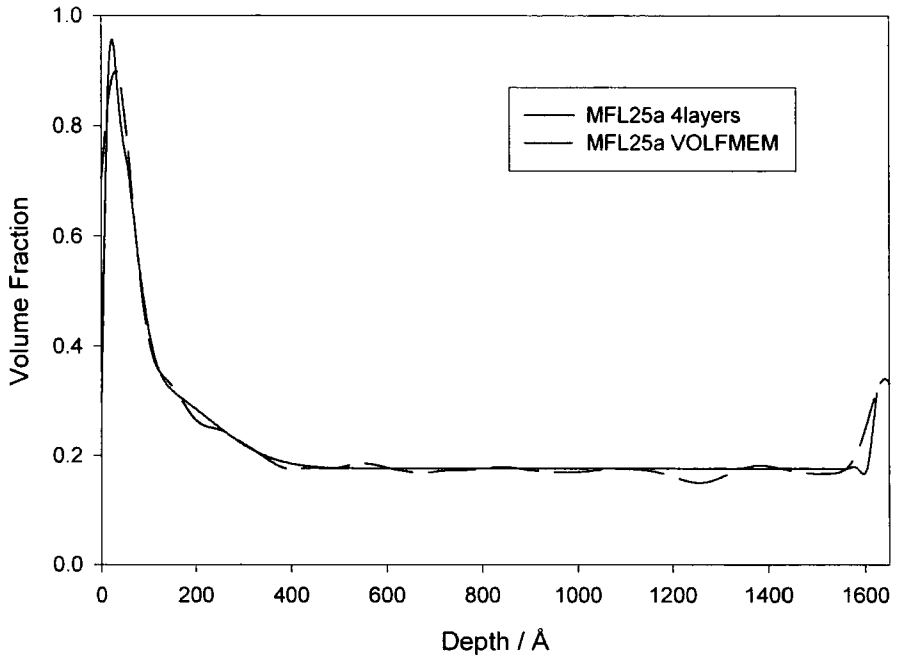


**Figure 2.9 Comparison of the 4 layer and VOLFMEM profiles for MFL25a.**

| Model | $\phi_b$ | $\phi_{air}$ | $z^*_{air}$/Å | $\phi_{Si}$ | $z^*_{Si}$/Å |
|---|---|---|---|---|---|
| **4 layers** | 0.18 | 0.91 | 76 | 0.32 | 12 |
| **VOLFMEM** | 0.18 | 0.90 | 78 | 0.34 | 10 |

**Table 2.6 Parameters obtained for MFL25a using two fitting methods.**

## 2.6 Nuclear Reaction Analysis (NRA)

Nuclear reaction analysis was carried out at the EPSRC Device Fabrication Facility at the University of Surrey, Guildford. Figure 2.10 shows the sample arrangement used for this work.

$^3He^+$ undergoes a nuclear reaction with deuterium present in the sample:

$$^{3}He^{+} + {}^{2}H \rightarrow {}^{4}He + {}^{1}H^{+} + 18.35\ MeV$$

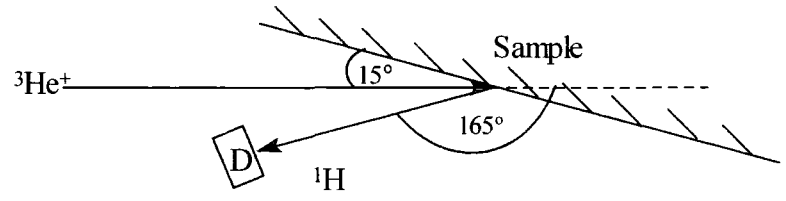


**Figure 2.10 A schematic to show the layout of an NRA experiment.**

$^{3}He^{+}$ ions are accelerated by a Van de Graaff generator and guided down the appropriate beam line. A beam energy of ~0.7MeV was used for this work, with a beam current of ~20nA. The beam line is held under high vacuum to maximise the flux of $^{3}He^{+}$ to the sample. An incidence angle of 9° or 15° was used to optimise the resolution perpendicular to the sample surface[15].

Samples are introduced individually to the chamber via an airlock. After data has been collected the sample is removed and the next sample added. A short time is required to allow the chamber to become fully evacuated again.

Particles from the sample, elastically scattered $^{3}He^{+}$; $^{4}He$ and $^{1}H^{+}$ are detected by a silicon surface detector, D at an angle of 165°. The backscattered protons were specifically detected in this work.

Data were collected as counts versus channel number. To calibrate the channel number to an absolute energy, a calibration package of α emitters of known energy ($^{244}Cm$, $^{241}Am$ and $^{239}Pu$) are used. Sampling time is related to the amount of deuterium in the sample and varied from 15 minutes to 90 minutes. A long sampling

time is desirable to improve the resolution, but this increases the possibility of sample damage. Hence care was taken to monitor the samples after analysis, and no signs of damage were seen.

The raw data were reduced using programs written at the University of Surrey. The data were converted to an absolute energy scale using the energy per channel determined using the calibration package. The sample counts are then corrected for the cross section of the nuclear reaction, by dividing by the counts from a thick 'pure' dPS sample. The dPS sample is measured at a slightly higher energy (typically 0.72 MeV), so that the front edge of the sample spectrum is at a slightly higher energy. This reduces the risk of a mismatch in beam energies giving poor correction at the front edge.

The data were then converted to counts versus depth using the known stopping powers of $^{3}He^{+}$ in polystyrene and the theory of elastic collisions. It was assumed that the proton energy was only affected by the energy of the $^{3}He^{+}$ at reaction, and did not lose energy itself in the sample. A file of volume fraction of deuterated material versus depth was obtained by using a normalisation constant such that the total volume fraction was equal to the volume fraction of deuterated polymer used. Errors were calculated from Poisson statistics, as the square root of the counts.

### 2.6.1 Data Analysis

The data were initially analysed using GENPLOT to obtain the bulk and surface volume fractions directly; the surface excess was determined by subtracting the bulk volume fraction from the data and then numerically integrating to obtain the area under the peak. The values thus obtained are lower than the actual values because of the effect of the instrumental resolution. The data have also been analysed using a

program FITTER adapted from a data analysis program from the University of Surrey. This fits a tanh function at the air surface and the instrumental resolution, which varied with individual experimental set-ups, but was in the range 150 to 250Å. The values for the surface excess were in reasonable agreement to those obtained from NR and followed the same trends. Due to the resolution the precise shape of the profile and surface volume fraction values were not obtained.

## 2.7 Small Angle Neutron Scattering (SANS)

The SANS experiments were carried out using LOQ (figure 2.11 below) on the ISIS pulsed spallation neutron source at the Rutherford Appleton Laboratory, Chilton. Full details of the instrument and the hardware and software used can be found in the LOQ instrument manual[16].

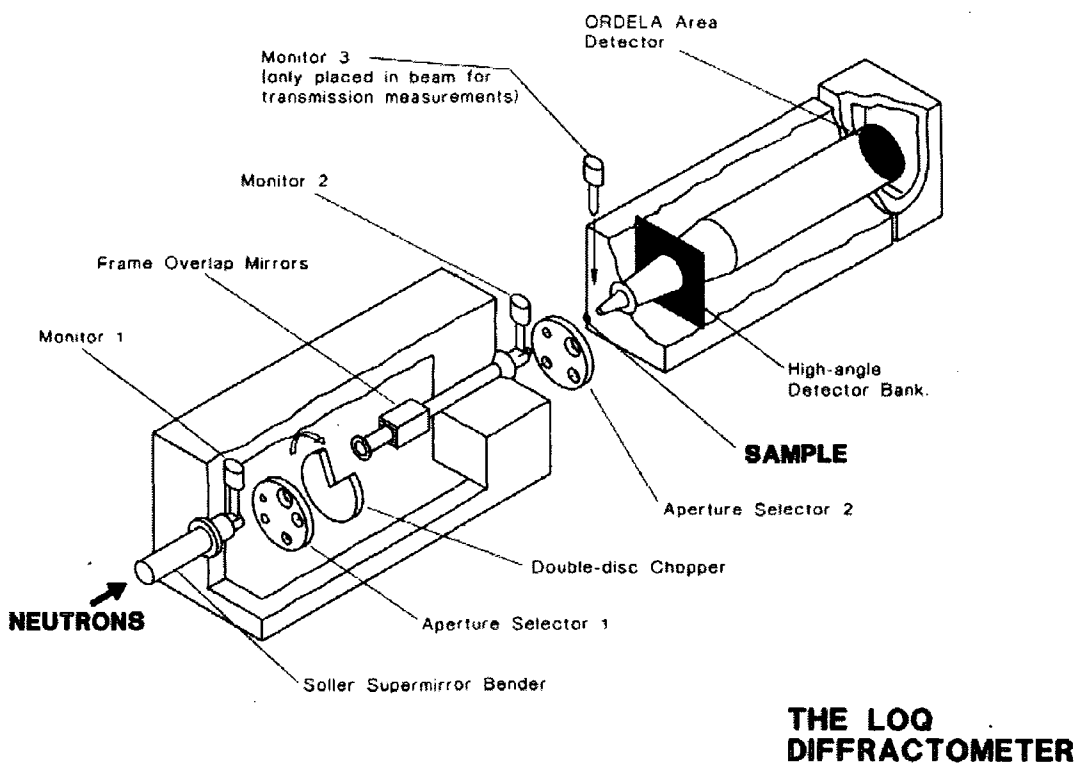


**Figure 2.11 Diagram of the layout of LOQ (from RAL)**

The disc chopper operates at 25Hz, which selects alternate pulses from the target. The neutron wavelength covered is 2.2 to 10.0Å, which gives a Q range of 0.008 to 0.25 $Å^{-1}$ when using the main detector. The Soller Supermirror deflects incident neutrons with a wavelength greater than 2Å and hence the source is not in direct line to the detector. The frame overlap mirror is used to remove neutrons with a wavelength greater than 12Å, thus preventing interference from neutrons from preceding pulses. The aperture selectors are used to collimate the beam so that the beam size at the sample is typically 8mm. Samples were placed in an eight position temperature controlled sample rack. This is controlled automatically by a command file from the LOQ computer. The neutron flight path is under vacuum apart from in the sample area to reduce air scattering. The scattered neutrons are detected using a $^{3}He$-$CF_4$ filled ORDELA "area" detector with an active area of 64 cm x 64 cm.

SANS data were obtained at two temperatures, room temperature and 413K. For each temperature two measurements were made, sample transmission and sample scattering. For transmission measurements a detector is placed immediately after the sample and the transmission measured with respect to a direct beam measurement with no sample in place. The sample scattering data is corrected by dividing by the monitor count, scaling by the direct beam for detector efficiency, by the transmission and sample volume and rebinned to give an ASCII file of cross section versus the scattering vector, Q. The above was carried out using COLETTE from GENIE at RAL. This reduced data file should be on an absolute scale (units $cm^{-1}$). However to correct for small deviations the LOQ standard should be used. The TK48/49 standard is a blend of 49% perdeuterated polystyrene in a hydrogenous polystyrene matrix. This blend gives strong scattering at low Q values so the calibration measurement is

relatively short. The standard has a special copolymer background. The calibrant has been well characterised having an intercept, $(d\sigma/d\Omega)_{Q=0}$ of 78.17cm$^{-1}$ and a radius of gyration ($R_g$) of 76.74Å. So, by fitting the scattering for the standard to obtain $(d\sigma/d\Omega)_{Q=0}$ it is possible to determine a normalisation constant for the experimental data.

The sample scattering as measured has a component due to elastic and inelastic incoherent scattering from the sample and the sample cell. This is referred to as background scatter. To account for this, measurements were made for the pure homopolymers and the proportional scattering values of these were subtracted from the blend data. The pure homopolymers do not produce elastic coherent scattering, but should provide a measure of the incoherent scattering that the blend will display. The majority of the background arises from incoherent scattering from the hydrogenous polymer.

### 2.7.1 Data Analysis of LOQ data

In this work the interest was in obtaining the radius of gyration of the functional polymers so that the values could be used when making comparisons to theory. It was also possible that there might have been aggregation between the functional groups, but there was no evidence to suggest that this occurred. For linear polymer blends the data were fitted with Debye's scattering function for monodisperse coils (equation 2.9), for the STAR polymer a function for monodisperse stars with f arms (f=3) was used (equation 2.10)[17].

$$I(Q) = \frac{2k}{u^2}\left(\exp(-u) - 1 + u\right) \qquad \text{eqn 2.9}$$
$$u = \langle S^2 \rangle Q^2$$

k is the intercept at Q=0, Q the scattering vector and S the radius of gyration ($R_g$) of the functional polymer.

$$I(Q) = \frac{2k}{fV^2}\left[V - (1 - \exp(-V)) + \frac{f-1}{2}(1 - \exp(-V))^2\right]$$
$$V = \frac{f}{3f-2}\left(\langle S^2\rangle Q^2\right)^2 \qquad \text{eqn 2.10}$$

## 2.8 References


1 J. Hunt, M. O., A. M. Belu, R. W. Linton, and J. M. DeSimone, *Macromolecules*, 1993, **26**, 4854.

2 J. Pasztor, A. J., in 'Encyclopedia of Polymer Science and Engineering', ed. H. F. Mark, N. M. Bikales, C. G. Overberger, and G. Menges, 1989.

3 'Polymer Handbook', ed. J. Brandrup and E. H. Immergut, Wiley Interscience, 1989.

4 M. Geoghegan, R. A. L. Jones, R. S. Payne, P. Sakellariou, A. S. Clough, and J. Penfold, *Polymer*, 1994, **35**, 2019.

5 C. Shackleton, J. Penfold, and A. Eaglesham, 'CRISP Instrument Manual', Rutherford Appleton Laboratory, 1991.

6 J. R. P. Webster, 'SURF Instrument Manual', Rutherford Appleton Laboratory, 1996.

7 T. P. Russell, *Materials Science Reports*, 1990, **5**, 171.

8 G. P. Felcher, A. Karim, and T. P. Russell, *Journal of Non-Crystalline Solids*, 1991, **131**, 703.

9 A. M. Mayes, R. D. Johnson, T. P. Russell, S. D. Smith, S. K. Satija, and C. F. Majkrzak, *Macromolecules*, 1993, **26**, 1047.

10 G. J. Fleer, M. A. Cohen Stuart, J. M. H. M. Scheutjens, T. Cosgrove, and B. Vincent, 'Polymers at Interfaces', Chapman and Hall, 1993.

11 I. Hopkinson, 'Surface Composition Profiles in Some Polymer Mixtures', Ph.D., Durham, 1994.

12 R. E. Ghosh, 'FITFUN - An Interactive/Graphical Fitting Routine', 89GH08T, Institut Laue Langevin, 1989.

13 D. Sivia, W. A. Hamilton, and G. S. Smith, *Physica B*, 1991, **173**, 121.

14 K. R. Shull, *Journal of Chemical Physics*, 1991, **94**, 5723.

15 R. S. Payne, A. S. Clough, P. Murphy, and P. J. Mills, *Nuclear Instruments and Methods in Physics Research B*, 1989, **42**, 130.

16 S. M. King, 'Small Angle Neutron Scattering', Rutherford Appleton Laboratory, 1995.

17 W. Burchard, 'Applied Fibre Science', ed. F. Happey, Academic Press, 1978.

# CHAPTER 3

# Linear Difunctional Polymer

## 3.1 Lower molecular weight double F end capped (L2F)

TK 145 dPSF2 was blended with TK 79 hPS (L2F samples), the volume fractions of dPSF2 used are given in table 3.1a. Films were prepared by spinning 7.5% solutions of the blended polymers in toluene onto the required silicon substrate. A sample of each blend was annealed so that the equilibrium surface composition was obtained; an unannealed sample of each blend was also prepared.

| Code | $\phi_{d\text{-}PSF2}$ |
|---|---|
| L2F02 | 0.020 |
| L2F05 | 0.050 |
| L2F10 | 0.100 |
| L2F15 | 0.150 |
| L2F20 | 0.200 |
| L2F25 | 0.250 |
| L2F30 | 0.300 |

**Table 3.1a Codes and volume fractions used for lower molecular weight double F end capped blends.**

### 3.1.1 Nuclear Reaction Analysis

For nuclear reaction analysis films were spun at 4000 rpm with an average thickness of 3450Å, thicker films of L2F02 (4820Å) were prepared at 2000 rpm due to problems with the film dewetting on annealing. Samples were annealed under vacuum at 423K for 70 hours.

NRA data were obtained at an incident angle of 15°. Figure 3.1.1 shows the profiles obtained for a range of the unannealed samples and no surface segregation could be seen. Segregation to the air / polymer interface could be seen in the annealed samples, a range of which are shown in figure 3.1.2.

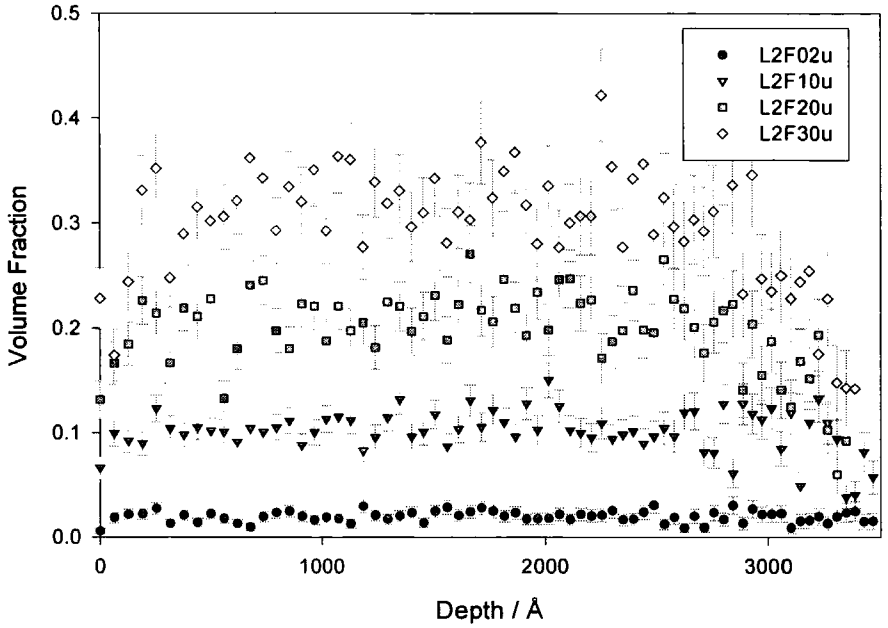


**Figure 3.1.1 NRA volume fraction profiles for unannealed L2F samples.**

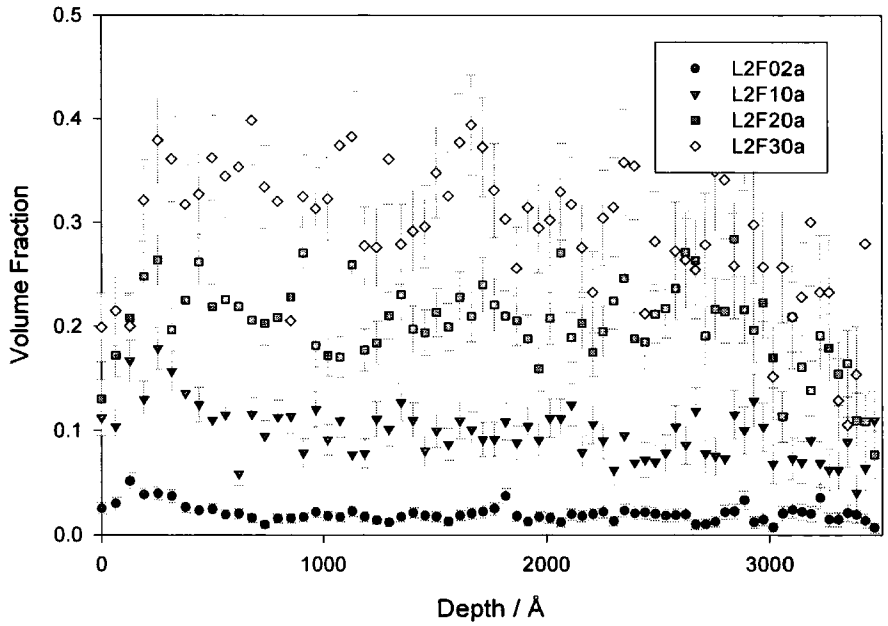


**Figure 3.1.2 NRA volume fraction profiles for the annealed L2F samples.**

The resolution of the technique meant that it was difficult to observe segregation in the higher volume fraction samples consequently L2F20 and L2F30 samples were repeated using an incidence angle of 9° to the sample. Thinner films

(thickness circa 2150Å as measured by contact profilometry) were prepared so that the beam would penetrate to the substrate at the lower angle. The profiles for these samples are shown in figure 3.1.3, the surface segregation could be seen more clearly, but the instrumental resolution was still a limiting factor in the analysis of the data.

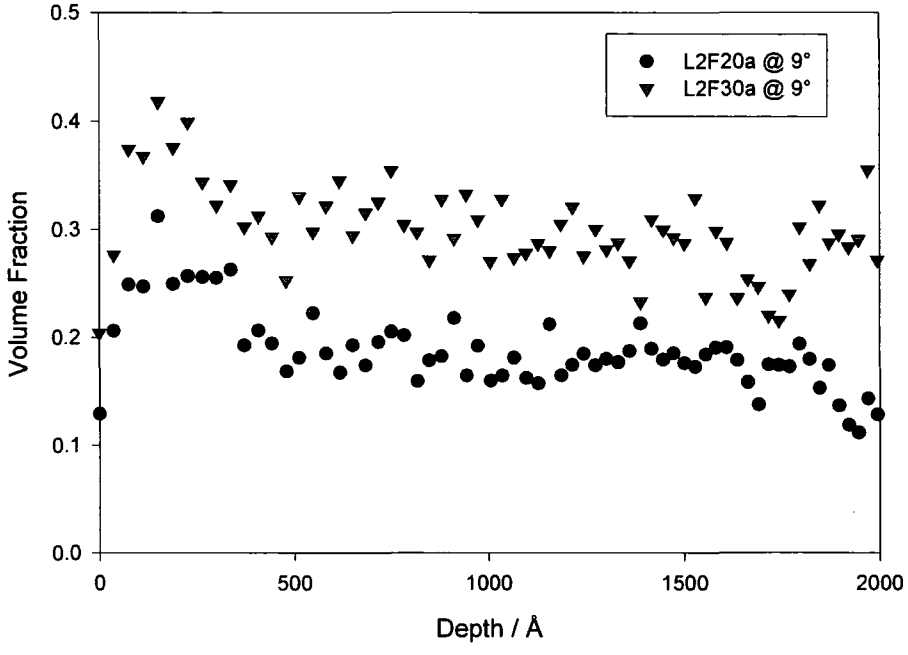


**Figure 3.1.3 NRA volume fraction profiles at a 9° incidence angle.**

From the profiles the bulk, $\phi_b$, and surface, $\phi_s$, volume fractions and surface excess, z*, values were determined using GENPLOT, $\phi_b$, and $\phi_s$ were taken directly from the plot, $\phi_b$ was subtracted from the normalised data which were then numerically integrated to determine z*. The values obtained are given in table 3.1b. The effect of the resolution can be seen in the low surface excess values as the bulk volume fraction increases. This was greatly improved using the lower angle, but there was insufficient time to repeat all the samples and the values obtained were still considerably lower than those obtained using NR.

| Sample | $\phi_b$ | $\phi_s$ | z*/Å |
|---|---|---|---|
| L2F02a | 0.02 | 0.04 | 8.3 |
| L2F05a | 0.04 | 0.09 | 15.9 |
| L2F10a | 0.10 | 0.17 | 14.6 |
| L2F15a | 0.15 | 0.19 | 7.8 |
| L2F20a | 0.19 | 0.22 | 6.6 |
| L2F25a | 0.26 | 0.32 | 9.9 |
| L2F30a | 0.30 | 0.30 | - |
| L2F20a 9° | 0.18 | 0.28 | 26.0 |
| L2F30a 9° | 0.29 | 0.40 | 23.6 |

**Table 3.1b Parameters obtained from the volume fraction profiles from NRA not taking into account the instrumental resolution.**

The data were also analysed using the program FITTER to fit a tanh profile, which was convoluted with the instrumental resolution, at the air surface. The parameters used to obtain the fits are given in table 3.1c; $\phi_b$ is the bulk volume fraction, $\phi_a$ is the approximate surface volume fraction, height is the thickness of the brush layer, width the width of the interface between the brush and the bulk polymer. Offset is used to adjust the starting position of the fitted profile to the experimental data and the resolution is the standard deviation of the Gaussian resolution function. Examples of the fitted profiles are shown in figure 3.1.4. From the fitted parameters the profile was determined and the surface excess value calculated. The values of surface volume fraction, $\phi_s$, bulk volume fraction, $\phi_b$ and surface excess, z* obtained are given in table 3.1d, figure 3.1.5 shows the surface excess values determined from the fits to the NRA data compared with those from NR data. The comparison is reasonable, though the surface excess determined from NRA data is greater than that from NR, but the error in these values is large due to the quality of the NRA data.

| Sample | $\phi_b$ | $\phi_a$ | height/Å | width/Å | offset/Å | resolution/ Å |
|---|---|---|---|---|---|---|
| L2F02a | 0.02 | 0.32 | 59 | 53 | 106 | 250 |
| L2F05a | 0.05 | 0.44 | 67 | 53 | 300 | 250 |
| L2F10a | 0.10 | 0.60 | 80 | 60 | 80 | 200 |
| L2F15a | 0.16 | 0.57 | 60 | 29 | 160 | 224 |
| L2F20a | 0.21 | 0.88 | 81 | 66 | 90 | 253 |
| L2F25a | 0.26 | 0.96 | 93 | 48 | 191 | 255 |
| L2F30a | 0.32 | 0.99 | 66 | 52 | 93 | 201 |
| L2F20a 9° | 0.18 | 0.90 | 80 | 41 | 86 | 152 |
| L2F30a 9° | 0.30 | 0.94 | 87 | 70 | 66 | 98 |

**Table 3.1c Parameters used to obtain fits to NRA data.**

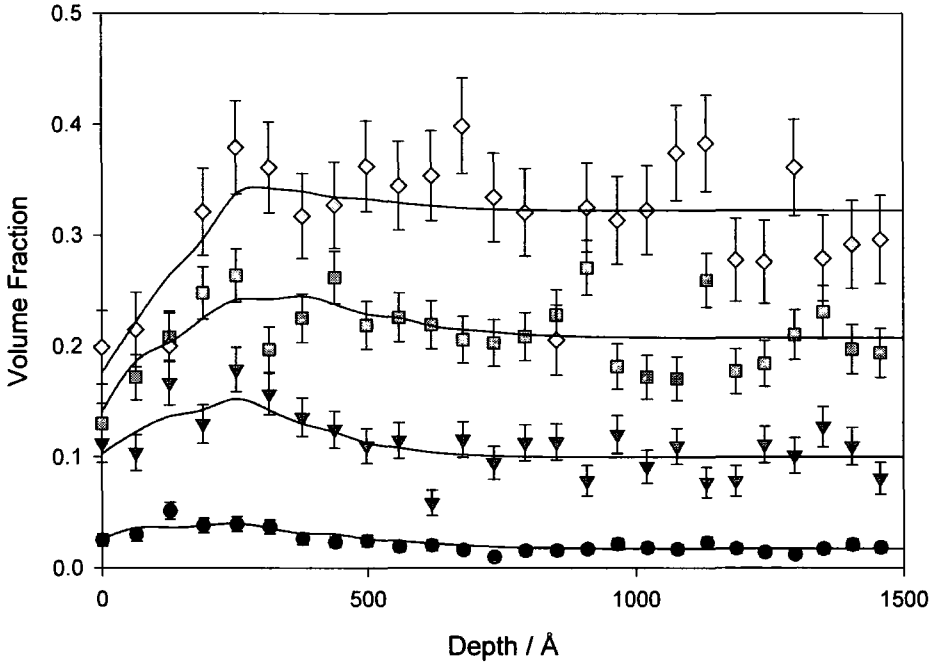


**Figure 3.1.4 NRA data with showing tanh fits. From the top L2F30a, L2F20a, L2F10a and L2F02a.**

| Sample | $\phi_b$ | $\phi_s$ | z*/Å |
|---|---|---|---|
| L2F02a | 0.02 | 0.31 | 17.4 |
| L2F05a | 0.05 | 0.44 | 26.1 |
| L2F10a | 0.10 | 0.60 | 40.2 |
| L2F15a | 0.16 | 0.57 | 24.9 |
| L2F20a | 0.21 | 0.87 | 54.3 |
| L2F25a | 0.26 | 0.97 | 65.4 |
| L2F30a | 0.32 | 0.99 | 44.1 |
| L2F20a 9° | 0.18 | 0.90 | 57.7 |
| L2F30a 9° | 0.30 | 0.93 | 55.9 |

**Table 3.1d Surface parameters for L2F annealed samples obtained from tanh profile fits to NRA data.**

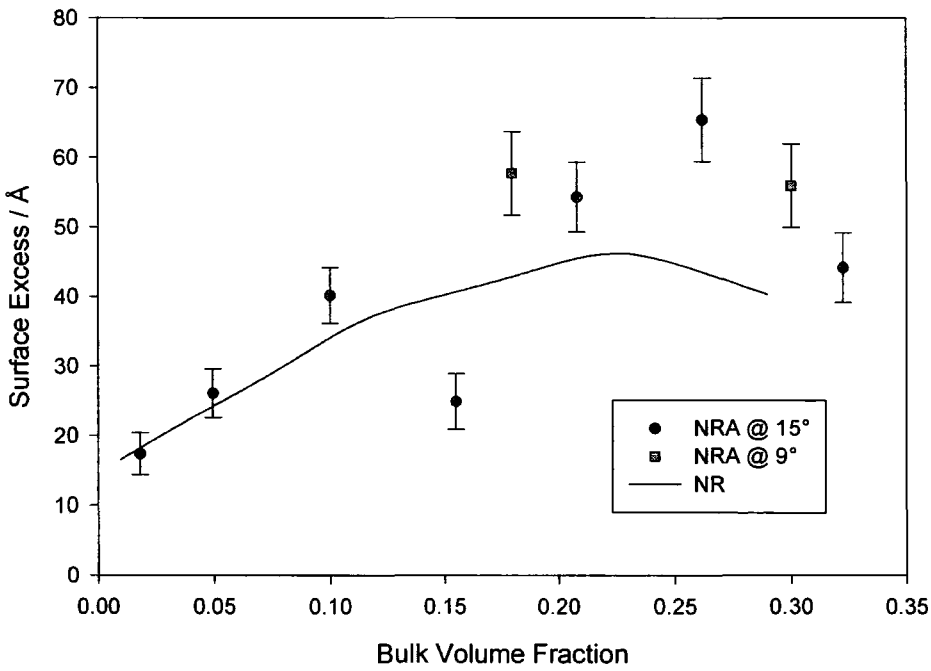


**Figure 3.1.5 Surface excess values from the fits to the NRA data with the line showing the comparison to the values obtained from NR data.**

### 3.1.2 Neutron Reflectometry

For neutron reflectometry measurements films were spun at 3500 rpm with an average thickness of 3900Å. There were problems with the film dewetting on annealing, so thicker films were used and an annealing temperature of 415K. An

unannealed sample of each composition was prepared but there was insufficient time to measure the L2F02u and L2F15u samples.

Due to the thickness of the films there were few features evident in the reflectivity profiles, also for the lower volume fraction samples the Q range was only just low enough to observe the critical edge especially for the unannealed samples. Hence the fits to the data were not particularly sensitive to slight changes in the surface composition parameters and had a tendency to over estimate the critical edge.

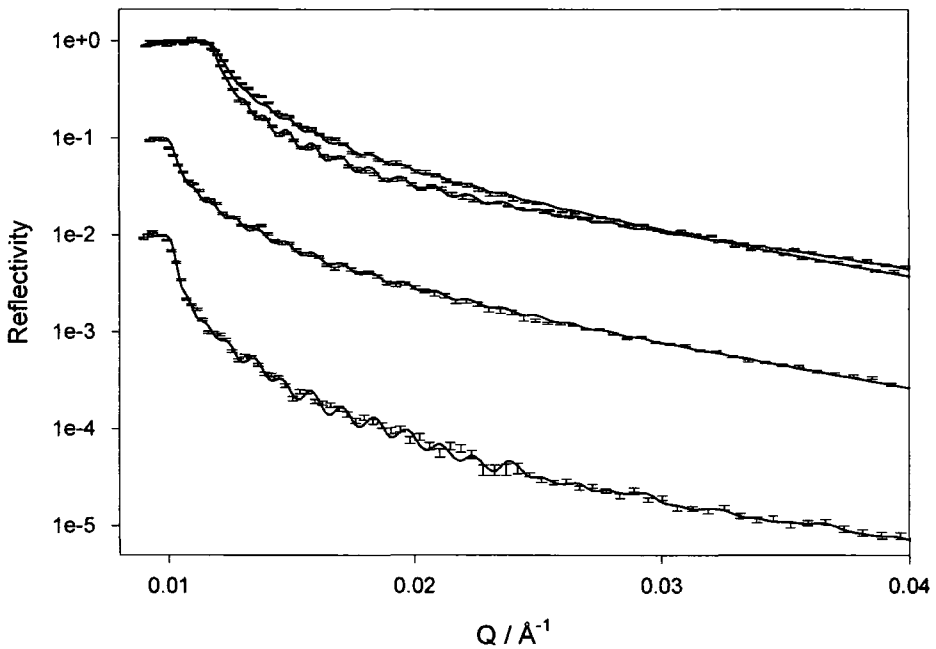


**Figure 3.1.6 Reflectivity profiles with fits obtained for L2F samples. From the top L2F30a, L2F30u, L2F15a and L2F02a. Data for subsequent blends are offset by a factor of 10 for clarity.**

Reflectivity profiles for L2F30a, L2F30u, L2F15a and L2F02a are shown in figure 3.1.6 along with the stretched exponential fit to the data for the annealed samples and a three layer fit to the data for the unannealed sample. The reflectivity for the annealed sample was greater than that of the unannealed sample in the region $0.012 < Q < 0.28$, indicating that there was a greater extent of segregation after

annealing. The difference was not large as there was already considerable segregation in the unannealed film as shown in the volume fraction profiles (figure 3.1.8). There was no evidence of segregation in the unannealed samples by NRA, but VOLFMEM analysis indicated the existence of surface segregation followed by a depletion layer and hence the data were analysed using a three layer model to account for this depletion layer. Two layer models were attempted and gave reasonable fits to the data, but the quality of the fits ($\chi^2$) were greatly improved by the inclusion of a depletion layer. The parameters used to obtain the fits are given in table 3.1.e for the annealed samples and table 3.1.g for the unannealed samples. From such fits to the NR data, the volume fraction profiles were obtained, figure 3.1.7 and figure 3.1.8, and the surface parameters (surface volume fraction, $\phi_s$, bulk volume fraction, $\phi_b$, surface excess, z*, brush height, L and surface grafting density, $\sigma$) determined. These values are given in table 3.1.f for the annealed samples and table 3.1.h for the unannealed samples.

| Sample | $\phi_b$ | $\phi_s$ | exponent | decay length/Å | $\chi^2$ |
|---|---|---|---|---|---|
| L2F02a | 0.01 | 0.20 | 1.7 | 95 | 15.6 |
| L2F05a | 0.04 | 0.41 | 2.8 | 68 | 23.0 |
| L2F10a | 0.08 | 0.74 | 2.4 | 63 | 3.3 |
| L2F15a | 0.12 | 0.75 | 2.0 | 67 | 5.6 |
| L2F20a | 0.18 | 0.86 | 2.1 | 71 | 5.3 |
| L2F25a | 0.23 | 0.96 | 2.1 | 71 | 7.7 |
| L2F30a | 0.29 | 0.99 | 1.8 | 65 | 7.3 |

**Table 3.1.e Parameters used for the stretched exponential model fits to the reflectivity data for the annealed L2F samples.**

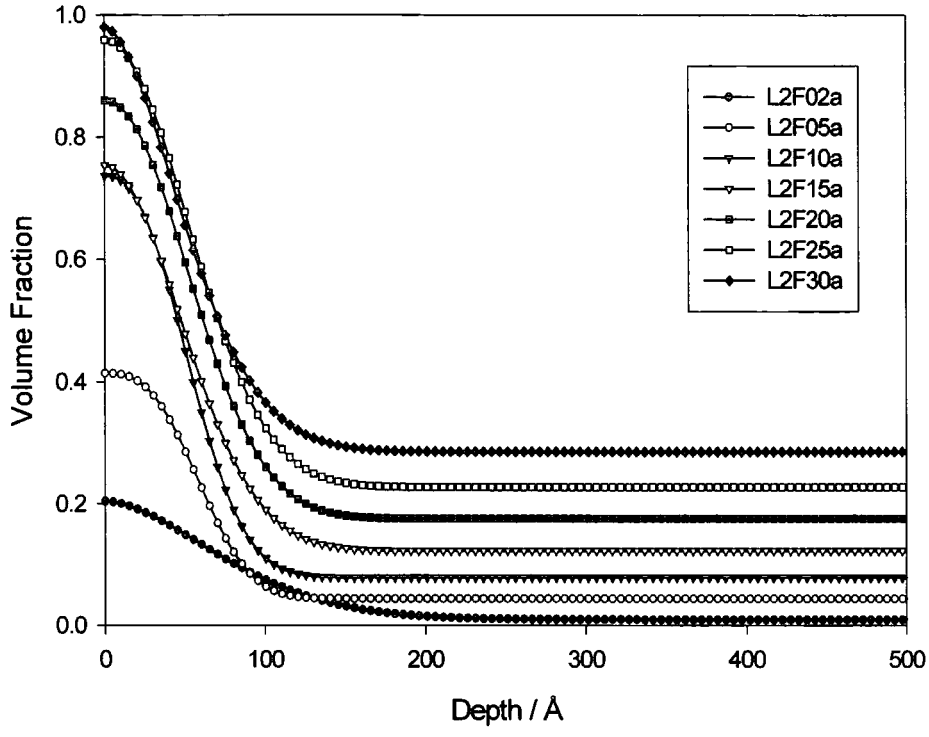


**Figure 3.1.7 Volume fraction profiles for the annealed L2F samples determined from stretched exponential model fits to the data. Symbols are not data points but are present to help identify different profiles.**

| Sample | $\phi_b$ | $\phi_s$ | z*/Å | L/Å | $\sigma$ |
|---|---|---|---|---|---|
| L2F02a | 0.01 | 0.20 | 16.6 | 77.4 | 0.0049 |
| L2F05a | 0.04 | 0.41 | 22.5 | 59.1 | 0.0067 |
| L2F10a | 0.08 | 0.74 | 37.0 | 53.9 | 0.0110 |
| L2F15a | 0.12 | 0.75 | 37.4 | 56.5 | 0.0111 |
| L2F20a | 0.18 | 0.86 | 42.9 | 58.2 | 0.0128 |
| L2F25a | 0.23 | 0.96 | 46.2 | 59.1 | 0.0138 |
| L2F30a | 0.29 | 0.99 | 40.3 | 53.0 | 0.0120 |

**Table 3.1.f Surface parameters for the annealed L2F samples determined from stretched exponential profiles.**

| sample | $\phi_1$ | $t_1$/Å | $\sigma_1$/Å | $\phi_2$ | $t_2$/Å | $\sigma_2$/Å | $\phi_3$ | $t_3$/Å | $\chi^2$ |
|---|---|---|---|---|---|---|---|---|---|
| L2F05u | 0.41 | 51 | 20 | 0.03 | 3968 | 5 | - | - | 66 |
| L2F10u | 0.58 | 47 | 19 | 0.04 | 100 | 41 | 0.08 | 3810 | 94 |
| L2F20u | 0.99 | 41 | 19 | 0.07 | 53 | 88 | 0.17 | 3694 | 4.0 |
| L2F25u | 0.96 | 44 | 21 | 0.16 | 79 | 73 | 0.22 | 3668 | 4.7 |
| L2F30u | 0.99 | 52 | 25 | 0.12 | 55 | 46 | 0.27 | 3667 | 4.8 |

**Table 3.1.g Parameters used for the 3 layer fits to the unannealed L2F samples.**

| Sample | $\phi_b$ | $\phi_{dep}$ | $\phi_s$ | z*/Å | $z^*_{dep}$/Å | $z^*_{total}$/Å |
|---|---|---|---|---|---|---|
| L2F05u | 0.03 | - | 0.29 | 15.5 | - | 15.5 |
| L2F10u | 0.10 | 0.04 | 0.40 | 17.4 | 3.8 | 22.5 |
| L2F20u | 0.16 | 0.11 | 0.95 | 26.3 | 3.4 | 29.4 |
| L2F25u | 0.22 | 0.18 | 0.93 | 28.4 | 3.8 | 28.7 |
| L2F30u | 0.27 | 0.20 | 0.96 | 30.9 | 3.9 | 34.0 |

**Table 3.1.h Surface parameters for the unannealed L2F samples obtained from the 3 layer model profiles.**

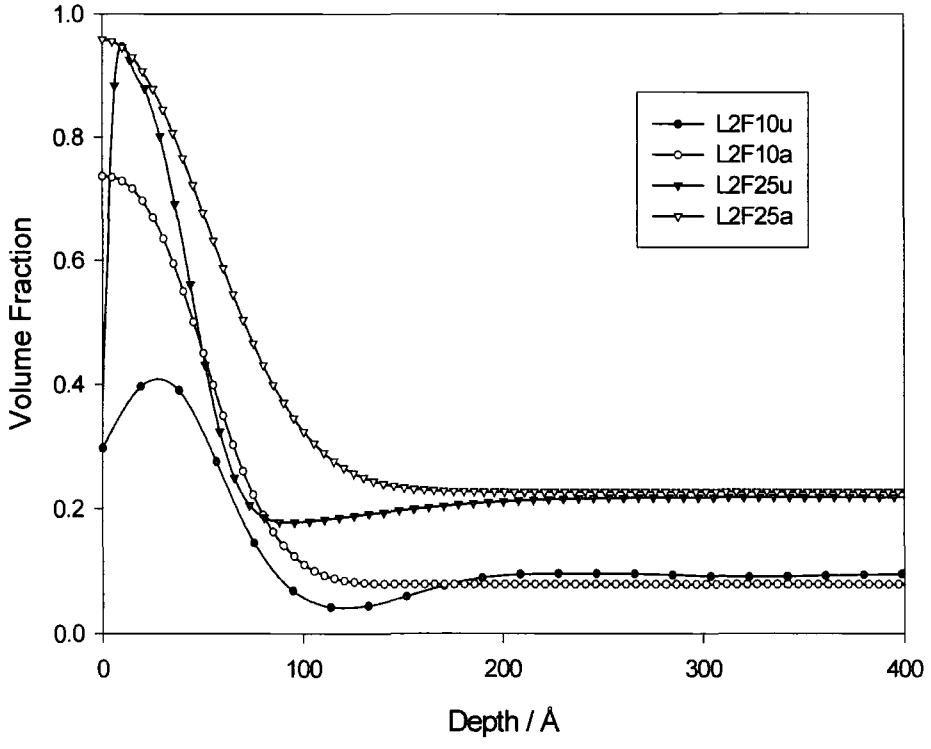


**Figure 3.1.8 Comparison of the unannealed and annealed volume fraction profiles for L2F10 and L2F25. Symbols used to identify individual profiles.**

### 3.1.3 Small Angle Neutron Scattering

Small angle neutron scattering experiments were carried out using LOQ at the Rutherford Appleton Laboratory. Polymer TK 145 dPSF2 was blended with TK 191 hPS and four compositions were prepared, the small angle scattering intensity as a function of Q was measured at room temperature and at 413K. Table 3.1i gives the sample codes and volume fractions used.

| Code | $\phi_{d\text{-}PSF2}$ |
|---|---|
| L2F05 | 0.049 |
| L2F10 | 0.100 |
| L2F15 | 0.151 |
| L2F20 | 0.200 |

**Table 3.1i Sample codes and volume fractions used for LOQ analysis.**

The data were fitted using Debye's scattering function as described in chapter 2 and figure 3.1.9 shows the data and fits for the blends ran at room temperature. There was no discernible difference in the scattering obtained for samples measured at different temperatures and the radius of gyration did not vary with sample composition. The value of radius of gyration obtained was 56.5±1.2Å which was in good agreement with that determined using $R_g = a\sqrt{(N/6)}$ where a is the statistical step length (6.7Å) and N the degree of polymerisation (value 61.0±3.0Å).

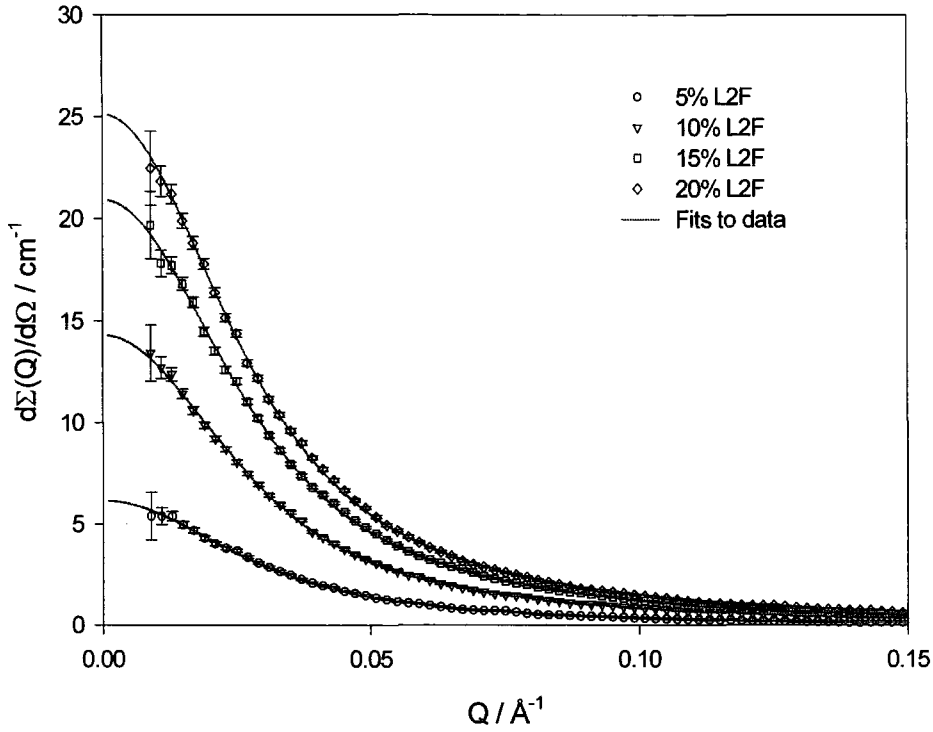


**Figure 3.1.9 Small angle neutron scattering data for L2F blends at 413K with fits to the data assuming Debye scattering.**

## 3.2 Higher molecular weight double F end capped

Polymer TK 181, ~100000 $M_w$ dPSF2 was blended with normal hydrogenous polystyrene, samples were annealed to equilibrium and the surface composition determined. Two experiments were carried out, symmetric blends where the matrix was the same molecular weight and asymmetric blends to determine the effect of matrix molecular weight.

### 3.2.1 Symmetric Blends (H2F)

The 100000 $M_w$ dPSF2 was blended with PL 120 to give a range of volume fractions (H2F samples), table 3.2.1a gives the codes and volume fraction values used. Samples were prepared by spinning onto the silicon substrate and annealed as described so that the equilibrium surface composition was obtained. An unannealed sample of each blend was prepared for comparison.

| Code | $\phi_{dPSF2}$ |
|---|---|
| H2F02 | 0.020 |
| H2F05 | 0.050 |
| H2F10 | 0.100 |
| H2F15 | 0.150 |
| H2F20 | 0.200 |
| H2F25 | 0.250 |
| H2F30 | 0. 301 |

**Table 3.2.1a Codes and volume fractions used for higher molecular weight double F end capped blends.**

#### 3.2.1.1 Nuclear Reaction Analysis

For the NRA experiments films were spun at 3000 rpm with an average thickness of 2740Å. Samples were annealed under vacuum at 423K for 70 hours. The

unannealed samples had a uniform distribution of the dPSF2, which is shown for a range of the unannealed samples in figure 3.2.1.1, error bars were calculated from Poisson statistics.

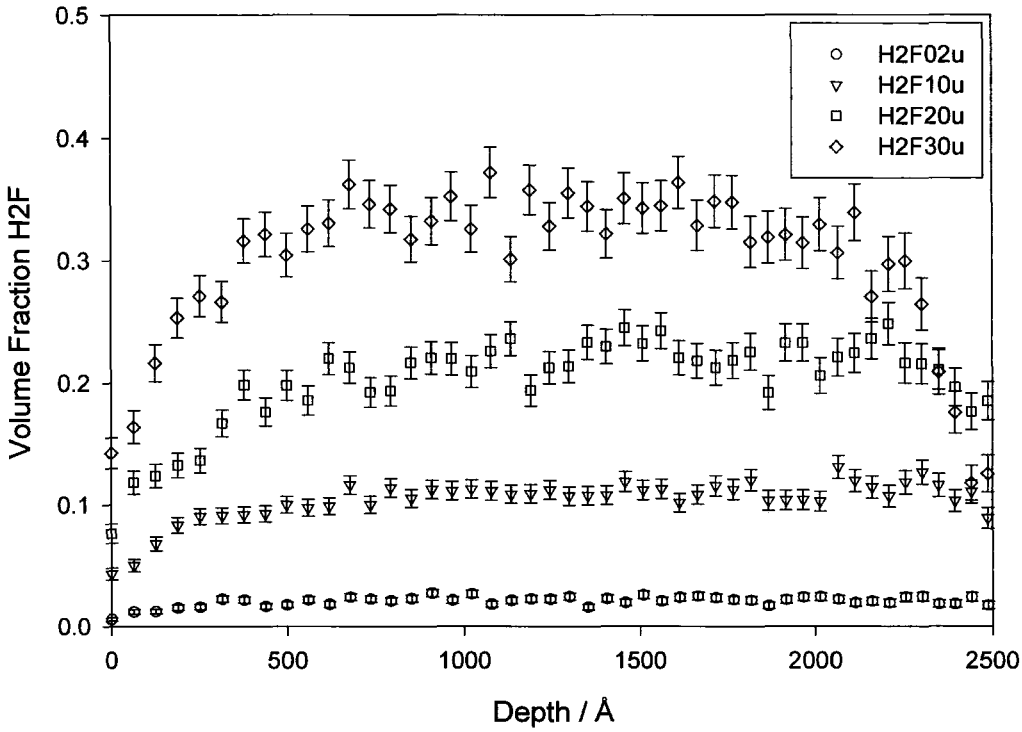


**Figure 3.2.1.1 Normalised NRA profiles for unannealed H2F samples.**

Surface segregation could be seen in all the annealed samples. This was not as clear in the higher volume fraction samples, particularly H2F30a, as in the lower volume fraction ones. Figure 3.2.1.2 shows the profiles obtained for a range of the annealed samples, the values of surface volume fraction, $\phi_s$, bulk volume fraction, $\phi_b$ and surface excess, z* were obtained directly from the profile using GENPLOT and are given in Table 3.2.1b.

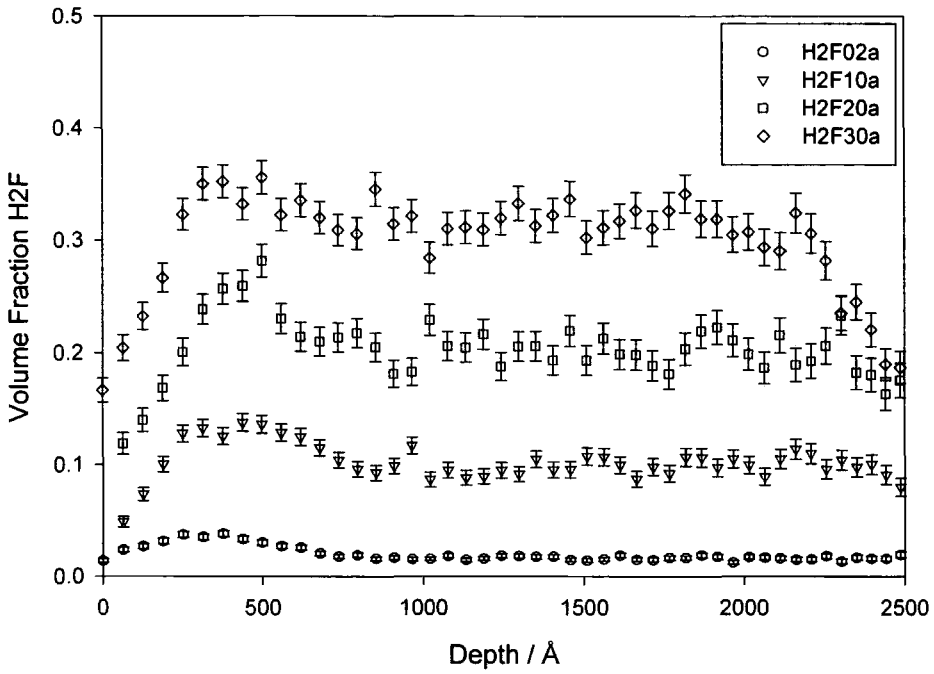


**Figure 3.2.1.2 Normalised NRA profiles for annealed H2F samples.**

| Sample | $\phi_b$ | $\phi_s$ | z*/Å |
|---|---|---|---|
| H2F02a | 0.02 | 0.04 | 9.1 |
| H2F05a | 0.04 | 0.08 | 15.1 |
| H2F10a | 0.10 | 0.14 | 15.5 |
| H2F15a | 0.14 | 0.19 | 15.3 |
| H2F20a | 0.20 | 0.27 | 15.6 |
| H2F25a | 0.25 | 0.31 | 17.3 |
| H2F30a | 0.30 | 0.33 | 7.7 |

**Table 3.2.1b Parameters determined from the NRA volume fraction profiles for the annealed H2F samples not taking into account the instrumental resolution.**

The data were also analysed using the program FITTER to fit a tanh profile convoluted with the instrumental resolution at the air surface, the parameters used to obtain the fits are given in table 3.2.1c and examples of the fitted profiles shown in figure 3.2.1.3. From the fitted parameters the profile was determined and the surface excess value calculated. The values of surface volume fraction, $\phi_s$, bulk volume fraction, $\phi_b$ and surface excess, z* obtained are given in table 3.2.1d, figure 3.2.1.4

shows the surface excess values determined from the fits to the NRA data compared with those from NR data given in the next section. The agreement between the two techniques is quite good, though the NRA values tended to be lower than those obtained by NR.

| Sample | $\phi_b$ | $\phi_s$ | height/Å | width/Å | offset/Å | resolution/ Å |
|---|---|---|---|---|---|---|
| H2F02a | 0.02 | 0.34 | 49 | 50 | 222 | 250 |
| H2F05a | 0.05 | 0.47 | 53 | 130 | 206 | 250 |
| H2F10a | 0.10 | 0.69 | 40 | 149 | 200 | 251 |
| H2F15a | 0.15 | 0.68 | 70 | 144 | 200 | 253 |
| H2F20a | 0.20 | 0.85 | 61 | 155 | 202 | 200 |
| H2F25a | 0.25 | 1.02 | 68 | 156 | 122 | 199 |
| H2F30a | 0.32 | 0.81 | 84 | 155 | 104 | 208 |

**Table 3.1c Parameters used to obtain fits to NRA data.**

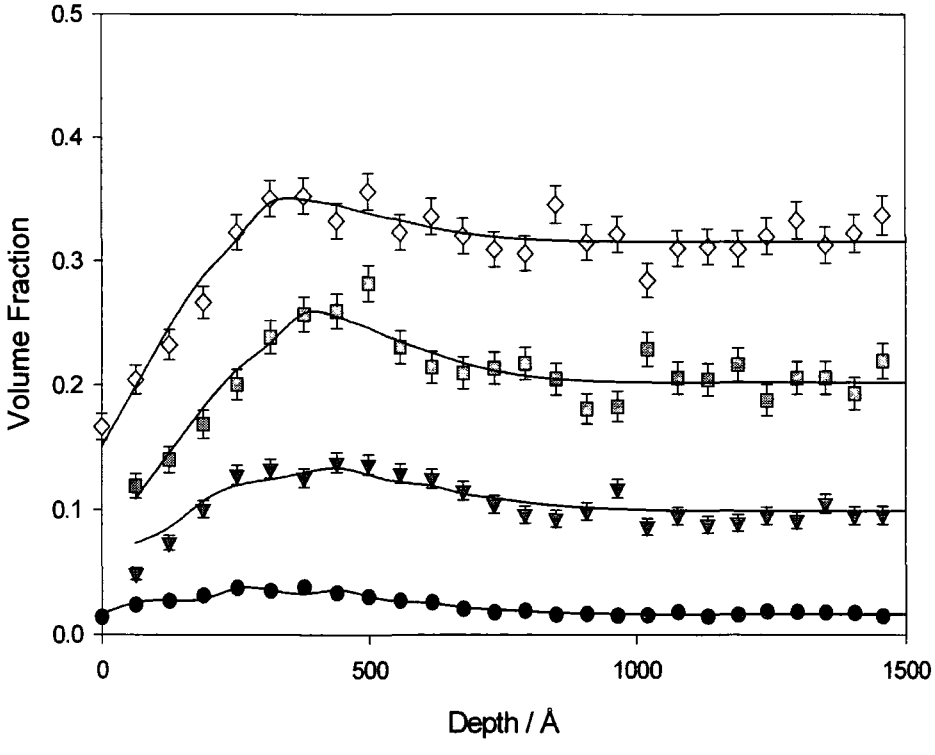


**Figure 3.2.1.3 NRA data with fitted tanh profiles. From the top H2F30a, H2F20a, H2F10a and H2F02a.**

| Sample | $\phi_b$ | $\phi_s$ | z*/Å |
|---|---|---|---|
| H2F02a | 0.02 | 0.33 | 15.6 |
| H2F05a | 0.05 | 0.40 | 24.8 |
| H2F10a | 0.10 | 0.53 | 30.0 |
| H2F15a | 0.15 | 0.61 | 39.5 |
| H2F20a | 0.20 | 0.74 | 44.0 |
| H2F25a | 0.25 | 0.91 | 56.7 |
| H2F30a | 0.32 | 0.76 | 43.7 |

**Table 3.2.1d Surface parameters for H2F annealed samples obtained from tanh profile fits to NRA data.**

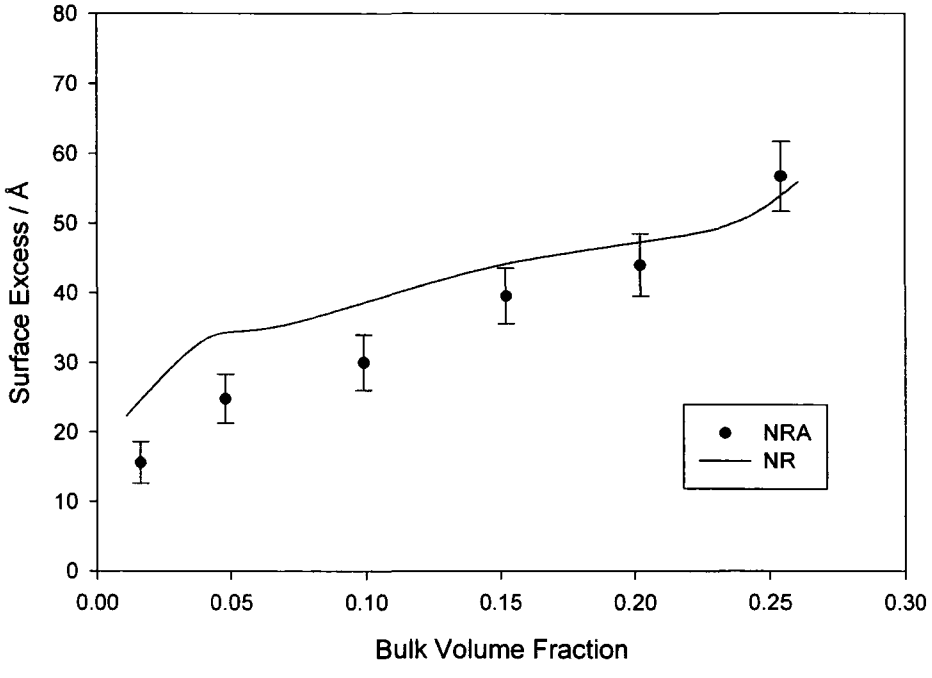


**Figure 3.2.1.4 Surface excess values from the fits to the NRA data with the line showing the comparison to the values obtained from NR data.**

### 3.2.1.2 Neutron Reflectometry

For the neutron reflectometry experiments films were spun at 3500 rpm with an average thickness of 4800Å, samples were annealed under vacuum for 7 days at 415K. Data were collected on CRISP using the single detector. Two angles were used, 0.25 and 0.6° covering the Q range 0.0084 to 0.20Å$^{-1}$ over the full wavelength

range of 0.5 to 6.5Å. The background was determined from the reflectivity at high Q. It is questionable as to whether two angles covers a sufficient Q range to determine the true background, but the values obtained ($\sim 1\times10^{-5}$) had only a small effect on the reflectivity values in the region fitted (up to Q=0.06Å$^{-1}$). Further experiments using the single detector covered three angles to ensure that background was reached.

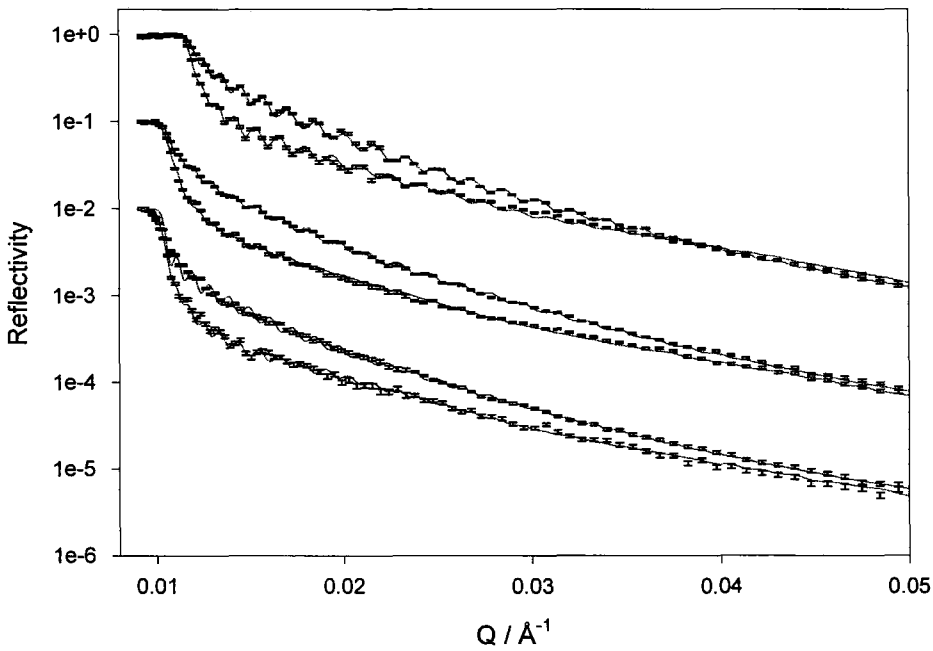


**Figure 3.2.1.5a Reflectivity profiles and fits to the data (from the top) for H2F30a, H2F30u, H2F20a, H2F20u, H2F10a and H2F10u. Data for subsequent blends offset by a factor of 10 for clarity.**

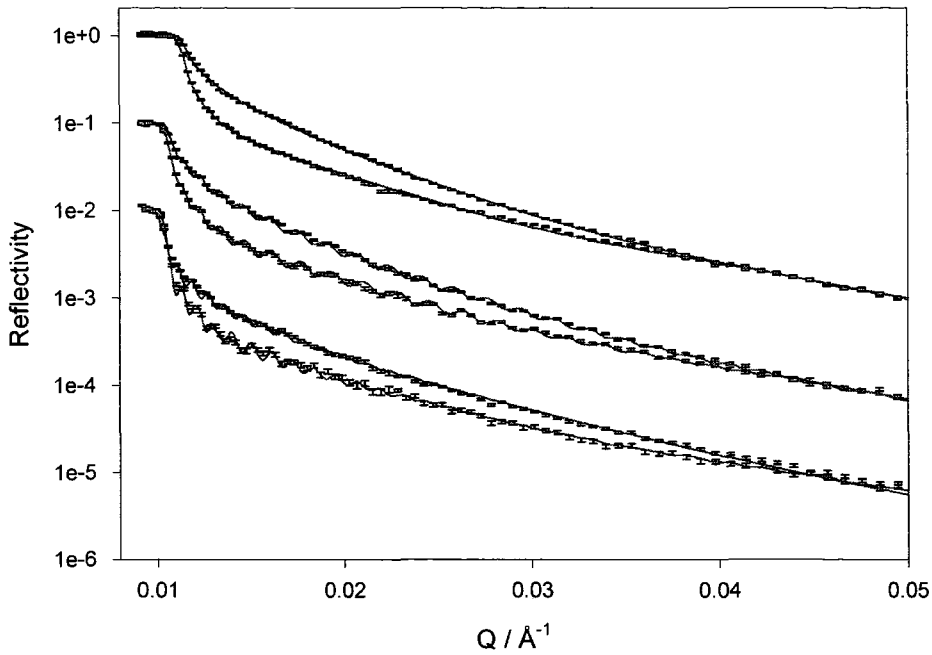


**Figure 3.2.1.5b Graph to show the reflectivity profiles and fits to the data (from the top) for H2F25a, H2F25u, H2F15a, H2F15u, H2F05a and H2F05u. Data for subsequent blends offset by a factor of 10 for clarity.**

The reflectivity profiles and fits to the data are shown in figures 3.2.1.5a and 3.2.1.5b. The data sets are paired in annealed and unannealed samples of the same blend. There is a considerable increase in the reflectivity on annealing, indicating that segregation has occurred. The annealed data show the fits obtained using a stretched exponential model, the parameters for the fits are given in table 3.2.1e. VOLFMEM analysis of the unannealed data show that some segregation had taken place during sample preparation and these have been fitted with a three layer model to account for a depletion layer that was seen. The parameters of these fits are given in table 3.2.1f. In the graphs data for subsequent blends are offset by a factor of 10 for clarity.

| Sample | $\phi_b$ | $\phi_s$ | exponent | decay length/Å | $\chi^2$ |
|---|---|---|---|---|---|
| H2F02a | 0.01 | 0.40 | 2.0 | 65 | 2.1 |
| H2F05a | 0.04 | 0.50 | 2.2 | 83 | 6.1 |
| H2F10a | 0.07 | 0.56 | 1.6 | 82 | 16.3 |
| H2F15a | 0.16 | 0.64 | 1.7 | 92 | 5.1 |
| H2F20a | 0.16 | 0.70 | 1.7 | 91 | 3.5 |
| H2F25a | 0.23 | 0.85 | 1.4 | 88 | 2.9 |
| H2F30a | 0.26 | 0.95 | 1.7 | 91 | 3.3 |

**Table 3.2.1e Parameters from stretched exponential fits to NR data for H2F annealed samples**

| sample | $\phi_1$ | $t_1$/Å | $\sigma_1$/Å | $\phi_2$ | $t_2$/Å | $\sigma_2$/Å | $\phi_3$ | $t_3$/Å | $\chi^2$ |
|---|---|---|---|---|---|---|---|---|---|
| H2F02u | 0.22 | 64 | 19 | 0.03 | 7300 | 35 | 0.07 | 322 | 4.7 |
| H2F05u | 0.34 | 62 | 7.5 | 0.03 | 198 | 27 | 0.05 | 4480 | 4.8 |
| H2F10u | 0.37 | 56 | 20 | 0.06 | 218 | 55 | 0.12 | 4040 | 4.2 |
| H2F15u | 0.49 | 57 | 19 | 0.12 | 235 | 45 | 0.15 | 2860 | 2.6 |
| H2F20u | 0.51 | 58 | 20 | 0.11 | 237 | 43 | 0.15 | 3140 | 4.9 |
| H2F25u | 0.62 | 64 | 18 | 0.18 | 242 | 31 | 0.22 | 6640 | 3.8 |
| H2F30u | 0.80 | 56 | 17 | 0.21 | 257 | 30 | 0.26 | 3040 | 4.2 |

**Table 3.2.1f Parameters from three layer fits to the NR data for unannealed H2F samples.**

The surface composition profiles obtained from the fits are shown in figure 3.2.1.6 for the annealed samples and figure 3.2.1.7 for the unannealed ones. In the unannealed samples the segregated layer was quite block like followed by a depletion layer for all the samples apart from H2F02u. In this sample which was over 7000Å thick, the amount of deuteration in the blend was so low that the reflectivity was insensitive to slight changes in volume fraction. Parameters determined from the surface composition profiles are given in table 3.2.1g for the annealed samples and table 3.2.1h for the unannealed samples.

On annealing the surface volume fraction increased and the segregated layer stretched into the bulk. This is shown in figure 3.2.1.8 where the composition profiles for the 5 and 30% annealed and unannealed samples are compared.

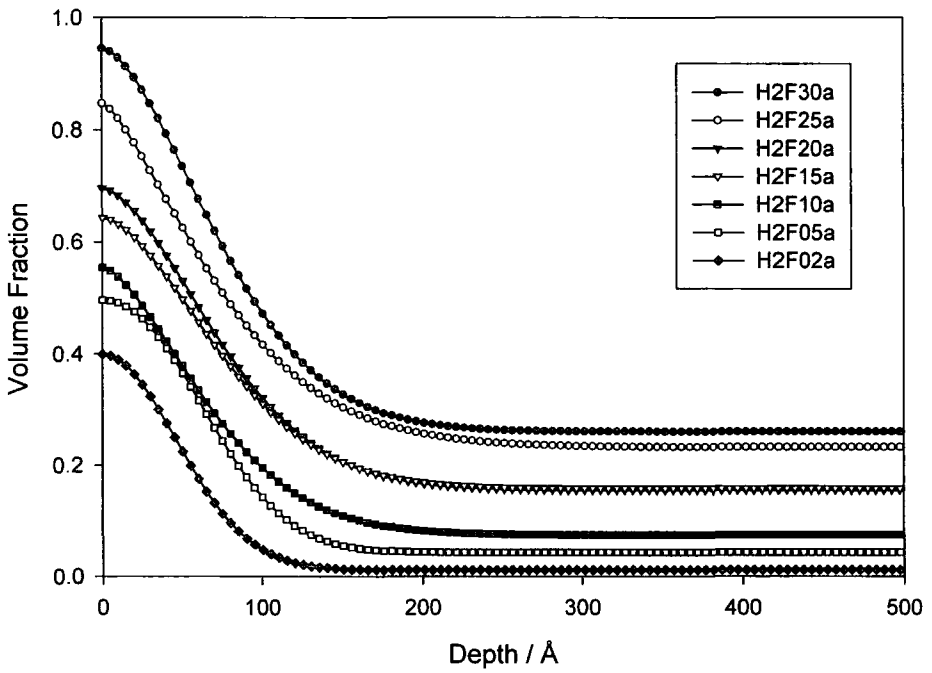


**Figure 3.2.1.6 Volume fraction profiles for H2F annealed samples obtained from stretched exponential model fits to the data. Symbols are to guide the eye.**

| Sample | $\phi_b$ | $\phi_s$ | z*/Å | L/Å | σ |
|---|---|---|---|---|---|
| H2F02a | 0.011 | 0.40 | 22.4 | 54.8 | 0.0037 |
| H2F05a | 0.04 | 0.50 | 33.3 | 69.5 | 0.0055 |
| H2F10a | 0.07 | 0.56 | 35.4 | 65.2 | 0.0058 |
| H2F15a | 0.16 | 0.64 | 39.9 | 73.9 | 0.0065 |
| H2F20a | 0.15 | 0.70 | 44.0 | 73.9 | 0.0072 |
| H2F25a | 0.23 | 0.85 | 49.2 | 67.8 | 0.0081 |
| H2F30a | 0.26 | 0.95 | 55.9 | 73.9 | 0.0092 |

**Table 3.2.1g Surface Parameters obtained from the stretched exponential profiles for the annealed H2F samples.**

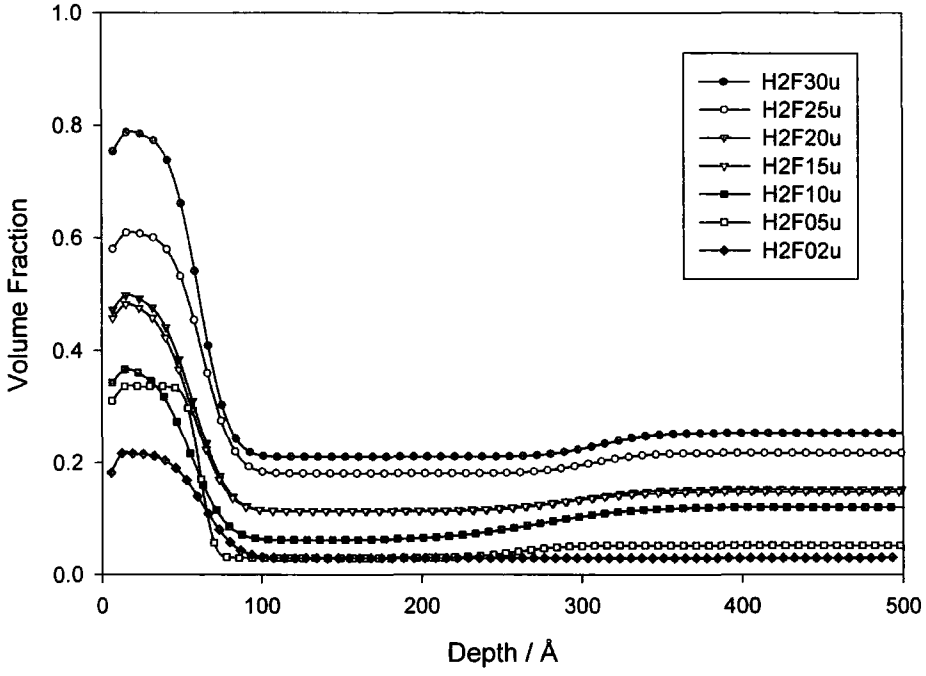


**Figure 3.2.1.7 Volume fraction profiles for H2F unannealed samples obtained using three layer fits to NR data. Symbols are to guide the eye.**

| Sample | $\phi_b$ | $\phi_{dep}$ | $\phi_s$ | z*/Å | $z^*_{dep}$/Å | $z^*_{total}$/Å |
|---|---|---|---|---|---|---|
| H2F02u | 0.029 | - | 0.22 | 10.9 | - | 10.9 |
| H2F05u | 0.05 | 0.03 | 0.34 | 15.2 | 4.1 | 16.7 |
| H2F10u | 0.12 | 0.06 | 0.37 | 10.6 | 11.4 | 14.9 |
| H2F15u | 0.15 | 0.11 | 0.48 | 15.3 | 7.2 | 18.1 |
| H2F20u | 0.15 | 0.11 | 0.50 | 16.3 | 7.9 | 19.3 |
| H2F25u | 0.22 | 0.18 | 0.61 | 20.9 | 7.7 | 24.0 |
| H2F30u | 0.25 | 0.21 | 0.79 | 27.5 | 9.5 | 30.8 |

**Table 3.2.1h Surface parameters obtained from 3 layer profiles for the unannealed H2F samples.**

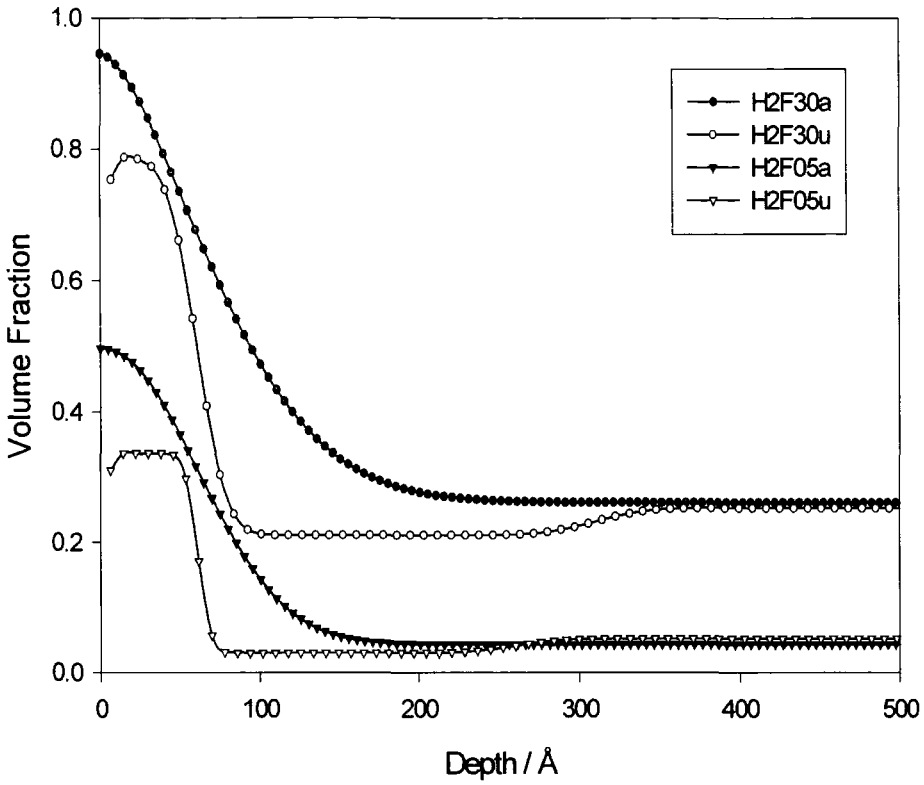


**Figure 3.2.1.8 Difference in surface composition profiles between the unannealed and annealed H2F samples. Symbols are to guide the eye.**

### 3.2.1.3 Small Angle Neutron Scattering

Small angle neutron scattering was carried out using LOQ at the Rutherford Appleton Laboratory. Polymer TK 181 dPSF2 was blended with TK 241 hPS and four compositions were prepared. The small angle neutron scattering for each sample was measured at room temperature and at 413K. Table 3.2.1i gives the sample codes and volume fractions used.

The data were fitted using Debye's scattering function as described in chapter 2 and figure 3.2.1.9 shows the data and fits for the blends measured at room temperature. There was no discernible difference in the small angle scattering of the samples measured at different temperatures and the radius of gyration did not vary with sample composition. The value of radius of gyration obtained was 83±2Å which

was in excellent agreement with that determined using $R_g = a\sqrt{(N/6)}$ where a is the statistical step length (6.7Å) and N the degree of polymerisation ($R_g$ value 82.5±1.5Å).

| Code | $\phi_{dPSF2}$ |
|---|---|
| H2F05 | 0.051 |
| H2F10 | 0.098 |
| H2F15 | 0.150 |
| H2F20 | 0.200 |

**Table 3.2.1i Sample codes and volume fractions used for LOQ analysis.**

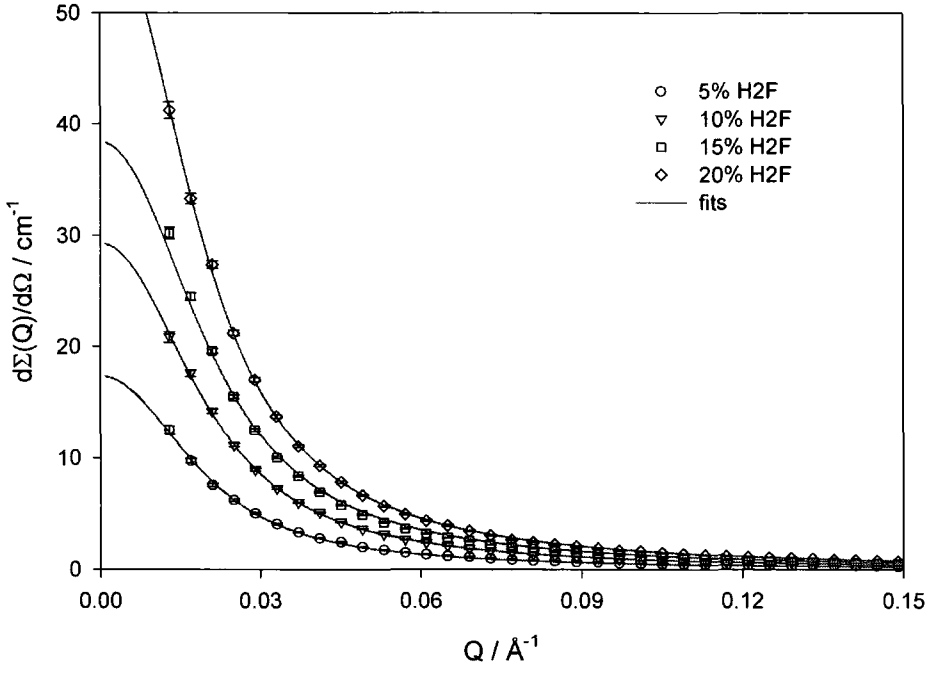


**Figure 3.2.1.9 Small angle neutron scattering data for H2F blends at room temperature with fits to the data assuming Debye scattering**

### 3.2.2 Asymmetric Blends

TK 181 dPSF2 was blended with a range of molecular weight hydrogenous polystyrenes covering a volume fraction range of 5 to 30% functional polymer. The molecular weights of the matrix polymers used are given in table 3.2.2a. As a comparison 20% TK 204 dPS was blended with the same range of matrix polystyrenes.

Solutions were prepared in toluene ranging from 2 to 7.5% polymer, with the highest concentration used for the lowest molecular weight matrix. Films were spun onto silicon blocks at 2000rpm giving uniform thin films of thickness 1600 to 5000Å. The thicker films were prepared for the lower molecular weight matrices because these were less stable to annealing than the higher molecular weight matrices.

Films were annealed at 413K in a vacuum oven. The 18k and 52k matrix samples were removed after 4 days, 100k after 6 days and the 330k and 1000k samples (labelled 1m) after 9 days to allow the equilibrium surface composition structure to be attained without causing sample damage.

| Polymer | $M_w$ | $M_w/M_n$ |
|---|---|---|
| TK 96 (18k) | 19 000 | 1.05 |
| PL 52 (52k) | 52 000 | 1.03 |
| TK 192 (100k) | 106 000 | 1.06 |
| PL 330 (330k) | 303 000 | 1.01 |
| PL 1m (1000k) | 1 080 000 | 1.05 |

**Table 3.2.2a Molecular weight and polydispersity of the polystyrene matrix samples.**

Neutron reflectometry experiments were carried out using the SURF reflectometer on the ISIS pulsed spallation source at the Rutherford Appleton Laboratory. Three angles of incidence were used (0.21, 0.5 and 1.35°) covering a Q range of ~0.007 to 0.14Å$^{-1}$. This was to ensure that background was reached as a single time of flight detector was used.

The data were analysed using VOLFMEM and a stretched exponential model at the air surface. The comparison between the two methods was extremely good as was discussed in chapter 2. For the 18k matrix, segregation was only seen in the 30% mixture. For the 20% dPS blends no segregation was seen for the 18k and 52k matrices, but there was some evidence of segregation for the higher molecular weight matrices and these were analysed using the stretched exponential model. The extent of this segregation was small, at least six times smaller than that seen for the equivalent difunctional polymer blend.

The normalised chi squared values, $\chi^2$, for the stretched exponential model fits were good with an average value of 6.7. The reflectivity profiles for the 20% functional polymer blends are shown in figure 3.2.2.1, the lines through the data are the stretched exponential fits to the data. The Q range shown has been reduced to show the Kiessig fringes and the differences in the reflectivity profile, but the data were fitted up to Q = 0.08Å$^{-1}$. The parameters used to obtain the fits are given in table 3.2.2b.

The fact that the reflectivity has increased with the matrix molecular weight indicates that the amount of segregation has also increased. This can be seen in the values of the surface volume fraction and surface excess given in table 3.2.2d.

| Sample | $\phi_b$ | $\phi_s$ | exponent | decay length/Å | $\chi^2$ |
|---|---|---|---|---|---|
| 52H2F20 | 0.15 | 0.61 | 1.5 | 93 | 1.9 |
| 100H2F20 | 0.15 | 0.71 | 1.7 | 102 | 2.6 |
| 330H2F20 | 0.14 | 0.84 | 1.9 | 106 | 3.8 |
| 1mH2F20 | 0.14 | 0.90 | 2.2 | 108 | 1.6 |

**Table 3.2.2b Parameters used for the stretched exponential model fits to the 20% dPSF2 polymer blends in different molecular weight hPS matrices.**

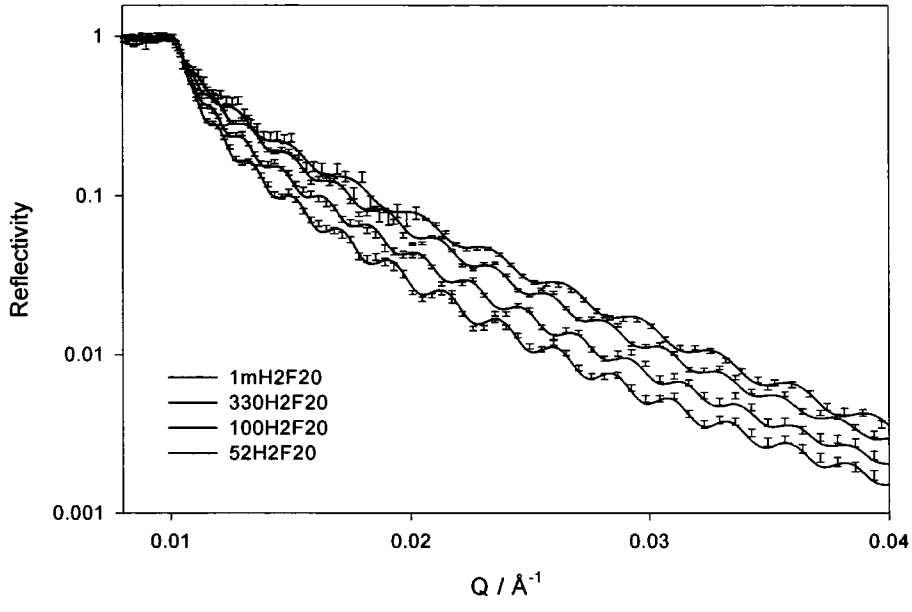


**Figure 3.2.2.1 Reflectivity profiles for the 20% functional polymer blends, from the top in order of decreasing matrix molecular weight.**

Figure 3.2.2.2 shows the reflectivity profiles for one matrix molecular weight, the 1000k hPS samples. Lines through the data are the stretched exponential model fits to the data, the parameters for which are given in table 3.2.2c. The pattern here is the same as for all the different matrices. The critical edge of the reflectivity extends to higher Q as the percentage of functional polymer is increased which is indicative of the higher total scattering length density of the mixture. As the volume fraction of functional polymer increases the reflectivity profile decays less quickly at the critical edge showing a higher surface volume fraction as the concentration of functional polymer is increased.

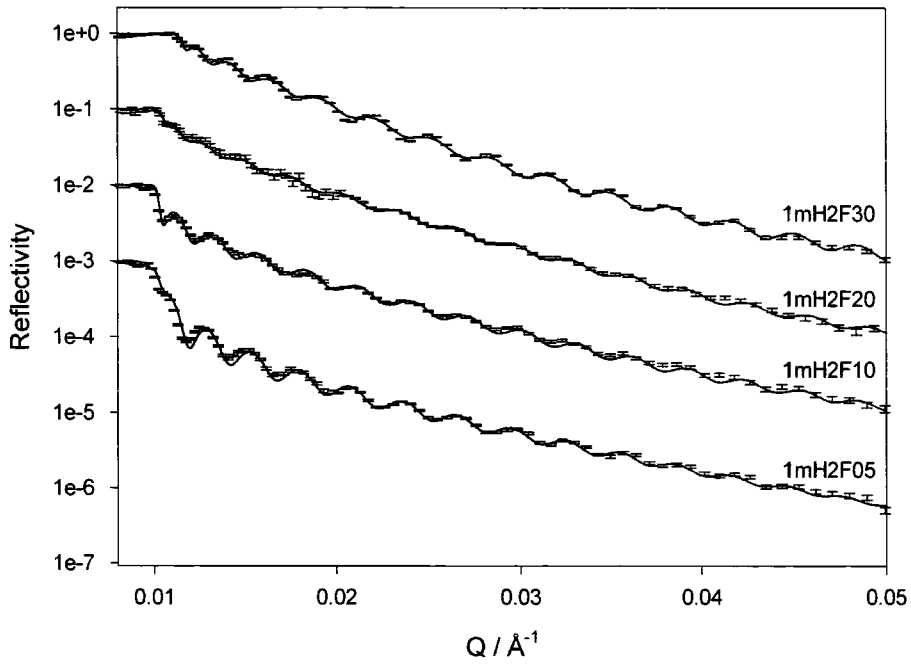


**Figure 3.2.2.2 Reflectivity profiles with stretched exponential model fits to the data for the 1000k hPS matrix samples. Subsequent data sets have been offset by a factor of 10 for clarity.**

| Sample | $\phi_b$ | $\phi_s$ | exponent | decay length/Å | $\chi^2$ |
|---|---|---|---|---|---|
| 1mH2F05 | 0.04 | 0.51 | 2.1 | 77 | 15.2 |
| 1mH2F10 | 0.06 | 0.87 | 1.7 | 84 | 5.6 |
| 1mH2F20 | 0.14 | 0.90 | 2.2 | 108 | 1.6 |
| 1mH2F30 | 0.22 | 0.99 | 1.9 | 129 | 5.7 |

**Table 3.2.2c Parameters used in the stretched exponential model fits for the 1000k molecular weight hPS matrix samples.**

As a general guide to the stretched exponential fits, the exponent increased with matrix molecular weight and the decay length of the profile increased with increasing volume fraction of functional polymer. This is shown in the composition profiles, which are more block like as the matrix molecular weight increased (figure 3.2.2.3), and the layer thickness increased with volume fraction (figure 3.2.2.4).

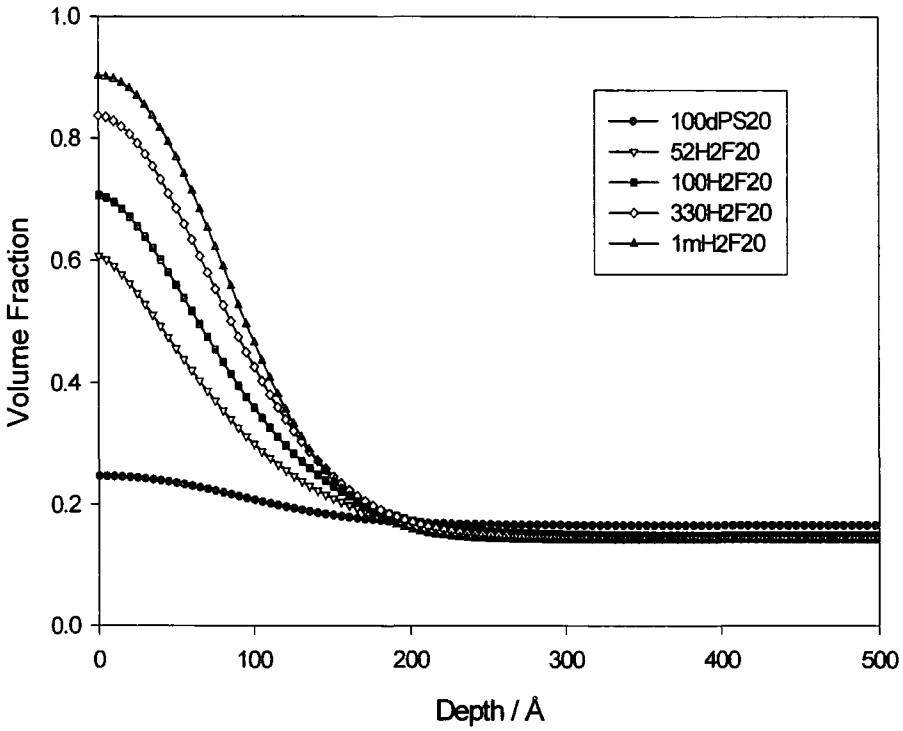


**Figure 3.2.2.3 Volume fraction profiles for 20% polymer blends. Symbols are used to guide the eye.**

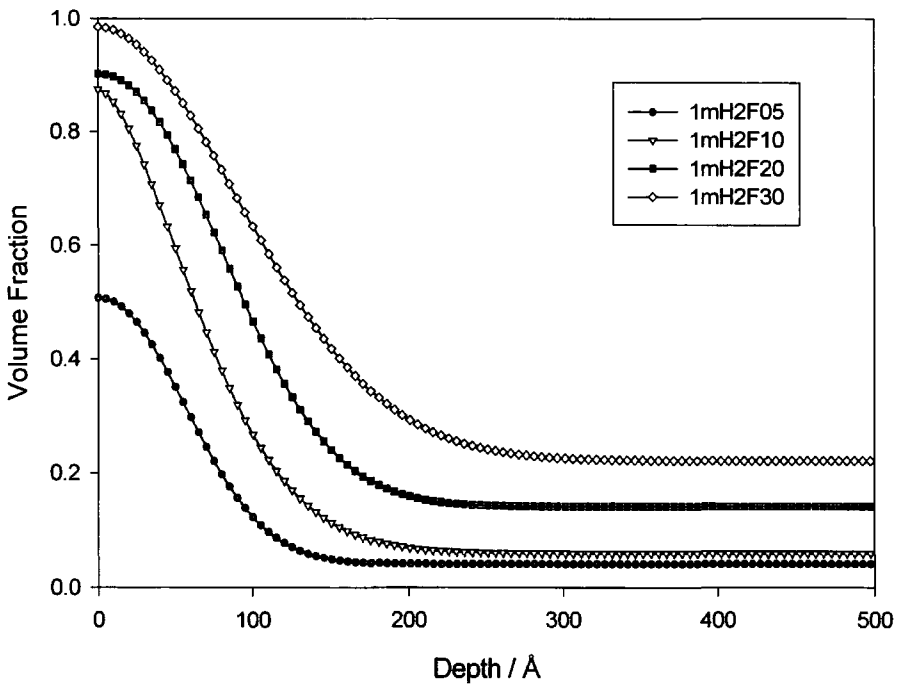


**Figure 3.2.2.4 Volume fraction profiles for 1000k hPS matrix samples. Symbols are used to guide the eye.**

| Sample | $\phi_b$ | $\phi_s$ | z*/Å | L/Å | σ |
|---|---|---|---|---|---|
| 18H2F30 | 0.24 | 0.36 | 11 | 83 | 0.002 |
| 52H2F05 | 0.03 | 0.31 | 19 | 63 | 0.003 |
| 52H2F10 | 0.06 | 0.42 | 26 | 72 | 0.004 |
| 52H2F20 | 0.15 | 0.61 | 38 | 73 | 0.006 |
| 52H2F30 | 0.25 | 0.75 | 42 | 70 | 0.007 |
| 100H2F05 | 0.02 | 0.39 | 25 | 68 | 0.004 |
| 100H2F10 | 0.08 | 0.46 | 27 | 68 | 0.004 |
| 100H2F20 | 0.15 | 0.71 | 51 | 82 | 0.008 |
| 100H2F30 | 0.23 | 0.85 | 56 | 82 | 0.009 |
| 100dPS20 | 0.17 | 0.25 | 8.7 | 103 | - |
| 330H2F05 | 0.03 | 0.41 | 26 | 67 | 0.004 |
| 330H2F10 | 0.04 | 0.58 | 43 | 76 | 0.007 |
| 330H2F20 | 0.15 | 0.84 | 65 | 87 | 0.011 |
| 330H2F30 | 0.23 | 0.98 | 76 | 90 | 0.012 |
| 330dPS20 | 0.16 | 0.26 | 9.8 | 94 | - |
| 1mH2F05 | 0.04 | 0.51 | 32 | 64 | 0.005 |
| 1mH2F10 | 0.06 | 0.87 | 61 | 68 | 0.010 |
| 1mH2F20 | 0.14 | 0.90 | 73 | 92 | 0.012 |
| 1mH2F30 | 0.22 | 0.99 | 87 | 107 | 0.014 |
| 1mdPS20 | 0.15 | 0.25 | 10 | 98 | - |

**Table 3.2.2d Surface parameters obtained from the stretched exponential profiles.**

Figure 3.2.2.5 shows the surface volume fraction and surface excess plotted against bulk volume fraction and matrix molecular weight on 3D plots. The data all follow the same trends with the surface volume fraction and surface excess both increasing with increasing bulk volume fraction and increasing matrix molecular weight.

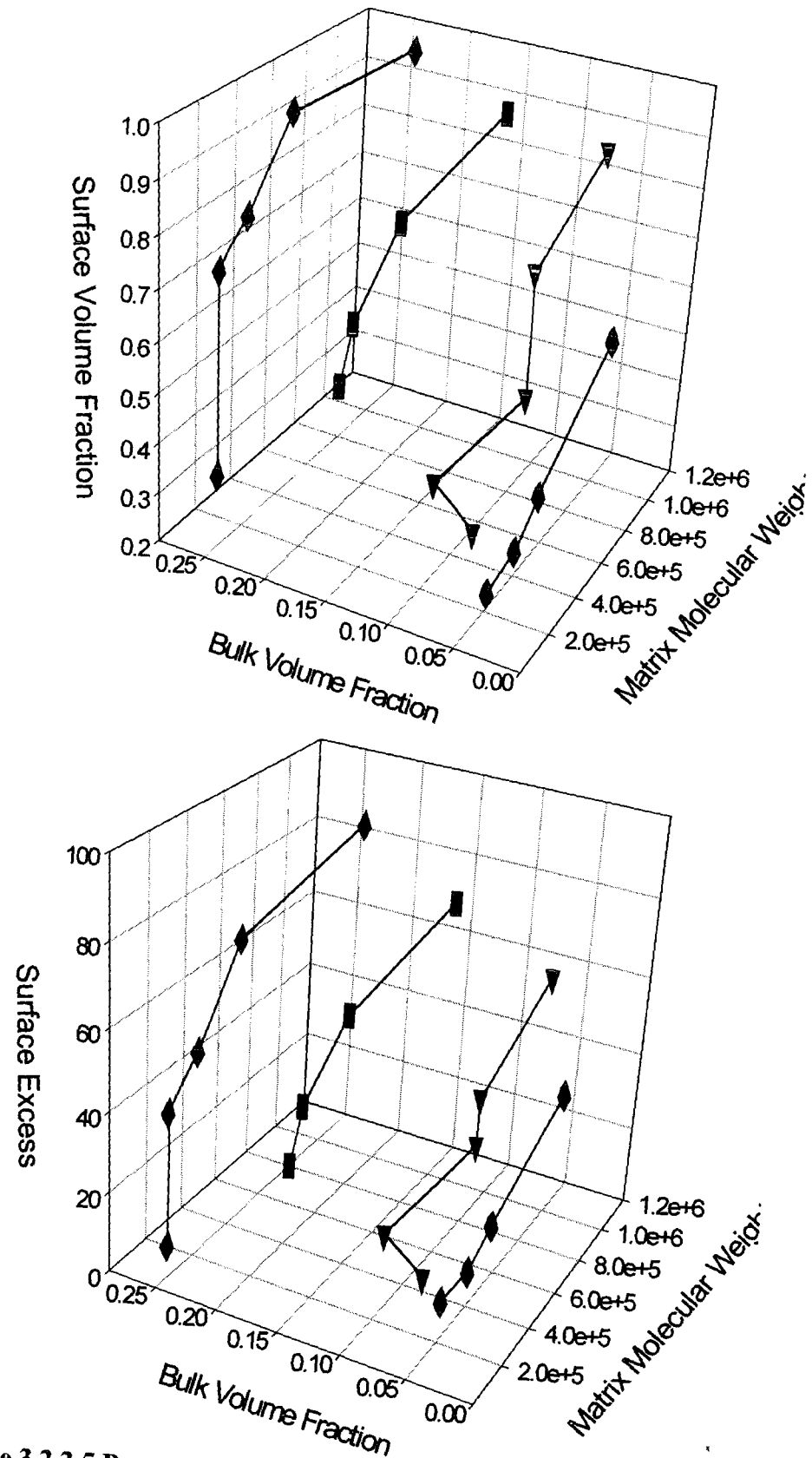


**Figure 3.2.2.5 Parameters obtained from NR profiles shown on 3D plots.**

## 3.3 Analysis and Discussion of Results

In isotopic blends of polystyrene, dPS has been seen to segregate to the surface when the molecular weight is sufficiently high and the mixture has been annealed at a temperature close to the coexistence curve[1, 2]. For the molecular weight range used in these linear blends segregation of dPS would not be expected. Even so, some segregation of 100000 $M_w$ dPS was seen when the matrix hPS was of equal or greater molecular weight. Nonetheless the amount of this segregation was small when compared with that of the functional polymer under the same conditions. It seems logical to conclude, therefore, that segregation was due to the end attachment of the fluorosilane group at the air / polymer interface. Confirmatory evidence for this conclusion was provided by Affrossman et al. They showed that there was an excess of fluorine at the surface of a thin film when using XPS and SIMS analysis on single fluorosilane end capped polystyrene[3] and on double fluorosilane end capped polystyrene[4] when blended with polystyrene of a similar molecular weight. They showed a slight affect due to the deuteration, i.e. whether the segregating polymer or the matrix polymer was the one which was deuterated, but this was outweighed by molecular weight effects, greater segregation seen when the matrix was of greater or equal molecular weight. They deduced that when both ends of the polymer have functional end groups, then both ends segregate to the surface, but suggest that the effect is limited by unfavourable configurational entropy caused by the reduction in possible chain configurations.

Hariharan[5] et al have also shown that there is a reversal of the isotopic segregation in asymmetric blends when the hPS is of lower molecular weight to the

dPS. For the samples with an 18k molecular weight matrix there was no evidence of segregation except for in the highest concentration of functional polymer. This indicates that the two driving forces for segregation are in balance, the entropy effects of having the shorter chains at the surface equalled by the energy gain in the fluorosilane groups being at the surface.

Initial work on segregation in polymers with the same functional end group was carried out by Hopkinson[6, 7]. He studied single end capped molecules and did some preliminary work on the L2F polymer blend system. In his work he found that, for the fluorosilane end groups in hPS, a value of $\left(\chi_e^b - \chi_e^s\right)$ = 4.0 gave the best comparisons to Shull's self consistent field theory predictions[8] using Shull's program LAYERS.

LAYERS calculates theoretical predictions of the composition profile of a polymer brush in a polymer matrix using the sticking energy of the segregating end group, $k_BT\beta$ (where $\beta = \left(\chi_e^b - \chi_e^s\right) + 1.1 \ln\sqrt{6/N_D}$) and the degree of polymerisation of the matrix, $N_H$ and segregating polymer, $N_D$. It is computationally intensive to carry out the calculations therefore the polymer chain dimensions are reduced whilst maintaining the ratio $N_H/N_D$. Hence the value of $\left(\chi_e^b - \chi_e^s\right)$ used in calculations is different to that of the actual experimental system.

For the L2F blends, $N_D$ is 500 and $N_H/N_D$ is equal to 0.86, $\beta$ is 1.5 when $\left(\chi_e^b - \chi_e^s\right)$ = 4.0. For the calculations a value of $N_D$ = 100 and $N_H$ = 86 were used giving a value of $\left(\chi_e^b - \chi_e^s\right)$ = 3.1. The results obtained from the theory are in lattice layers and therefore to normalise to the actual polymer dimensions the depth scale is multiplied by the polymer radius of gyration (61Å for L2F) and divided by the model

system radius of gyration (4.082 when $N_D$ = 100). Examples of theoretical profiles compared with the stretched exponential model profiles are shown in figure 3.3.1.

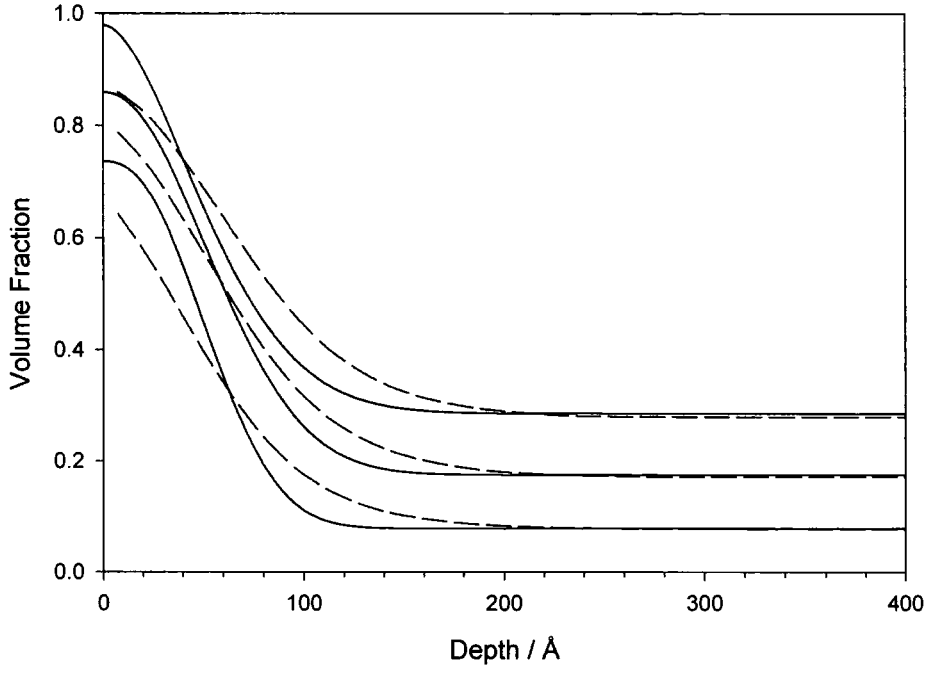


**Figure 3.3.1 Stretched exponential profiles (solid lines) compared with theoretical predictions (dashed lines) for L2F10a, L2F20a and L2F30a.**

The profiles obtained match the experimental data reasonably well, but they tend to under estimate the surface volume fraction and over estimate the extent of the brush layer. Jones[9] and Clarke[10, 11] have also seen that SCF theory predicts a greater interface width when data for a single end capped polystyrene, which segregated to the silicon / polymer interface was analysed. Figure 3.3.2 shows the surface volume fraction vs. equilibrium bulk volume fraction and the surface excess vs. equilibrium bulk volume fraction for the L2F annealed samples compared to the predictions of self-consistent field theory.

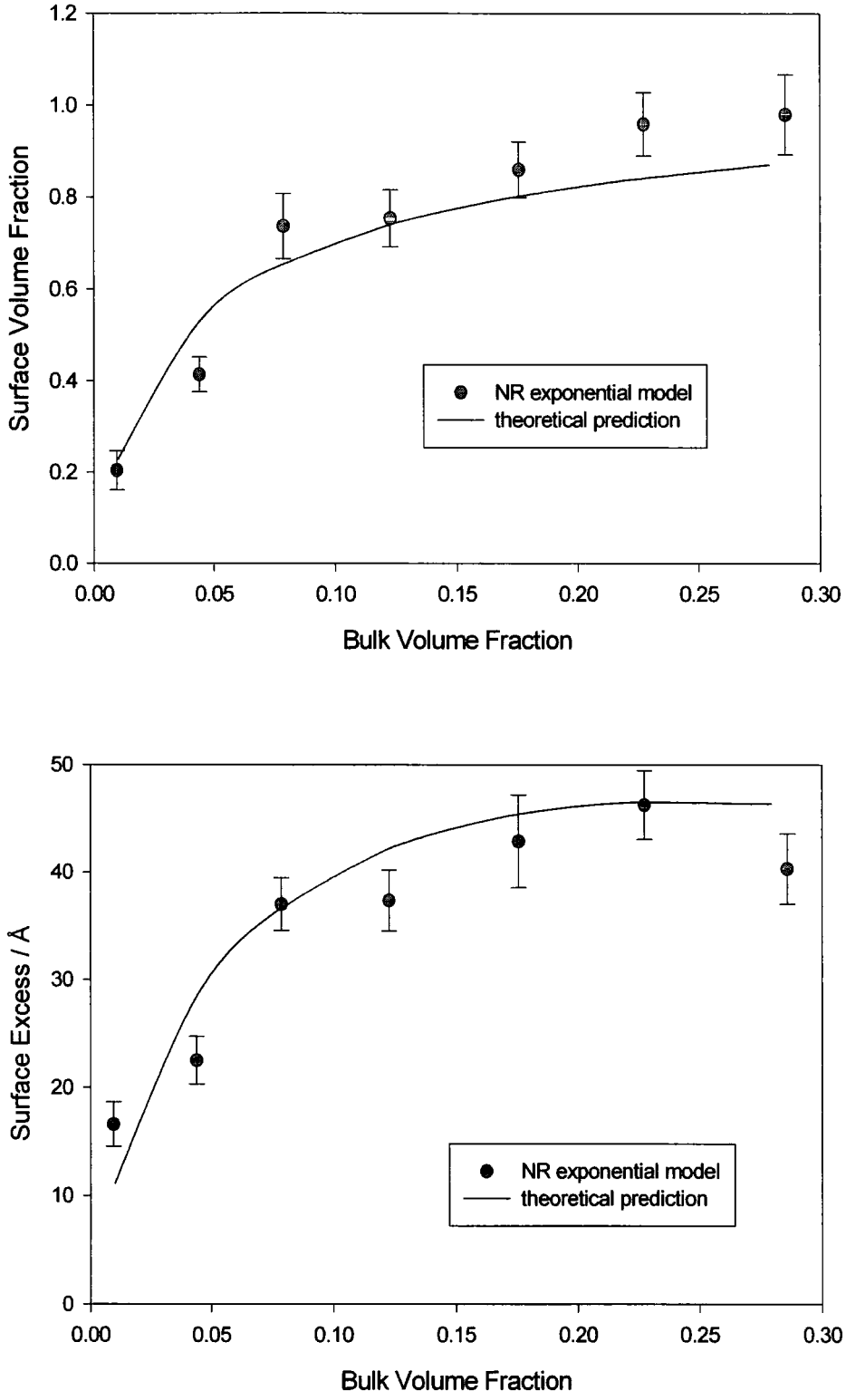


**Figure 3.3.2 Data from stretched exponential model profiles for L2F annealed samples compared with SCF theory predictions.**

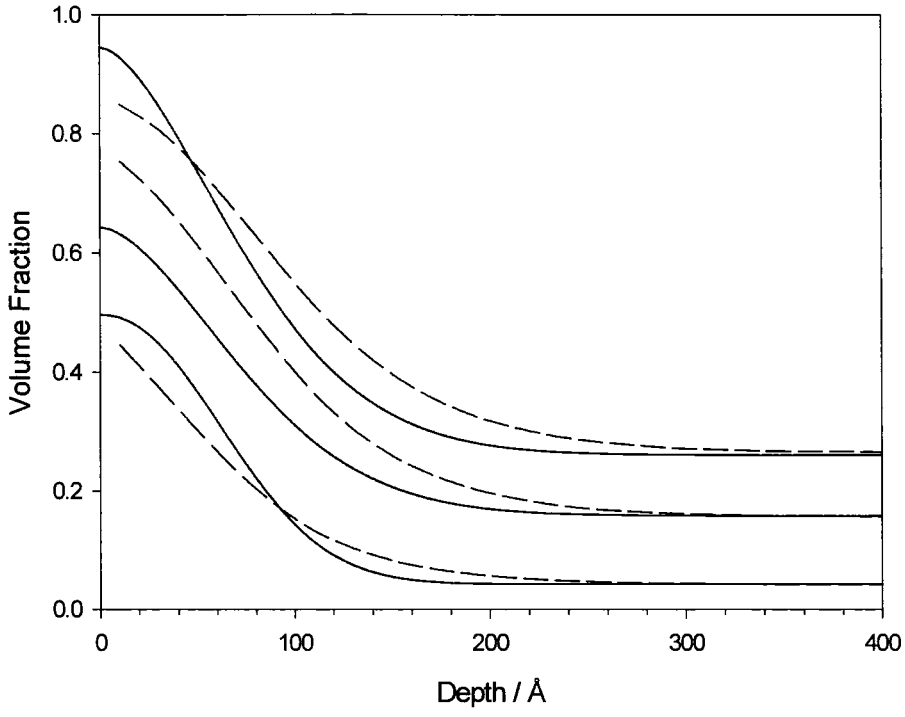


**Figure 3.3.3 Stretched exponential profiles (solid lines) compared with theoretical predictions, β = 1.24, (dashed lines) for H2F05a, H2F15a and H2F30a.**

For the H2F samples, $N_D$ = 910 and $N_H/N_D$ = 1.26 so in the calculations values of $N_D$ = 100 and $N_H$ = 126 were used. For $\left(\chi_e^b - \chi_e^s\right)$ = 4.0, β = 1.24, so $\left(\chi_e^b - \chi_e^s\right)$ = 2.79 in the calculations. Figure 3.3.3 shows examples of the experimental data compared to the results of the theoretical predictions. The agreement at the low and high volume fractions used was good and similar to that obtained for the L2F system, but for intermediate volume fractions the theoretical volume fraction profile overestimates the experimental at all positions, shown for H2F15a. If the volume fraction profiles calculated by self consistent field theory were non-linearly least squares fitted to the experimental profiles where the value of the $\left(\chi_e^b - \chi_e^s\right)$ was the only fitting parameter, values of β were obtained ranging from 0.77 - 1.55 with an average value of 1.11±0.29. This reduced to 0.97±0.15 if the lowest and highest volume fraction samples were excluded. The comparisons

between the profiles calculated by SCF theory using a value of $\beta = 0.97$ with the experimental profiles are shown in figure 3.3.4.

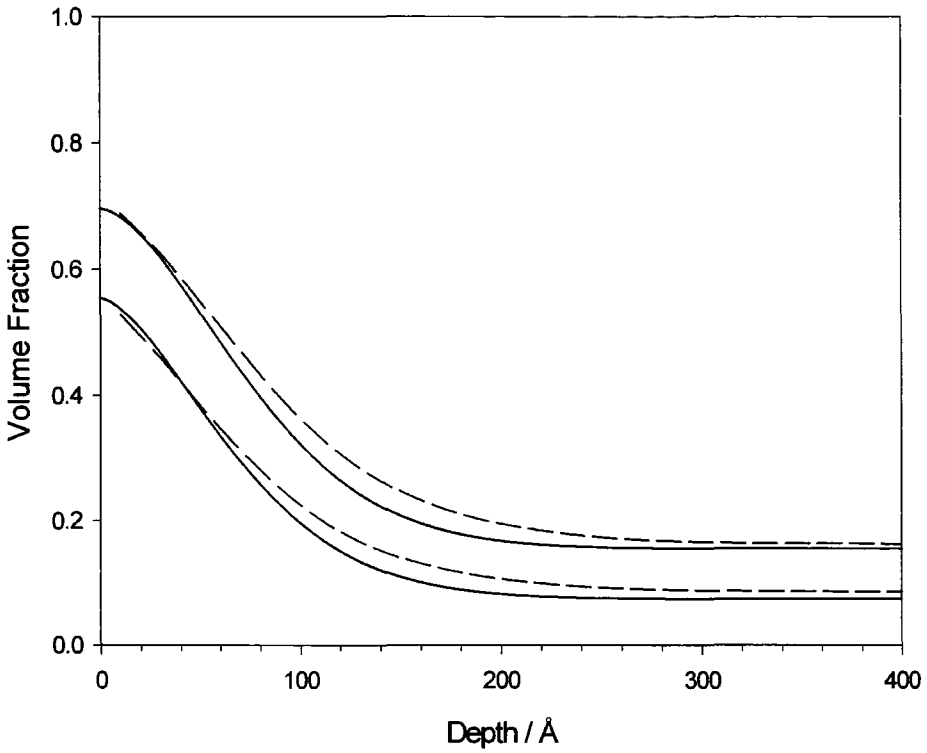


**Figure 3.3.4 Stretched exponential profiles (solid lines) compared with theoretical predictions, $\beta = 0.97$, (dashed lines) for H2F10a, and H2F20a.**

Figure 3.3.5 shows the stretched exponential surface volume fraction against equilibrium bulk volume fraction and surface excess against equilibrium bulk volume fraction with lines from theory using $\beta = 0.97$ and $\beta = 1.24$. The latter matched the experimental surface volume fraction well but overestimated the surface excess whereas the former underestimated the surface volume fraction but matched the surface excess well. This would suggest that the greater molecular weight was affecting the behaviour of the end group to a greater extent than predicted. However, when the same polymer was blended with different polystyrene matrices, a value of $\beta = 1.24$ gave excellent agreement to the data so the problem would appear to be with these samples.

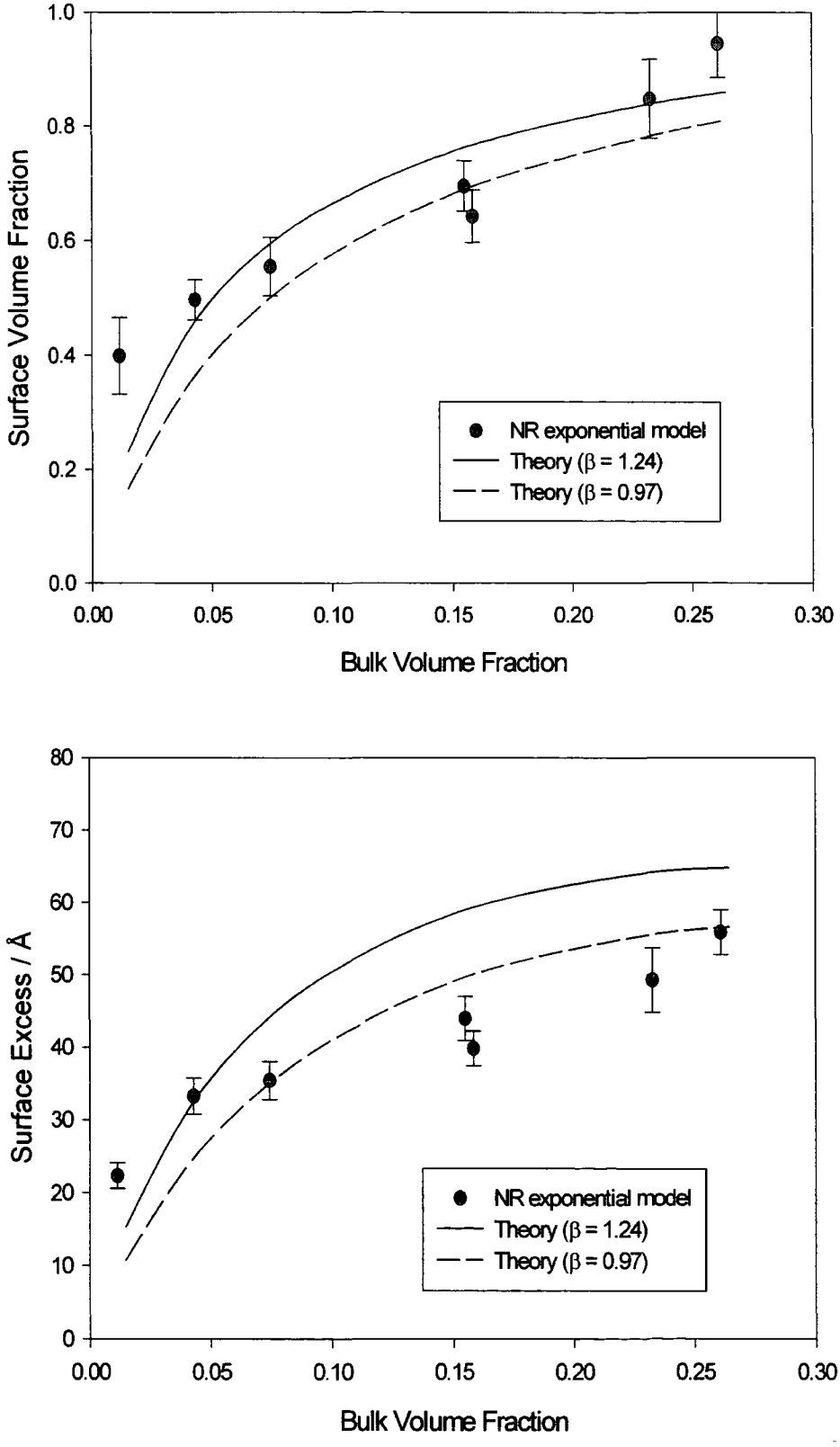


**Figure 3.3.5 Data from stretched exponential model profiles for H2F annealed samples compared with SCF theory predictions.**

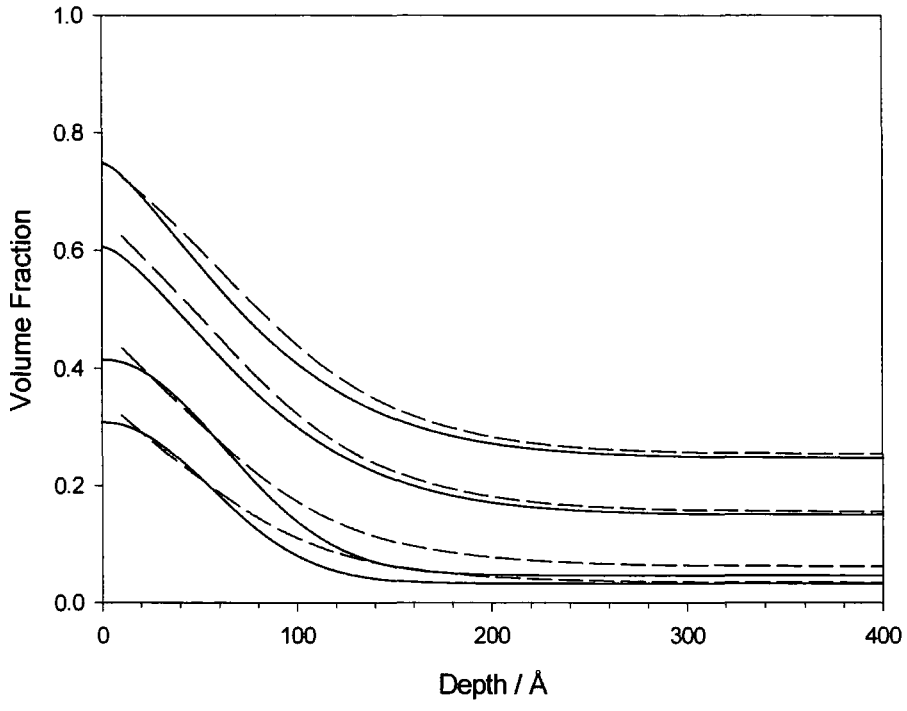


**Figure 3.3.6 Stretched exponential profiles (solid lines) and comparisons with theoretical predictions (dashed lines) for the 52k matrix molecular weight samples: from the top 52H2F30, 52H2F20, 52H2F10 and 52H2F05.**

Figures 3.3.6 and 3.3.7 show comparisons with theoretical profiles determined from LAYERS and experimental profiles for the 52k and 330k hPS matrices respectively. For the calculations a value of $\beta = 1.24$ was used. For the 52k and 100k matrix samples a value of $N_D = 100$ was used with $N_H = 54.7$ and 112 respectively. For the higher matrix molecular weights the values had to be scaled down because the calculations did not converge and values of $N_D = 30$ with $N_H = 104$ for the 330k hPS and $N_D = 20$ with $N_H = 226$ for the 1000k hPS were used. This had the effect of cutting the polymer chain up into larger pieces and the lattice layers were bigger to account for this, but the results compared well. The most obvious disagreement was for the surface volume fraction because of the large lattice spacing.

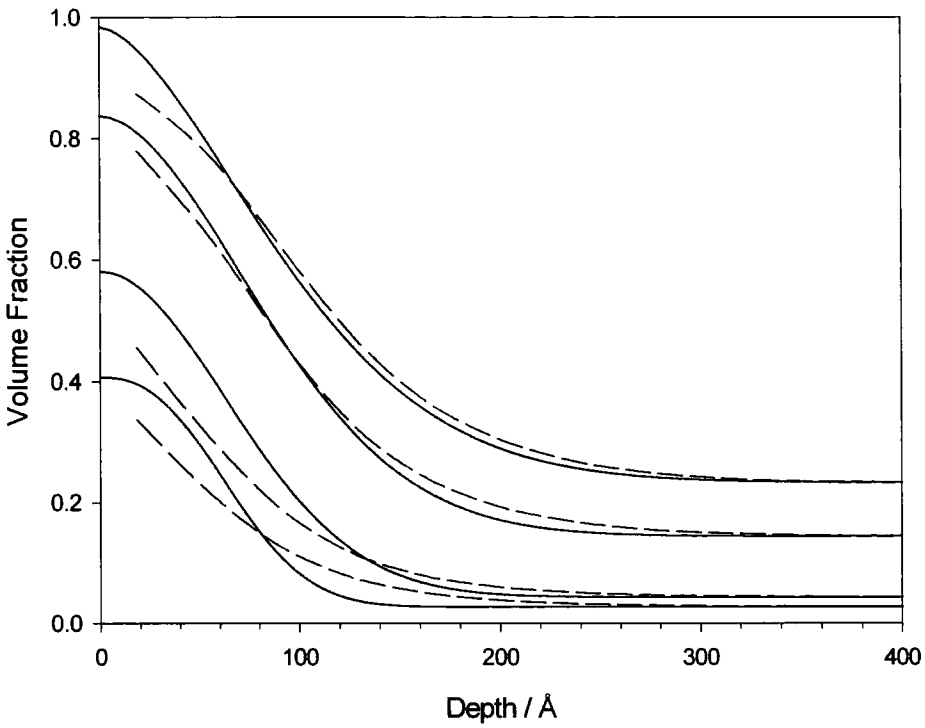


**Figure 3.3.7 Stretched exponential profiles (solid lines) and comparisons with theoretical predictions (dashed lines) for 330k matrix molecular weight samples: from the top 330H2F30, 330H2F20, 330H2F10 and 330H2F05.**

Figure 3.3.8 shows the experimental data points determined from the stretched exponential profiles with lines determined from theory for the different molecular weight matrices. The effect of the reduced number of lattice layers can be seen in the surface volume fraction comparisons for the greater molecular weight matrices, especially for the 1000k matrix where the theoretical line is offset relative to the other theoretical predictions. The surface excess values are in good agreement to those determined by theory, though theory does overestimate for the 52k and 100k hPS matrix as was seen for the L2F and H2F systems.

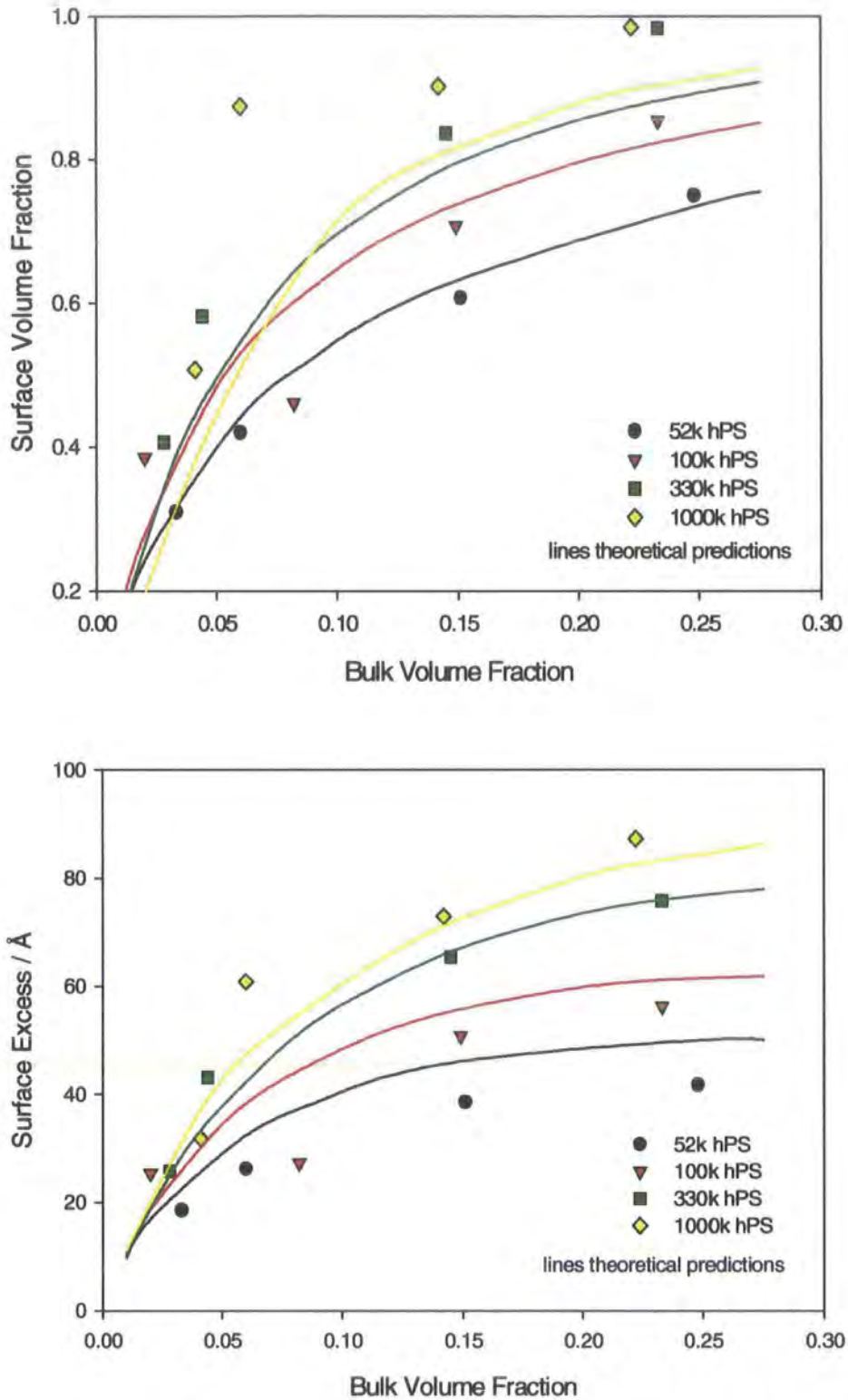


**Figure 3.3.8 Data from the stretched exponential model profiles for the varying matrix molecular weight samples compared with SCF theory predictions ($\beta$=1.24).**

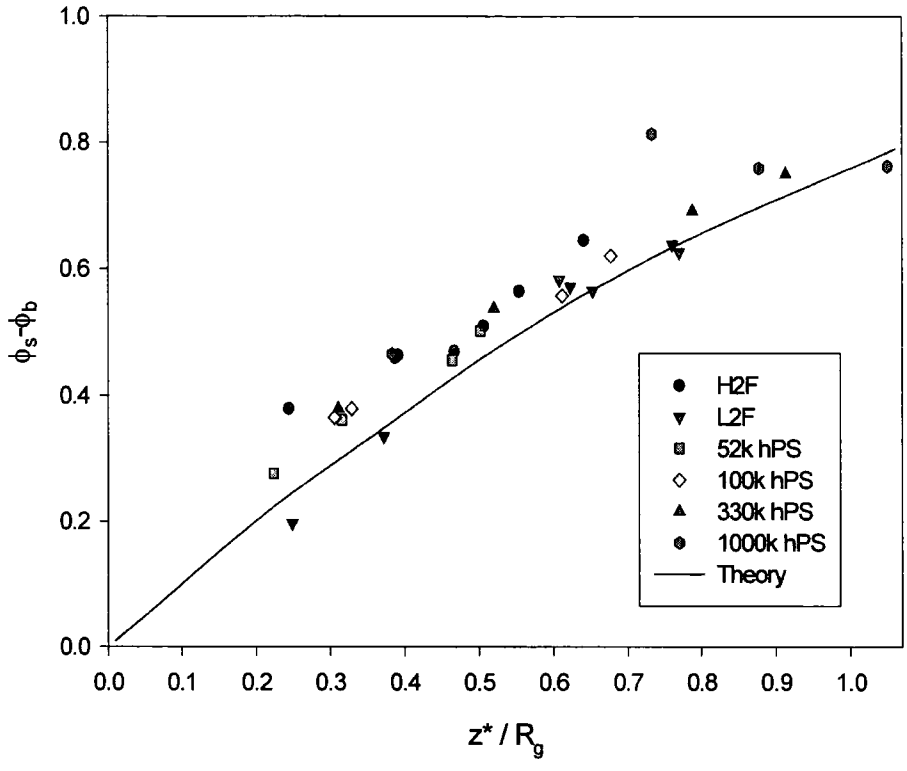


**Figure 3.3.9 Equilibrium surface volume fraction minus bulk volume fraction against normalised excess, $z^*/R_g$ for all the linear dPSF2 samples. Line is from Shull's SCF theory predictions for the dry brush limit.**

The comparisons of the experimental profiles with SCF theory profiles have been very good especially as the theory was initially developed for single end, strong adsorption (i.e. the surface volume fraction profile of the brush polymer decays to zero). LAYERS has been adapted to allow for two functional end groups, these in principal can have different affinities for the surface but the profile obtained is the same as two ends with the same average sticking energy.

Shull[8] has predicted that for strong segregation in the dry brush regime the brush profile is characterised by the surface excess normalised by the brush polymer radius of gyration, $z^*/R_g$ and has calculated brush parameters. The systems studied here are only weakly segregated with a substantial amount of functional polymer remaining in the bulk, but this can be regarded as a strongly adsorbed brush on a

uniform background. The values of surface volume fraction minus the bulk volume fraction (background) are shown in figure 3.3.9 against the normalised excess, the theoretical line is the predicted surface volume fraction value for a strongly adsorbed brush. The data for L2F match the theory well; the data for the 100k dPSF2 follow the same trend but are greater than the theoretical value. The two functional end groups mean that if both ends attach to the surface the brush layer will tend to be taller but thinner than the equivalent single functional end group polymer which would give rise to the greater $\phi_s$ - $\phi_b$ values for the same $z^*/R_g$. Affrossman etal[4] studied both single and double functional end capped polymers up to the molecular weight of the L2F system, for these they said that there was no difference in the polymer profile, but both ends segregated to the surface for the difunctional polymer. This would support the fact that the L2F polymer follows the theoretical prediction but as the chain length increases the brush layer will be narrower when both ends are confined to the surface as opposed to only one end.

Figure 3.3.10 shows the adsorption isotherms of normalised surface excess against equilibrium bulk volume fraction. Lines are guides to the eye and only one line is shown for the H2F and 100k matrix samples, as these were both symmetrical blends of 100000 $M_w$.

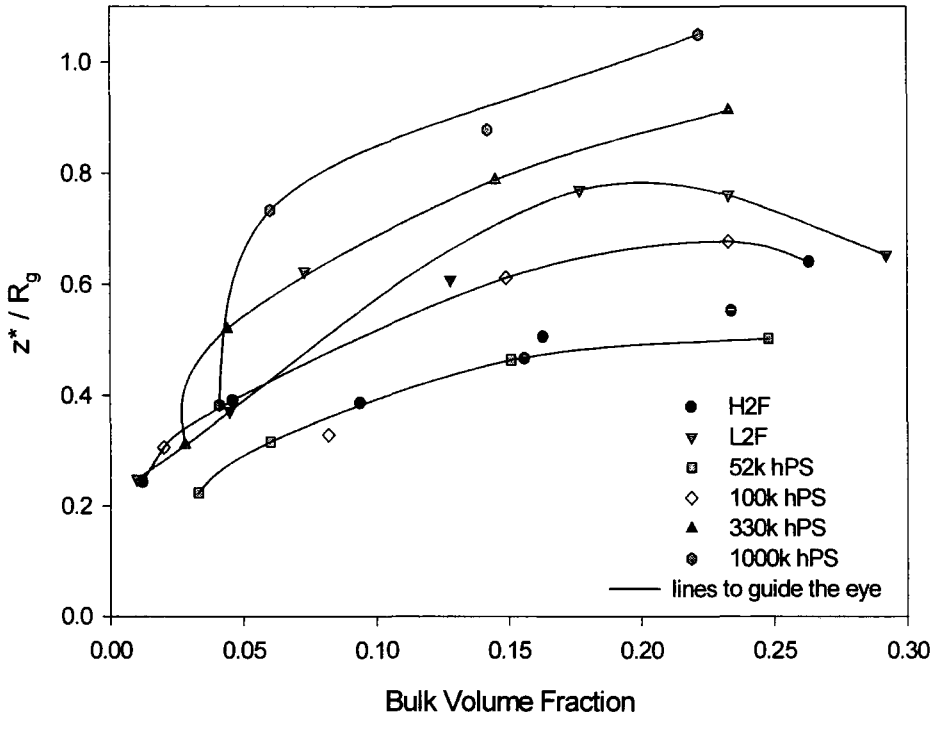


**Figure 3.3.10 Normalised excess, $z^*/R_g$ against equilibrium bulk volume fraction for all the linear dPSF2 polymer systems. Lines are to guide the eye for same matrix molecular weight.**

For the L2F system $z^*/R_g$ is greater than for the 100k dPSF2 in approximately the same or lower molecular weight polystyrene which would be expected due to the greater sticking energy of the polymer because of its lower molecular weight. For the 100k dPSF2 the sticking energy was the same but $z^*/R_g$ increases with increasing matrix molecular weight. This could be due to an increase in the value of $\chi_{ab}N_b$ where $\chi_{ab}$ is the interaction parameter between the brush and matrix polymer and $N_b$ is the degree of polymerisation of the brush polymer. In this work it has been assumed that the interaction parameter is very small and hence $\chi_{ab}N_b$ is effectively zero which is true for the equal molecular weight systems, but it has been shown that $\chi$ can be slightly positive for higher molecular weight isotopic blends. Molecular weight

effects mean that there is an entropic gain in having the lower molecular weight polymer at the surface, which will enhance the segregation caused by the fluorosilane groups.

The L2F and 100k matrix profiles show a downturn at high bulk volume fractions, the other data are reaching a plateau but do not go to sufficiently high bulk volume fraction to show a maximum. The data for the equal or greater matrix molecular weight appear to converge at low bulk volume fractions, though in this region there is greater uncertainty in the values because the NR data is less sensitive to small changes. The 52k data lie below this and give generally low values as the low molecular weight matrix penetrates the brush layer more.

De Gennes[12] developed a scaling theory for polymer brushes immersed in a solution of polymer chains of the same or smaller degree of polymerisation. Aubouy and Raphael[13] extended this to polymer chains in polymeric matrices. As all the matrices studied here had a degree of polymerisation, P, greater than $N^{1/2}$ there are four possible regions of interest: ideal mushroom, stretched wet brush, unstretched brush and stretched dry brush. When the actual dimensionless surface grafting density values ( $\sigma = z^*/aN_D$ ) obtained experimentally are plotted against the degree of polymerisation of the matrix all the 100k dPSF2 samples appear to be in the unstretched brush region (see figure 3.3.11).

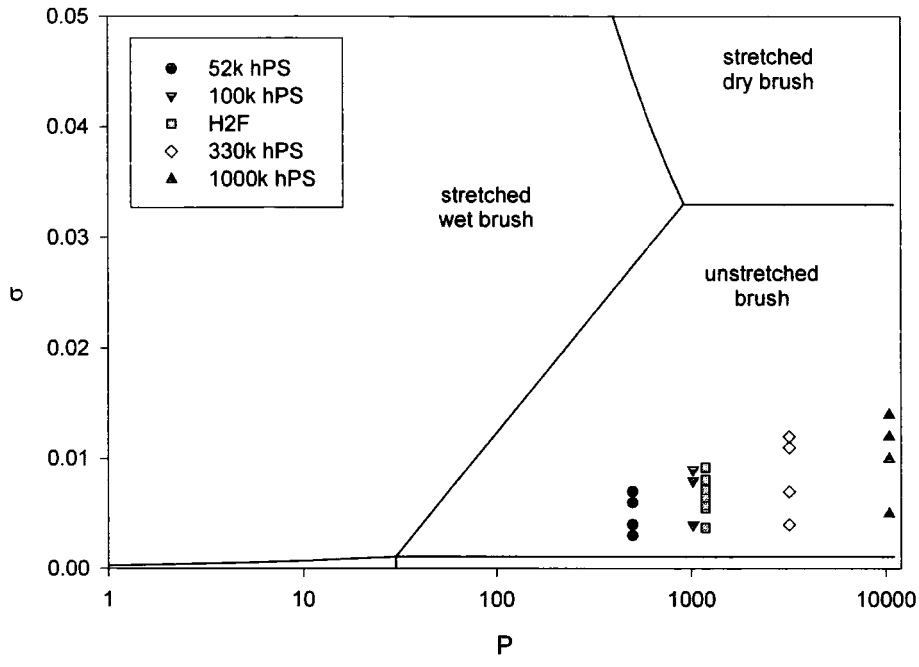


**Figure 3.3.11 Graph to show the various scaling regions predicted for 100k dPSF2 brush in varying molecular weight matrix. Data points show the experimental values obtained.**

In the unstretched region, the thickness of the brush, L, is predicted to be $\approx aN^{1/2}$ with no dependence on σ. For the L2F system there was no dependence on σ with an average brush height (width at half height of the segregated layer) of 56.6±2.7Å, this is about the $R_g$ of the polymer and follows the expected trend.

The values of brush height (width at half height of the segregated layer) obtained for the 100k dPSF2 have ranged from 55 to 107Å with an average excluding the high molecular weight and surface grafting density samples of 72±6Å. The $R_g$ for the 100k dPSF2 is 83Å and is generally larger than the brush height obtained. If both ends have segregated to the interface, this places a constraint on the polymer dimensions and will probably reduce the brush height value from that of the radius of gyration. There is some ambiguity in how the brush height is determined, but whichever method is used the trend between values is the same, the brush height

scaled as $\sigma^{0.29}$, shown in figure 3.4.12. This would not be expected in the unstretched region, but is predicted for a stretched wet brush. In the stretched wet brush region the brush height is predicted to be $\approx aNP^{-1/3}\sigma^{1/3}$ and so a dependence on the matrix molecular weight would also be expected. When the brush height was looked at as a function of matrix molecular weight, P, there was no effect for the low volume fractions, for the 30% samples there was a possible dependence of $\sim P^{0.13}$, but this does not agree with scaling theory predictions and was not particularly strong.

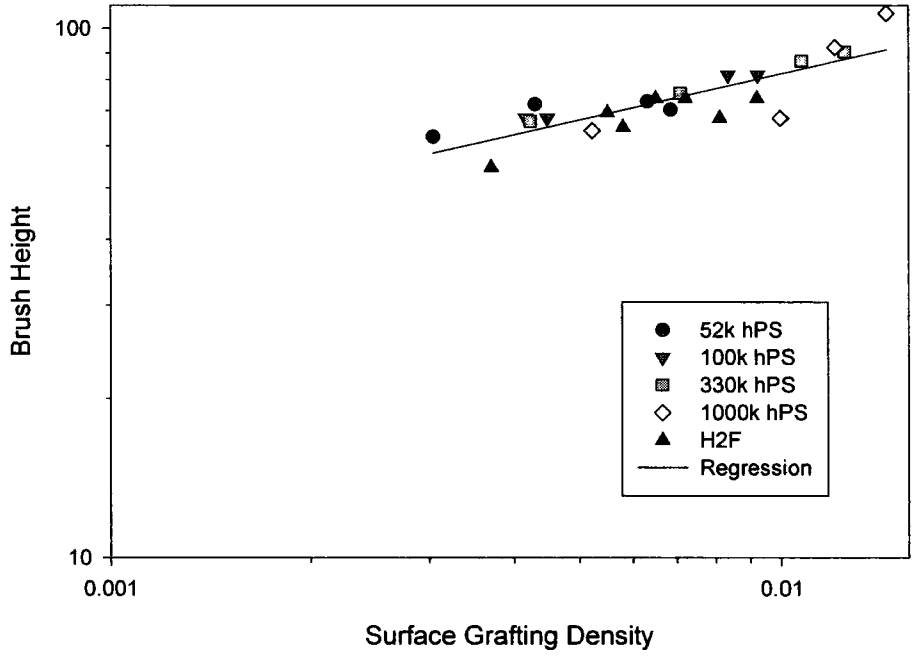


**Figure 3.3.12 Brush height against surface grafting density for 100k dPSF2 polymer in various hPS matrices.**

Another factor which is important here is the fact that with two functional ends the surface grafting density could be up to a factor of two greater. This would still place all the experimental data in the unstretched brush region, but some of the values would be close to the boundary with the stretched brush region that does scale with $\sigma^{1}$. Budkowski etal[14] studied perdeuterated polystyrene with a short

polyisoprene block at one end that segregated to the air interface when blended with polystyrene and annealed above the glass transition. They found a dependence of brush height on surface coverage of $\sigma^{0.54}$, and suggested that this could be due to a transition region from the unstretched to the dry stretched brush regime. They did find the expected wet brush behaviour for a low molecular weight matrix. Aubouy and Raphael[13] suggested that this unexpected behaviour could be due to a small value of $\chi$ for the high molecular weight matrix and proposed adjustments to scaling theory to account for it. Whilst they managed to justify a region which scaled as $\sigma^{1/2}$, unfortunately this did not apply when the matrix was equal or greater molecular weight. However they feel that the influence of a small $\chi$ value could explain the unusual scaling behaviour.

Jones[15] made direct comparisons between the brush height predicted by scaling theory and that determined using SCF calculations and found that the sharp boundaries assumed by scaling theory are actually replaced with a broad region of cross-over when SCF theory calculations are used. This is shown in figure 3.3.13 with the experimental data points for the systems studied here. The experimental values are generally lower than those predicted which would be expected because of the thinner brush layer that is formed when both ends segregate to the surface, but the values follow the trend shown by SCF theory calculations. This would explain the unusual scaling behaviour observed as the data points all fall in the transition region between unstretched and stretched dry brush regimes.

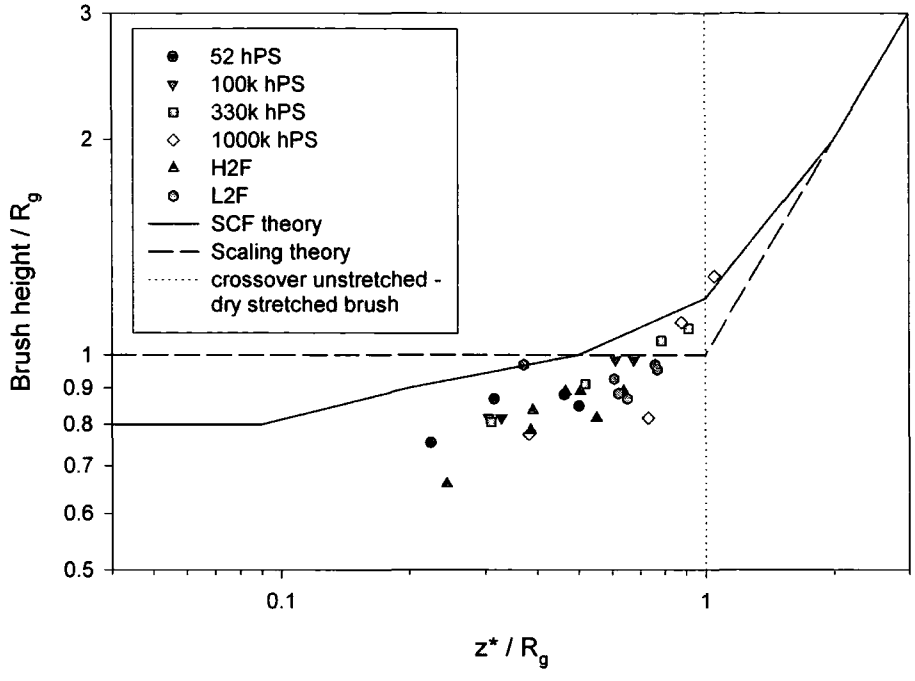


**Figure 3.3.13 Self consistent field theory and scaling theory predictions of brush height for a single end attached polymer in a chemically identical matrix of molecular weight ~100k showing the experimental values obtained for the difunctional polymers used.**

The average volume fraction ($\phi_{Av} = z^*/L$) in the brush ranged from 0.2 to 0.9 so the matrix was never completely expelled from the brush. When the average volume fraction was plotted against surface grafting density on a log-log plot, figures 3.3.14 and 3.3.15, L2F scaled as $\sigma^1$, H2F scaled as $\sigma^{0.71}$ and for the 100k dPSF2 in different molecular weight matrices a scaling of $\sigma^{0.72}$ was obtained. This behaviour follows from the scaling of the brush height of the polymer, if $L \propto \sigma^n$ then $\phi_{Av} \propto \sigma^{1-n}$.

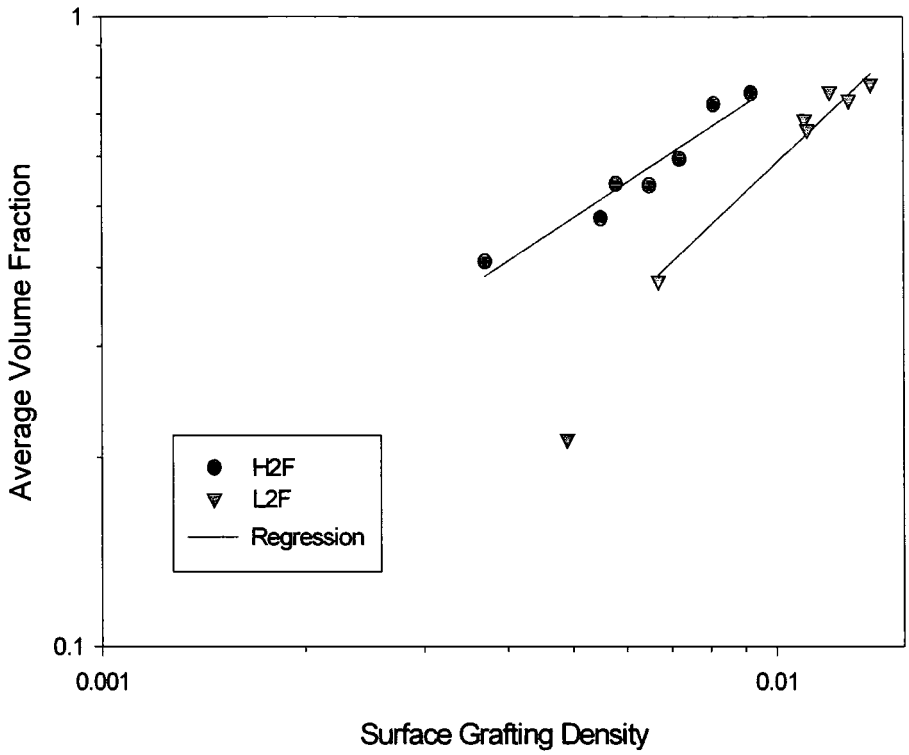


**Figure 3.3.14 Average volume fraction against surface grafting density for H2F and L2F samples**

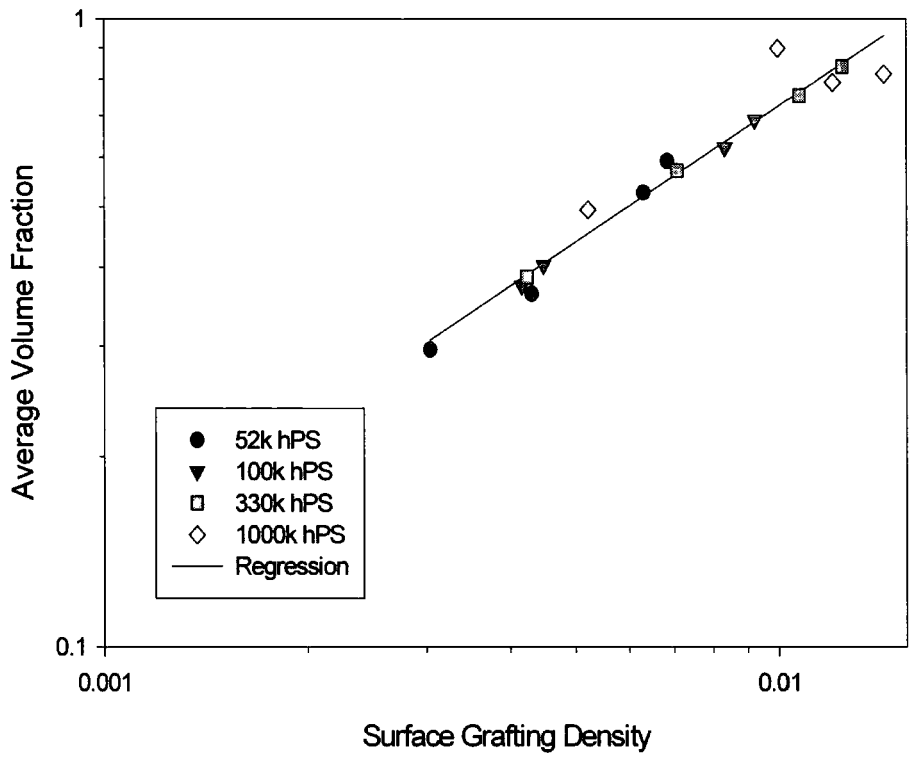


**Figure 3.3.15 Average volume fraction against surface grafting density for 100k dPSF2 in various hPS matrices.**

In conclusion, the surface volume fraction profiles obtained for difunctional end capped linear polystyrene in hPS showed good agreement with SCF calculations with $\left(\chi_e^b - \chi_e^s\right)$ = 4.0. The surface grafting density values obtained fell into the unstretched dry brush regime, however the scaling of the brush thickness for 100000 $M_w$ dPSF2 samples gave $\sigma^{1/3}$ behaviour which is not predicted but is accounted for by a broad crossover from unstretched to stretched brush behaviour.

## 3.4 References


1 R. A. L. Jones, L. J. Norton, E. J. Kramer, R. J. Composto, R. S. Stein, T. P. Russell, A. Mansour, A. Karim, G. P. Felcher, M. H. Rafailovich, J. Sokolov, X. Zhao, and S. A. Schwarz, *Europhysics Letters*, 1990, **12**, 41.

2 R. A. L. Jones and E. J. Kramer, *Philosophical Magazine B-Physics of Condensed Matter Structural Electronic Optical and Magnetic Properties*, 1990, **62**, 129.

3 S. Affrossman, M. Hartshorne, F. T. Kiff, R. A. Pethrick, and R. W. Richards, *Macromolecules*, 1994, **27**, 1588.

4 S. Affrossman, P. Bertrand, M. Hartshorne, F. T. Kiff, D. Leonard, R. A. Pethrick, and R. W. Richards, *Macromolecules*, 1996, **29**, 5432.

5 A. Hariharan, S. K. Kumar, and T. P. Russell, *Journal of Chemical Physics*, 1993, **98**, 4163.

6 I. Hopkinson, 'Surface Composition Profiles in Some Polymer Mixtures', Ph.D., Durham, 1994.

7 I. Hopkinson, F. T. Kiff, R. W. Richards, D. G. Bucknall, and A. S. Clough, *Polymer*, 1997, **38**, 87.

8 K. R. Shull, *Journal of Chemical Physics*, 1991, **94**, 5723.

9 T. Nicolai, C. J. Clarke, R. A. L. Jones, and J. Penfold, *Colloids and Surfaces A-Physicochemical and Engineering Aspects*, 1994, **86**, 155.

10 C. J. Clarke, R. A. L. Jones, J. L. Edwards, K. R. Shull, and J. Penfold, *Macromolecules*, 1995, **28**, 2042.

11 C. J. Clarke, R. A. L. Jones, J. L. Edwards, A. S. Clough, and J. Penfold, *Polymer*, 1994, **35**, 4065.

12 P. G. de Gennes, *Macromolecules*, 1980, **13**, 1069.

13 M. Aubouy and E. Raphael, *Journal de Physique II*, 1993, **3**, 443.

14 A. Budkowski, U. Steiner, J. Klein, and L. J. Fetters, *Europhysics Letters*, 1992, **20**, 499.

15 R. A. L. Jones and R. W. Richards, 'Polymer Surfaces and Interfaces', Cambridge University Press, To be published 1998.

# CHAPTER 4

# Three Armed STAR Polymer

## 4.1 Experimental Results

To determine the extent of segregation in thin films, the first fraction of TK 200 STAR was blended with PL 120 hPS. Table 4.1 gives the volume fractions of STAR used and the codes to refer to them. Films were spun from 5% solution in toluene at 3500 rpm. A sample of each blend was annealed at 415K for 7 days to ensure the equilibrium surface composition was obtained and an unannealed sample of each was prepared for comparison.

| Code | $\phi_{STAR}$ |
|---|---|
| STAR02 | 0.021 |
| STAR05 | 0.050 |
| STAR10 | 0.100 |
| STAR15 | 0.150 |
| STAR20 | 0.200 |
| STAR25 | 0.251 |
| STAR30 | 0. 300 |

**Table 4.1 Codes and volume fractions used in the STAR blends**

Attempts to carry out nuclear reaction analysis on these samples proved to be unsuccessful with no clear segregation that could be discerned with confidence within the spatial resolution of the instrument. Hence all surface segregation results reported were obtained using neutron reflectometry.

### 4.1.1 Neutron Reflectometry

Neutron reflectivity data on STAR05 and STAR30, average thickness 3000Å, were obtained on CRISP using the single detector, the remaining samples, average thickness 2700Å, were measured on CRISP using the multidetector. The data were analysed using VOLFMEM, and a stretched exponential model for the annealed data and a 3 layer model for the unannealed samples. Figure 4.1 shows the reflectivity

profiles for the 10, 20 and 30% STAR samples, with the fitted profiles shown as lines. The parameters used for the stretched exponential fits to the annealed samples are given in table 4.2. VOLFMEM analysis showed some segregation and a depletion layer in the unannealed samples, as was seen previously for the difunctional polymers, therefore a three layer model was used to fit the data. The parameters resulting from the best non-linear least squares fits are given in table 4.3, where $\phi$ is the volume fraction of STAR, t is the layer thickness, $\sigma$ is the roughness between the layer and the succeeding layer, and $\chi^2$ is the normalised chi squared goodness of fit. The subscript is the number of the layer with 1 being the uppermost layer and the roughness at the air and substrate interfaces was fixed at 5Å.

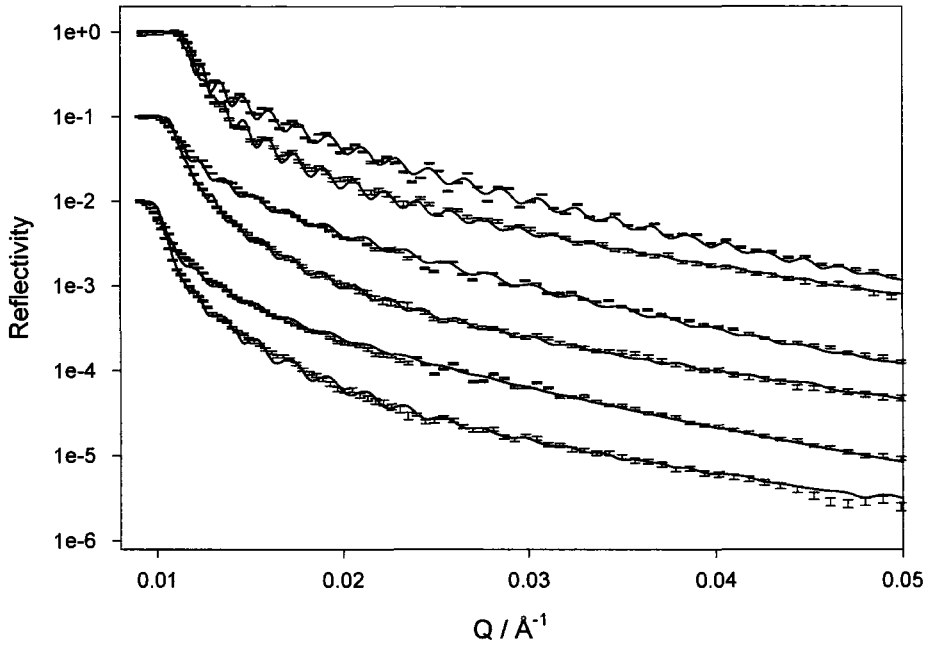


**Figure 4.1 Reflectivity profiles and fits to the data (from the top) for STAR30a, STAR30u, STAR20a, STAR20u, STAR10a and STAR10u. Data for subsequent blends offset by a factor of 10 for clarity.**

| Sample | $\phi_b$ | $\phi_s$ | exponent | decay length/Å | $\chi^2$ |
|---|---|---|---|---|---|
| STAR02a | 0.01 | 0.15 | 1.2 | 82 | 8 |
| STAR05a | 0.04 | 0.44 | 2.1 | 62 | 28 |
| STAR10a | 0.10 | 0.71 | 1.7 | 62 | 13 |
| STAR15a | 0.12 | 0.79 | 2.0 | 67 | 16 |
| STAR20a | 0.18 | 0.93 | 1.6 | 68 | 10 |
| STAR25a | 0.22 | 0.94 | 1.7 | 71 | 9 |
| STAR30a | 0.23 | 0.91 | 1.6 | 72 | 8 |

**Table 4.2 Parameters used to obtain stretched exponential model fits to the annealed STAR neutron reflectometry data.**

| sample | $\phi_1$ | $t_1$/Å | $\sigma_1$/Å | $\phi_2$ | $t_2$/Å | $\sigma_2$/Å | $\phi_3$ | $t_3$/Å | $\chi^2$ |
|---|---|---|---|---|---|---|---|---|---|
| STAR02u | 0.11 | 55 | 23 | 0.01 | 29 | 12 | 0.02 | 2680 | 8 |
| STAR05u | 0.20 | 65 | 6 | 0.03 | 60 | 17 | 0.06 | 3270 | 36 |
| STAR10u | 0.22 | 56 | 2 | 0.07 | 40 | 17 | 0.10 | 2620 | 21 |
| STAR15u | 0.25 | 60 | 2 | 0.09 | 40 | 17 | 0.13 | 2540 | 10 |
| STAR20u | 0.32 | 67 | 2 | 0.08 | 17 | 22 | 0.19 | 2860 | 5 |
| STAR25u | 0.38 | 76 | 2 | 0.08 | 19 | 19 | 0.24 | 3000 | 6 |
| STAR30u | 0.55 | 50 | 6 | 0.24 | 119 | 16 | 0.25 | 2910 | 6 |

**Table 4.3 Parameters used to obtain three layer fits to the unannealed STAR neutron reflectometry data.**

Volume fraction profiles obtained from the fits are shown in figure 4.2 for the annealed samples and in figure 4.3 for the unannealed ones. In the unannealed samples the amount of segregation was quite small and block like when compared with the equilibrium structure, figure 4.4 shows the comparison between the annealed and unannealed samples. From the volume fraction profiles the bulk volume fraction, $\phi_b$, surface volume fraction, $\phi_s$, surface excess, z*, and the segregated layer thickness, L, were determined for the annealed samples and are given in table 4.4. The values for the unannealed samples are given in table 4.5 where $\phi_{dep}$ is the volume fraction in the depletion layer and $z^*_{total}$ the total surface excess determined from $\phi_{dep}$, $z^*_{dep}$ is an approximation of the size of the depleted region.

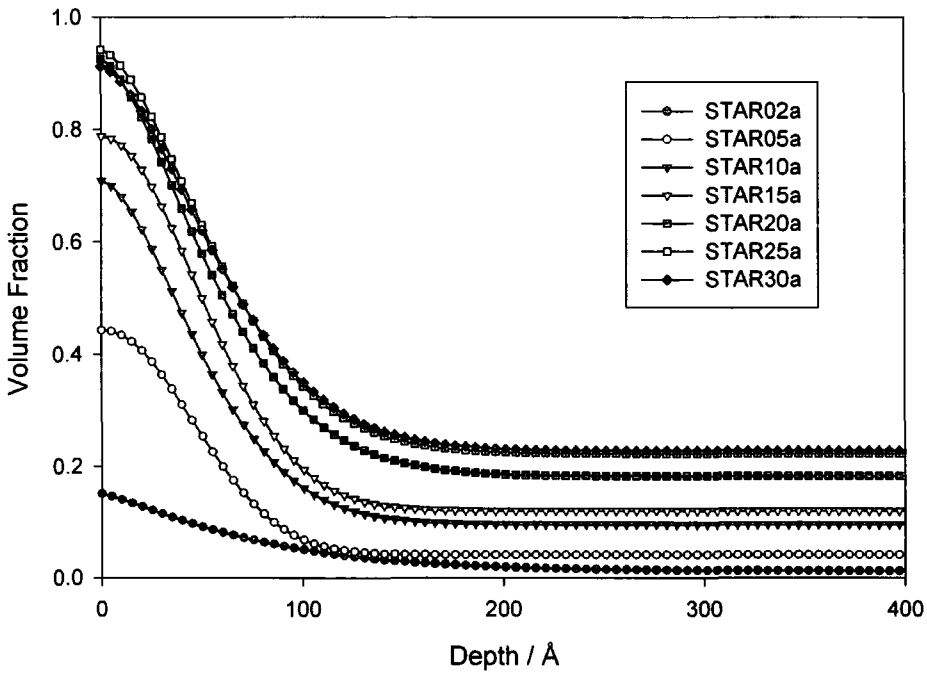


**Figure 4.2 Volume fraction profiles obtained for the STAR annealed samples from stretched exponential model fits to the data. Symbols are not data points but to guide the eye.**

| Sample | $\phi_b$ | $\phi_s$ | z*/Å | L/Å | σ |
|---|---|---|---|---|---|
| STAR02a | 0.01 | 0.15 | 11 | 62 | 0.002 |
| STAR05a | 0.04 | 0.44 | 22 | 53 | 0.004 |
| STAR10a | 0.10 | 0.71 | 34 | 50 | 0.006 |
| STAR15a | 0.12 | 0.79 | 40 | 57 | 0.008 |
| STAR20a | 0.18 | 0.93 | 45 | 55 | 0.009 |
| STAR25a | 0.22 | 0.94 | 45 | 57 | 0.009 |
| STAR30a | 0.23 | 0.91 | 44 | 58 | 0.008 |

**Table 4.4 Surface parameter values obtained from volume fraction profiles for the annealed STAR samples.**

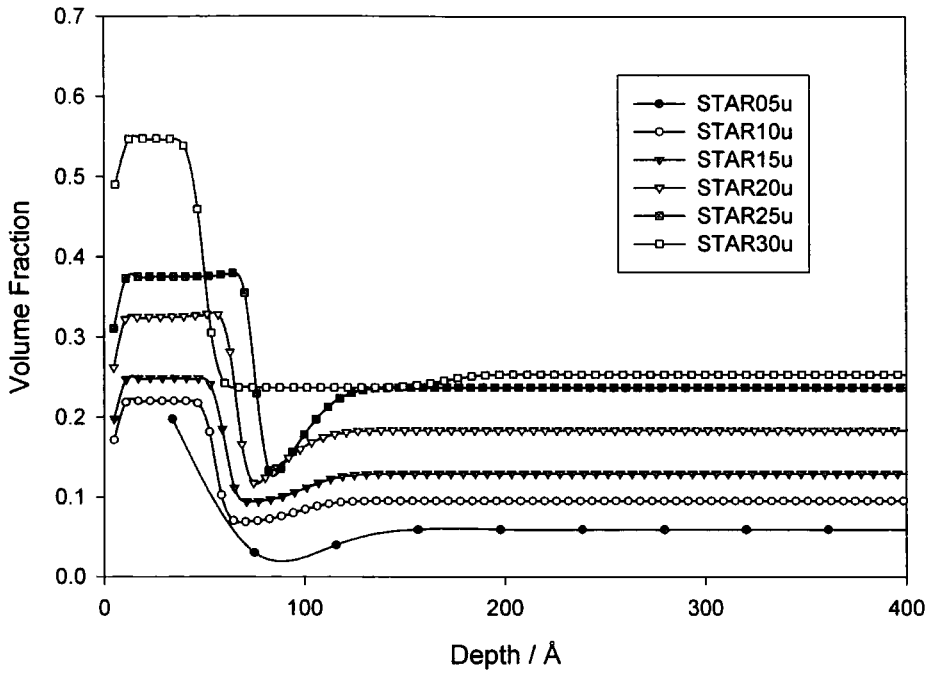


**Figure 4.3 Volume fraction profiles obtained for STAR unannealed samples using a three layer model to fit the data. Symbols are not data points but to guide the eye.**

| Sample | $\phi_b$ | $\phi_{dep}$ | $\phi_s$ | z*/Å | $z^*_{dep}$/Å | $z^*_{total}$/Å |
|---|---|---|---|---|---|---|
| STAR02u | 0.02 | 0.01 | 0.11 | 4 | 0.3 | 4.5 |
| STAR05u | 0.05 | 0.03 | 0.20 | 2 | 1.4 | 3.5 |
| STAR10u | 0.10 | 0.07 | 0.22 | 6 | 0.9 | 7.5 |
| STAR15u | 0.13 | 0.09 | 0.25 | 6 | 1.2 | 8 |
| STAR20u | 0.18 | 0.12 | 0.33 | 8 | 1.6 | 13 |
| STAR25u | 0.24 | 0.13 | 0.38 | 9 | 2.6 | 17 |
| STAR30u | 0.25 | 0.24 | 0.55 | 13 | 1.9 | 14 |

**Table 4.5 Surface parameter values obtained from volume fraction profiles for the unannealed STAR samples.**

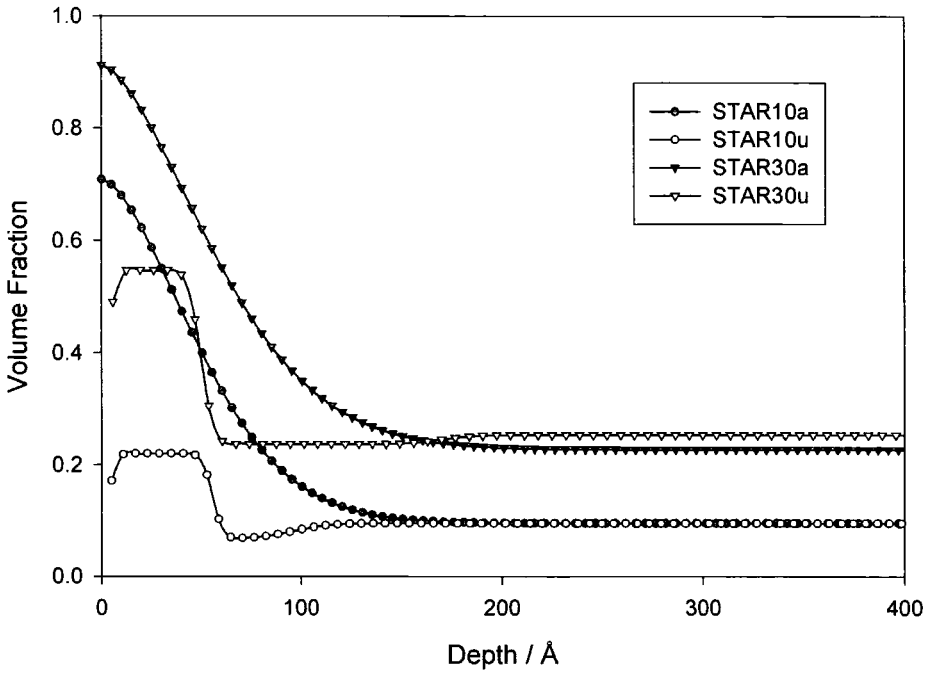


**Figure 4.4 Comparison of the volume fraction profiles for the unannealed and annealed STAR samples. Symbols to guide the eye.**

### 4.1.2 Small Angle Neutron Scattering

Small angle neutron scattering was carried out using LOQ at the Rutherford Appleton Laboratory to determine the radius of gyration of the polymer and also to ensure that aggregation was not occurring between the molecules. Polymer TK 200 STAR was blended with TK 241 hPS and four compositions were prepared. The small angle neutron scattering for each sample was measured at room temperature and at 413K. Table 4.6 gives the sample codes and volume fractions studied.

| Code | $\phi_{STAR}$ |
|---|---|
| STAR05 | 0.050 |
| STAR10 | 0.101 |
| STAR15 | 0.149 |
| STAR20 | 0.198 |

**Table 4.6 Sample codes and volume fractions used for LOQ analysis.**

The data were fitted to obtain the radius of gyration, $R_g$, using the scattering function for stars as described in chapter 2. It was assumed at the molecular weight used that the interaction parameter would be negligible. Figure 4.5 shows the small angle neutron scattering data and the fits obtained for the samples measured at 413K. There was no discernible difference in the samples measured at the two temperatures and the values of radius of gyration obtained did not vary with sample composition, the value obtained 67.8±2.5Å.

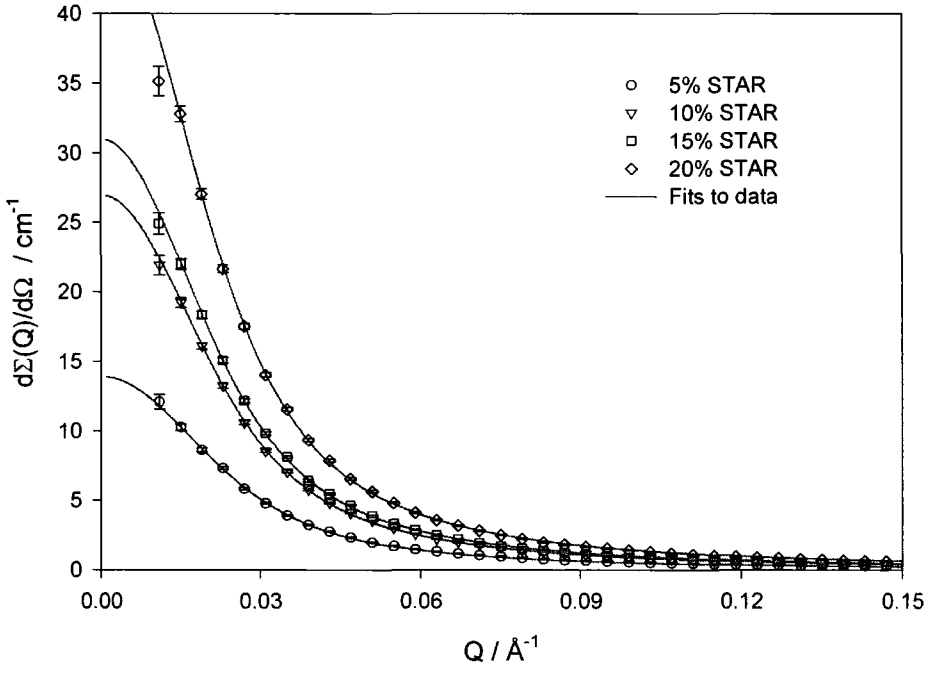


**Figure 4.5 Small angle neutron scattering data for the STAR polymer blends at 413K with fits to the data.**

Zimm and Stockmayer[1] showed that the ratio of the radius of gyration of a star molecule to that of a linear polymer of the same degree of polymerisation is equal to $\sqrt{\frac{3f-2}{f^2}}$, where f is the number of arms on the star. Hence, the radius of gyration was calculated for a monodisperse star[2] using $R_g = \sqrt{\frac{a^2}{6}\frac{(3f-2)}{f^2}N}$, where

a is the statistical step length (=6.7Å) and N is the degree of polymerisation of the star, the value obtained was 68Å, i.e. excellent agreement between theory and experiment. The agreement between theory and experiment and with no variation in $R_g$ with composition would suggest that there was no aggregation of the functional polymer, certainly over the concentration range studied.

Raphael et al[3] discussed the conformation of star molecules in a melt of chemically identical solvent where the solvent, P had a lower degree of polymerisation than the 'arm' of the star, $N_{arm}$. They found that in the limit $N_{arm} << f^{1/2}P^{3/4}$ that $R_g = aN_{arm}^{1/3}f^{1/3}$. For the system studied here although P (1150) was greater than $N_{arm}$ (266), the relation given above should hold and the radius of gyration so calculated was 62Å in satisfactory agreement with experimental data.

A master equation for the radius of gyration of a star calculated from the molecular weight, $M_w$ of the star molecule is, $R_g = KM_w^{\nu}f^{\beta}$. The factors K, ν and β are polymer specific and dependent upon the solvent conditions, for polystyrene under θ conditions they are 0.34, 0.50 and –0.346 respectively[4]. Assuming that a polymer in a chemically identical melt behaves as that in a θ solvent, the radius of gyration obtained is 69Å and again in excellent agreement with the experimental data.

## 4.2 Analysis and discussion of results

The surface composition profiles obtained have been compared with SCF theory predictions using LAYERS. For the calculations the degree of polymerisation of the segregating polymer, $N_D$, is required to calculate the sticking energy, $k_BT\beta$, and hence the value of $\left(\chi_e^b - \chi_e^s\right)$ to be used in calculations. For the calculations

only one plane of the lattice is used so $N_D$ for the STAR molecule was determined for one arm (= 266). Although 3 arms were emanating from the core, essentially one singly attached chain would be seen and no account was made for the fact that in the immediate vicinity of the core this assumption would not be true. From the previous chapter on the linear difunctional polymer blends a value of $(\chi_e^b - \chi_e^s) = 4.0$ gave good results for the experimental systems. Using this value as a starting point a value of $\beta = 1.91$ was obtained. To allow the calculations to converge successfully the degree of polymerisation values needed to be scaled down and hence values of $N_D = 50$, $N_H = 222$ and $(\chi_e^b - \chi_e^s) = 3.08$ were used. The results obtained gave profiles that matched the extent of the surface segregation well, but greatly underestimated the surface volume fraction and hence the surface excess values. The value of $(\chi_e^b - \chi_e^s)$ was varied whilst keeping $N_D$ and $N_H$ the same, and a value of 3.58 was found to match all the data well, just overestimating the surface excess for the highest bulk volume fraction samples. This gave a value of $(\chi_e^b - \chi_e^s) = 4.5$ and $\beta = 2.42$ for the experimental system. Figure 4.6 shows experimental profiles with theoretical comparisons using both $(\chi_e^b - \chi_e^s)$ values. The higher value of $(\chi_e^b - \chi_e^s)$ for essentially the same functional group indicates that the architecture of the polymer has increased the surface segregation compared to linear polymers.

The value of $(\chi_e^b - \chi_e^s)$ that gave the best theoretical comparison to the experimental volume fraction profile decreased with increasing bulk volume fraction. This would suggest that at low grafting densities the three arms enhance segregation, but at higher grafting densities this advantage is gradually lost due to the constraint on the configurational entropy of three polymer chains emanating from the same

point. For the STAR30a sample the value of $\left(\chi_e^b - \chi_e^s\right)$ was the same as that obtained for the difunctional linear polymers.

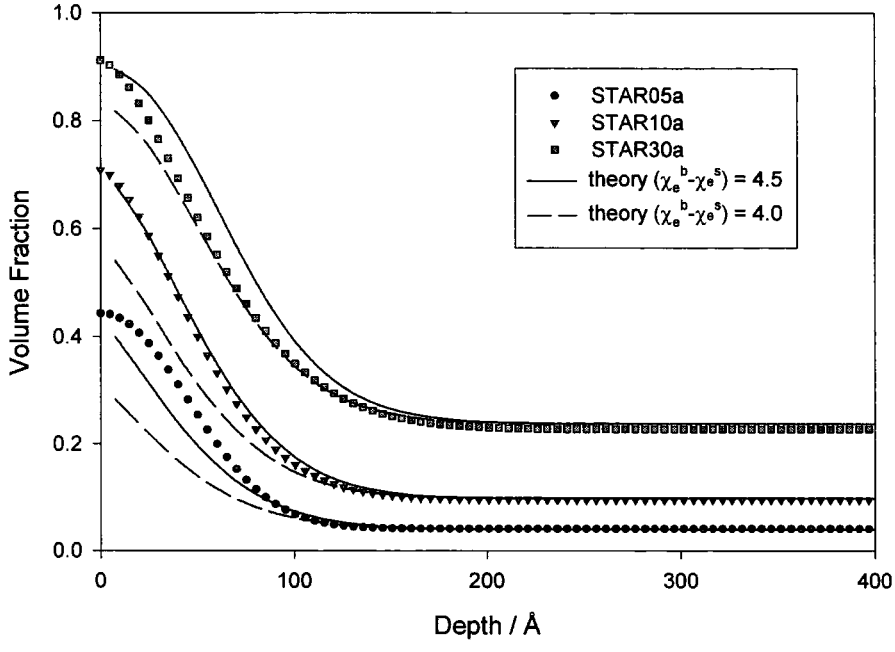


**Figure 4.6 Volume fraction profiles from stretched exponential fits to NR data (symbols) compared with theoretical predictions (lines).**

Figure 4.7 shows the experimental data points from the NR data with lines determined from theory using $\left(\chi_e^b - \chi_e^s\right) = 4.0$ and $\left(\chi_e^b - \chi_e^s\right) = 4.5$. The error bars for the experimental data were calculated from the standard deviation in the fitted parameters. The bulk volume fraction for the 10 and 15% samples show a greater error as the scattering length density of the bulk was about the same as that of the substrate giving poor contrast. There was some variation in the surface volume fraction values obtained which were partly due to differences in the model chosen and also possibly due to the fact that the core of the STAR is hydrogenous with a scattering length density of $\sim 1\times10^{-6}$Å$^{-2}$. If there were a layer of this core at the surface it would have the effect of reducing the volume fraction determined relative

to the actual volume fraction. Attempts were made to fit a three layer model at the air surface to account for a lower scattering length density layer. Fits with a ~10Å layer of a scattering length density around 10% less than the peak value were obtained but gave no significant improvement in the quality of the fit.

Walton and Mayes[5] carried out a self consistent mean field theory treatment of branched polymers in a linear polymer matrix and found that configurational entropy caused branched chains to segregate to the surface more favourably than a linear polymer chain, with the chain ends segregating to the surface. This might account for the apparent increase in the sticking energy of the functional group as the chain ends would enhance the segregation of the polymer to the surface. Walton and Mayes also showed that there is a maximum in the volume fraction profile that disappears when the number of branches is small or the branch length is long. For the STAR polymer used here with only 3 arms their results would not predict a maximum, but this possibility would also account for the degree of uncertainty in the shape of the profile at the immediate surface.

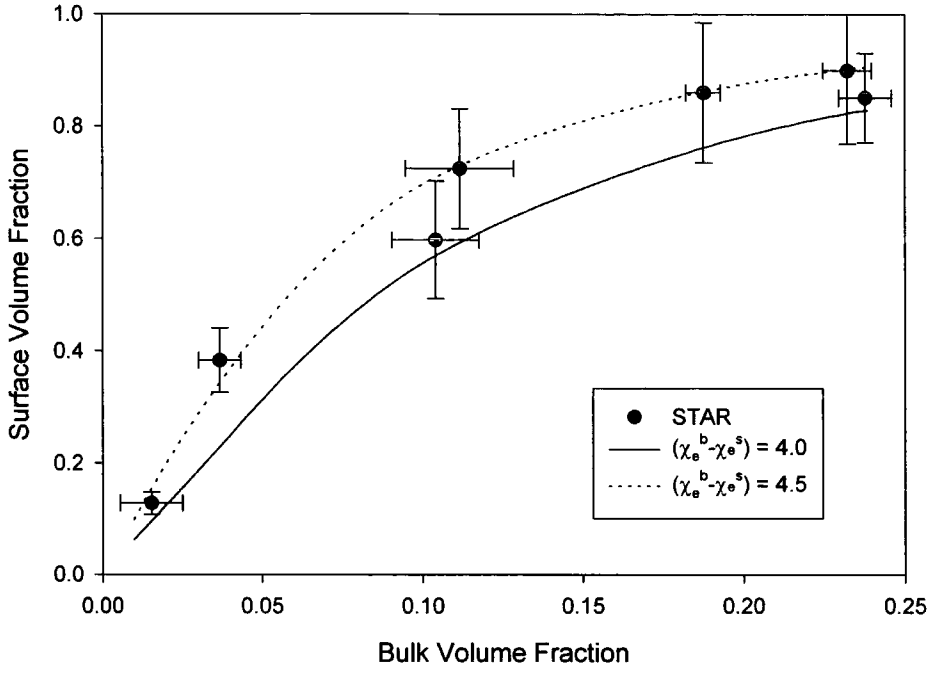


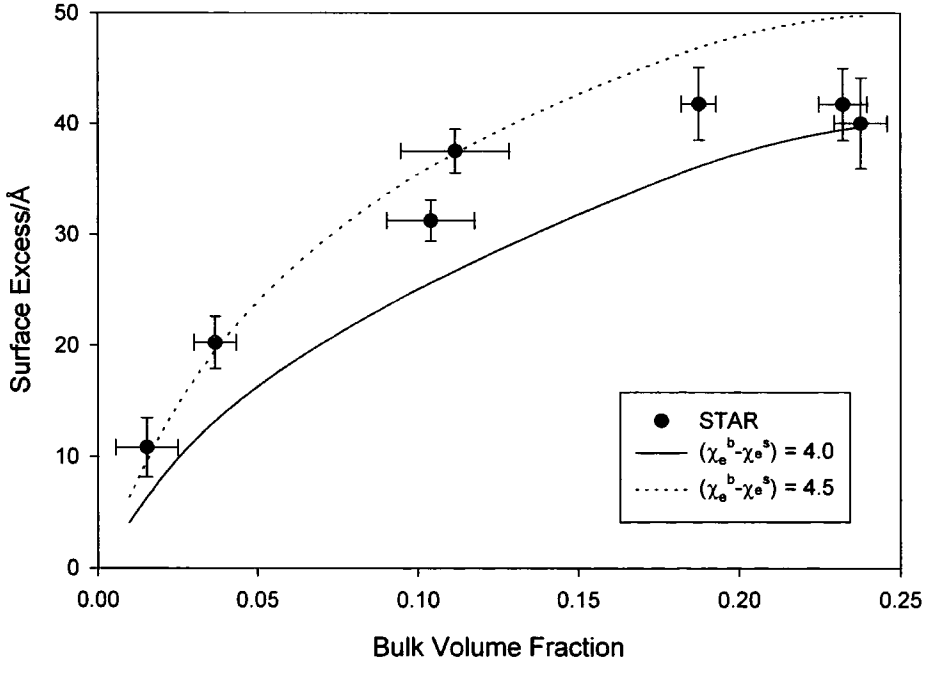


**Figure 4.7 Parameters from the NR fits to the STAR annealed data with lines from SCF theory calculations.**

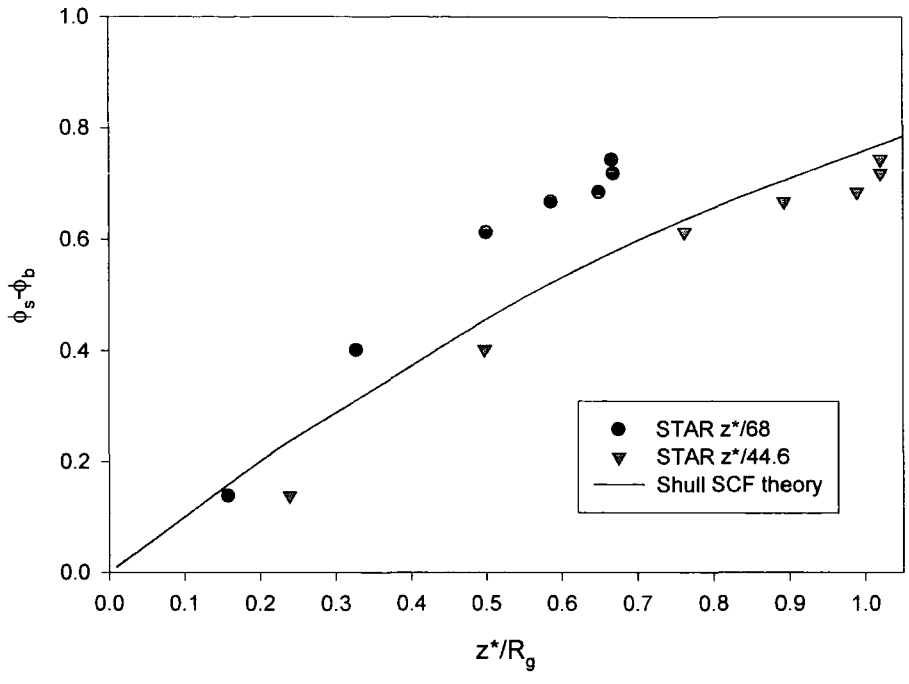


**Figure 4.8 The difference in equilibrium surface volume fraction and bulk volume fraction against normalised excess, $z^*/R_g$ for the STAR polymer. Line is from Shull's SCF theory predictions for the dry brush limit.**

Figure 4.8 shows ($\phi_s$ - $\phi_b$) against the normalised excess using the radius of gyration determined for a single arm (44.6Å) and that of the whole molecule (68Å) compared with SCF theory predictions[6]. The data normalised by the $R_g$ of the arm follow the theory well, which supports the use of the arm degree of polymerisation for carrying out the LAYERS calculations. Taking the polymer as a whole, the STAR polymer gave a higher ($\phi_s$ - $\phi_b$) for the same normalised excess than the linear difunctional polymers.

The surface grafting density, $\sigma = z^*/aN_D$, requires the degree of polymerisation of the segregating polymer, in this case it could be the arm or the whole molecule, values range from 0.006 to 0.026 for the arm and 0.002 to 0.009 for the molecule. Whichever method was used the values all fell into the unstretched dry brush regime from scaling predictions and the scaling behaviour of the brush height with surface grafting density was the same. Figure 4.9 shows the brush height against

the dimensionless grafting density calculated using the degree of polymerisation of the whole molecule on a log-log plot, and shows that the brush height was not dependent upon the grafting density as is predicted in the unstretched brush regime. The average brush height obtained was 62±2Å and is of the order of the radius of gyration of the molecule. However, if the polymer has attached to the surface by the functional core to give the brush like behaviour that is seen, then the layer thickness would be expected to be of the order of the radius of gyration of the arm (44.6Å). This might suggest that the local confinement of three chains from one attachment point has caused the chains for individual molecules to stretch away from the surface. If this was the case the extent of stretching was only dependent upon localised confinement and not the grafting density of individual molecules.

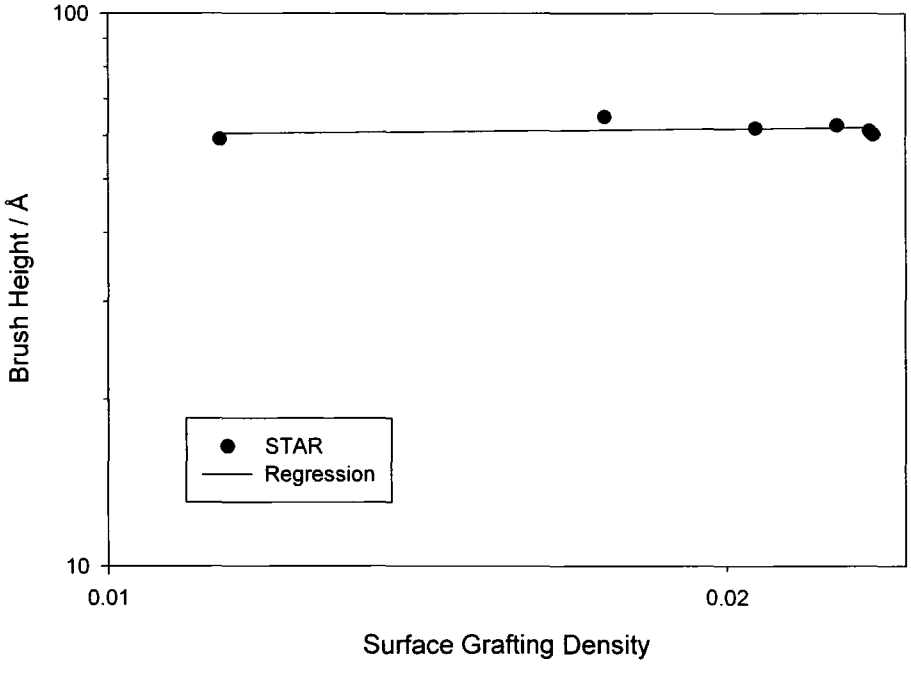


**Figure 4.9 Variation in the brush height with surface grafting density for the annealed STAR polymer blends.**

Zhulina and Vilgis[7] looked at the scaling behaviour of polymer brushes formed by branched polymers in solution. They found that branched polymers

attached at a surface followed conventional σ dependencies similar to those predicted for linear chains of degree of polymerisation of the arm, N/f. It would appear that this holds for stars in polymer matrices, as here, but as the scaling behaviour observed was only for the unstretched brush regime this cannot be said definitively.

The normalised surface excess is shown plotted against the bulk volume fraction, figure 4.10, with lines to show the values obtained for the linear difunctional polymers, 50k dPSF2 in 50k hPS (L2F) and the 100k dPSF2 in 52k and 100k hPS matrices. There was little difference in the profile obtained to that of the 100k dPSF2 in 100k hPS when the radius of gyration of the molecule was used. If the radius of gyration of the arm was used the normalised excess would be greater than that of the linear polymer blends. However, when comparing against other polymer architectures the value for the whole molecule should be used.

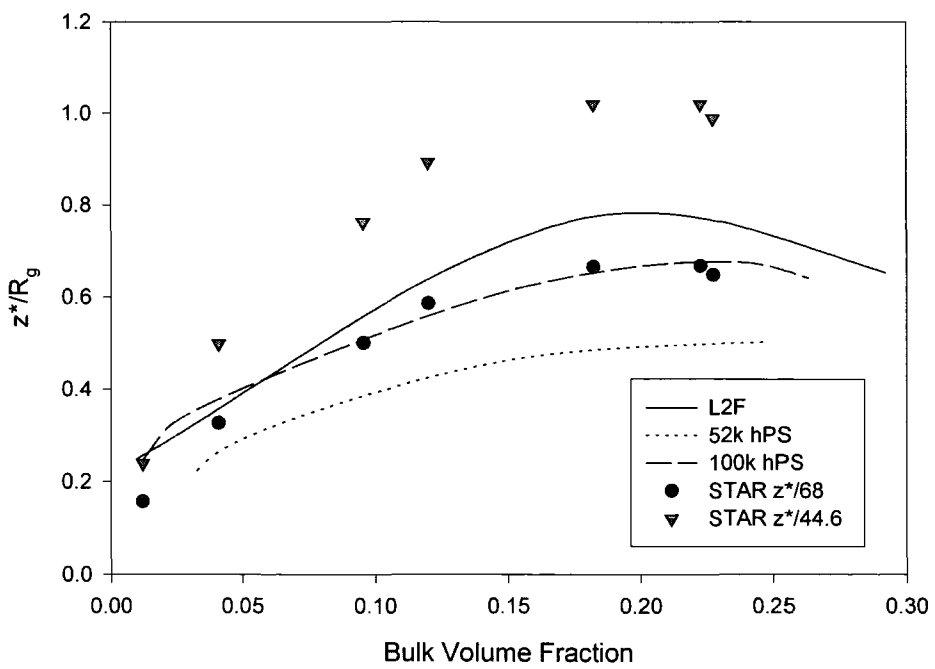


**Figure 4.10 Normalised excess against equilibrium bulk volume fraction for the STAR polymer. Lines are from the dPSF2 samples.**

Hence, from these experiments, considering the more complex synthesis required for the STAR polymer, there would appear to be no obvious advantage in using the STAR polymer over the functionalised linear polystyrene. These measurements only consider the amount of deuterated polymer in the surface layer and do not measure the amount of functionality at the surface, which would be important if a low energy surface was required.

## 4.3 References


1 B. H. Zimm and W. H. Stockmayer, *Journal of Chemical Physics*, 1949, **17**, 1301.

2 W. Burchard, 'Applied Fibre Science', ed. F. Happey, Academic Press, 1978.

3 E. Raphael, P. Pincus, and G. H. Fredrickson, *Macromolecules*, 1993, **26**, 1996.

4 G. S. Grest, L. J. Fetters, J. S. Huang, and D. Richter, in 'Star Polymers: Experiment, Theory, and Simulation', *Advances in Chemical Physics*, ed. I. Prigogine and S. A. Rice, 1996, **94**.

5 D. G. Walton and A. M. Mayes, *Physical Review E*, 1996, **54**, 2811.

6 K. R. Shull, *Journal of Chemical Physics*, 1991, **94**, 5723.

7 E. B. Zhulina and T. A. Viligis, *Macromolecules*, 1995, **28**, 1008.

# CHAPTER 5

## Multiple Fluorine Labelled Polymer

## 5.1 Experimental Results

The second fraction of TK 213 MFL was taken and blended with PL 330 hPS. Table 5.1 gives the range of volume fractions used and the codes assigned. Films were spun at 3500 rpm from 3% solution in toluene and samples with an average thickness of 2000Å were prepared for NRA whilst those for NR were 1700Å thick. Thinner films of this blend were prepared as the higher molecular weight of the polymers made them more stable to annealing. A sample of each blend was annealed to equilibrium at a temperature of 415K, with an unannealed sample prepared for comparison.

| Code | $\phi_{MFL}$ |
|---|---|
| MFL02 | 0.020 |
| MFL05 | 0.050 |
| MFL10 | 0.100 |
| MFL15 | 0.150 |
| MFL20 | 0.200 |
| MFL25 | 0.250 |
| MFL30 | 0. 300 |

**Table 5.1: Codes and volume fractions used for the multiple fluorine labelled blends**

### 5.1.1 Nuclear Reaction Analysis

NRA data were obtained at an incident beam angle of 9°, no data were obtained for MFL02 due to time constraints. The NRA profiles after normalisation are shown in figure 5.1 for the unannealed and annealed pairs and in figure 5.2 to show the variation with bulk volume fraction. In contrast to the difunctional polymers, segregation could be seen more clearly in the higher volume fraction samples. There was clear segregation to the air/polymer interface and there was some evidence of segregation to the polymer/substrate interface (particularly seen in

MFL15 and MFL20). The MFL25 samples were much thicker (3450Å), so at 9° incidence the beam did not penetrate through to the substrate.

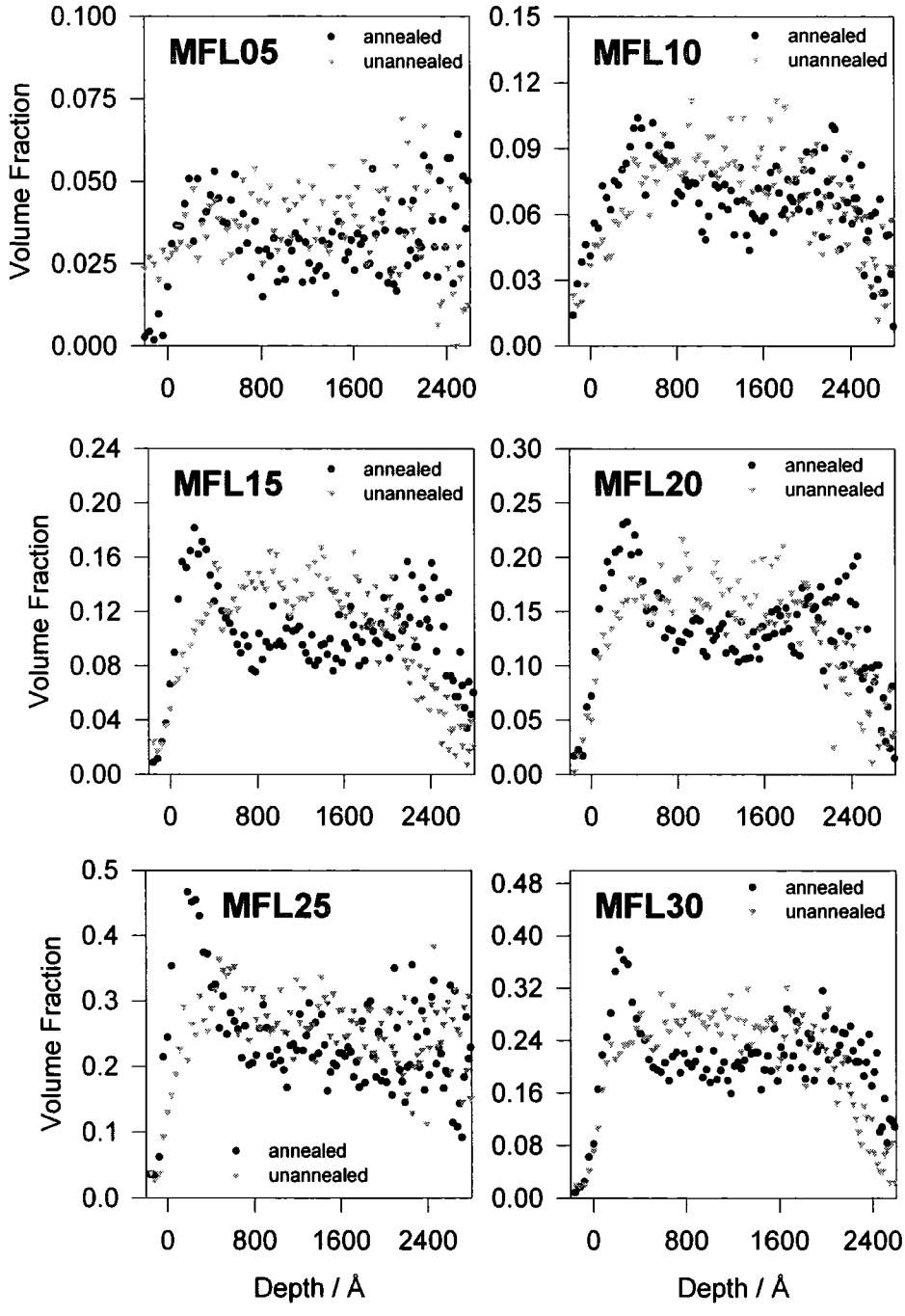


**Figure 5.1 Volume fraction profiles for MFL samples by NRA showing the comparison between the annealed and unannealed samples.**

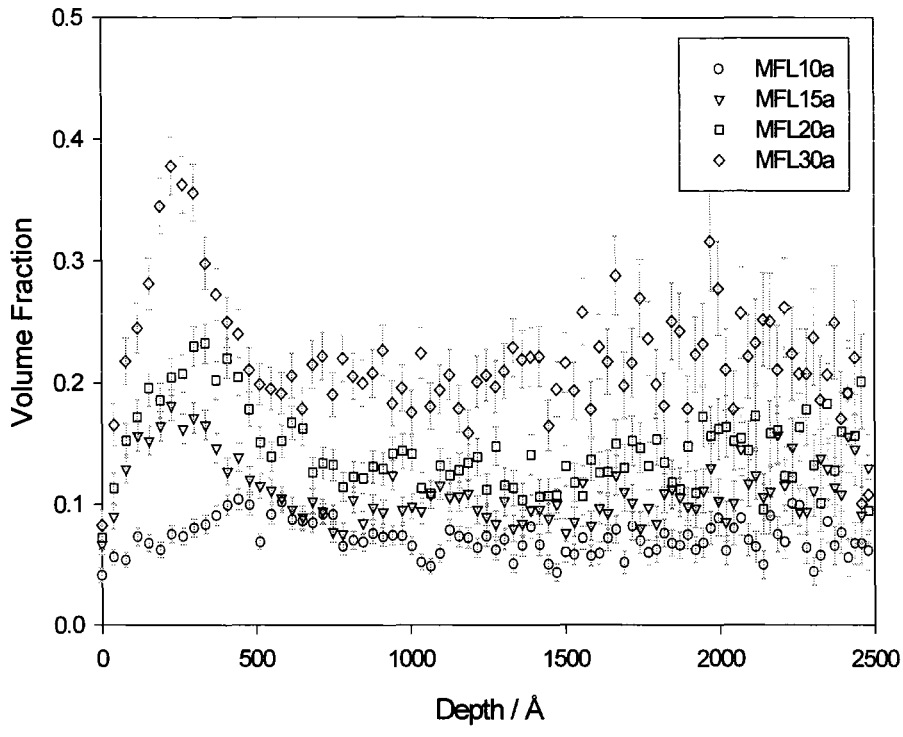


**Figure 5.2 Volume fraction profiles obtained from NRA showing the effect of bulk volume fraction on the annealed samples.**

The data were rather noisy, increasingly so as the beam penetrated further into the sample, which meant that obtaining quantitative data was difficult. The data were analysed using the data analysis and graphics package, GENPLOT to obtain the bulk, $\phi_b$, air, $\phi_{air}$ and substrate, $\phi_{Si}$ volume fractions directly and the surface excess at the air, $z^*_{air}$ and substrate, $z^*_{Si}$ interfaces by numerical integration. The values obtained are given in table 5.2 and are shown plotted in figures 5.3 and 5.4. The values obtained follow the same trend as the NR data given later, but the values were generally much lower especially the volume fraction data. This was largely due to the poorer resolution of the NRA measurement compared to NR. MFL25a agreed most closely with the NR results and this sample data was obtained separately from the other samples and at a time when the beam was well defined and hence gave better resolution.

| Sample | $\phi_b$ | $\phi_{air}$ | $\phi_{Si}$ | $z^*_{air}$/Å | $z^*_{Si}$/Å |
|---|---|---|---|---|---|
| MFL05a | 0.03 | 0.05 | 0.05 | 10 | 10 |
| MFL10a | 0.06 | 0.10 | 0.09 | 17 | 8 |
| MFL15a | 0.09 | 0.17 | 0.14 | 31 | 21 |
| MFL20a | 0.12 | 0.22 | 0.18 | 41 | 17 |
| MFL25a | 0.21 | 0.58 | - | 73 | - |
| MFL30a | 0.19 | 0.37 | 0.24 | 46 | 18 |

**Table 5.2 Surface parameter values obtained directly from NRA profiles.**

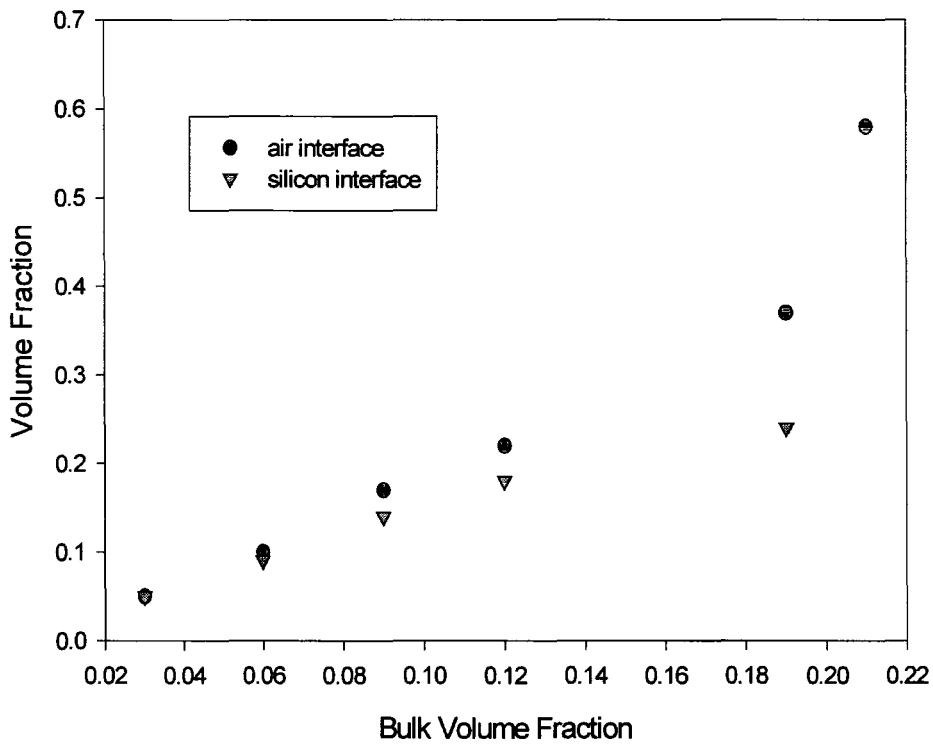


**Figure 5.3 Volume fraction data obtained from NRA profiles at the air (circles) and substrate (triangles) interfaces.**

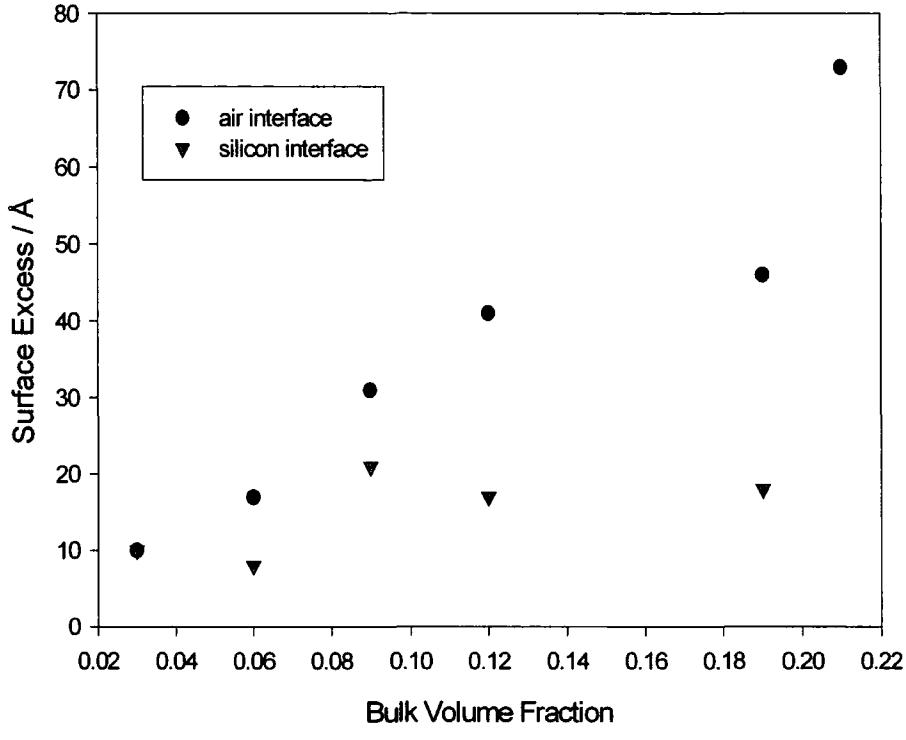


**Figure 5.4 Surface excess values obtained from NRA profiles at the air (circles) and substrate (triangles) interfaces.**

As already mentioned the experimental data are convoluted with the resolution function of the instrument. No attempt was made to deconvolute the resolution from the data, but the data were further analysed by using the program FITTER. This program convolutes a tanh function with the instrumental resolution function, the resultant function then non-linearly least squares fitted to the data at the air surface. The parameters used to obtain the fits are given in table 5.3, $\phi_b$ is the bulk volume fraction, $\phi_a$ is the approximate surface volume fraction, height is the thickness of the brush layer, width the width of the interface between the brush and the bulk polymer. Offset is used to adjust the starting position of the fitted profile to the experimental data and the resolution is the standard deviation of the Gaussian resolution function, examples of the fitted profiles are shown in figure 5.5.

Unfortunately the loss of resolution with depth into the sample, meant that the data at the silicon substrate were too noisy for functional form fits to be carried out.

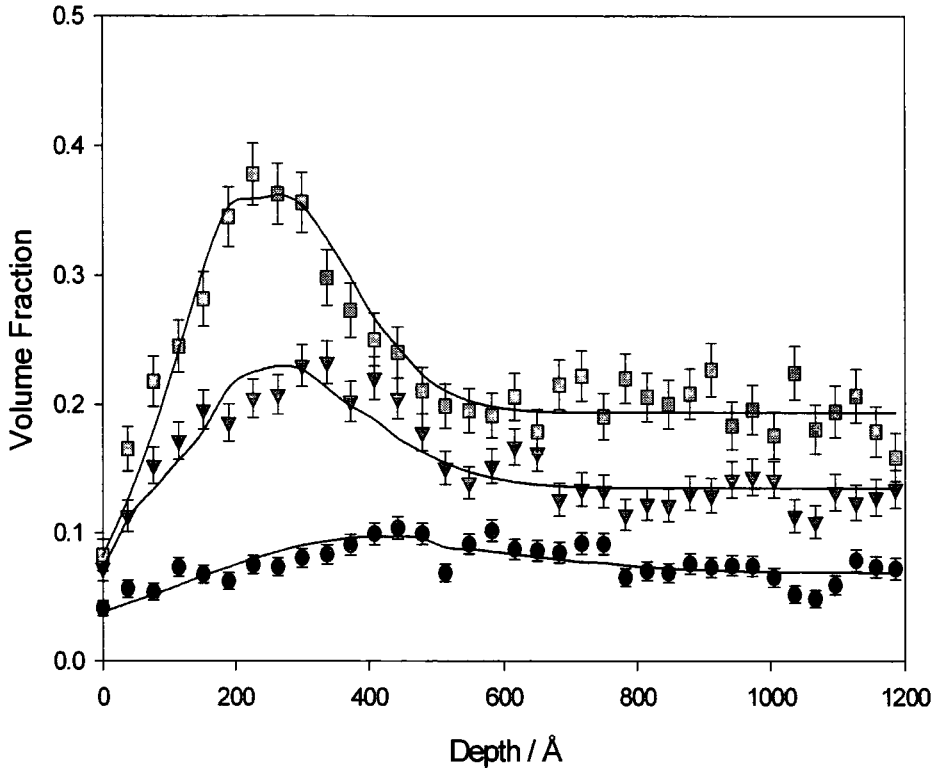


**Figure 5.5 NRA data for MFL30a, MFL20a and MFL10a showing fits obtained to the data**

| Sample | $\phi_b$ | $\phi_a$ | height/Å | width/Å | offset/Å | Resolution /Å |
|---|---|---|---|---|---|---|
| MFL05a | 0.03 | 0.16 | 116 | 30 | 195 | 202 |
| MFL10a | 0.07 | 0.37 | 102 | 38 | 224 | 250 |
| MFL15a | 0.10 | 0.52 | 102 | 41 | 138 | 156 |
| MFL20a | 0.14 | 0.85 | 66 | 100 | 144 | 154 |
| MFL25a | 0.25 | 1.10 | 70 | 221 | 32 | 50 |
| MFL30a | 0.20 | 0.96 | 97 | 94 | 128 | 150 |

**Table 5.3 Parameters used to obtain tanh functional form fits to NRA data for the annealed MFL samples.**

The magnitude of the resolution meant that obtaining the accurate shape of the volume fraction profiles was not possible. In fact the fits obtained, especially for the lower volume fractions were very block like, but should still give an accurate

representation of the values of the surface excess. From the fits the surface composition profiles were determined and the values of bulk, $\phi_b$ and surface, $\phi_s$ volume fraction and the surface excess, z* were obtained. These values are given in table 5.4 and figure 5.6 shows the comparison in the values of the surface excess obtained from NRA and NR (discussed in section 5.1.2). The agreement is very good and certainly within the error of the two techniques.

| Sample | $\phi_b$ | $\phi_s$ | z*/Å |
|---|---|---|---|
| MFL05a | 0.035 | 0.17 | 15.8 |
| MFL10a | 0.07 | 0.37 | 30.4 |
| MFL15a | 0.10 | 0.52 | 42.9 |
| MFL20a | 0.14 | 0.80 | 48.3 |
| MFL25a | 0.25 | 0.91 | 71.3 |
| MFL30a | 0.20 | 0.95 | 74.7 |

**Table 5.4 Surface parameters obtained from the fits to the MFL annealed samples.**

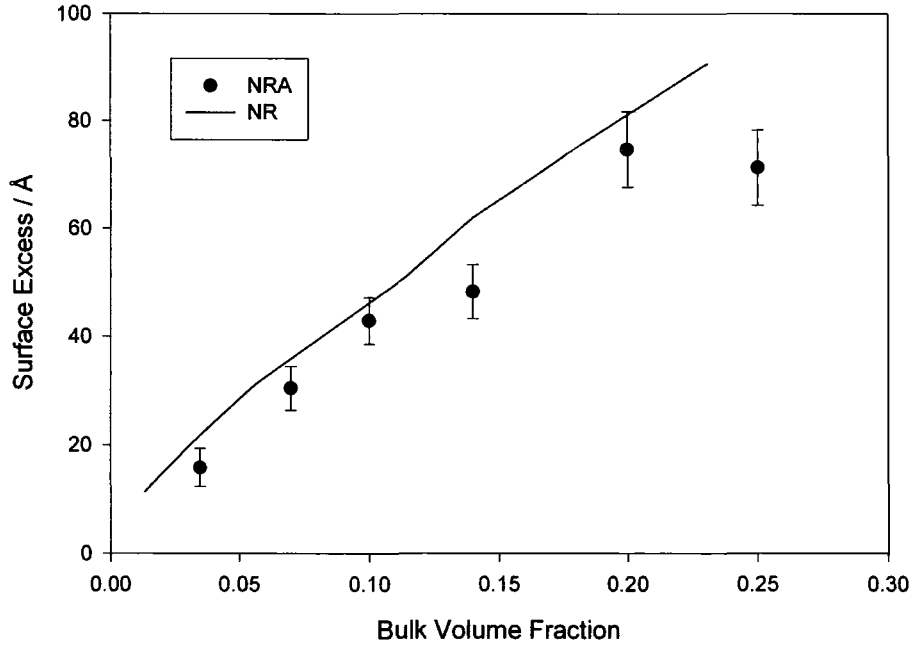


**Figure 5.6 Surface excess values determined from the fits to the NRA data with the line showing the comparison to the NR data.**

### 5.1.2 Neutron Reflectometry

NR data were collected using CRISP at the Rutherford Appleton Laboratory; samples were analysed at two different angles, 0.25 and 0.6°, using the multidetector. The oxide layer on the substrate affected the reflectivity of these thinner samples and was taken into account during data analysis. For the unannealed samples there was no evidence of segregation from VOLFMEM analysis so these samples were not analysed further. Functional form fitting (tanh and stretched exponential) to the annealed samples did not prove successful, the quality of the best fit obtained was poor ($\chi^2$ values obtained approximately double) compared to those from four layer models (both PCMULF and helix3) and VOLFMEM. The comparison in the fits obtained is shown for MFL30a in figure 5.7a along with the comparison in the volume fraction profiles for MFL10a, MFL20a and MFL30a in figure 5.7b. The volume fraction profiles follow the same general profile, however the surface excess is over estimated in the exponential profile and the sample decays to the bulk volume fraction too quickly. Initially four layers were used because it was thought that if the functional groups were all located at the air interface, the top layer could have a lower scattering length density. This did not prove to be the case, but it was found that the surface segregation was best fitted with a top layer of ~65Å at a high volume fraction of functional polymer followed by a thicker layer of approximately twice the bulk volume fraction. The thickness of this second layer increased as the bulk volume fraction was increased. A segregated layer of much lower surface excess was included at the substrate interface, but the reflectivity was less sensitive to variations in this layer. The reflectivity data and four layer fits are shown in figure 5.8.

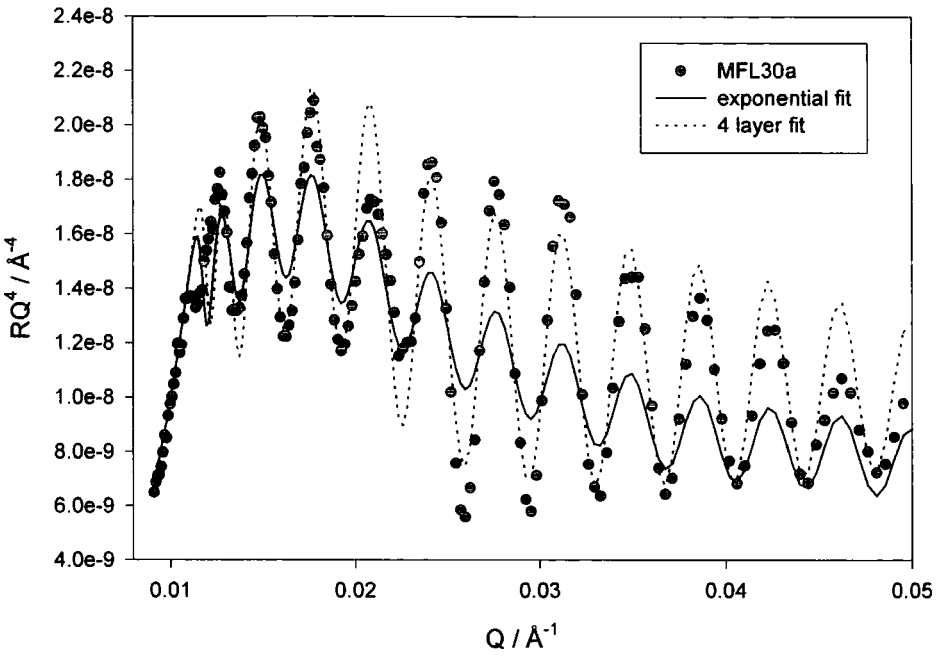


**Figure 5.7a Comparison in the fits obtained for sample MFL30a using and exponential model and a 4 layer fit, shown on a $RQ^4$ plot for clarity.**

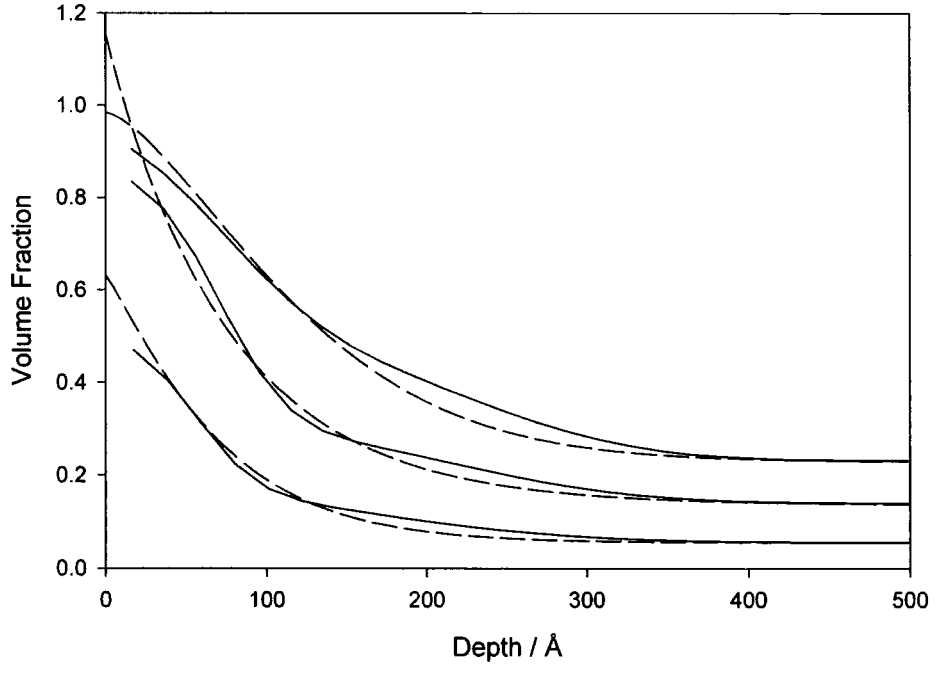


**Figure 5.7b Comparison in the volume fraction profiles obtained using an exponential model (dashed line) and a 4 layer model (solid line) for MFL30a, MFL20a and MFL10a respectively from the top.**

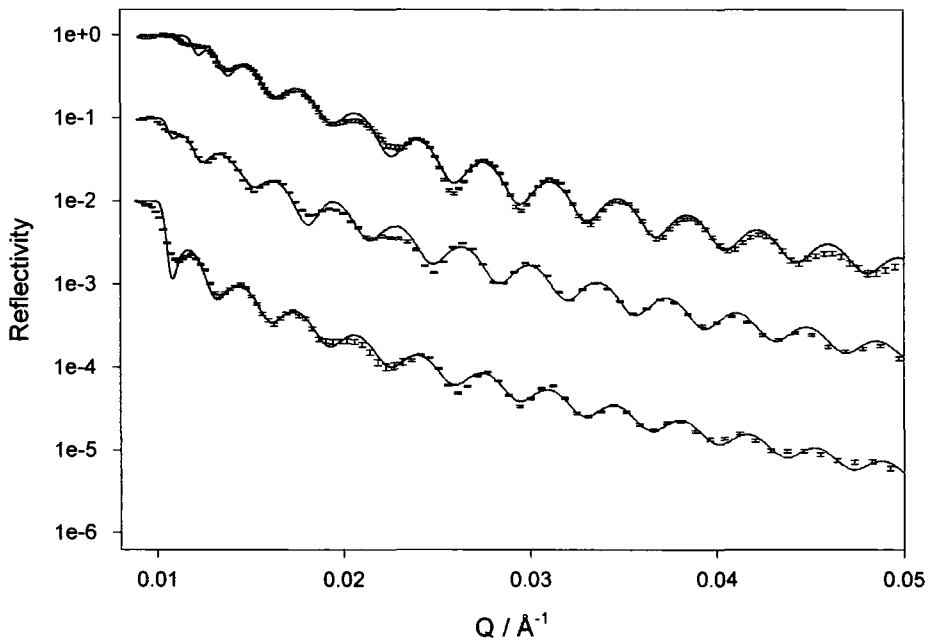


**Figure 5.8a Reflectivity profiles for (from the top) MFL30a, MFL20a and MFL10a, showing 4 layer fits to the data. Subsequent data sets offset by a factor of 10 for clarity.**

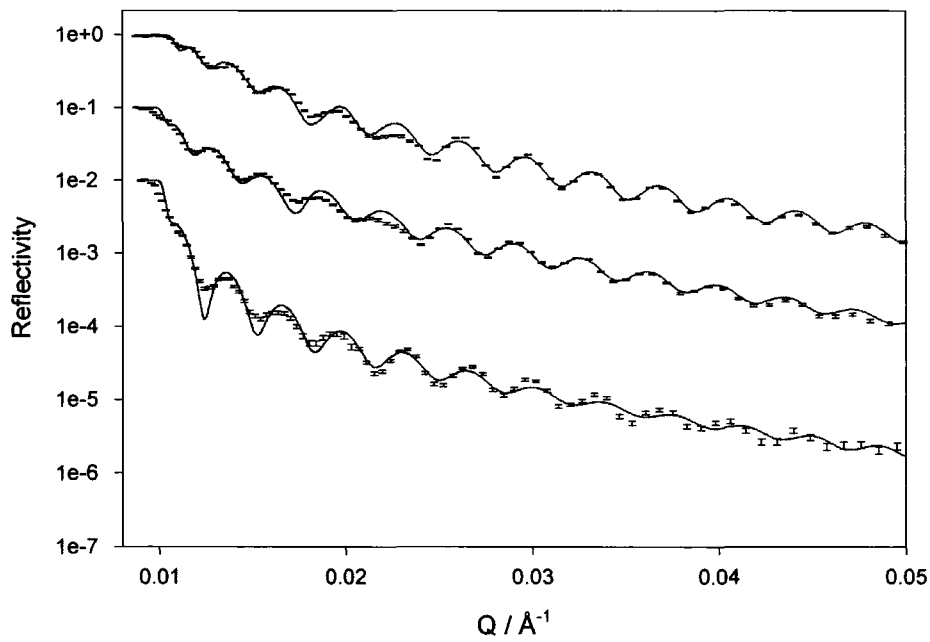


**Figure 5.8b Reflectivity profiles for (from the top) MFL25a, MFL15a and MFL02a, showing 4 layer fits to the data. Subsequent data sets offset by a factor of 10 for clarity.**

The parameters used to obtain the fits to the data are given in table 5.5, $\phi$ is the volume fraction, t is the layer thickness, $\sigma$ is the roughness between the layer and the succeeding layer and $\chi^2$ is the normalised chi squared goodness of fit. The subscript is the number of the layer with 1 being the uppermost layer. The normalised chi squared values for the fits to these data were not as good as those obtained for other experimental systems with values ~20. The reason for this was an apparent mismatch in the resolution of the data at the low angle compared to the data obtained at the higher angle, particularly evident at the region of overlap (Q = 0.020 to 0.028Å$^{-1}$). This was thought to be due to large-scale ripples on the surface of the polymer layer, which have a greater affect on the reflectivity at lower incidence angles than at higher angles.

| MFL | $\phi_1$ | $t_1$/Å | $\sigma_1$/ Å | $\phi_2$ | $t_2$/Å | $\sigma_2$/Å | $\phi_3$ | $t_3$/Å | $\sigma_3$/Å | $\phi_4$ | $t_4$/Å | $\chi^2$ |
|---|---|---|---|---|---|---|---|---|---|---|---|---|
| 02a | 0.12 | 91 | 16 | 0.06 | 39 | 104 | 0.01 | 1600 | 158 | 0.06 | 52 | 31 |
| 05a | 0.41 | 49 | 32 | 0.18 | 40 | 146 | 0.02 | 1530 | 108 | 0.09 | 101 | 19 |
| 10a | 0.52 | 61 | 35 | 0.20 | 80 | 138 | 0.05 | 1560 | 7 | 0.17 | 29 | 26 |
| 15a | 0.80 | 63 | 37 | 0.25 | 81 | 176 | 0.11 | 1480 | 7 | 0.26 | 38 | 15 |
| 20a | 0.88 | 72 | 38 | 0.32 | 146 | 107 | 0.14 | 1360 | 5 | 0.38 | 44 | 10 |
| 25a | 0.94 | 76 | 38 | 0.35 | 163 | 121 | 0.17 | 1390 | 3 | 0.55 | 30 | 8 |
| 30a | 1.00 | 72 | 65 | 0.50 | 158 | 99 | 0.23 | 1320 | 5 | 0.51 | 53 | 21 |

**Table 5.5 Parameters used to obtain four layer fits to the neutron reflectometry data for the annealed MFL samples.**

Volume fraction composition profiles were constructed from the parameters obtained from the 4 layer fits. Figure 5.9 shows the profiles obtained using PCMULF for some of the samples, comparisons with VOLFMEM were very good and an example was given in section 2.5.1, figure 2.9. The bulk, $\phi_b$, air, $\phi_{air}$ and substrate, $\phi_{Si}$ volume fractions and the surface excess at the air, $z^*_{air}$ and substrate, $z^*_{Si}$ interfaces

were determined from these profiles and are given in table 5.6. The surface excess values determined from all three fitting methods are shown plotted in figure 5.10 with lines showing the values from NRA data.

| Sample | $\phi_b$ | $\phi_{air}$ | $\phi_{Si}$ | $z^*_{air}$/Å | $z^*_{Si}$/Å |
|---|---|---|---|---|---|
| MFL02a | 0.01 | 0.12 | 0.06 | 11 | 3 |
| MFL05a | 0.03 | 0.33 | 0.09 | 21 | 6 |
| MFL10a | 0.06 | 0.47 | 0.17 | 32 | 2 |
| MFL15a | 0.11 | 0.74 | 0.26 | 48 | 4 |
| MFL20a | 0.14 | 0.84 | 0.38 | 71 | 7 |
| MFL25a | 0.18 | 0.91 | 0.55 | 76 | 12 |
| MFL30a | 0.23 | 0.91 | 0.51 | 91 | 16 |

**Table 5.6 Surface parameters determined from the composition profiles from PCMULF fits to NR data for MFL samples.**

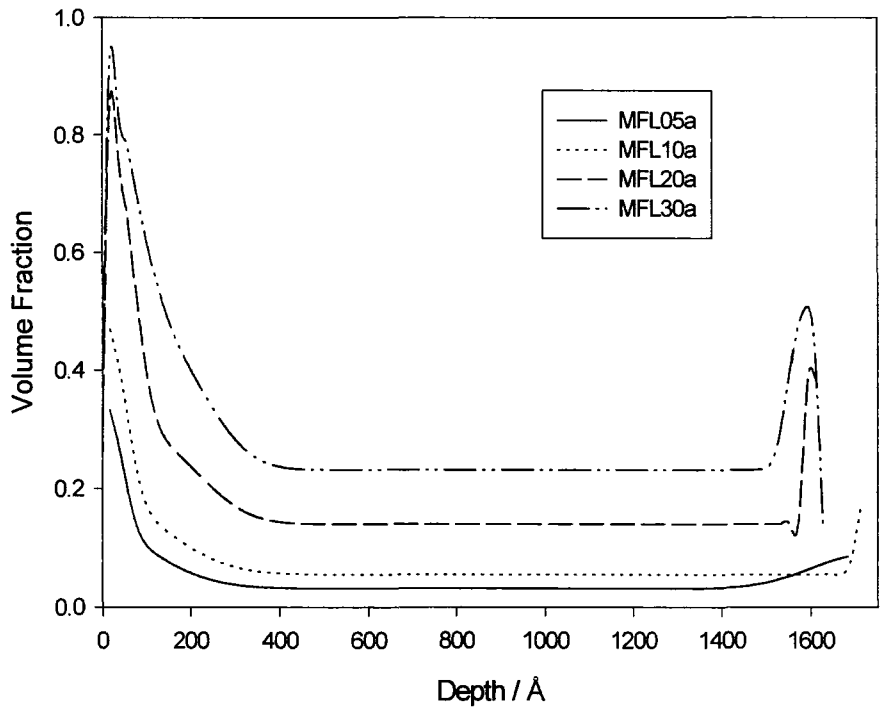


**Figure 5.9 Composition profiles for MFL30a, MFL20a, MFL10a and MFL05a obtained from PCMULF fits to the data.**

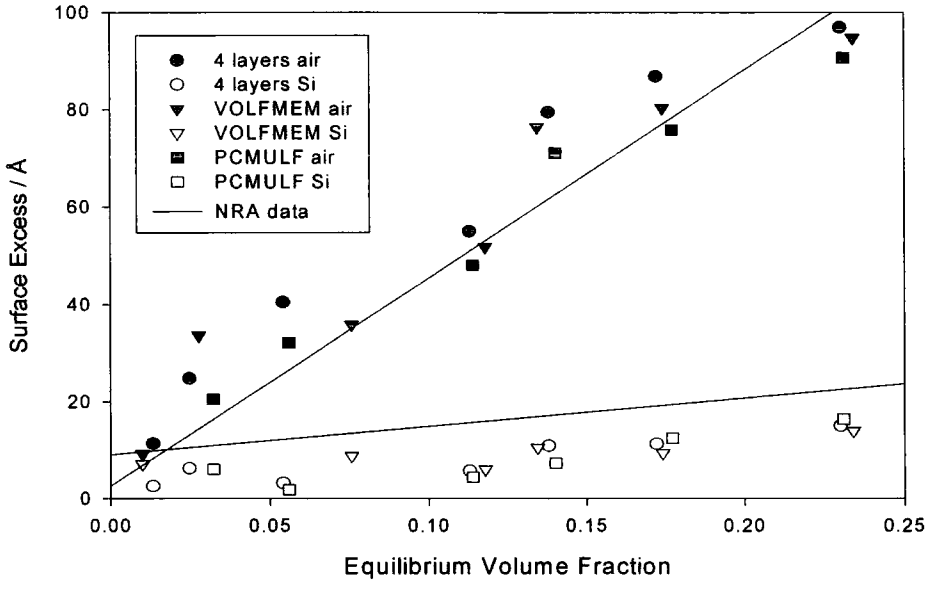


**Figure 5.10 Surface excess values determined from the surface composition profiles for MFL samples. Symbols are for the values obtained by the various fitting programs and the line is the comparison with NRA.**

The surface excess values from the different NR fitting methods were in good agreement, PCMULF gave generally lower values partly because the profiles were convoluted with a 5Å surface roughness, and also the profile had a restricted number of data points which limited the accuracy. The surface excess at the silicon interface was generally lower than that found for the samples measured using NRA. The NR fits are less sensitive in this region when there is a large excess at the air surface, and the NRA data had poor resolution at the substrate interface at the incident angle used giving large errors in the actual values determined.

## 5.2 Analysis and discussion of results

Balazs and co-workers[1-5] have theoretically investigated a variety of polymer structures, diblock, random, alternating and branched copolymers at polymer-polymer interfaces, which have the ability to act as a compatibiliser

between two immiscible polymers reducing the interfacial tension and improving the strength of the interface between the polymers. In these experiments discussed here, the aim was to investigate the segregation of low energy functional groups to the surface and to compare the extent of the segregation with respect to the other architectures studied. The aim had been to have a molecular weight of ~100000 so direct comparison between the H2F and STAR polymer systems could be made but unfortunately the synthesis was more difficult than anticipated and the resulting molecular weight of the polymer was 364000.

Di Marzio[6] et al showed that a polymer chain with a few strong bonds (sparse but strong bonds, SBSB) has a different adsorption profile at the surface than an equivalent polymer chain with an averaged bond attraction to the surface. They predicted that block and random copolymers would show different behaviour from each other and from that of linear homopolymer chains.

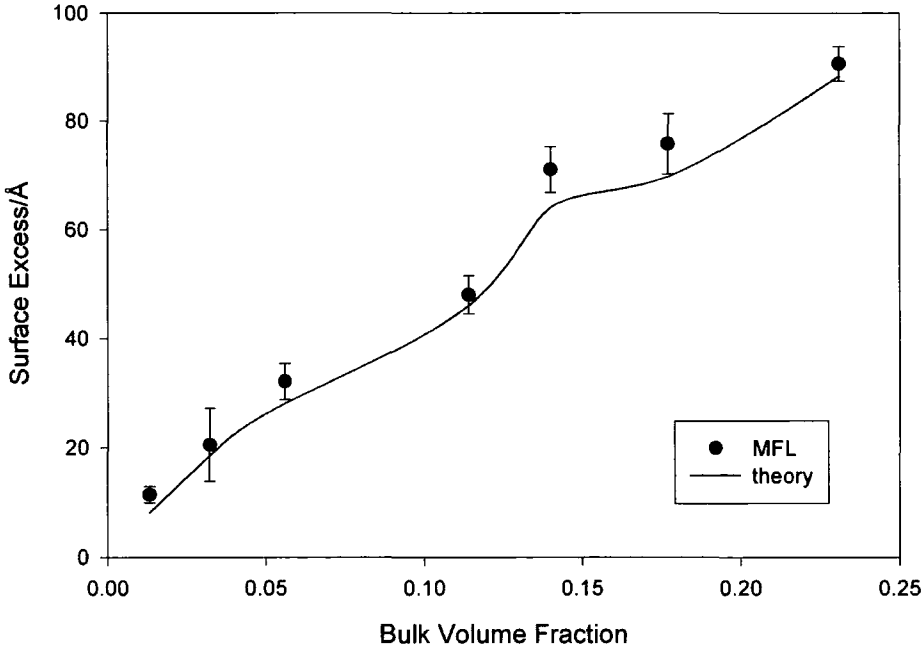


**Figure 5.11 Surface excess of MFL as a function of the equilibrium bulk volume fraction, with the line showing the values obtained from LAYERS.**

The unusual structure of the MFL polymer has meant that obtaining theoretical predictions of the volume fraction profile has been difficult. SCF theory calculations using LAYERS have been for polymer brushes with either one end or both ends of the chain attached at the surface. In this polymer there were ~7 functional groups evenly spaced along the chain, so a brush structure would not be expected. Subsequent attempts to use LAYERS to obtain the volume fraction profile failed to match the surface volume fraction and the shape of the profile though the surface excess calculated was in surprisingly good agreement (figure 5.11). The value of $\beta$ obtained varied, the samples up to and including MFL15 were the same with $\beta = 0.4$, for the higher volume fractions $\beta$ increased to a maximum of 0.84 for MFL30.

Another program generously donated by Professor Shull, LAYFIX, calculates the volume fraction profile for a given normalised surface excess value. The polymer chain in the calculation could have up to five 'sticky' groups along the chain. Calculations were carried out for a polymer with 4 functional groups located at positions 1, 34, 67 and 100 of a chain of degree of polymerisation 100, in a matrix polymer of the same degree of polymerisation. The degree of polymerisation was limited to 100 so that the calculations would converge in a reasonable time. However, the actual polymer used had 7 functional groups not 4, so the theoretical chain needed to be doubled in size making the effective degree of polymerisation 50 ($R_g = 2.041$Å) (figure 5.12). The number of lattice layers used in the calculation were determined by dividing the polymer film thickness by the radius of gyration of the MFL polymer (156Å) and multiplying by the radius of gyration of the theoretical polymer (around 23 layers); and the calculation was for segregation to both the air and substrate interfaces.

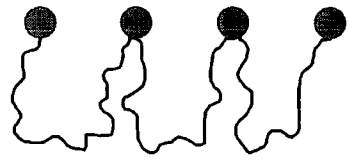

Polymer chain with four functional groups

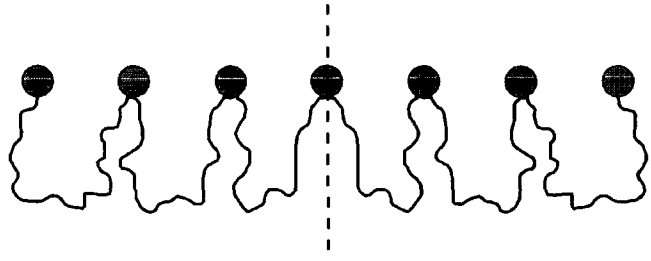

Above chain doubled in size

**Figure 5.12 Diagram to illustrate the model used to carry out self-consistent field calculations for the MFL polymer system.**

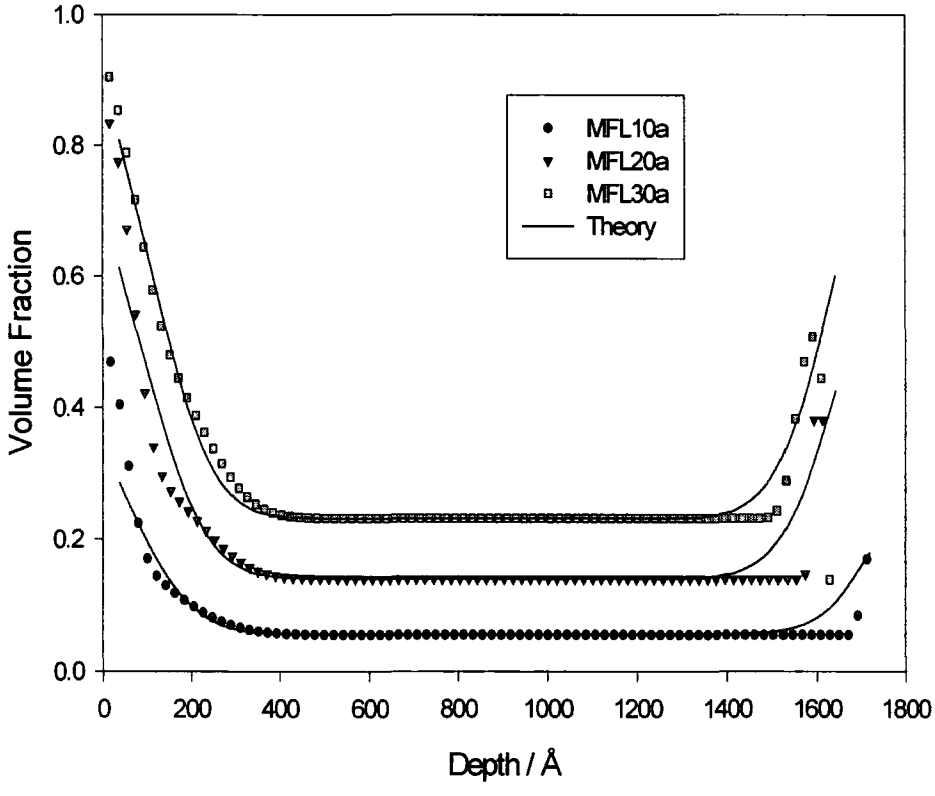


**Figure 5.13 Comparison of the experimental volume fraction profiles with those obtained using LAYFIX.**

Examples of the profiles obtained compared to the experimental data are given in figure 5.13. The profiles obtained still underestimated the surface volume fraction, partly due to the fact that the first value obtained is not at the very surface of the profile but at the halfway point of the lattice layer. After the first two lattice layers the comparison between the experimental and theoretical profiles was very good. Figure 5.14 shows the comparison in the theoretical values for the volume fraction at the air and silicon interfaces compared with the experimental values, the open circles are the volume fraction values at the depth in the experimental volume fraction profile where the theoretical profiles start.

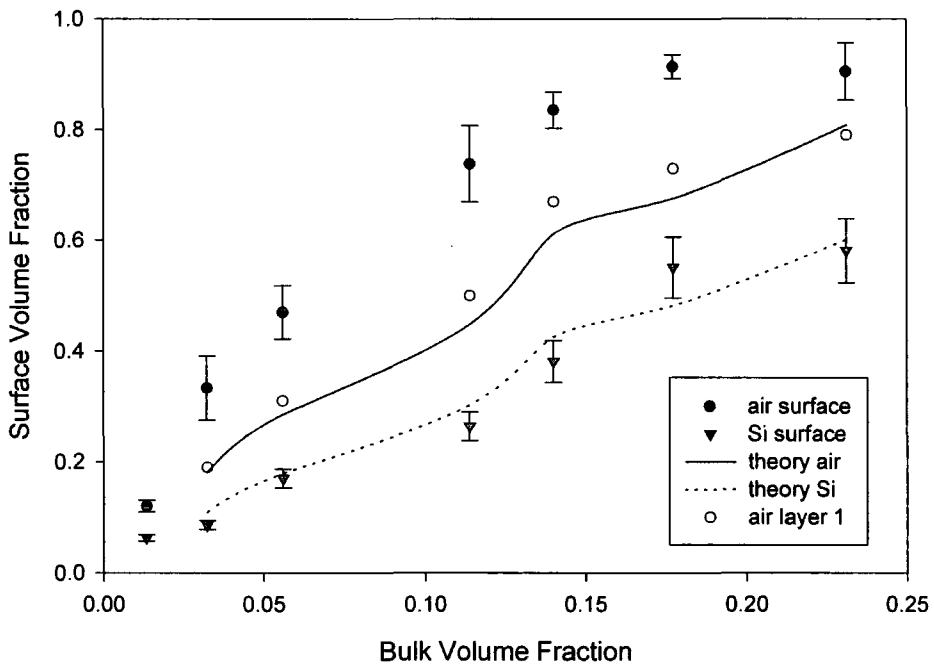


**Figure 5.14 Surface volume fraction values obtained from NR data as a function of the equilibrium bulk volume fraction, with the line showing values obtained using LAYFIX. Air surface is the experimental volume fraction at the immediate surface whereas air layer 1 is the volume fraction at the halfway point of the first lattice layer.**

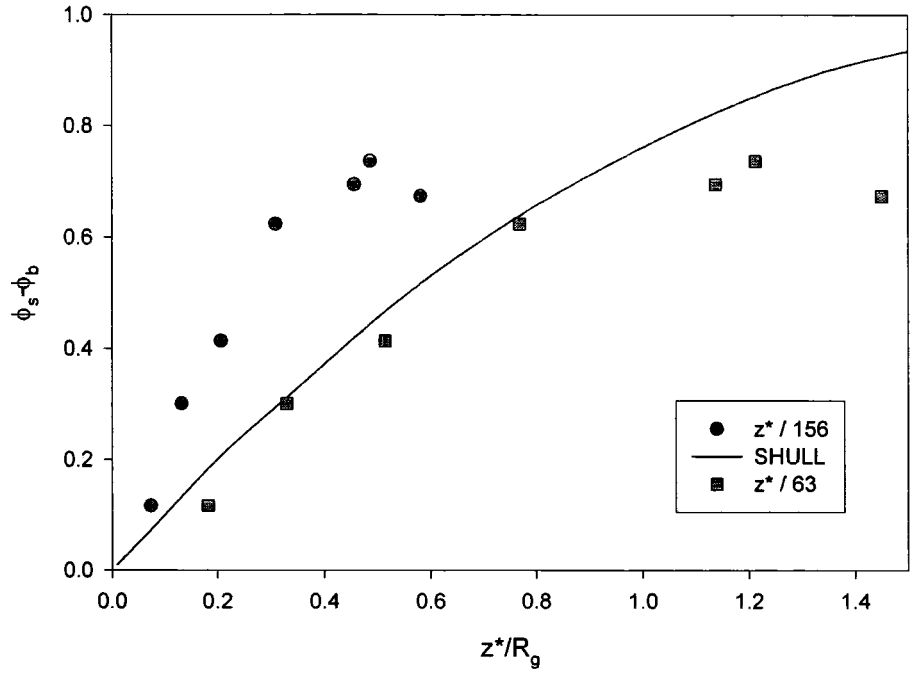


**Figure 5.15 The difference between the surface and bulk volume fractions against normalised excess for MFL samples. Line shows the values predicted by Shull for polymer brushes in the dry brush limit.**

Figure 5.15 shows the difference between the surface and bulk volume fractions, $\phi_s - \phi_b$ as a function of the normalised surface excess, $z^*/R_g$ compared with the predicted values for polymer brushes in the dry brush limit. The experimental values for the MFL samples when normalised by the radius of gyration calculated for a linear chain of 364000 $M_w$ ($R_g$ = 156) were greater than those predicted, which indicated that the segregated layer was much taller and thinner than a single end attached polymer brush would be. When the experimental values were normalised by the radius of gyration of the average connecting length between two functional groups ($R_g$ = 63Å), the values for all apart from the highest $z^*/R_g$ values fell on the line predicted by Shull[7] for polymer brushes in the dry brush limit. This suggested that most of the functional groups in the polymer chain have segregated to the air surface on annealing. Shull stated that the assumption that weak adsorption is the

same as strong adsorption on a uniform background (i.e. the bulk volume fraction) is not valid when the surface volume fraction reaches 0.8, this occurred at the values of $z^*/R_g$ where the data diverged from the predicted curve.

When the surface excess was normalised by the radius of gyration of the whole polymer (156Å) and plotted against the bulk volume fraction (figure 5.16) the values obtained were lower than those for the linear difunctional polymer systems apart from when the matrix was of lower molecular weight. So, there was greater segregation at the immediate air surface when compared to the linear polymers but the normalised excess was much lower. However, the values of normalised excess had not reached a plateau over the range of equilibrium bulk volume fractions studied so may rise to greater values than the linear systems.

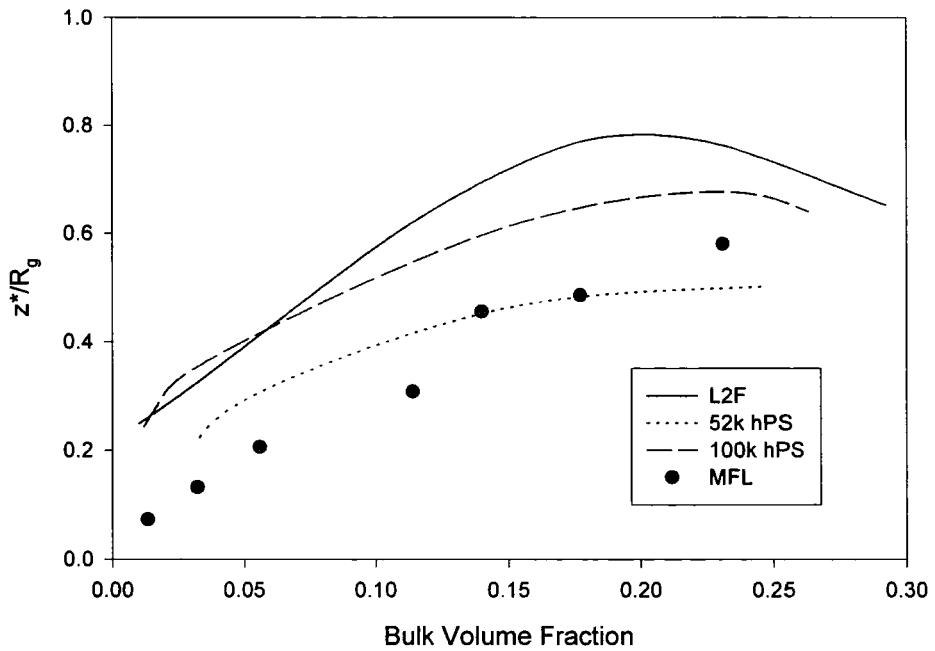


**Figure 5.16 Normalised excess against bulk volume fraction for the MFL polymer samples. Lines show the comparison with the results for the linear difunctional polymer blends, 50000 $M_w$ dPSF2 in 50000 $M_w$ hPS (L2F) and 100000 $M_w$ dPSF2 in 52k and 100k $M_w$ hPS (section 3.2.2).**

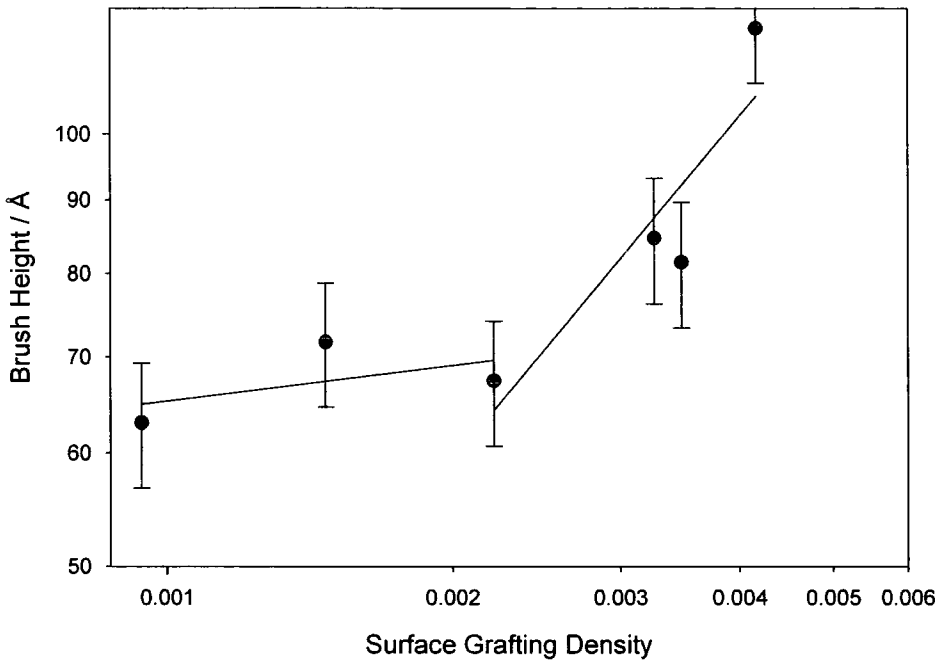


**Figure 5.17 Variation in the segregated layer thickness with surface grafting density.**

The dimensionless surface grafting density values, σ, calculated for the adsorbed layer using the degree of polymerisation of the polymer (3250) ranged from 0.0005 to 0.0042, all of which fall into the unstretched brush regime. However, if all seven functional groups were at the surface the σ values would be up to seven times higher and the σ values thus obtained ranged from 0.0037 to 0.029. The predicted crossover from unstretched to stretched dry brush behaviour is for a grafting density of $N^{-½}$, which is 0.0175 for the polymer studied here, but accounting for seven attachment points, the crossover would occur at a dimensionless grafting density of 0.0025. Figure 5.17 shows the variation in the segregated layer thickness (brush height) with the dimensionless grafting density on a log-log plot. The lines are linear regression fits with the value at a grafting density of ~0.0022 included in both. There are insufficient data to prove conclusively, but a difference in the slope of brush height was seen at a grafting density of ~0.0025. The slopes of the two lines were 0.1

and 0.8, which are in reasonable agreement with the scaling predictions of $\sigma^0$ and $\sigma^1$ for unstretched and stretched brush behaviour respectively.

The thickness of the brush layer in the unstretched regime was ~67Å which was considerably less than the predicted radius of gyration of a linear polymer chain of this molecular weight (156Å). If the radius of gyration was calculated for the connecting length of polystyrene joining two functional groups the value obtained was 63Å, which is of the same order as the layer thickness. The brush height almost doubled to a value of 119Å at the highest grafting density achieved. This was still lower than the end to end distance for the connecting length between functional groups (153Å). If it was assumed that both functional groups were attached to the surface, the degree of polymerisation of the effective chain would be reduced by a factor of two, and the end to end distance value obtained for this was 110Å. Raphael et al[8] looked at an adsorbed polymer layer at an interface in terms of loops and tails and suggested that a loop could be regarded as 2 pseudotails of half the degree of polymerisation of the loop, supporting the above assumption (figure 5.18).

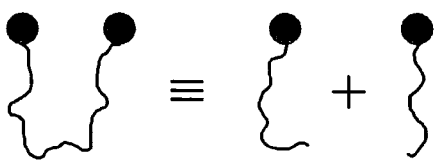

One loop equivalent to two chains of
half the degree of polymerisation

**Figure 5.18 Diagram to illustrate how a polymer loop can be regarded as two single tails.**

## 5.3 Conclusions

A perdeuterated polystyrene chain with functional groups evenly spaced along the polymer chain was blended with linear polystyrene. Thin films were

prepared and annealed above the glass transition to allow the equilibrium surface composition to be formed. Nuclear reaction analysis and neutron reflectometry were used to determine the volume fraction profile. There was evidence of segregation of the functional polymer to both the air and silicon substrate interface, which had previously not been seen for the other polymer architectures studied. This could be due to the greater molecular weight rather than the different architecture as the larger polymer size gave larger surface excess values, which could be observed by the experimental techniques. Alternatively, the greater number of functional groups might have caused the segregation, but without further work concentrating on the substrate interface it is impossible to tell. Comparison of the surface excess of functional polymer at the air surface between the two techniques used (NRA and NR) was in excellent agreement.

More detailed information on the shape of the segregated layer was obtained from NR data. The layer could not be modelled using a stretched exponential model that normally can be used when a polymer has enriched at the surface. Indeed, from comparison with both scaling and self-consistent field theories for polymer brushes, it would appear that the polymer chain has segregated to the surface and formed a looped structure with the functional groups attached to the interface and the connecting polymer chain stretching into the bulk. The degree of stretching of the connecting polymer chain has increased as the grafting density of the functional groups has increased. As the bulk volume fraction of the functional polymer was increased there was a crossover from unstretched behaviour to stretched brush behaviour as predicted by scaling theories. The multiple labelling could provide an easy means of increasing the grafting density in a segregated layer and allow the

study of the crossover between different regimes, which has previously been difficult to investigate.

## 5.4 References


1 A. C. Balazs, *Accounts of Chemical Research*, 1993, **26**, 63.

2 Y. Lyatskaya, D. Gersappe, and A. Balazs, *Macromolecules*, 1995, **28**, 6278.

3 Y. Lyatskaya, D. Gersappe, N. A. Gross, and A. Balazs, *Journal of Physical Chemistry*, 1996, **100**, 1449.

4 G. T. Pickett, A. C. Balazs, and D. Jasnow, *Trends in Polymer Science*, 1997, **5**, 128.

5 Y. Lyatskaya and A. C. Balazs, in 'Improved Compatibilization of Immiscible Homopolymer Blends Using Copolymer Mixtures', ed. D. J. Lohse, T. P. Russell, and L. H. Sperling, New York, 1997.

6 E. A. Di Marzio, C. M. Guttman, and A. Mah, *Macromolecules*, 1995, **28**, 2930.

7 K. R. Shull, *Journal of Chemical Physics*, 1991, **94**, 5723.

8 M. Aubouy, O. Guiselin, and E. Raphael, *Macromolecules*, 1996, **29**, 7261.

# CHAPTER 6

# Kinetics of Segregation

It has been shown in the preceding chapters that a low surface energy moiety placed in the polymer chain causes the molecule to segregate to the air / polymer interface when blended with unfunctionalised polymer. Having found this, the aim was then to understand the kinetics of the segregation process. Two approaches were used, blends were prepared in solution as before and several samples were spun cast onto a silicon substrate and then annealed under vacuum for different times. The growth of the surface excess was observed using NR and NRA. In the second method a bilayer was prepared where the pure or blended functional polymer was spun directly onto the substrate and overlaid with a layer of pure hPS and annealed for various times. The surface composition profile was then determined using NRA and NR and the broadening of the interface and the growth in the surface excess were observed and used to determine diffusion coefficients.

## 6.1 Blend Kinetics

Samples of 30% of L2F, H2F and STAR polymer in a linear matrix were prepared in toluene. For each polymer system the same solution was used if possible, and several samples were spun onto silicon blocks. Each sample was annealed under vacuum at 413K for different known times, samples investigated are shown in table 6.1.1 (0 is the unannealed sample and 'a' the fully annealed sample discussed earlier). Fifteen minutes was the shortest annealing time that could be achieved with reliability.

| Sample | Volume Fraction functional polymer | Annealing time / minutes |
|---|---|---|
| L2F30 | 0.300 | 0, 15, 30, 40, 50, 59, a |
| H2F30 | 0.301 | 0, 90, 120, 240, 720, a |
| H2F30 | 0.300 | 15, 30, 40, 50, 60, 2880 |
| STAR30 | 0.300 | 0, 60, 480, a |
| STAR30 | 0.300 | 15, 30, 40, 50, 120 |

**Table 6.1.1 Samples that were used in the blend kinetics experiment, each row represents samples from the same solution.**

### 6.1.1 L2F kinetics results

Neutron reflectivity data were obtained on CRISP using the multidetector. The sample files have been fitted using VOLFMEM and multilayer models (Helix3 and PCMULF) to obtain the volume fraction profile. Initially VOLFMEM was used to obtain the volume fraction profile, if there was evidence of a depletion layer a three layer model was used in Helix3 and PCMULF. After only 15 minutes there was no depletion layer, but a three layer model still gave a better fit to the data than a stretched exponential model. Examples of the fitted profiles are shown in figure 6.1.1. The parameters used to obtain the fits to the data are given in table 6.1.2, $\phi$ is the volume fraction, t is the layer thickness, $\sigma$ is the roughness between succeeding layers and $\chi^2$ is the normalised chi squared goodness of fit. The subscript is the number of the layer with 1 being the uppermost layer.

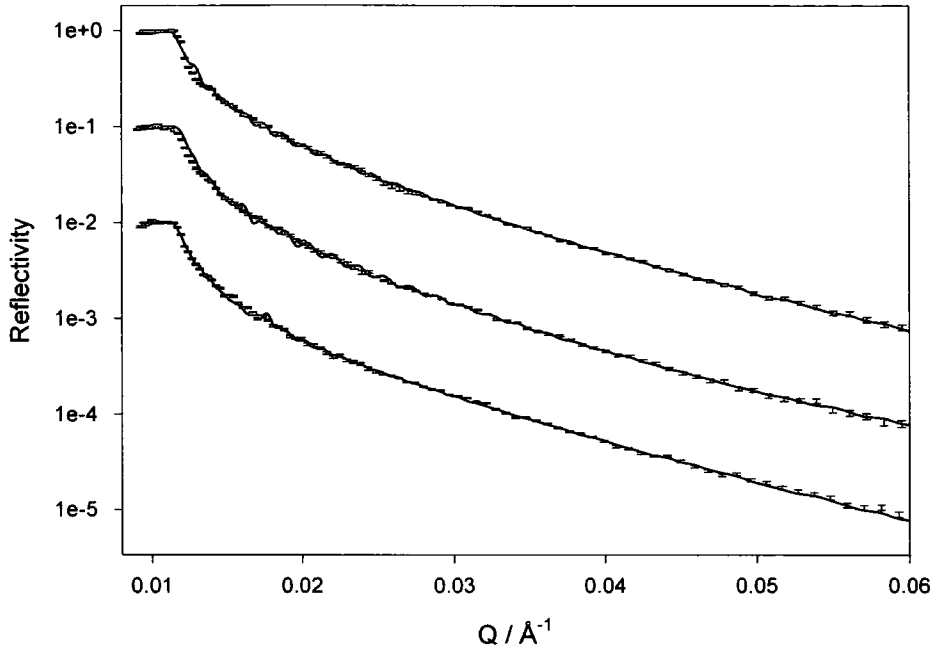


**Figure 6.1.1 Reflectivity profiles showing the multilayer fits obtained for (from the top) L2F30a15, L2F30a30 and L2F30a40. Subsequent data sets are offset by a factor of 10 for clarity.**

| sample | $\phi_1$ | $t_1$/Å | $\sigma_1$/Å | $\phi_2$ | $t_2$/Å | $\sigma_2$/Å | $\phi_3$ | $t_3$/Å | $\chi^2$ |
|---|---|---|---|---|---|---|---|---|---|
| L2F30u | 0.99 | 52 | 25 | 0.12 | 55 | 46 | 0.27 | 3667 | 5 |
| a15 | 0.95 | 65 | 17 | 0.39 | 58 | 32 | 0.26 | 3486 | 11 |
| a30 | 0.99 | 54 | 17 | 0.48 | 53 | 28 | 0.30 | 3112 | 12 |
| a40 | 0.99 | 57 | 15 | 0.46 | 40 | 22 | 0.27 | 4287 | 7 |
| a50 | 0.99 | 68 | 21 | 0.37 | 66 | 71 | 0.27 | 4905 | 5 |
| a59 | 0.99 | 52 | 19 | 0.49 | 47 | 24 | 0.26 | 4243 | 7 |

**Table 6.1.2 Parameters used to obtain three layer fits to NR data for the L2F kinetics samples.**

In the unannealed sample there was already significant segregation at the air surface followed by a depletion layer. After only 15 minutes of annealing the reflectivity profile had changed considerably and the depletion layer had disappeared. The reflectivity profiles for the 15 to 59 minutes annealed samples actually showed very little difference that could be discerned with confidence, shown in figure 6.1.2.

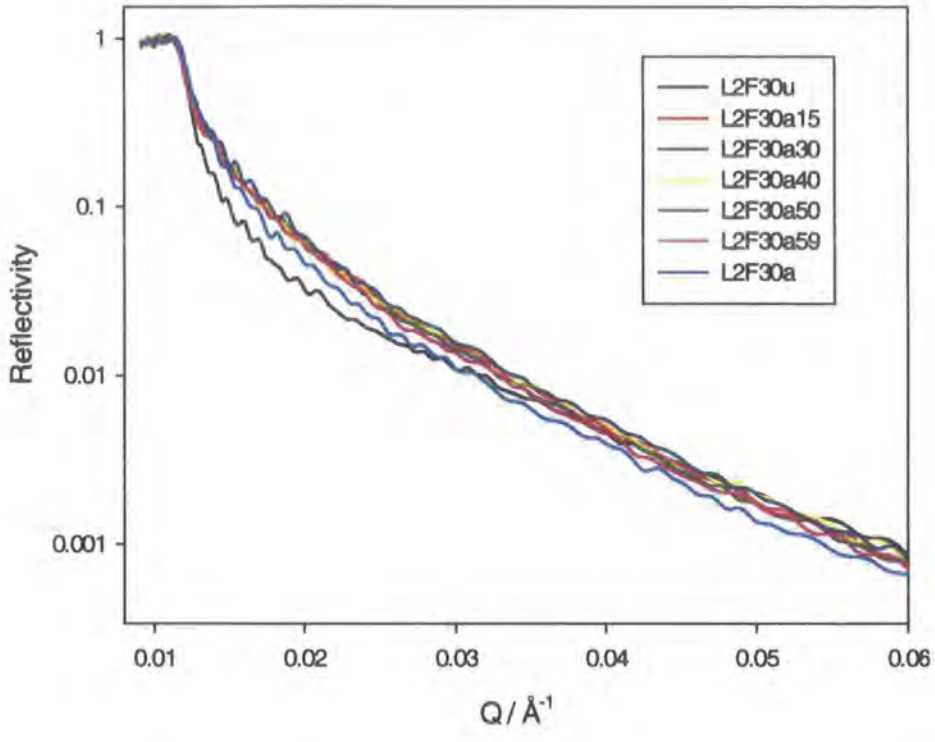


**Figure 6.1.2 Neutron reflectivity profiles for the L2F kinetics samples.**

Assuming that there was no difference in the profiles, the results gave an indication of the reproducibility of the technique. From the fitted profiles, figure 6.1.3, the standard deviation in the bulk, $\phi_b$ and surface, $\phi_s$ volume fraction and surface excess, z* were obtained (table 6.1.3). Values obtained for individual samples are given in table 6.1.4 and figure 6.1.4 shows the variation in surface excess with annealing time.

| | $\phi_b$ | $\phi_s$ | z* / Å |
|---|---|---|---|
| Mean | 0.28 | 0.95 | 45.4 |
| SD | 0.015 | 0.037 | 3.5 |

**Table 6.1.3 Mean and standard deviation in the surface parameters for the L2F30 samples annealed for 15minutes or longer.**

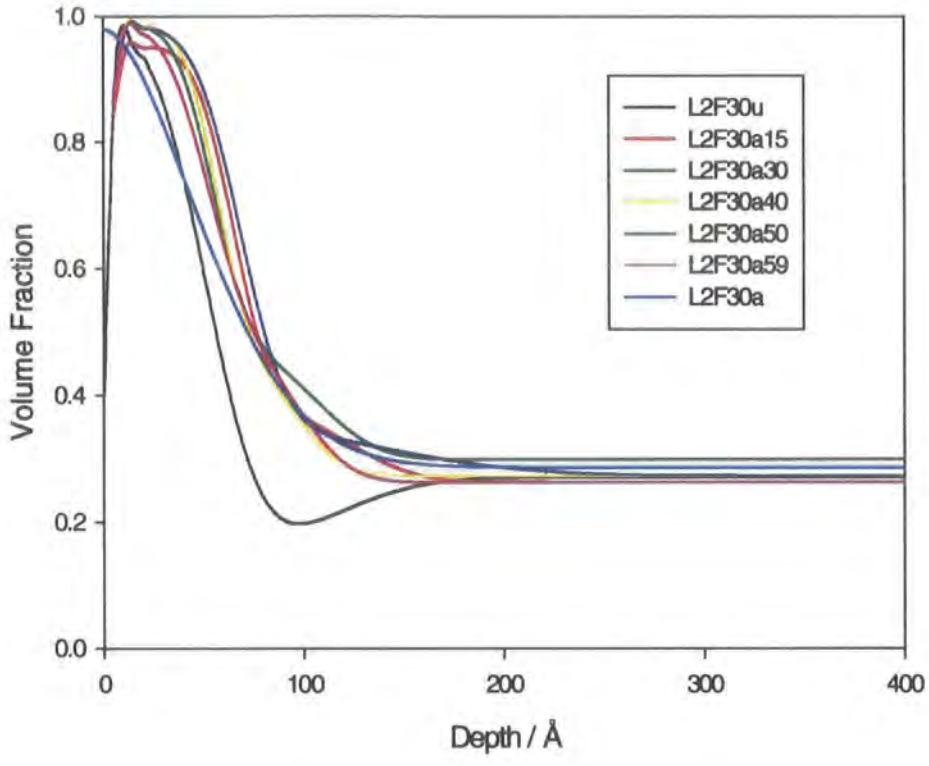


**Figure 6.1.3 Volume fraction profiles from multilayer fits to the NR data for the L2F kinetics samples.**

| Sample | $\phi_b$ | $\phi_s$ | z*/Å |
|---|---|---|---|
| L2F30u | 0.20 | 0.96 | 34 |
| a15 | 0.26 | 0.95 | 48 |
| a30 | 0.30 | 0.99 | 43 |
| a40 | 0.27 | 0.99 | 44 |
| a50 | 0.27 | 0.99 | 50 |
| a59 | 0.26 | 0.98 | 44 |
| a | 0.29 | 0.99 | 40 |

**Table 6.1.4 Parameters obtained from the volume fraction profiles for the L2F kinetics samples.**

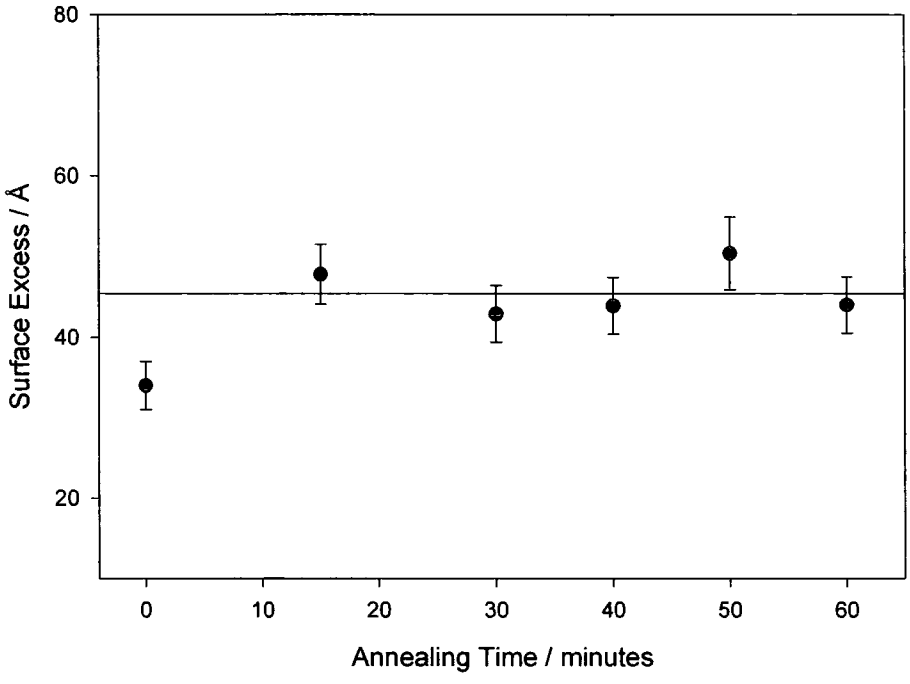


**Figure 6.1.4 Surface excess as a function of annealing time for the L2F30 kinetics samples. The line indicates the mean surface excess value after annealing.**

The fully annealed sample did show a slight difference in reflectivity, the volume fraction profile obtained was less blocky than the shorter annealing times. This could be due to sample damage after the long annealing time (possibly dewetting of the polymer film from the substrate) or perhaps showed that there was rapid initial segregation followed by a much slower local rearrangement at the surface that was not observable in the time scale used.

### 6.1.2 H2F kinetics results

The H2F samples were analysed in a similar manner to that used for the L2F samples except the single detector was used on CRISP. A stretched exponential model was also used to obtain the volume fraction profile. Initially VOLFMEM was used to obtain the volume fraction profile, if there was evidence of a depletion layer a

three layer model was used. For the 60 minute sample there was no evidence of a depletion layer, but a three layer model gave a better fit to the data than a stretched exponential model. For two of the samples with a depletion layer (H2F30a40 and H2F30a50) a better fit was obtained if four layers were used to model the profile. Increasing the number of layers will improve the fit, consequently the number of layers used were kept to the minimum number necessary to obtain a good fit without having too many fitting variables. Examples of the fitted reflectivity profiles are shown in figure 6.1.5. The parameters used to obtain the multilayer fits to the data are given in tables 6.1.5 and 6.1.6.

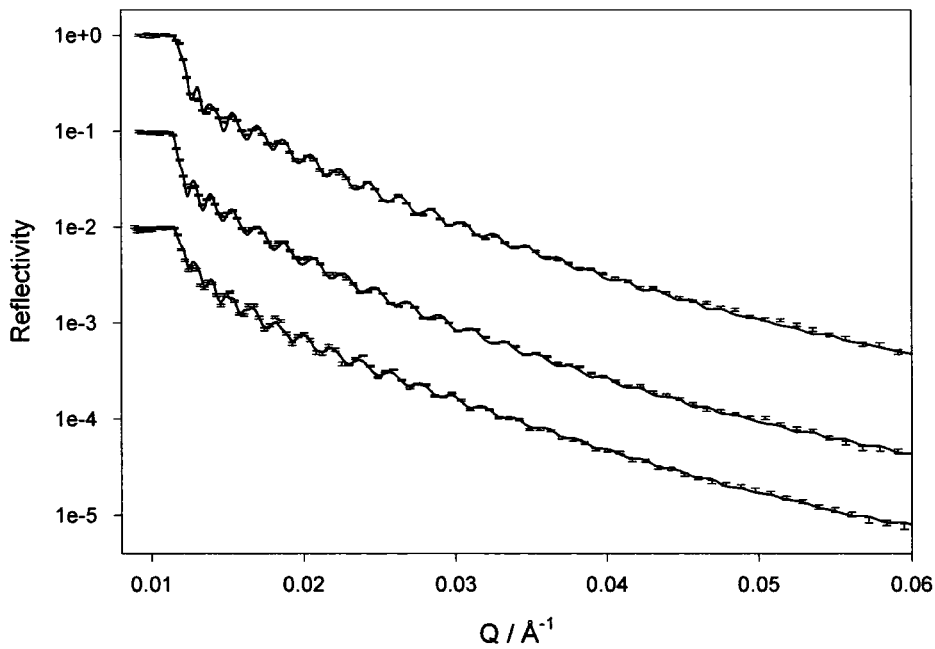


**Figure 6.1.5 Reflectivity profiles showing the multilayer fits obtained for (from the top) H2F30a15, H2F30a30 and H2F30a60. Subsequent data sets are offset by a factor of 10 for clarity.**

| sample | $\phi_1$ | $t_1$/Å | $\sigma_1$/Å | $\phi_2$ | $t_2$/Å | $\sigma_2$/Å | $\phi_3$ | $t_3$/Å | $\chi^2$ |
|---|---|---|---|---|---|---|---|---|---|
| H2F30u | 0.80 | 56 | 17 | 0.21 | 257 | 30 | 0.26 | 3040 | 4 |
| a15 | 0.94 | 60 | 58 | 0.21 | 297 | 102 | 0.28 | 2434 | 10 |
| a30 | 0.87 | 57 | 68 | 0.20 | 416 | 135 | 0.24 | 2243 | 7 |
| a40 | 0.89 | 34 | 86 | 0.24 | 484 | 149 | 0.29 | 2576 | 54 |
| a50 | 0.89 | 64 | 62 | 0.26 | 373 | 71 | 0.29 | 2483 | 26 |
| a60 | 1.00 | 57 | 19 | 0.45 | 63 | 20 | 0.26 | 2738 | 6 |

**Table 6.1.5 Parameters used to obtain three layer fits to NR data for the H2F and kinetics samples.**

| H2F30 | $\phi_1$ | $t_1$/Å | $\sigma_1$/Å | $\phi_2$ | $t_2$/Å | $\sigma_2$/Å | $\phi_3$ | $t_3$/Å | $\sigma_3$/Å | $\phi_4$ | $t_4$/Å | $\chi^2$ |
|---|---|---|---|---|---|---|---|---|---|---|---|---|
| a40 | 0.82 | 62 | 37 | 0.47 | 45 | 81 | 0.22 | 288 | 60 | 0.25 | 2487 | 12 |
| a50 | 0.83 | 61 | 29 | 0.56 | 36 | 65 | 0.23 | 307 | 60 | 0.25 | 2749 | 18 |

**Table 6.1.6 Parameters used to obtain four layer fits to NR data for H2F30 annealed for 40 and 50 minutes.**

After 60 minutes of annealing there was no evidence of a depletion layer and good fits were obtained using a stretched exponential model. Earlier annealing time samples could also be fitted using a stretched exponential model, but the fits did not account for any depletion and were not as good as the three layer fits as can be seen in the value of $\chi^2$ obtained. The parameters used to obtain the stretched exponential model fits are given in table 6.1.7.

| Sample | $\phi_b$ | $\phi_s$ | exponent | decay length/Å | $\chi^2$ |
|---|---|---|---|---|---|
| H2F30a15 | 0.26 | 0.84 | 2.1 | 80 | 35 |
| a30 | 0.23 | 0.77 | 2.0 | 90 | 25 |
| a40 | 0.24 | 0.78 | 1.8 | 93 | 30 |
| a50 | 0.24 | 0.84 | 1.7 | 90 | 20 |
| a60 | 0.22 | 0.99 | 1.7 | 80 | 10 |
| a90 | 0.25 | 0.88 | 1.8 | 93 | 6 |
| a120 | 0.24 | 0.86 | 1.6 | 95 | 3 |
| a240 | 0.25 | 0.85 | 1.6 | 101 | 3 |
| a720 | 0.26 | 0.91 | 1.6 | 93 | 2 |
| a | 0.26 | 0.95 | 1.7 | 91 | 3 |

**Table 6.1.7 Parameters used to obtain stretched exponential fits to NR data for H2F kinetics samples.**

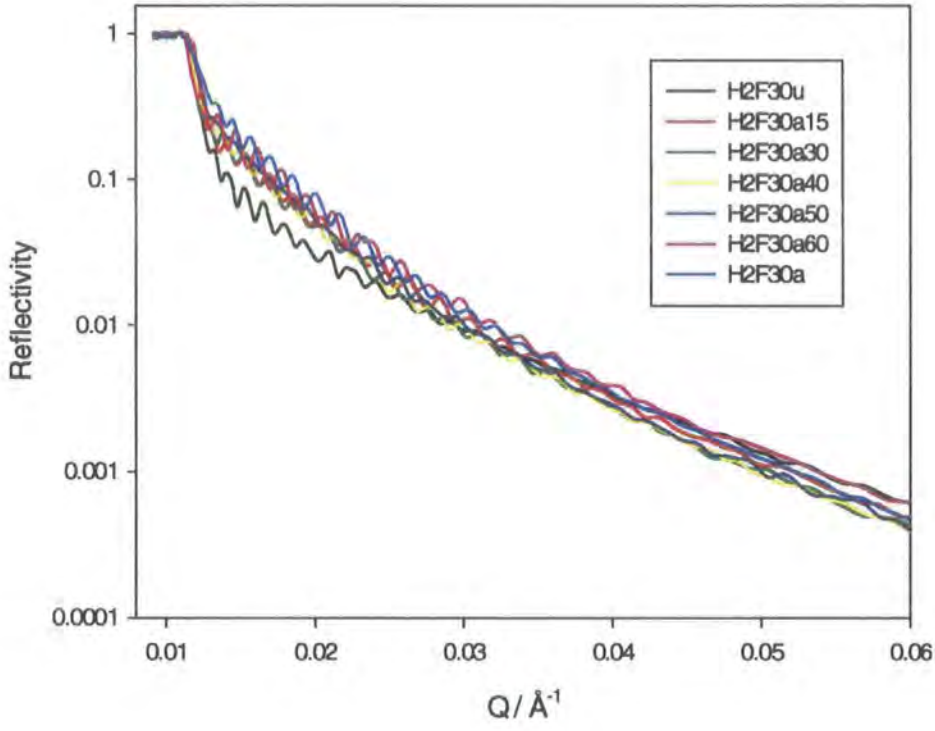


**Figure 6.1.6 Reflectivity profiles for the unannealed to 60 minutes annealed H2F samples and the fully annealed sample.**

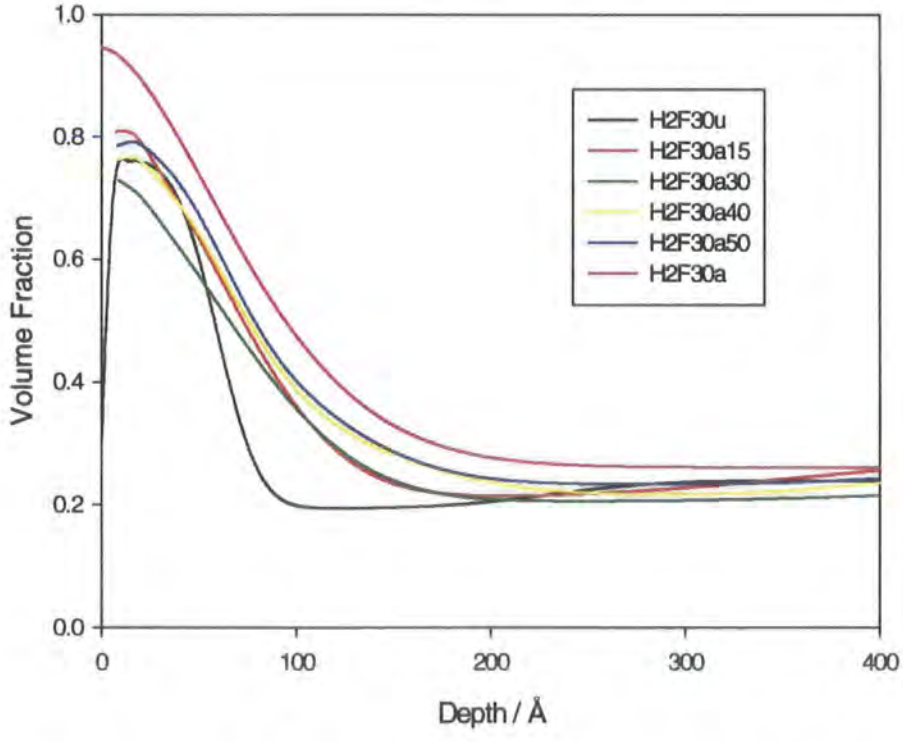


**Figure 6.1.7 Volume fraction profiles from the multilayer fits to the H2F samples.**

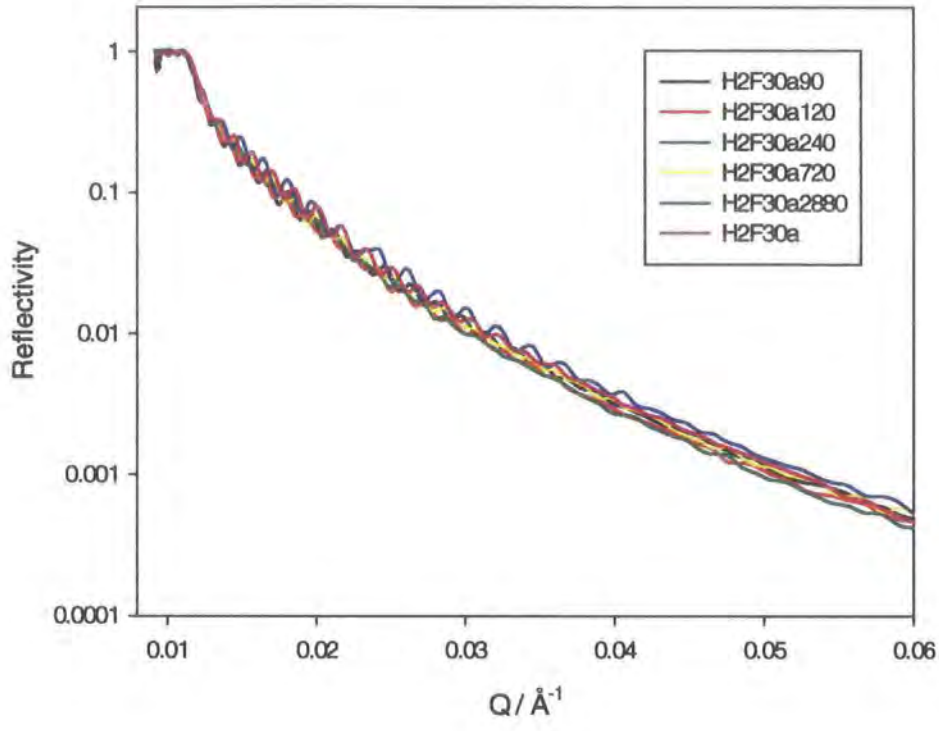


**Figure 6.1.8 Neutron reflectivity profiles for the H2F long annealing times.**

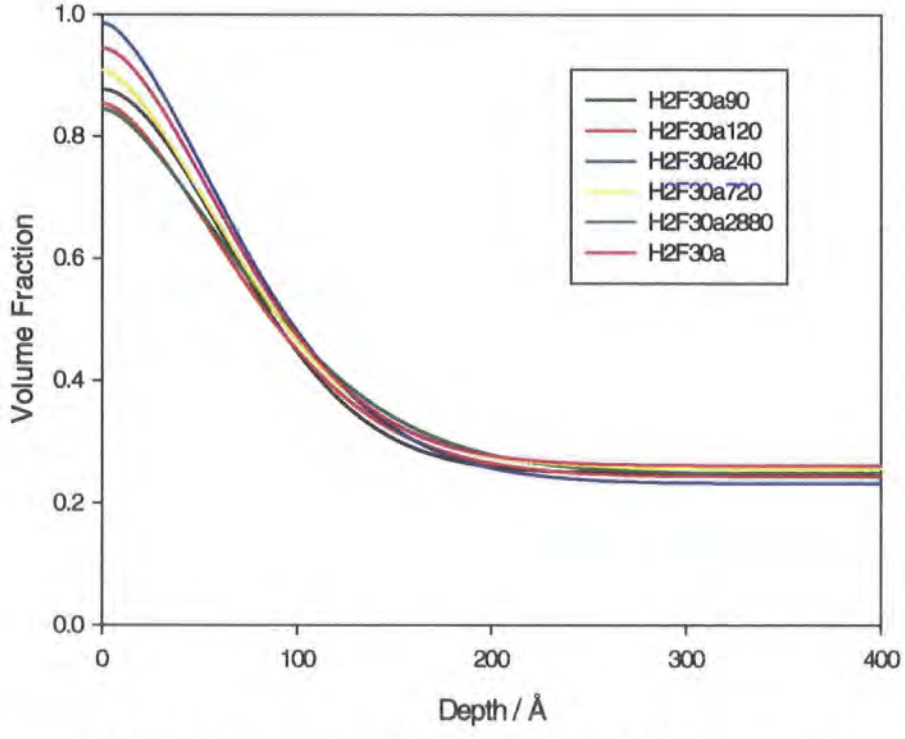


**Figure 6.1.9 Volume fraction profiles from stretched exponential fits to the longer annealed H2F samples.**

In the H2F samples as in the L2F samples there was some segregation in the unannealed sample and after just 15 minutes the reflectivity profile had changed quite considerably. However the increased molecular weight of the polymer was sufficient to slow the diffusion of the polymer and the reflectivity profiles showed some variation up to ~60 minutes annealing time, figure 6.1.6. There was still evidence of a depletion layer, but this now extended much further into the bulk of the sample (figure 6.1.7). After 60 minutes there was very little difference in the profiles that could be distinguished from sample variation, shown in figure 6.1.8, the stretched exponential profiles are shown in figure 6.1.9. From the fitted profiles the standard deviation in the bulk, $\phi_b$ and surface, $\phi_s$ volume fraction and surface excess, z* were obtained (table 6.1.8). Surface parameter values for all the samples are given in table 6.1.9, for samples where there was a depletion layer, values are given for $\phi_{dep}$ and $z^*_{dep}$ as well. z* was determined using the equilibrium bulk volume fraction, $z^*_{total}$ is the surface excess calculated using $\phi_{dep}$, assuming the surface excess to be in local equilibrium with the depletion layer and $z^*_{dep}$ is the area of the depleted region. Figure 6.1.10 shows the variation in the surface excess with annealing time.

| | $\phi_b$ | $\phi_s$ | z* / Å |
|---|---|---|---|
| Mean | 0.24 | 0.83 | 53.0 |
| SD | 0.012 | 0.045 | 3.0 |

**Table 6.1.8 Mean and standard deviation in the surface parameters for the H2F30 samples annealed for 60 minutes or longer.**

| Sample | $\phi_b$ | $\phi_{dep}$ | $\phi_s$ | z*/Å | $z^*_{dep}$/Å | $z^*_{total}$/Å |
|---|---|---|---|---|---|---|
| H2F30u | 0.24 | 0.19 | 0.76 | 28 | 6 | 32 |
| a15 | 0.28 | 0.21 | 0.81 | 31 | 14 | 40 |
| a30 | 0.24 | 0.21 | 0.73 | 30 | 12 | 36 |
| a40 | 0.25 | 0.22 | 0.77 | 36 | 7 | 44 |
| a50 | 0.25 | 0.24 | 0.79 | 39 | 4 | 43 |
| a60 | 0.26 | - | 0.99 | - | - | 50 |
| a90 | 0.25 | - | 0.88 | - | - | 48 |
| a120 | 0.24 | - | 0.85 | - | - | 52 |
| a240 | 0.25 | - | 0.85 | - | - | 54 |
| a720 | 0.26 | - | 0.91 | - | - | 54 |
| a2880 | 0.23 | - | 0.99 | - | - | 64 |
| a | 0.26 | - | 0.95 | - | - | 56 |

**Table 6.1.9 Parameters obtained from the volume fraction profiles for the H2F kinetics samples.**

The unannealed sample had a thin layer of material segregated to the surface, after 15 minutes annealing at 413K the surface volume fraction and surface excess increased but after 30 minutes these values fell. On subsequent annealing the surface volume fraction and surface excess increased until the equilibrium values were reached after 60 minutes. This variation suggests that the layer, which had initially segregated to the surface during spinning, stretched and rearranged itself and was then followed by the slower diffusion from the bulk. The fully segregated layer was obtained after ~60 minutes, which then rearranged locally to give the equilibrium structure.

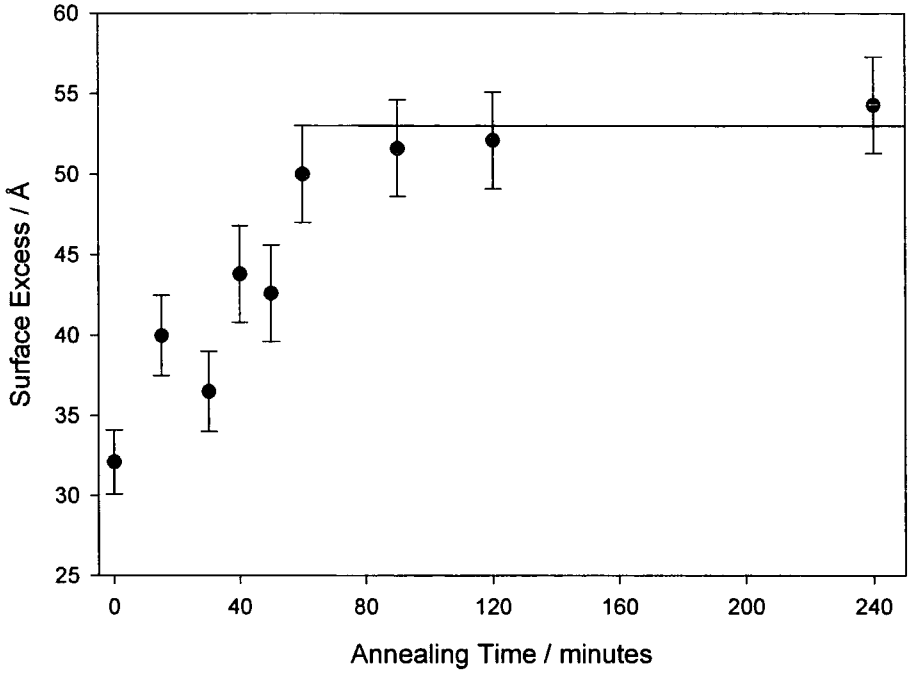


**Figure 6.1.10 Surface excess as a function of annealing time for the H2F30 kinetics samples. The line shows the mean surface excess value after more than 60 minutes of annealing.**

### 6.1.3 STAR kinetics results

Neutron reflectivity data were obtained on CRISP using the multidetector for the STAR kinetic samples; STAR30u and STAR30a were measured at a different time using the single detector. There was evidence of a depletion layer in the samples annealed for up to 50 minutes and a three layer model was used for these, otherwise just two layers were used. Examples of the reflectivity profiles showing the fits obtained to the data are shown in figure 6.1.11 and the parameters used to obtain the fits to the data are given in table 6.1.10.

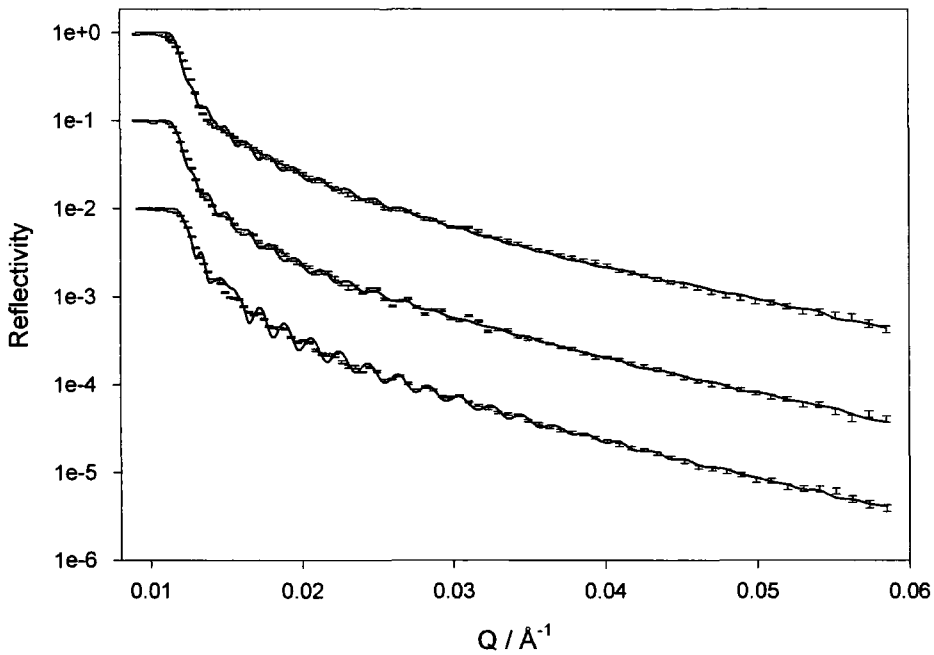


**Figure 6.1.11 Reflectivity profiles showing multilayer fits to the data for (from the top) STAR30a15, STAR30a30 and STAR30a60. Subsequent data sets are offset by a factor of 10 for clarity.**

| sample | $\phi_1$ | $t_1$/Å | $\sigma_1$/Å | $\phi_2$ | $t_2$/Å | $\sigma_2$/Å | $\phi_3$ | $t_3$/Å | $\chi^2$ |
|---|---|---|---|---|---|---|---|---|---|
| STAR30u | 0.55 | 50 | 6 | 0.24 | 119 | 16 | 0.25 | 2910 | 6 |
| a15 | 0.64 | 58 | 21 | 0.24 | 200 | 20 | 0.26 | 2746 | 19 |
| a30 | 0.79 | 62 | 19 | 0.25 | 151 | 28 | 0.26 | 2769 | 8 |
| a40 | 0.63 | 64 | 18 | 0.27 | 58 | 15 | 0.28 | 2774 | 23 |
| a50 | 0.69 | 66 | 19 | 0.28 | 106 | 21 | 0.28 | 2372 | 31 |
| a60 | 0.67 | 63.9 | 26 | 0.30 | 2745 | - | - | - | 29 |
| a120 | 0.93 | 42 | 47 | 0.28 | 2977 | - | - | - | 19 |
| a480 | 0.91 | 82 | 33 | 0.30 | 5232 | - | - | - | 22 |

**Table 6.1.10 Parameters used to obtain two and three layer fits to NR data for the STAR kinetics samples.**

In the STAR samples some segregation occurred during spinning, but this was not to the same extent as was seen in the linear polymer blends. Hence the reflectivity profiles and subsequent volume fraction profiles showed a greater variation (figures 6.1.12 and 6.1.13). A depletion layer was seen in the samples annealed for up to 50 minutes and the volume fraction profiles were quite blocky, as

increased the profiles showed a smoother decay from the surface. Table 6.1.11 gives the volume fraction and surface excess values obtained from the profiles. The surface excess showed a rapid increase at 15 minutes, which fell slightly before rising gradually to the equilibrium value (figure 6.1.14). This further supports the belief that there is an immediate, rapid segregation at the surface followed by a more gradual equilibration with the bulk.

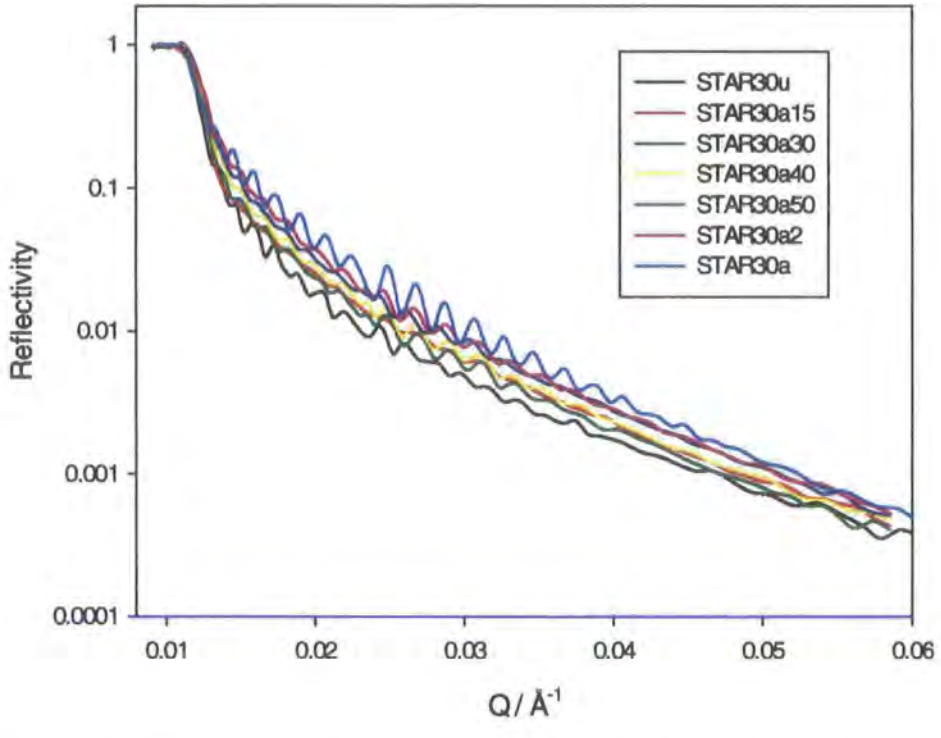


**Figure 6.1.12 Neutron reflectivity profiles for the STAR kinetics samples.**

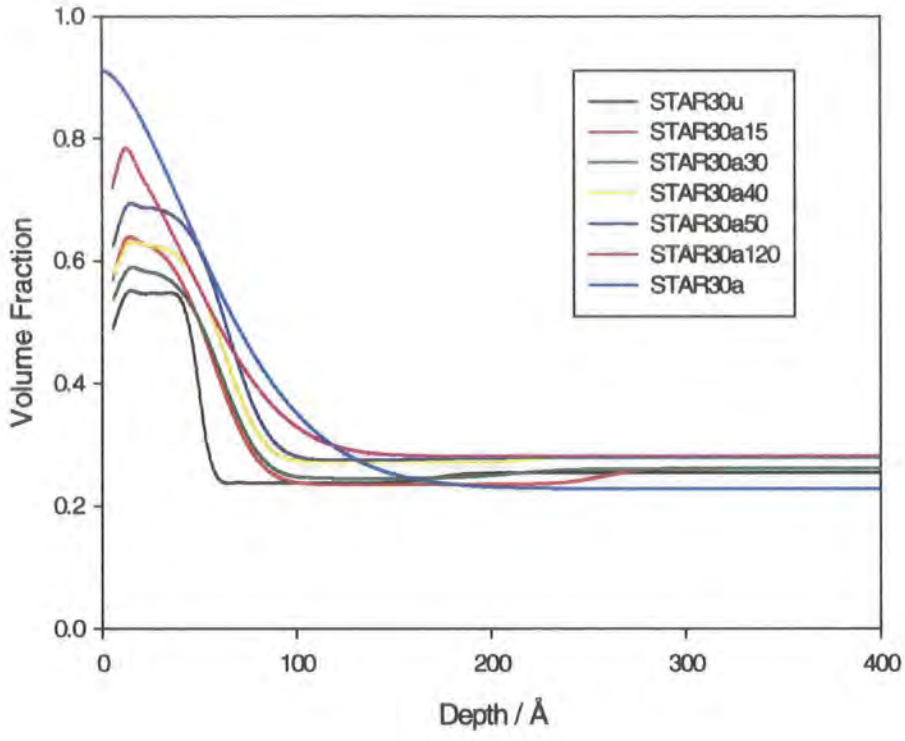


**Figure 6.1.13 Volume fraction profiles for the STAR kinetics samples.**

| Sample | $\phi_b$ | $\phi_{dep}$ | $\phi_s$ | z*/Å | $z^*_{dep}$/Å | $z^*_{total}$/Å |
|---|---|---|---|---|---|---|
| STAR30u | 0.25 | 0.24 | 0.55 | 13 | 2 | 14 |
| a15 | 0.26 | 0.24 | 0.63 | 18 | 4 | 21 |
| a30 | 0.26 | 0.25 | 0.59 | 17 | 2 | 19 |
| a40 | 0.28 | 0.27 | 0.63 | 19 | 1 | 20 |
| a50 | 0.28 | 0.27 | 0.69 | 24 | 0.5 | 24 |
| a60 | 0.30 | - | 0.66 | - | - | 21 |
| a120 | 0.28 | - | 0.78 | - | - | 26 |
| a480 | 0.30 | - | 0.90 | - | - | 46 |
| a | 0.23 | - | 0.91 | - | - | 44 |

**Table 6.1.11 Parameters obtained from the volume fraction profiles for the STAR kinetics samples.**

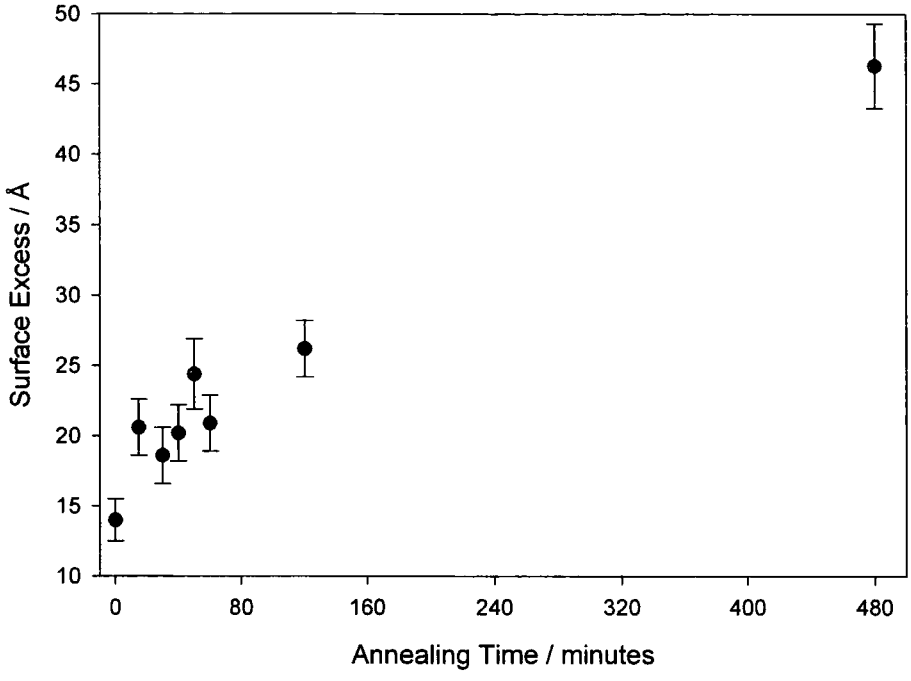


**Figure 6.1.14 Surface excess as a function of annealing time for the STAR30 kinetics samples.**

Although the surface excess attained at equilibrium was of the same order as that seen for the L2F system, the time taken for this to be achieved was much longer than for the linear system. There are two contributing factors to this slower approach to equilibrium, the STAR only has one functional group compared to two in the linear polymer and the three arms mean that the polymer cannot diffuse by normal polymer reptation mechanisms[1, 2].

### 6.1.4 10% dPSF2 kinetics samples

For all the 30% samples the amount of initial segregation during spinning made it difficult to see variations in the segregated layer, especially as neutron reflectometry is insensitive to gradual changes, but the greater amount of deuterated

material gave better reflectivity profiles. NRA did not show segregation in the 30% samples so it was impossible to obtain supporting evidence using this technique.

NRA showed the segregated layer better in the lower volume fraction samples, but as the amount of deuterated material in the sample decreased the time taken to obtain data of acceptable signal to noise increased and hence the risk of sample damage also increased. As a compromise, 10% samples of L2F and H2F were prepared by spinning the blended polymer solution onto silicon wafers. The wafers were broken into pieces of the correct size for the technique; each piece was annealed under vacuum at 413K for known times.

NRA data were obtained at an incident angle of 15°. For the L2F10 samples data were only obtained for 15, 30 and 60 minutes of annealing and it was difficult to see any variation in the results both from analysing the profiles directly and after fitting a tanh function at the air surface using FITTER (figure 6.1.15). The tanh function was convoluted with the instrumental resolution and the parameters used to obtain the fits to the data are given in table 6.1.12; the surface parameters obtained from the volume fraction profiles thus obtained are given in table 6.1.13.

| Sample | $\phi_b$ | $\phi_a$ | height/Å | width/Å | offset/Å | Resolution /Å |
|---|---|---|---|---|---|---|
| L2F10a15 | 0.08 | 0.40 | 94 | 61 | 173 | 198 |
| L2F10a30 | 0.09 | 0.75 | 58 | 59 | 204 | 199 |
| L2F10a60 | 0.09 | 0.68 | 62 | 52 | 203 | 200 |

**Table 6.1.12 Parameters used to obtain fits to NRA data using FITTER.**

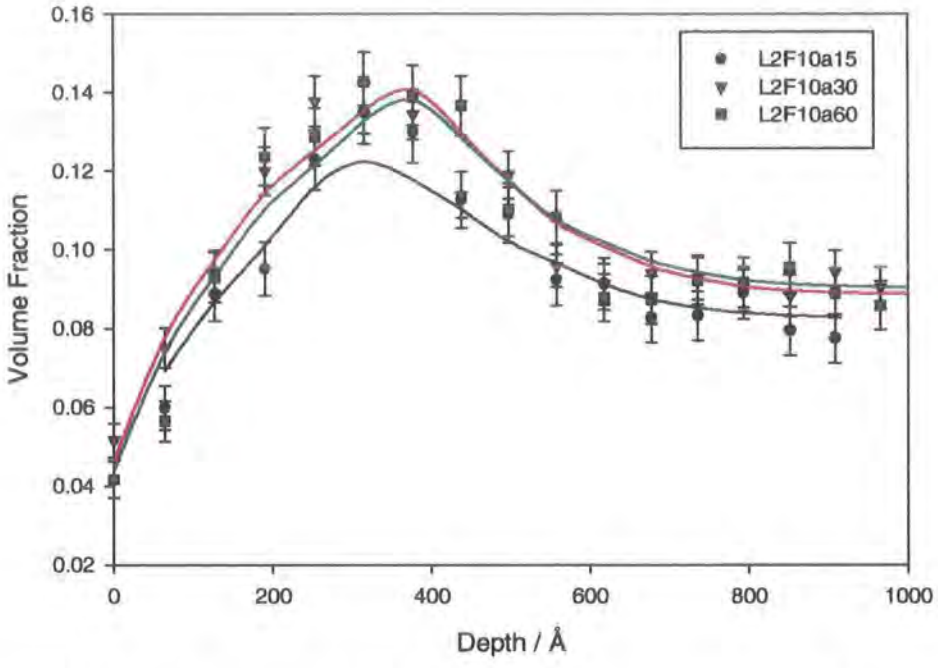


**Figure 6.1.15 NRA data for L2F10 kinetics samples showing tanh function fits to data.**

| Sample | $\phi_b$ | $\phi_s$ | z*/Å |
|---|---|---|---|
| L2F10a15 | 0.08 | 0.40 | 30 |
| L2F10a30 | 0.09 | 0.73 | 38 |
| L2F10a60 | 0.09 | 0.68 | 36 |

**Table 6.1.13 Parameters obtained from the fits to NRA data.**

These results support the NR data for L2F30 where after only 15 minutes there was no change in the profiles obtained. Figure 6.1.16 shows the surface excess values obtained from NRA along with the values obtained by NR for the unannealed and fully annealed samples.

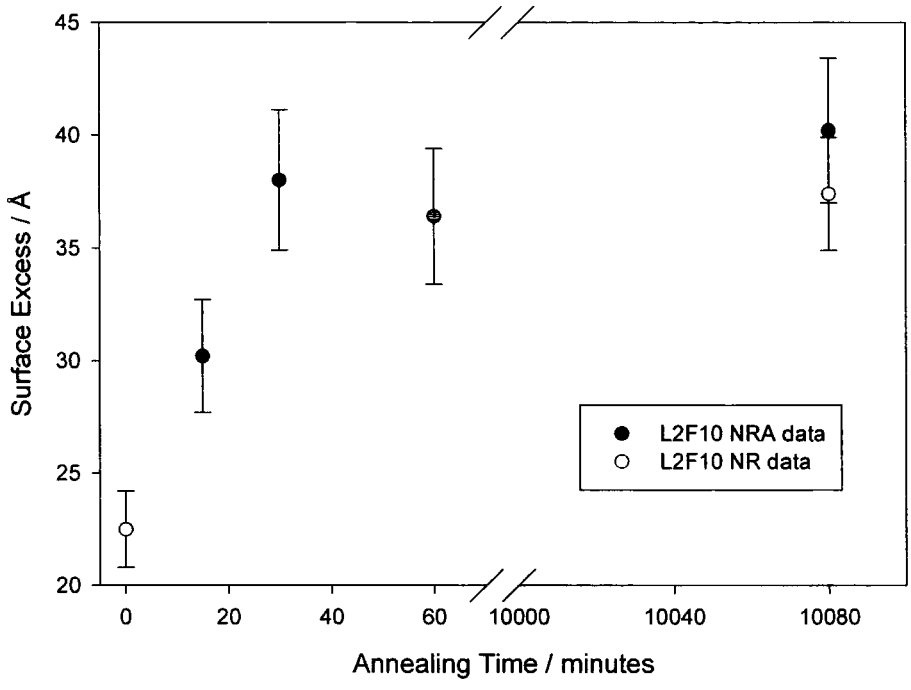


**Figure 6.1.16 Surface excess as a function of annealing time for L2F10 kinetics samples with values for the unannealed and fully annealed sample by NR shown for comparison.**

For the H2F10 samples some variation could be seen in the NRA profiles. The parameters used to obtain fits using FITTER are given in table 6.1.14; figure 6.1.17 shows examples of the NRA data along with the fitted profile. From the fitted profile values of the bulk, $\phi_b$ and surface, $\phi_s$ volume fractions and surface excess, z* were obtained, given in table 6.1.15.

| Sample | $\phi_b$ | $\phi_a$ | height/Å | width/Å | offset/Å | Resolution /Å |
|---|---|---|---|---|---|---|
| H2F10a15 | 0.08 | 0.33 | 89 | 30 | 153 | 204 |
| H2F10a30 | 0.08 | 0.35 | 98 | 70 | 119 | 204 |
| H2F10a50 | 0.08 | 0.34 | 102 | 68 | 149 | 201 |
| H2F10a60 | 0.08 | 0.34 | 116 | 68 | 166 | 159 |
| H2F10a90 | 0.08 | 0.34 | 120 | 60 | 150 | 187 |
| H2F10a2 | 0.08 | 0.41 | 120 | 50 | 150 | 201 |
| H2F10a4 | 0.08 | 0.44 | 106 | 52 | 148 | 201 |

**Table 6.1.14 Parameters used to obtain fits to NRA data.**

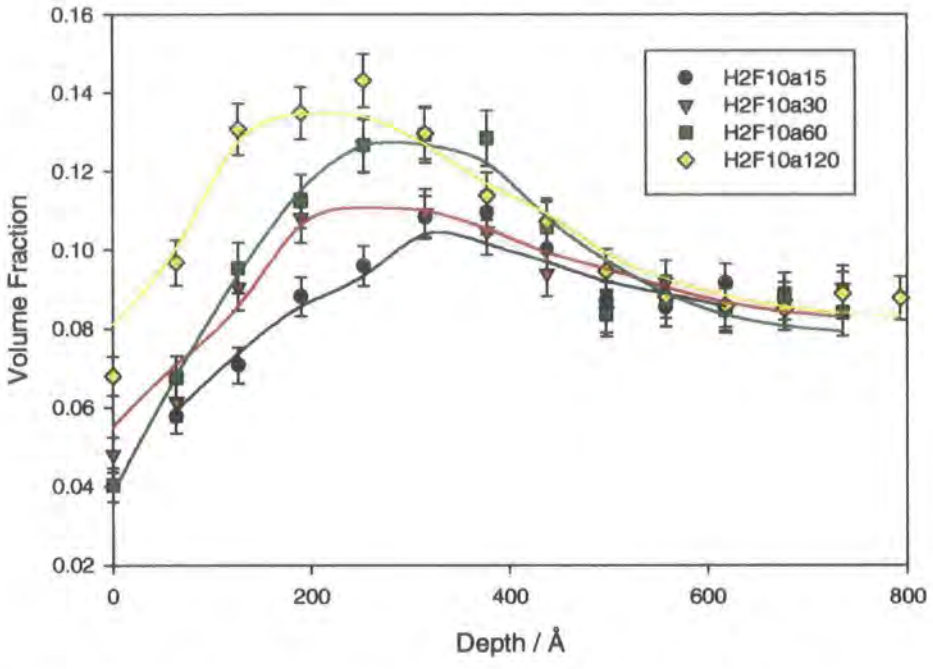


**Figure 6.1.17 NRA data for H2F10 kinetics samples showing tanh function fits to data.**

| Sample | $\phi_b$ | $\phi_s$ | z*/Å |
|---|---|---|---|
| H2F10a15 | 0.08 | 0.33 | 22 |
| H2F10a30 | 0.08 | 0.35 | 26 |
| H2F10a50 | 0.08 | 0.34 | 26 |
| H2F10a60 | 0.08 | 0.34 | 30 |
| H2F10a90 | 0.08 | 0.34 | 31 |
| H2F10a2 | 0.08 | 0.41 | 39 |
| H2F10a4 | 0.08 | 0.43 | 38 |

**Table 6.1.15 Parameters obtained from fits to NRA data.**

Four samples of H2F10 annealed between 15 and 120 minutes were also analysed using neutron reflectometry on the SURF reflectometer at the Rutherford Appleton Laboratory. The reflectivity profiles (figure 6.1.18) showed some variation up to 2 hours of annealing. The 2 hour sample was indistinguishable from the fully annealed sample measured previously on CRISP.

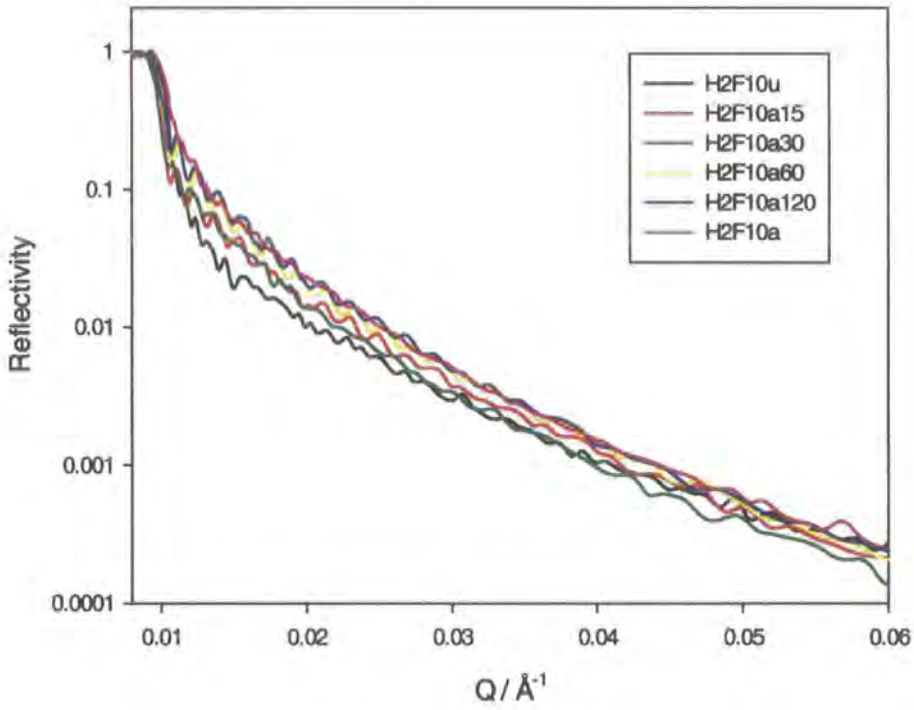


**Figure 6.1.18 Neutron reflectivity profiles for H2F10 kinetics samples.**

The reflectivity data were obtained during the commissioning of SURF, and at this time there were problems with the instrument alignment at low incident angles. This, along with the small quantity of deuterated material in the sample affected the quality of the NR data at low Q values and hence the subsequent fits. The data were analysed using VOLFMEM, and figure 6.1.19 shows the profiles and VOLFMEM fits to the data. Values of the surface parameters obtained from the volume fraction profiles (figure 6.1.20) are given in table 6.1.16.

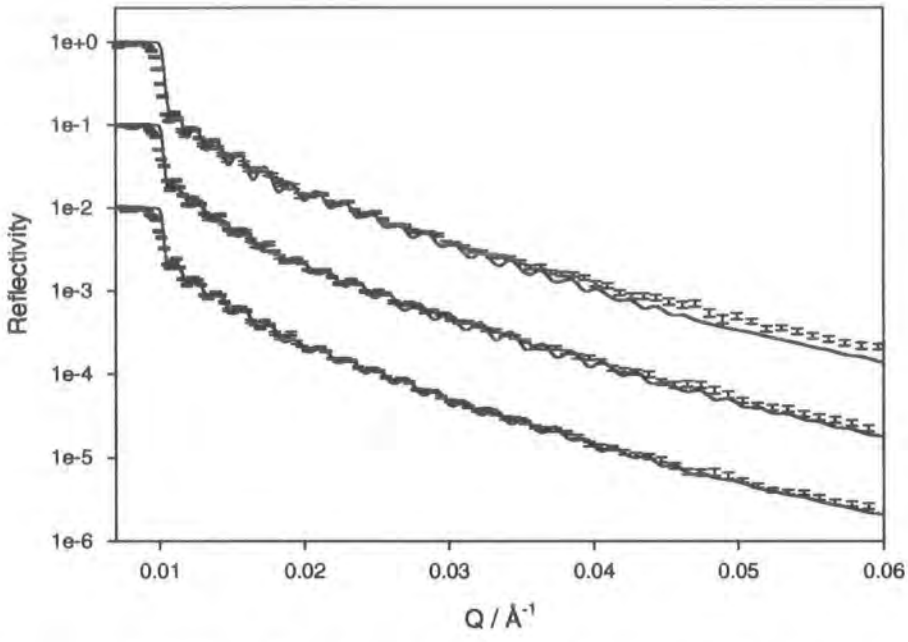


**Figure 6.1.19 NR profiles showing the VOLFMEM fits for (from the top) H2F10a15, H2F10a60 and H2F10a120. Subsequent data sets are offset by a factor of 10 for clarity.**

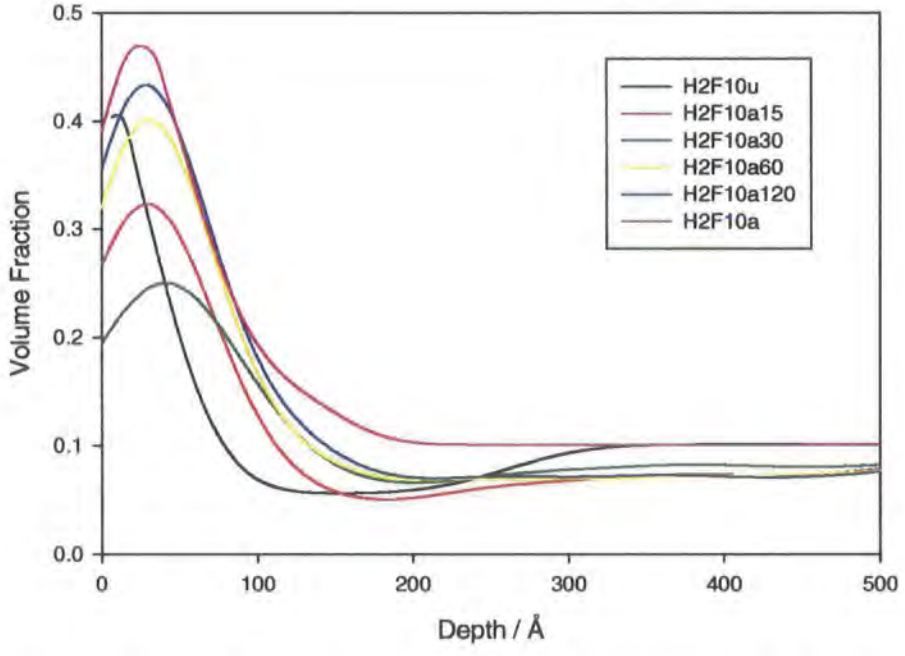


**Figure 6.1.20 Volume fraction profiles from the VOLFMEM fits to the NR data for the H2F10 kinetics samples**

| Sample | $\phi_b$ | $\phi_s$ | z*/Å |
|---|---|---|---|
| H2F10u | 0.09 | 0.40 | 15 |
| H2F10a15 | 0.05 | 0.32 | 22 |
| H2F10a30 | 0.07 | 0.25 | 18 |
| H2F10a60 | 0.07 | 0.40 | 28 |
| H2F10a120 | 0.07 | 0.43 | 30 |
| H2F10a | 0.09 | 0.47 | 31 |

**Table 6.1.16 Parameters obtained from VOLFMEM fits to NR data.**

The volume fraction profiles show that during spinning segregation occurred which gave a thin layer of functional polymer at the air surface. On annealing this layer stretched further into the bulk with a reduction in the surface volume fraction; but on further annealing there was diffusion from the bulk which maintained the layer thickness and increased the surface volume fraction. The values of surface excess obtained from NRA and NR are shown plotted on figure 6.1.21. The agreement between the two techniques is good and within the experimental error.

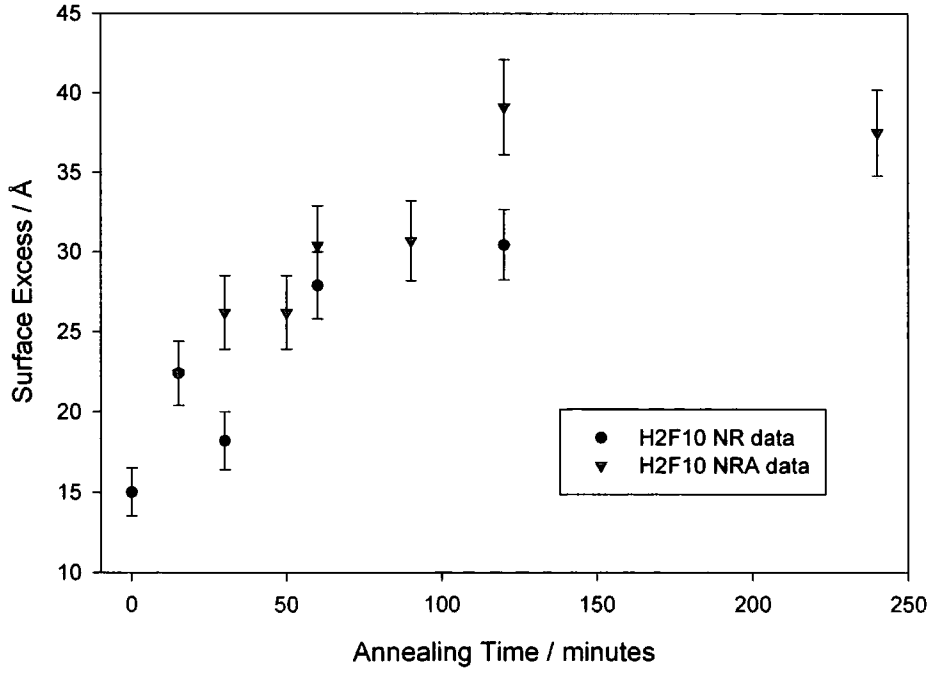


**Figure 6.1.21 Surface excess values obtained using both NR and NRA as a function of annealing time for H2F10 kinetics samples.**

### 6.1.5 Discussion of Blend Kinetics

For the blended samples segregation has been shown to occur in the unannealed samples as a result of the spinning process. As this is not fully understood, and the amount of segregation thought to depend upon the solution concentration, the duration of time before spinning and on the spinning speed, each sample studied would have a different surface composition profile before annealing commenced. The segregation during sample preparation will influence the kinetics of segregation due to the annealing process, and the extent of this effect could vary between individual samples. However, notwithstanding the above, interesting observations of the process of surface segregation have been obtained by investigating the surface composition profile as a function of annealing time.

For the low molecular weight difunctional polymer (L2F), the full extent of segregation occurred after 15 minutes of annealing. The data obtained gave an indication in the reproducibility of the neutron reflectometry results for different specimens of the same sample and was very good. The volume fraction profiles for the high molecular weight difunctional polymer (H2F) showed some variation up to one hour of annealing, but again the majority of the segregation occurred during sample preparation and after 15 minutes of annealing. The results for this system were further supported by NRA data on a 10% sample; the agreement in the surface excess values between the two techniques was excellent. The lower bulk volume fraction allowed variation in the volume fraction profiles to be seen more clearly and indicated that the segregation that occurred during spinning produced a thin layer of functional polymer at the surface. Initially, on annealing this layer stretched into the

bulk, and was then supplemented by the diffusion of further material from the bulk of the sample.

The STAR polymer system showed the greatest variation in the volume fraction profile over the annealing times, with only a small amount of segregation occurring during sample preparation in comparison to the linear polymer systems. After two hours the surface excess was still increasing and had changed considerably by eight hours of annealing at 413K when the equilibrium segregation had been attained. It would therefore have been useful to have measured further samples in the 2 to 8 hour range. Whilst at equilibrium the architecture has had little effect on the extent of the surface segregated layer, a longer annealing time is required for the equilibrium surface excess to be achieved. This supports the Monte Carlo simulations of Sikorski and Romiszowski[3], which suggest that the dynamics of a star polymer are slower than for a linear polymer of the same degree of polymerisation. Walton and Mayes[4] suggest that the more branched component would segregate more favourably, i.e. produce a larger surface excess over a linear chain of equivalent molecular weight. However, they do not indicate any time scales or account for the presence of functional groups in the polymer stating that enthalpic contributions tend to dominate over configurational entropy.

Determination of the diffusion coefficient has been difficult because of the extent of segregation seen in the as prepared samples, especially the L2F blends where equilibrium was achieved after 15 minutes. However, estimations of the diffusion coefficients have been made from the variation in the surface excess with annealing time. Log-log plots of the surface excess against annealing time gave straight lines, $z^* \sim t^v$ where v was equal to 0.23 for 10% H2F measured by NRA and

0.19 by NR, and 0.23 for the 30% STAR blends. These are in agreement with the value obtained by Clarke for carboxy terminated polystyrene in different molecular weight hPS (0.18±0.07)[5]. However, diffusion theories predict a square root of annealing time, $t^{1/2}$ dependence and indeed for the 10 and 30% H2F samples and the 30% STAR samples there is a linear variation in surface excess with $t^{1/2}$. Figure 6.1.22 shows the variation of surface excess with $t^{1/2}$, from the slopes of these lines diffusion coefficients were calculated, 10% H2F $5.2\times10^{-16}cm^2s^{-1}$, 30% H2F $8.8\times10^{-17}cm^2s^{-1}$ and 30% STAR $3.6\times10^{-17}cm^2s^{-1}$. However, these values do not take into account that the intercept is not at zero due to the segregation that had occurred during sample preparation and assume a constant bulk volume fraction of functional polymer for all the annealing times. If the surface excess of the unannealed sample was subtracted the slope would be the same, but the rate of change of the surface excess might be different if there was no segregation during sample preparation.

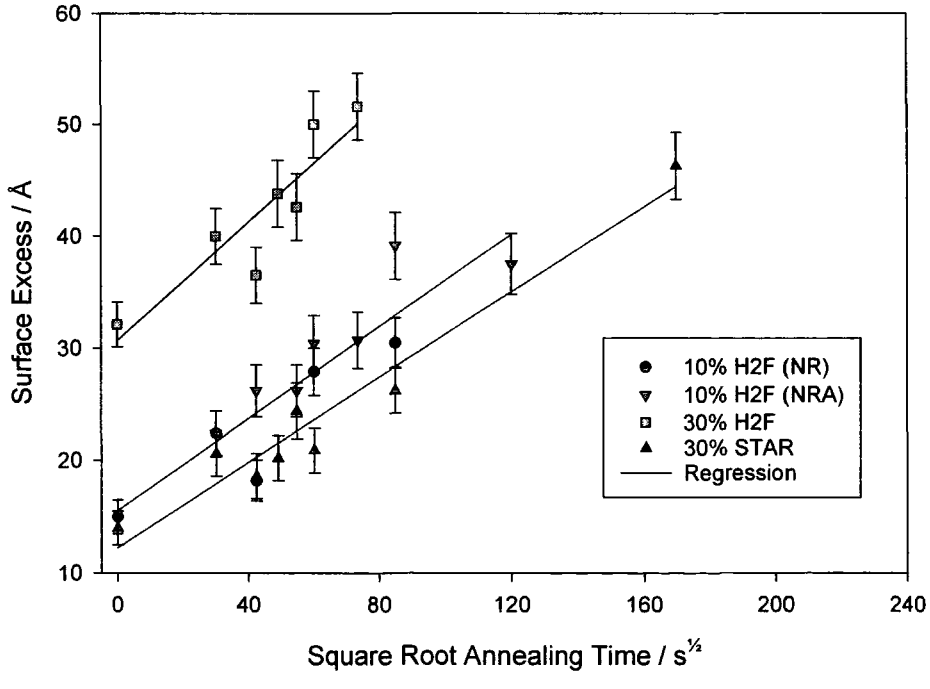


**Figure 6.1.22 Surface excess values plotted against the square root of the annealing time showing a linear relationship.**

If the slope in figure 6.1.22 is taken through the origin, the regression lines through the data are not as good, but the diffusion coefficients thus obtained are 10% H2F $1.4\times10^{-15}cm^2s^{-1}$, 30% H2F $5.9\times10^{-16}cm^2s^{-1}$ and 30% STAR $8.7\times10^{-17}cm^2s^{-1}$.

When the surface excess value is smaller than the radius of gyration of the segregating polymer (i.e. before chain stretching occurs restricting penetration into the brush layer by polymer diffusing from the bulk), $z^* = \frac{2}{\sqrt{\pi}}\phi_b\sqrt{Dt}$. Diffusion coefficients calculated were constant for one set of samples except for the first value (15 minutes annealed sample) and values where the surface excess was approaching the equilibrium value. The values are higher than those obtained from the slope of figure 6.2.22 because of the surface excess that occurred during sample preparation. If the initial surface excess value is subtracted the values obtained are approximately the same as those obtained from the slope of figure 6.2.22. However, the surface excess values attained after 30 minutes or more annealing could actually be about the same as if there had been no segregation during sample preparation and then the diffusion coefficient should be calculated for the surface excess at that time. The values obtained are shown plotted in figure 6.1.23 and the average values for each of the compositions studied are given in table 6.1.17. The values obtained for H2F are around a factor of 10 lower than that estimated by Clarke[5] for carboxy terminated dPS. However, the polymer used by Clarke was of slightly lower molecular weight and the samples were annealed at 423K, ten degrees higher than the annealing temperature used here.

| Sample | Diffusion Coefficient / $cm^2s^{-1}$ |
|---|---|
| L2F10 | $7.8\times10^{-15}$ |
| L2F30 | $5.0\times10^{-15}$ |
| H2F10 | $3.0\times10^{-15}$ |
| H2F30 | $1.1\times10^{-15}$ |
| STAR30 | $1.8\times10^{-16}$ |

**Table 6.1.17 Diffusion coefficients determined from the surface excess values at intermediate annealing times.**

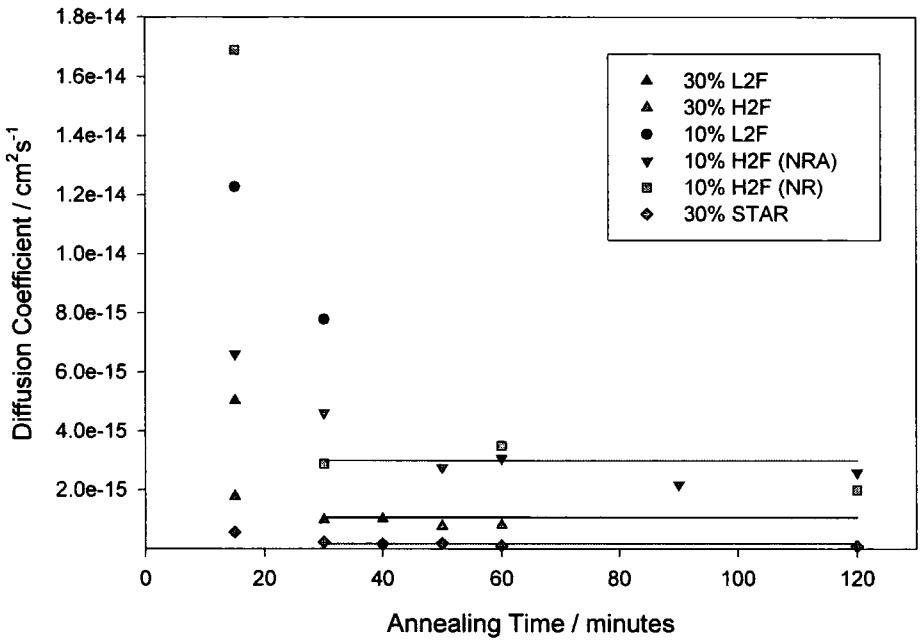


**Figure 6.1.23 Diffusion coefficients calculated from the surface excess value at each annealing time. Lines show the average values after 30 minutes annealing.**

Klein et al[6] predicted diffusion coefficients, D(N), assuming reptative motion dependent upon the degree of polymerisation, N, of the polymer, $D(N)=\frac{D_0}{N^2}$. For dPS diffusing at 140°C they found that $D_0 = 1.5\times10^{-9}cm^2s^{-1}$. This gives values for D(N) of $6\times10^{-15}cm^2s^{-1}$ for the L2F polymer and $2\times10^{-15}cm^2s^{-1}$ for the H2F polymer, both in good agreement with the experimental values calculated using the surface excess values for annealing times between 30 and 120 minutes. The STAR polymer

would not undergo reptation so the diffusion coefficient could not be estimated in this manner. However, the polymer would be expected to diffuse more slowly and the diffusion coefficient was a factor of 10 lower than that of the H2F polymer of a similar total molecular weight.

## 6.2 Bilayer Kinetics

A layer of the pure functional polymer or a blend of the functional polymer with linear hPS was spun cast onto the silicon substrate. This was then overlaid with a layer of hPS, which had been spun onto a microscope slide (76mm × 52mm) and then floated off onto the surface of distilled water before being picked up onto the substrate. The sample was allowed to dry in the air before drying under vacuum overnight at room temperature. Contact profilometry was used to determine the thickness of the base layer, the hPS layer on the microscope slide, and the thickness of the full sample. The two separate layer thickness measurements were in good agreement with both the final bilayer measurement and with the experimental results.

For NRA two or three samples of each composition were prepared which were then broken into four to six pieces about 10mm × 20mm, each individual piece was annealed under vacuum for a different time at 413K. For NR three samples of each composition were prepared, one was annealed for 48 hours and the others left as prepared. NR data were collected for one of the unannealed samples, after measurement the sample was annealed under vacuum at 413K for a known time and then the neutron reflectivity was measured again. The same sample was used to collect data over a range of annealing times; the third sample was used to cover a

wider range of annealing times. Annealing times up to 24 hours were covered using the two samples.

### 6.2.1 NRA Bilayer Kinetics

For NRA studies samples were prepared with a hPS top layer of ~1000Å. This thickness was chosen so that the segregation could be seen in the layer but without the $He^{3+}$ beam having to penetrate so far into the sample that the resolution at the interface would be lost. The base layer ranged from 20% deuterated polymer to pure deuterated polymer and was also of the order of 1000Å thick. This layer thickness was chosen so that a low incident angle could be used to increase the resolution but allow the beam to penetrate through to the substrate for normalisation of the data.

An initial investigation was carried out using samples prepared with a base layer of 20 and 30% TK 181 dPSF2 in TK 192 hPS and 20% TK 204 dPS in the same hPS. Samples were measured as prepared and after annealing for 7 days to ensure that the technique and sample preparation methods were valid. The volume fraction profiles of these samples are shown in figure 6.2.1. In all the as prepared samples the bilayer structure could be clearly seen. After annealing the 20% dPS sample showed a uniform distribution of dPS throughout the sample, whereas the dPSF2 samples showed a segregated layer at the air surface followed by a uniform bulk layer. For the 30% dPSF2 a sample was measured that had only been annealed for 48 hours. The volume fraction profile was identical to that of the 7 days annealed sample showing that the sample had fully diffused and equilibrium had been attained after 48 hours of annealing.

Clearly bilayers were a viable method of studying the mechanism of segregation of the functional polymer without already having a segregated layer at the air surface (though segregation may presumably have occurred in the base layer and could affect the initial interdiffusion). Samples were prepared with 30, 50, 75 and 100% TK 249 dPSF2 in the base layer with samples with pure TK 204 dPS base layer as controls. All the toplayers were TK 192 hPS, which was also used to prepare the blended samples. Unannealed samples and samples after annealing at 413K for between 5 minutes and 48 hours were measured using NRA.

| **Base Layer** | **Thickness / Å** | **hPS layer / Å** | **Annealing times / minutes** | $\phi_D$ |
|---|---|---|---|---|
| 30% dPSF2 | 930 | 1080 | **U, 5, 15** | 0.14 |
| | 920 | 1080 | 90, **90** | 0.14 |
| | 920 | 1070 | U, 180, 240, 480, 1440, 2880 | 0.14 |
| 50% dPSF2 | 1200 | 940 | U, 5, 15, 30, 60, 2880 | 0.28 |
| | 1230 | 920 | 90, 120, 180, 240, 480 | 0.29 |
| 75% dPSF2 | 780 | 960 | U, 5, 15, 30, 60, 2880 | 0.34 |
| | 860 | 970 | 90, 120, 180, 240, 480 | 0.35 |
| 100% dPSF2 | 840 | 1180 | **U**, 5, **5**, **15**, 60 | 0.42 |
| | 840 | 1140 | **60**, **90**, 120, **180**, 240 | 0.42 |
| | 860 | 1090 | **U**, 240, **480**, 1440, **2880** | 0.44 |
| | 890 | 900 | U, 15, 480, 2880 | 0.50 |
| 100% dPS | 720 | 1130 | U, 5, 60, 240, 2880 | 0.39 |
| | 1140 | 910 | 15, 30, 90, 120, 180, 480 | 0.56 |

**Table 6.2.1 Composition of bilayer samples and annealing times measured using NRA. Times in bold were measured at an incident beam angle of 6°.**

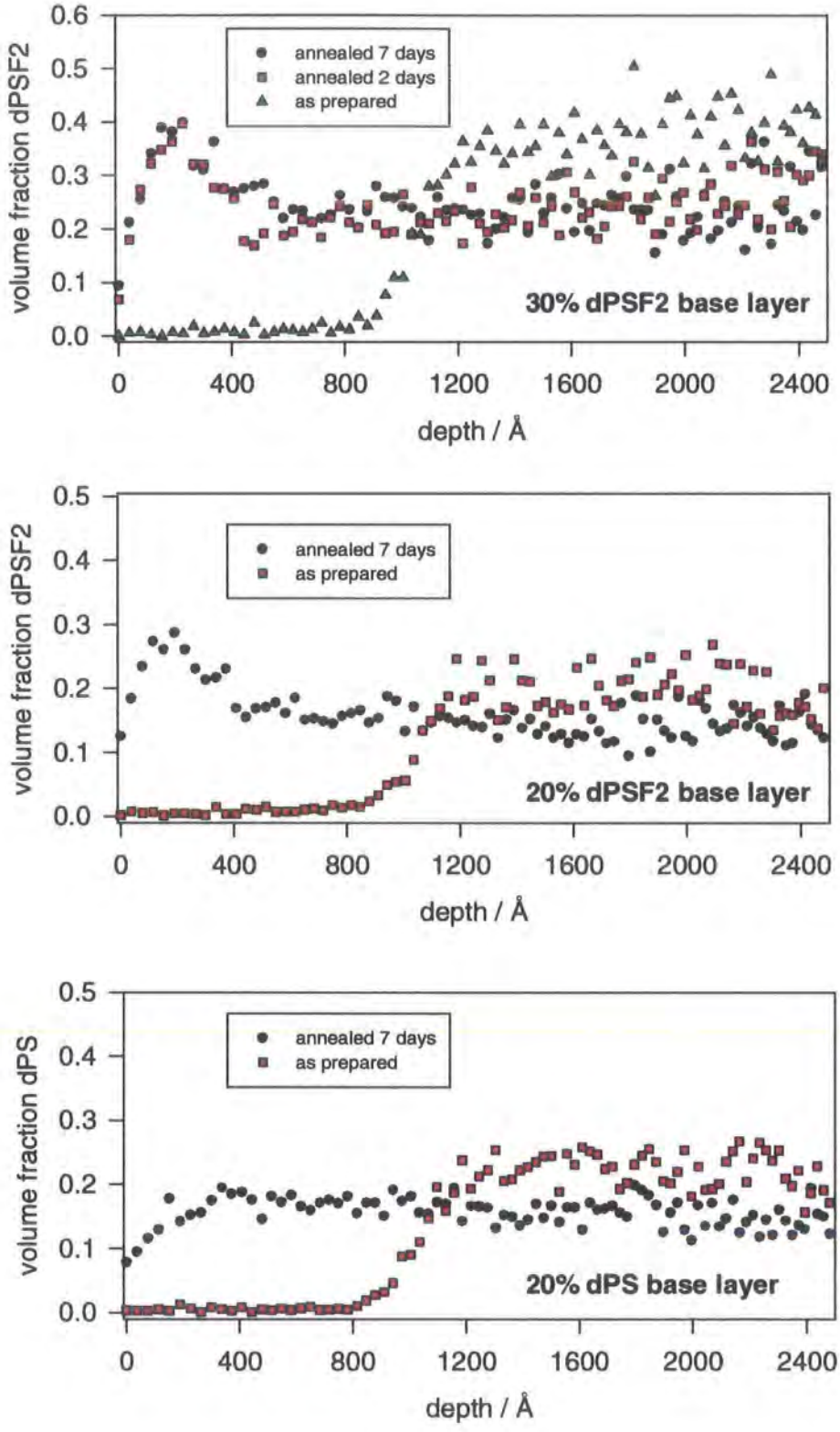


**Figure 6.2.1 Comparison between the annealed and unannealed NRA volume fraction profiles for the initial bilayer studies.**

When preparing the samples, the aim was to make as many NRA measurements as possible from samples from the same silicon wafer to minimise the variation, and also to try to keep the film thickness of samples prepared from different wafers similar. Table 6.2.1 shows the film thickness and annealing times of samples measured by NRA. The volume fraction of deuterated polymer, $\phi_D$ was calculated assuming a uniform distribution of the deuterated polymer throughout the total sample thickness and was used to normalise the data in order to obtain the volume fraction profiles. Measurements were made at an incident beam angle of 9°, on one occasion there were problems with the instrumental set-up and measurements were made at 6°. This gave increased resolution at the immediate air surface, but the resolution at the interface was poor and the beam did not penetrate through to the substrate, which made it difficult to normalise the data.

Figures 6.2.2 to 6.2.7 show the normalised NRA profiles obtained for the bilayer samples. The data were obtained on a number of separate occasions; where possible the different annealing times for the same sample were measured at the same time. The variation in the resolution of the technique under different experimental set-ups can be seen in the data especially the results of the dPS / hPS bilayer. The first set of data (figure 6.2.6) has good signal to noise and the volume fraction profiles are smooth, in the second set (figure 6.2.7) the signal to noise is not as good and the data points show a greater degree of scatter. The resolution of the data also varies with depth into the sample, due to beam straggling, giving greater noise in the data at the substrate interface, particularly evident in figure 6.2.5 where the lower incident angle increases the effect.

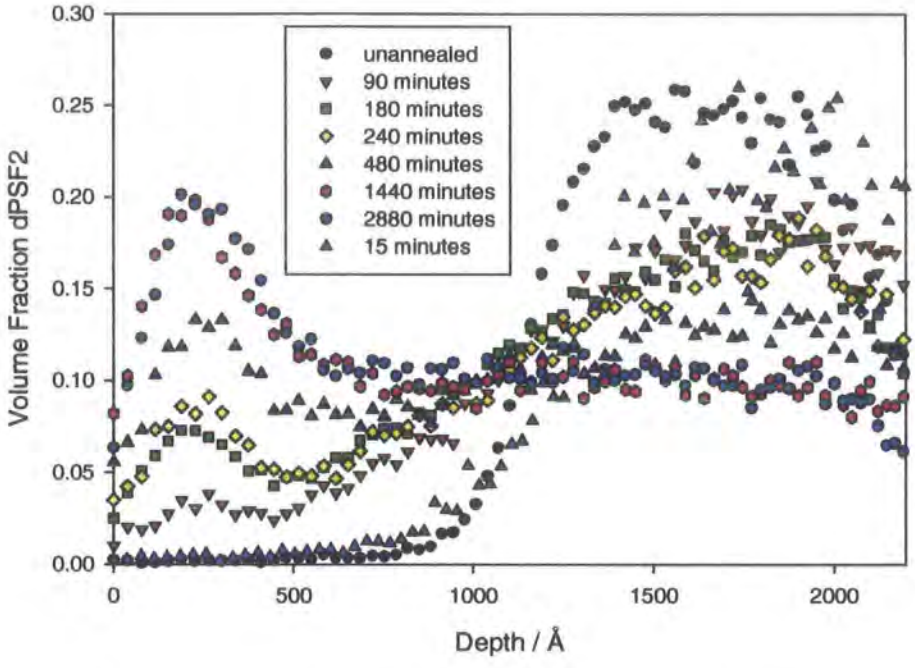


**Figure 6.2.2 Normalised NRA data for the 30% dPSF2 base layer bilayer samples**

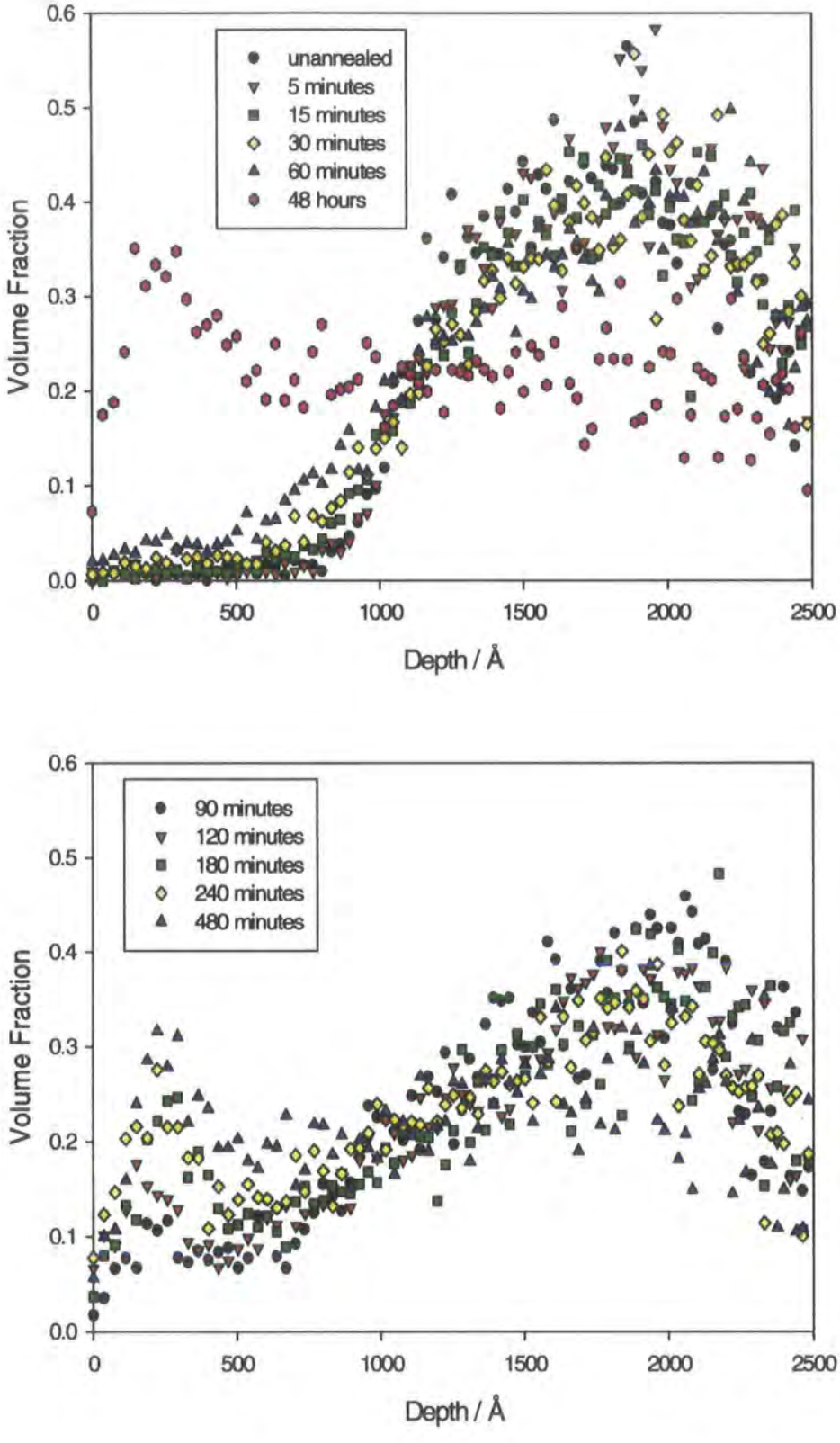


**Figure 6.2.3 Normalised NRA data for 50% dPSF2 base layer bilayer samples. Each graph shows samples from the same wafer.**

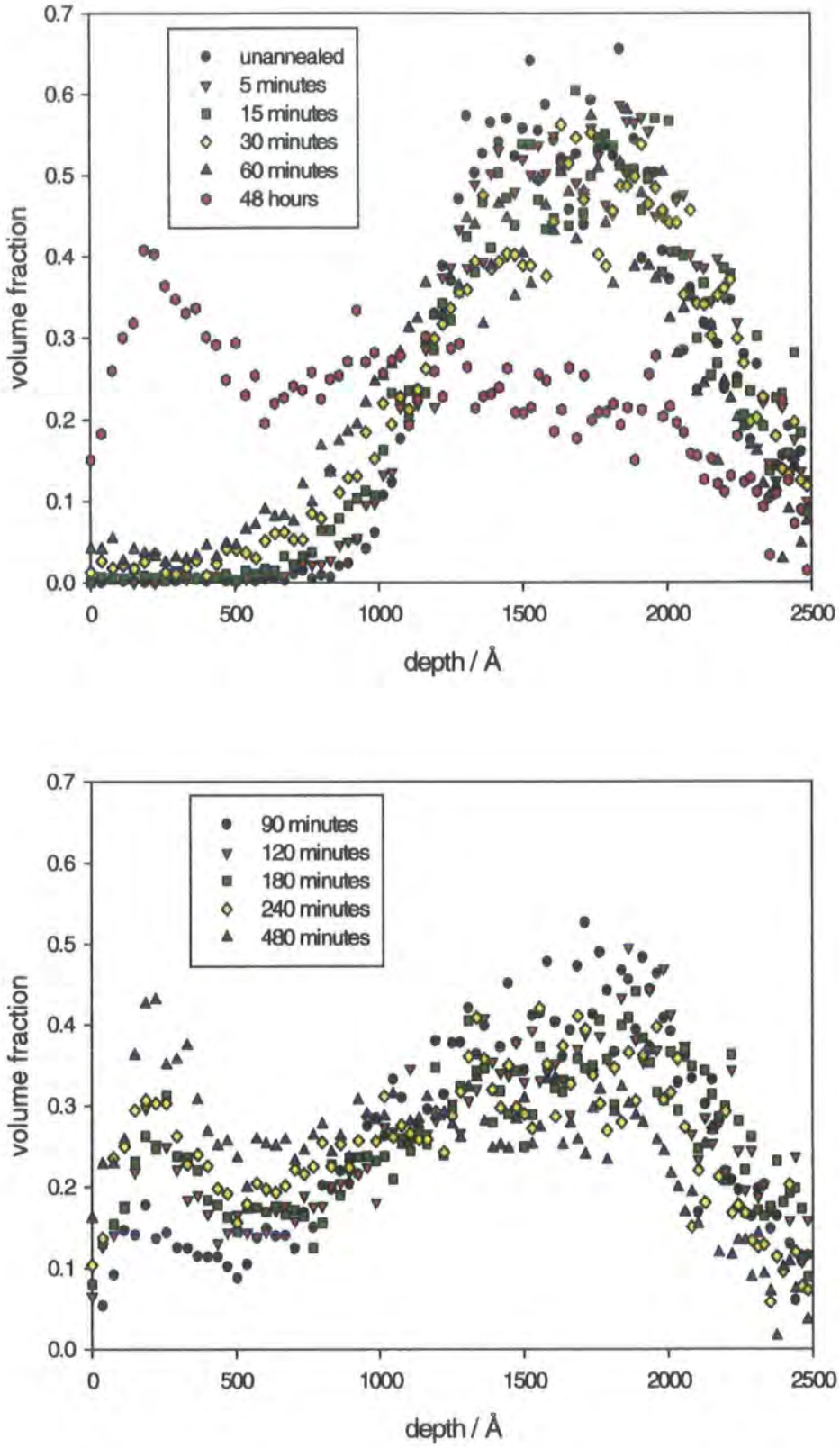


**Figure 6.2.4 Normalised NRA data for 75% dPSF2 base layer bilayer samples. Each graph shows samples from the same wafer.**

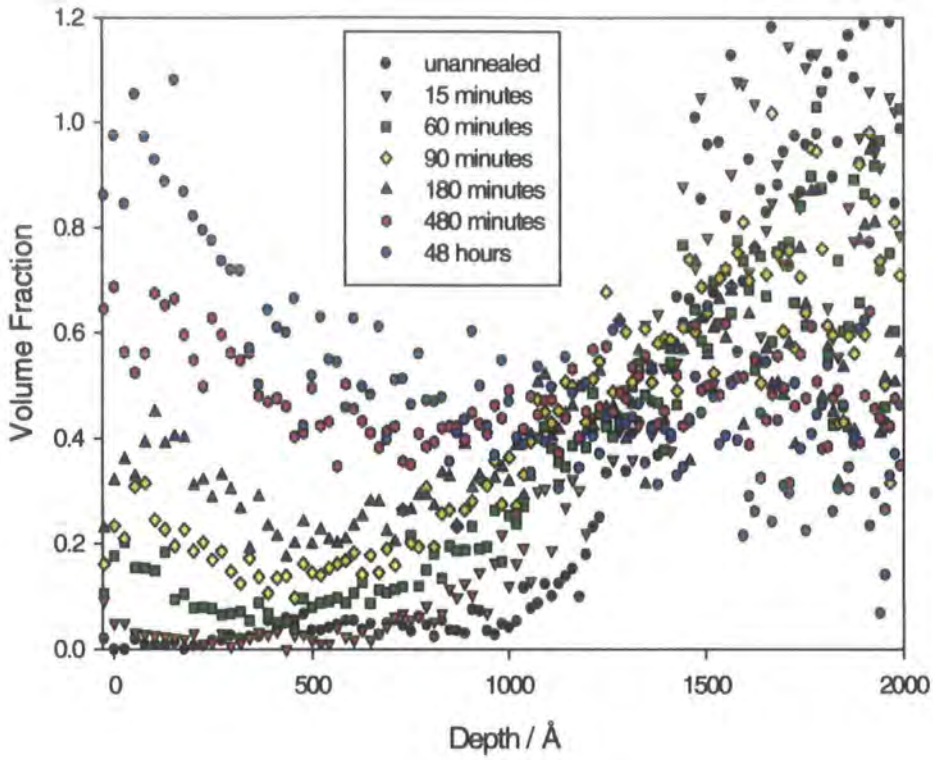


**Figure 6.2.5 Normalised NRA data for dPSF2 / hPS bilayer at an incident angle of 6°.**

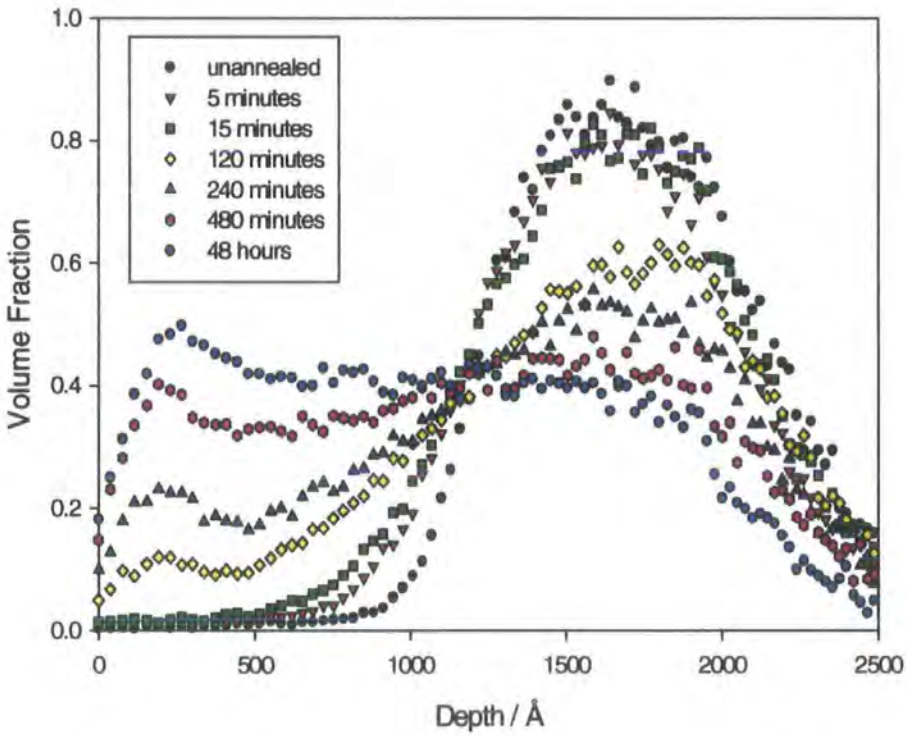


**Figure 6.2.6 Normalised NRA data for dPSF2 / hPS bilayer at an incident angle of 9°.**

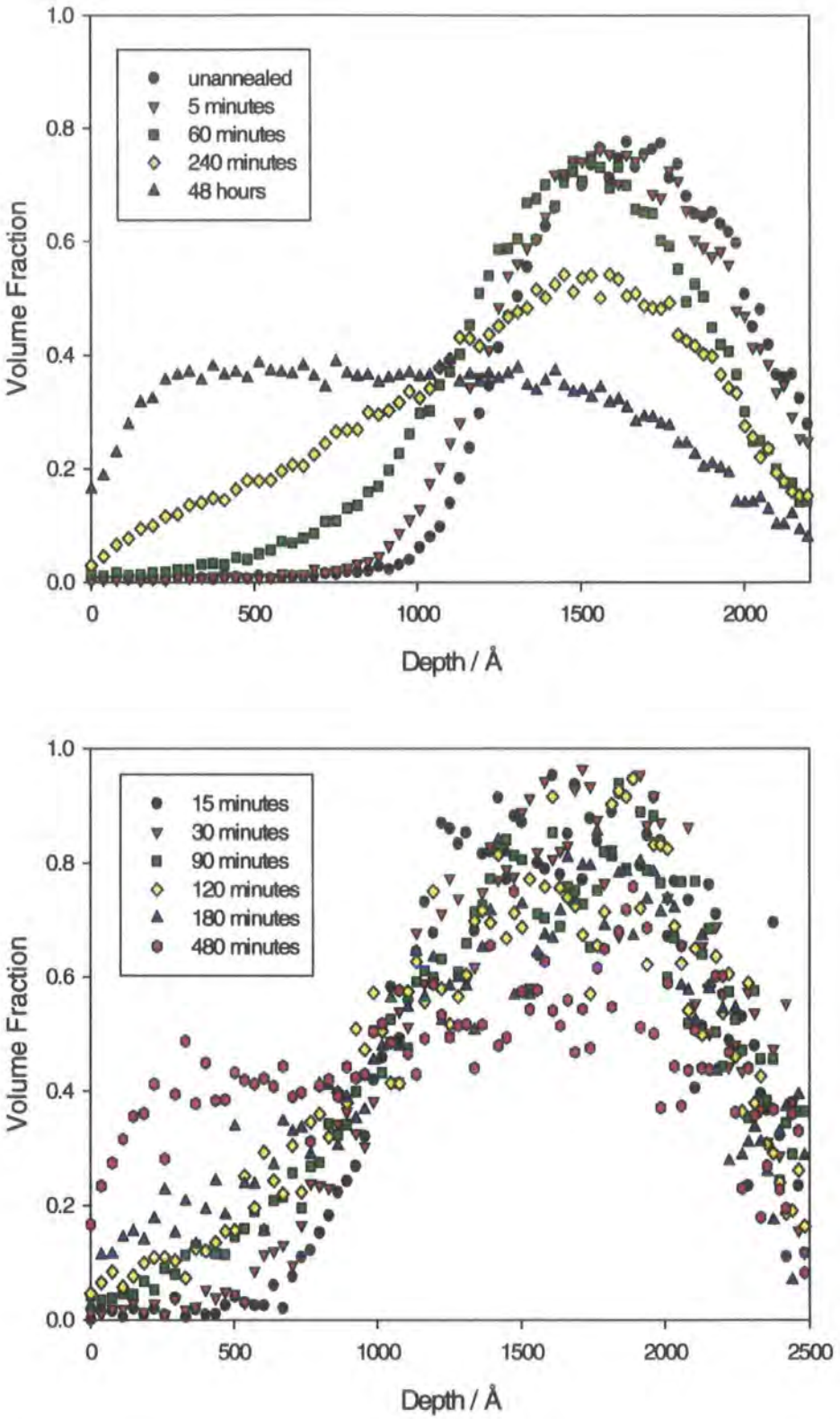


**Figure 6.2.7 Normalised NRA data for hPS / dPS bilayer samples. Each graph shows samples from the same wafer, the instrumental resolution was worse for the second set of data.**

From the profiles, interdiffusion between the two layers could be seen as interfacial broadening and the amount of deuterated material in the top layer increased with annealing time. In the samples with dPSF2 in the base layer, initially only interfacial broadening could be seen, but after 60 minutes of annealing a segregated layer at the surface was observed. For annealing times greater than 60 minutes the surface excess continued to grow along with further interfacial broadening. After 480 minutes of annealing the sample was close to equilibrium with a surface excess followed by a uniform bulk layer. Only a slight variation could be seen between this and the 48 hours annealed sample.

Previous studies of interdiffusion have used Fick's solutions to the diffusion equation and have measured the interface width by fitting with an error function[7-10]. The interface width, w is equal to $(4Dt)^{½}$ where D is the diffusion coefficient and t the annealing time. For the dPS/hPS bilayer samples it was possible to measure the increase in the interface width on annealing. This increased linearly with the square root of the annealing time shown in figure 6.2.8 and from the slope a diffusion coefficient of $4.0\times10^{-15}cm^2s^{-1}$ was obtained. This value is in good agreement with values obtained in the literature[11], though many values quoted for polystyrene are for greater molecular weight and / or a much higher annealing temperature. It was impossible to use this method for the functional polymer bilayers because after only short annealing times it was difficult to separate the surface segregating layer from the increase in the interface width. The interface width appearing to be much less than expected because of the increase in the volume fraction of functional polymer in the top hPS layer.

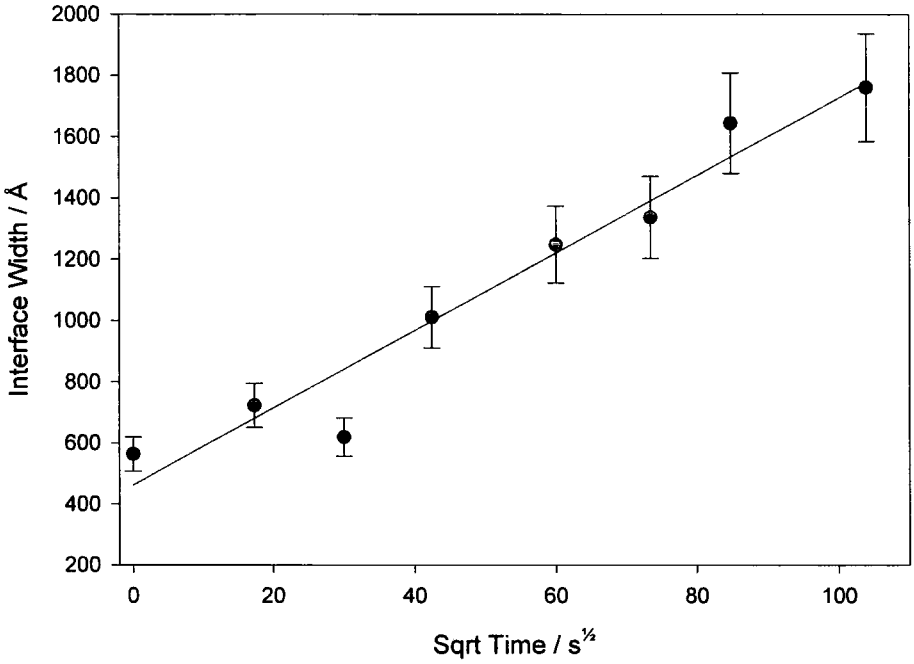


**Figure 6.2.8 Interface width between hPS layer and dPS layer.**

For the bilayers with functional polymer, the samples were analysed by integration to find the area under the curve in the top 500Å layer of the sample. The amount of deuterated polymer in this region increased with annealing time and is shown plotted in figures 6.2.9 and 6.2.10. To determine the diffusion coefficients the amount of segregated material at time t, $z^*_t$, was divided by the amount at equilibrium, $z^*_\infty$, and then multiplied by the diffusion distance, which was the thickness of the top hPS layer, $l^{12}$. This process should have normalised the slight variations between different samples. These values and the amount of segregated material for each annealing time are given in tables 6.2.2 to 6.2.6 for each polymer system and are shown plotted against the square root of annealing time in figures 6.2.11 and 6.2.12. When $l \times z^*_t/z^*_\infty$ was plotted against the square root of the annealing time for samples annealed between 60 minutes and 480 minutes a straight line graph was produced (figures 6.2.13 to 6.2.16). The slope of the line equal to $2D^{½}$

and hence the diffusion coefficient could be determined. Before 60 minutes there was no segregation to the air surface, and after 480 minutes the increase in the surface excess was slowing in the approach to the equilibrium value. In the 50 and 75% dPSF2 base layer samples there was a change in the slope after annealing for 120 minutes and the diffusion coefficient was determined for both values. For the 30% dPSF2 sample there was no evidence for a change in slope, though due to instrumental problems less samples had been measured for this system. For the pure dPSF2 base layer samples the instrumental resolution had a greater effect on the values and again there was no obvious change in the slope, the difference between the samples measured at different incident angles was negligible. The values of diffusion coefficient obtained are given in table 6.2.7.

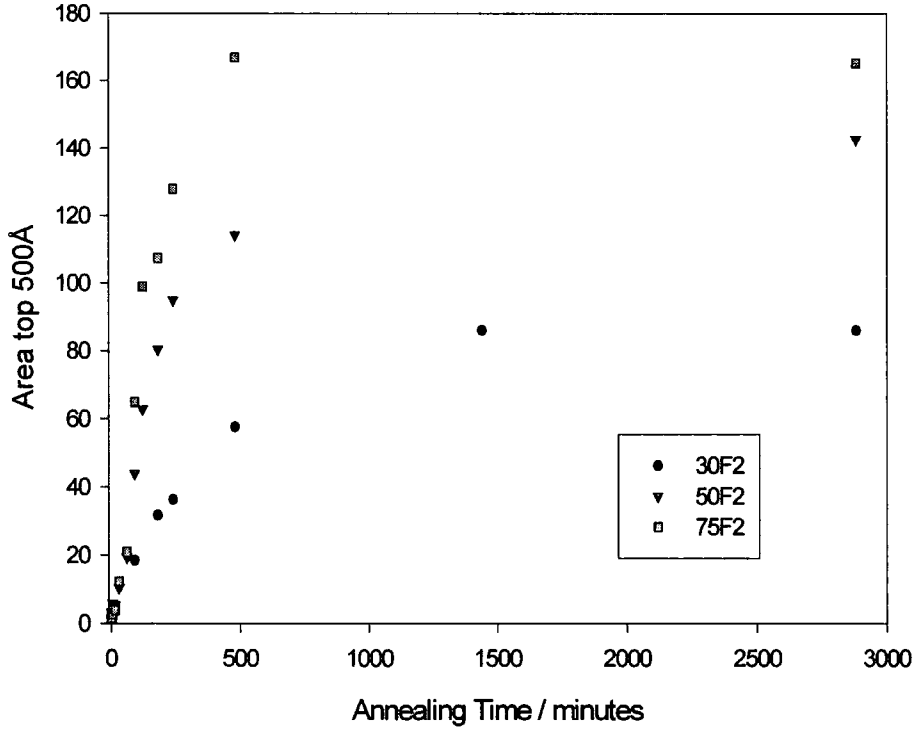


**Figure 6.2.9 Segregated material in the top 500Å of the 30%, 50% and 75% dPSF2 bilayers after annealing.**

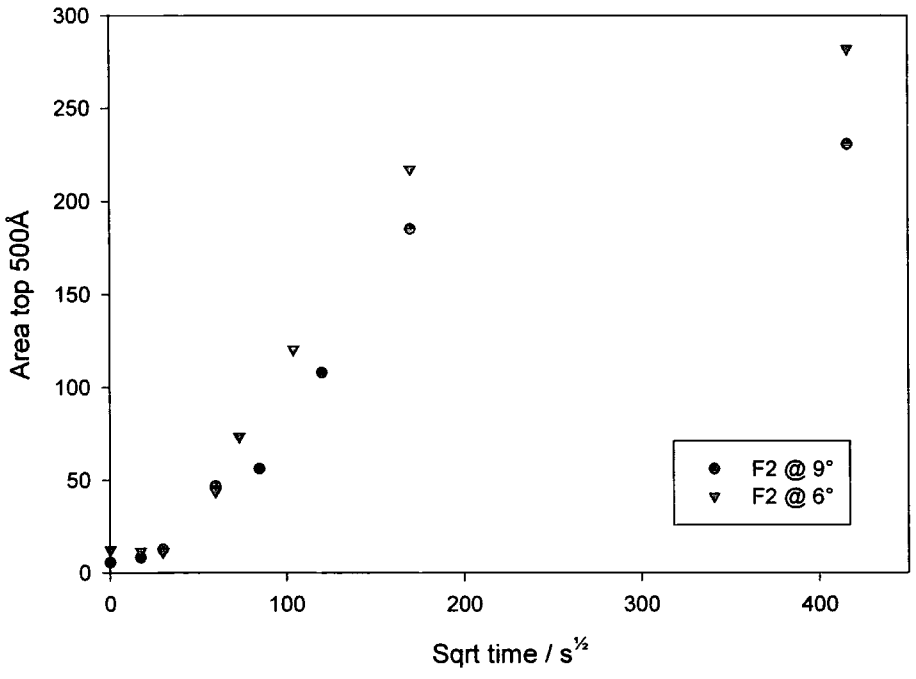


**Figure 6.2.10 Segregated material in the top 500Å of the dPSF2 bilayers after annealing. Slightly lower values were obtained at the higher incident angle due to the poorer resolution.**

| Annealing time / minutes | Sqrt time / $s^{½}$ | Area top 500Å / Å | $l \times z^*_t / z^*_\infty$ / cm ($\times 10^{-7}$) |
|---|---|---|---|
| 0 | 0 | 2.1 | 2.62 |
| 5 | 17.3 | 1.4 | 1.77 |
| 15 | 30.0 | 3.6 | 4.48 |
| 90 | 73.5 | 18.4 | 23.1 |
| 180 | 103.9 | 31.7 | 39.4 |
| 240 | 120.0 | 36.4 | 45.2 |
| 480 | 169.7 | 57.6 | 71.6 |
| 1440 | 293.9 | 86.1 | 107 |
| 2880 | 415.7 | 86.1 | 107 |

**Table 6.2.2 Segregated dPSF2 in the top 500Å and as a proportion of the equilibrium value for the 30% dPSF2 base layer bilayer samples.**

| Annealing time / minutes | Sqrt time / $s^{1/2}$ | Area top 500Å / Å | $l \times z^*_t / z^*_\infty$ / cm ($\times 10^{-7}$) |
|---|---|---|---|
| 0 | 0 | 3.2 | 2.12 |
| 5 | 17.3 | 5.8 | 3.80 |
| 15 | 30.0 | 5.4 | 3.56 |
| 30 | 42.4 | 10.3 | 6.82 |
| 60 | 60.0 | 19.4 | 12.8 |
| 90 | 73.5 | 43.8 | 28.3 |
| 120 | 84.9 | 62.8 | 40.5 |
| 180 | 103.9 | 80.3 | 51.9 |
| 240 | 120.0 | 94.9 | 61.3 |
| 480 | 169.7 | 114.2 | 73.7 |
| 2880 | 415.7 | 142.6 | 94.0 |

**Table 6.2.3 Segregated dPSF2 in the top 500Å and as a proportion of the equilibrium value for the 50% dPSF2 base layer bilayer samples.**

| Annealing time / minutes | Sqrt time / $s^{1/2}$ | Area top 500Å / Å | $l \times z^*_t / z^*_\infty$ / cm ($\times 10^{-7}$) |
|---|---|---|---|
| 0 | 0 | 1.5 | 0.87 |
| 5 | 17.3 | 2.6 | 1.53 |
| 15 | 30.0 | 3.8 | 2.19 |
| 30 | 42.4 | 12.2 | 7.07 |
| 60 | 60.0 | 20.9 | 12.1 |
| 90 | 73.5 | 64.9 | 38.1 |
| 120 | 84.9 | 98.9 | 58.1 |
| 180 | 103.9 | 107.4 | 63.1 |
| 240 | 120.0 | 127.8 | 75.0 |
| 480 | 169.7 | 166.9 | 98.0 |
| 2880 | 415.7 | 165.2 | 96.0 |

**Table 6.2.4 Segregated dPSF2 in the top 500Å and as a proportion of the equilibrium value for the 75% dPSF2 base layer bilayer samples.**

| Annealing time / minutes | Sqrt time / $s^{1/2}$ | Area top 500Å / Å | $l \times z^*_t / z^*_\infty$ / cm ($\times 10^{-7}$) |
|---|---|---|---|
| 0 | 0 | 12.4 | 4.79 |
| 5 | 17.3 | 11.6 | 4.86 |
| 15 | 30.0 | 11.3 | 4.72 |
| 60 | 60.0 | 43.8 | 17.7 |
| 90 | 73.5 | 73.5 | 29.7 |
| 180 | 103.9 | 120.5 | 48.7 |
| 480 | 169.7 | 217.2 | 84.0 |
| 2880 | 415.7 | 281.9 | 109 |

**Table 6.2.5 Segregated dPSF2 in the top 500Å and as a proportion of the equilibrium value for the dPSF2 base layer bilayer samples measured using NRA at an incident angle of 6°.**

| Annealing time / minutes | Sqrt time / $s^{1/2}$ | Area top 500Å / Å | $l \times z^*_t / z^*_\infty$ / cm ($\times 10^{-7}$) |
|---|---|---|---|
| 0 | 0 | 5.6 | 2.19 |
| 5 | 17.3 | 8.3 | 4.24 |
| 15 | 30.0 | 12.7 | 4.97 |
| 60 | 60.0 | 46.9 | 24.0 |
| 120 | 84.9 | 56.3 | 27.8 |
| 240 | 120.0 | 108.3 | 53.4 |
| 480 | 169.7 | 185.3 | 72.3 |
| 1440 | 293.9 | 171.8 | 81.2 |
| 2880 | 415.7 | 230.7 | 90.0 |

**Table 6.2.6 Segregated dPSF2 in the top 500Å and as a proportion of the equilibrium value for the dPSF2 base layer bilayer samples measured using NRA at an incident angle of 9°.**

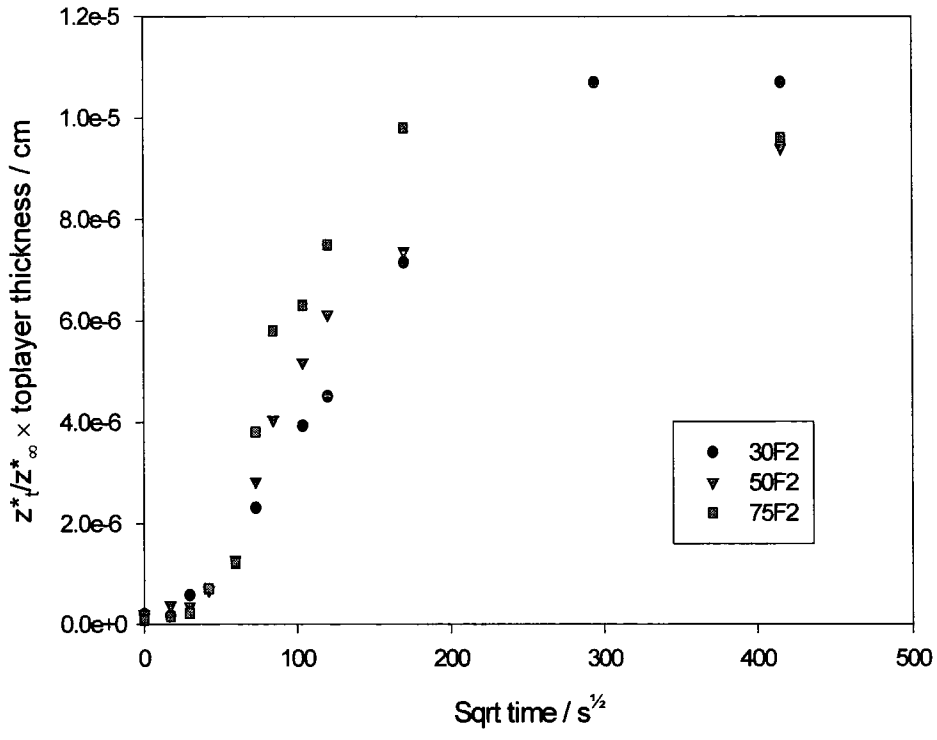


**Figure 6.2.11 Ratio of the surface excess at time t to the equilibrium excess multiplied by the hPS layer thickness against the square root of annealing time for the 30%, 50% and 75% dPSF2 bilayer samples**

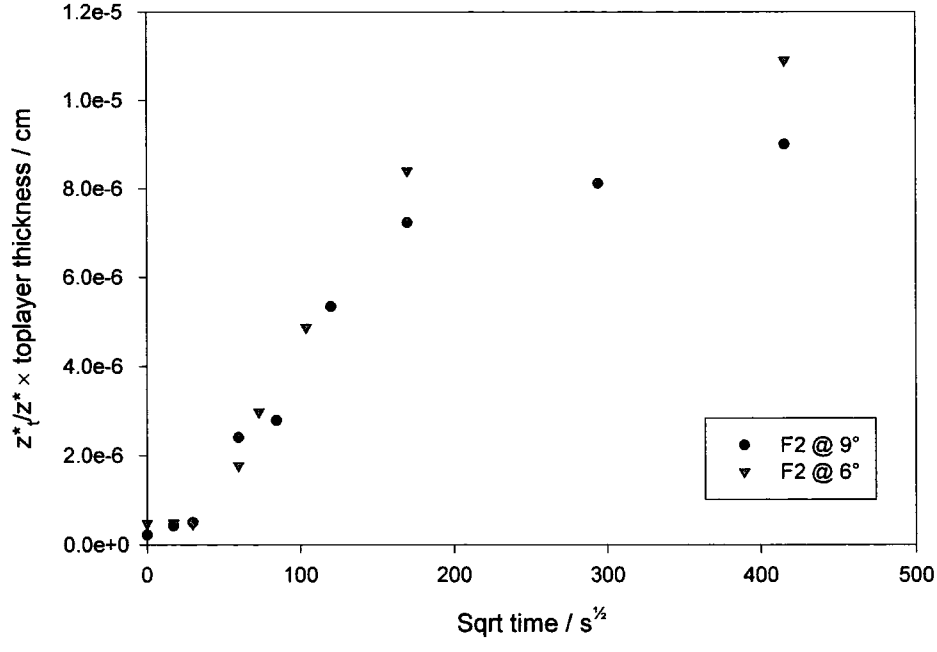


**Figure 6.2.12 Ratio of the surface excess at time t to the equilibrium excess multiplied by the hPS layer thickness against the square root of annealing time for the dPSF2 bilayer samples.**

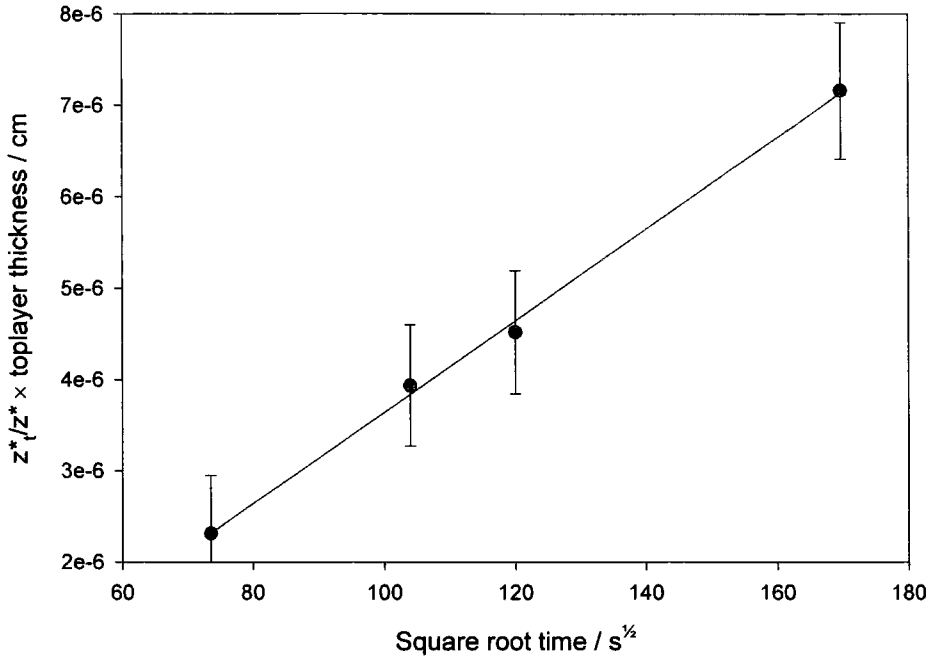


**Figure 6.2.13 30% dPSF2/hPS bilayer samples.**

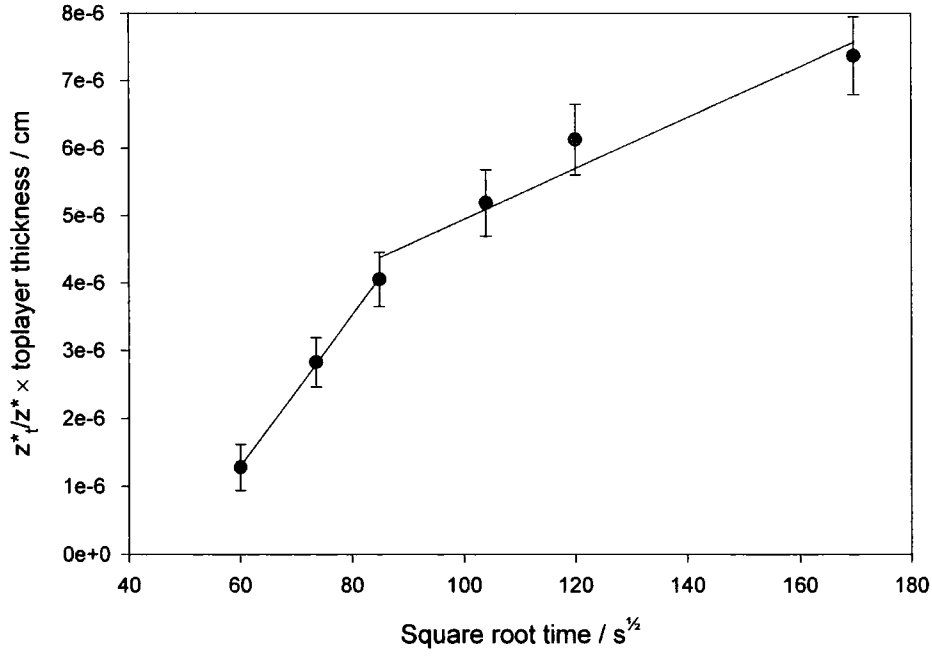


**Figure 6.2.14 50% dPSF2/hPS bilayer samples.**

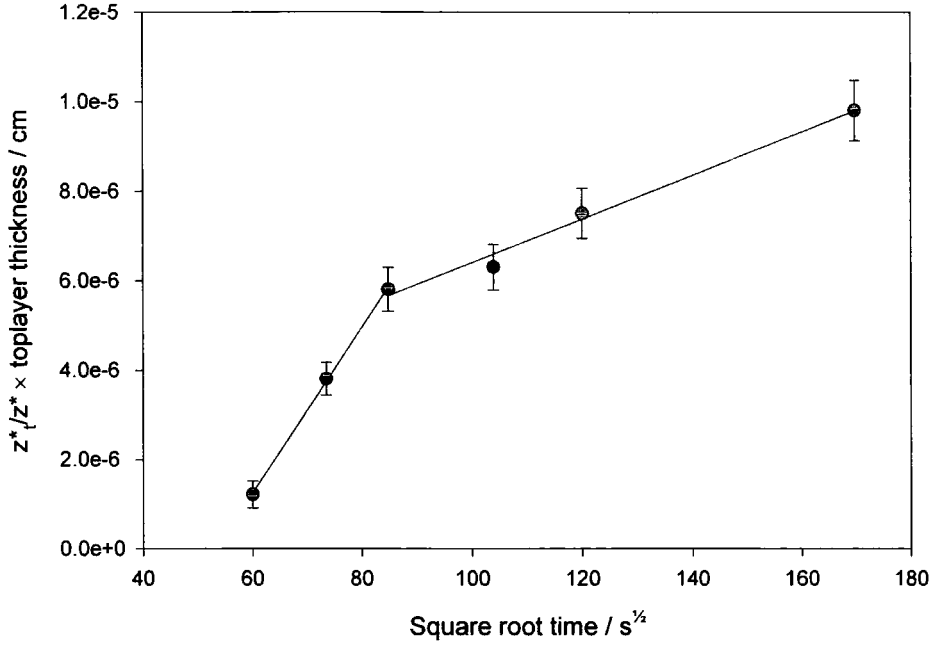


**Figure 6.2.15 75% dPSF2/hPS bilayer samples.**

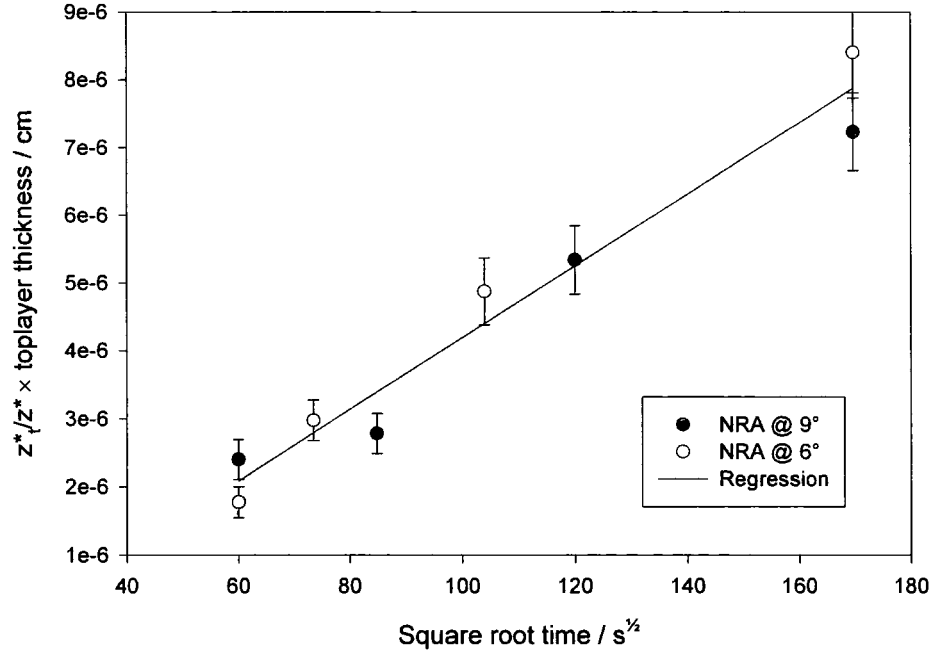


**Figure 6.2.16 dPSF2/hPS bilayer samples.**

| Sample | Slope / $cms^{-½}$ ($\times 10^{-8}$) | Diffusion Coefficient / $cm^2s^{-1}$ ($\times 10^{-16}$) |
|---|---|---|
| 30% dPSF2 | 5.00 | 6.3 |
| 50% dPSF2 | 11.17 | 31.1 |
| | 3.76 | 3.5 |
| 75% dPSF2 | 18.50 | 85.6 |
| | 4.86 | 5.9 |
| 100% dPSF2 | 5.28 | 12.0 |

**Table 6.2.7 Diffusion coefficients determined from bilayer samples measured using NRA.**

The values of diffusion coefficient are slightly lower than obtained for the dPS/hPS bilayer samples. This was not expected as the functional groups were expected, if anything, to increase the rate of diffusion, however, this could be due to the different method used. For the 50 and 75% dPSF2 samples there was a larger diffusion coefficient at earlier times. This suggests that the functional groups have an immediate effect, especially as there will probably have been an increase of dPSF2 at the interface formed during sample preparation. In the 30% base layer sample there might not be enough functional polymer for an appreciable affect to be seen, and the pure polymer cannot have a surface excess as the polymer is the same throughout, though the functional end groups might have segregated to some extent. At later times the material already diffused to the surface will be a barrier to further diffusion and the movement of the non-functional polymer will also be a limiting step. The number of data points used to determine the diffusion coefficients were limited, but the linear regressions obtained were within the error bars of the data points.

The above calculations have assumed that diffusion is a function of the square root of time and based upon reptative motion of the diffusing polymer chains.

Indeed, plots against $t^{1/2}$ do give straight lines. However, the slope, v, from log-log plots of the surface excess against annealing time ($z^* \sim t^v$) was not always equal to ½. For the samples annealed for longer times (120 to 240 minutes) the slope, within the error, was equal to ½, but for the 50% dPSF2 and 75% base layers values for v of 1.7 and 2.3 were obtained respectively for annealing times up to 120 minutes. The values for times greater than 120 minutes suggest that the system is behaving as predicted for polymer diffusion. The increased values of v for earlier times gives the greater diffusion coefficients and suggests that the functional polymer is important during the initial annealing process as this is the only obvious difference present in the system. Previous studies have shown variations in the time dependency, but this has generally been for times before the reptation time of the polymer and has given values lower than ½[9, 11].

### 6.2.2 NR Bilayer Kinetics

The samples analysed using neutron reflectometry are given in table 6.2.8. Initially samples were prepared with a TK 192 hPS toplayer of ~1000Å with a base layer of 30, 50 and 100% TK 249 dPSF2. The thickness of the base layer was ~1000Å for the pure functional polymer, and for the blended layers ~3000Å. Thicker layers of the blends were prepared to ensure that there was sufficient deuterated material to provide good contrast in the reflectivity. Samples with 30% TK 204 dPS base layers were prepared as control samples.

| Base Layer | Thickness / Å | hPS layer / Å | Annealing times / minutes | $\phi_D$ |
|---|---|---|---|---|
| 30% dPSF2 | 1090 | 3380 | U, 15, 30, 60, 120, 240, 480, 1440 | 0.23 |
| | 1050 | 3360 | 2880 | 0.23 |
| | 1030 | 3420 | 5, 90, 180 | 0.23 |
| 50% dPSF2 | 1080 | 3080 | U, 5, 10, 60, 90, 120, 180, 240, 480 | 0.37 |
| | 1010 | 3190 | 2880 | 0.38 |
| 100% dPSF2 | 1040 | 930 | U, 5, 15, 60, 120, 180, 240 | 0.47 |
| | 1060 | 970 | 2880 | 0.48 |
| | 830 | 410 | U, 5, 15, 60, 91, 120, 180 | 0.35 |
| | 870 | 390 | 240, 480 | 0.32 |
| | 810 | 400 | 2880 | 0.34 |
| 30% dPS | 1030 | 3460 | U, 15, 60, 120, 240 | 0.23 |
| | 1060 | 3560 | 2880 | 0.23 |
| | 1130 | 3130 | 5 | 0.22 |

**Table 6.2.8 Composition of bilayer samples and annealing times measured using NR.**

The reflectivity profiles for these samples are shown in figures 6.2.17 to 6.2.21. In the unannealed samples Kiessig fringes can be seen from the toplayer thickness and the sharp interface between this and the base layer, however these rapidly disappear on annealing when the interface has broadened. To keep structure in the reflectivity profile and to reduce the problems in analysing the symmetrical bilayer, some further samples of the hPS / dPSF2 bilayer were prepared, reducing the thickness of the dPSF2 base layer to ~400Å. Neutron reflectometry is a non-destructive technique, which allowed the same sample to be used for a number of measurements the limiting factor being the ability to anneal the samples sufficiently in the allocated neutron beam time.

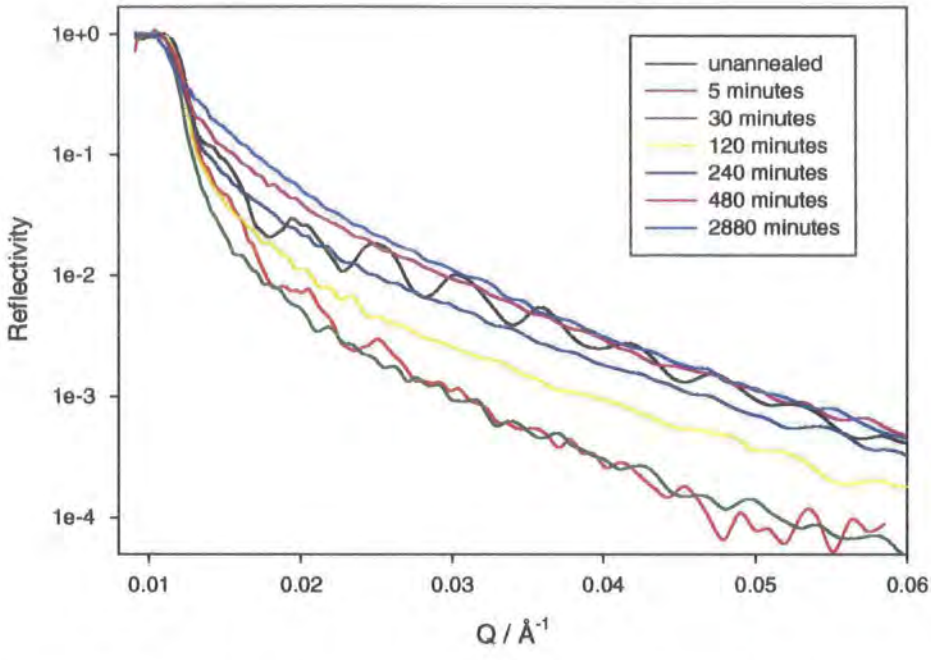


**Figure 6.2.17 Neutron reflectivity profiles for 30% dPSF2/hPS bilayer samples after annealing for different times.**

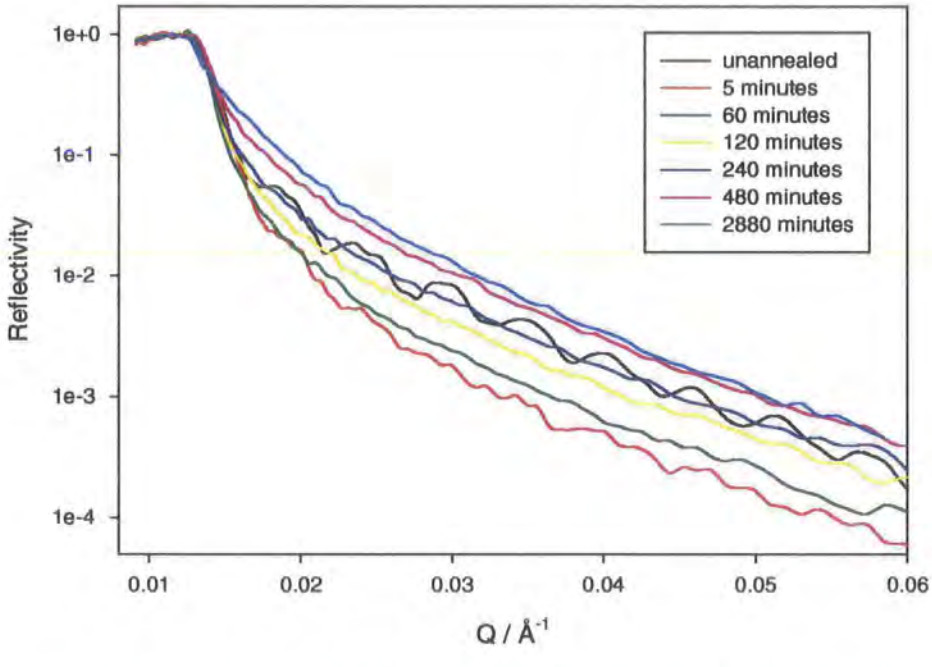


**Figure 6.2.18 Neutron reflectivity profiles for 50% dPSF2/hPS bilayer samples after annealing for different times.**

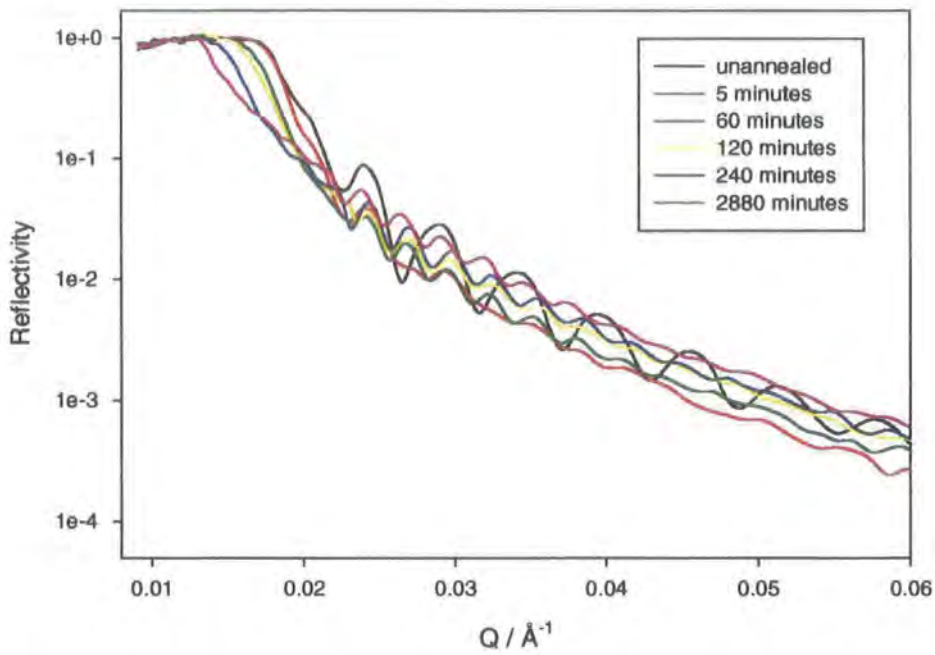


**Figure 6.2.19 Neutron reflectivity profiles for dPSF2 (1000Å) /hPS (1000Å) bilayer samples after annealing for different times.**

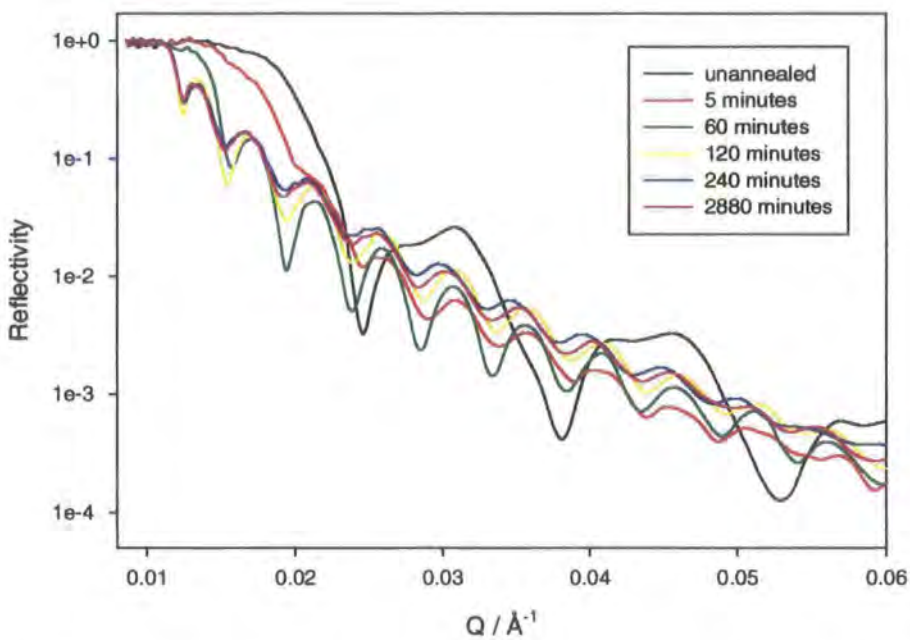


**Figure 6.2.20 Neutron reflectivity profiles for dPSF2 (400Å) /hPS (850Å) bilayer samples after annealing for different times.**

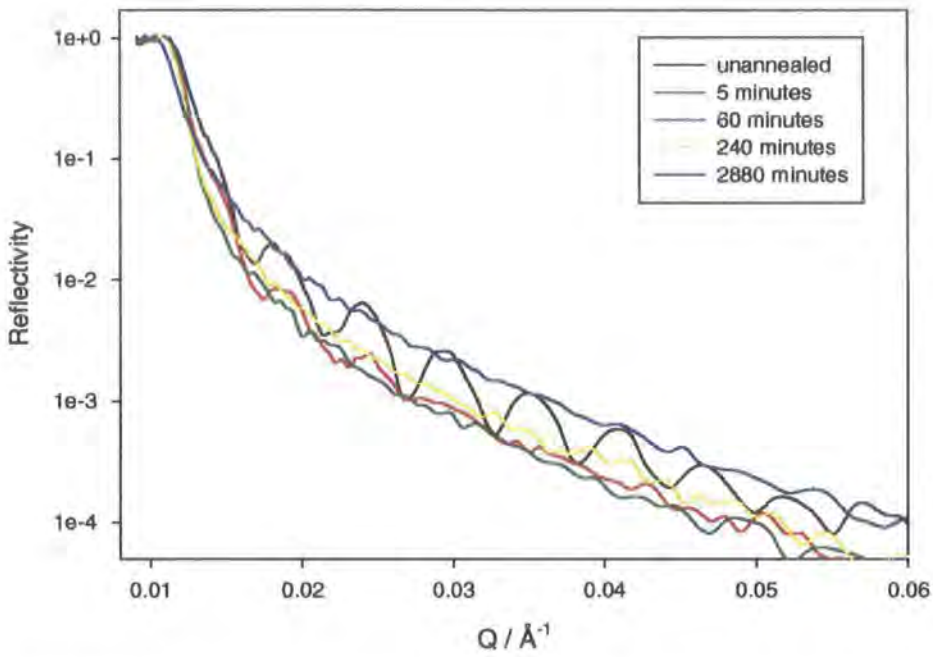


**Figure 6.2.21 Neutron reflectivity profiles for 30% dPS/hPS bilayer samples after annealing for different times.**

The reflectivity data have been fitted using multilayer models (helix3 and PCMULF), for the longer annealed samples VOLFMEM and a stretched exponential model were also used. Attempts were made to fit a profile that used an error function for the broadening interfacial region and a stretched exponential at the air surface to account for segregation. However this gave identical profiles to the multilayer fits and was more computer intensive with a large number of fitting variables. The parameters used to obtain the fits are given in tables 6.2.9 to 6.2.14; figures 6.2.22 and 6.2.23 show some examples of the fits to the data.

| Time/ min | $t_1$/Å | $\phi_1$ | $\sigma_1$/Å | $t_2$/Å | $\phi_2$ | $\sigma_2$/Å | $t_3$/ Å | $\phi_3$ | $\sigma_3$/Å | $t_4$/Å | $\phi_4$ |
|---|---|---|---|---|---|---|---|---|---|---|---|
| 0 | 1080 | 0.0 | 5 | 64 | 0.78 | 20 | 126 | 0.22 | 22 | 3200 | 0.30 |
| 5 | 1080 | 0.0 | 78 | 69 | 0.45 | 20 | 133 | 0.26 | 8 | 3200 | 0.29 |
| 15 | 860 | 0.10 | 157 | 78 | 0.26 | 20 | 149 | 0.24 | 7 | 3200 | 0.25 |
| 30 | 855 | 0.10 | 161 | 82 | 0.26 | 20 | 152 | 0.24 | 8 | 3200 | 0.24 |
| 60 | 54 | 0.14 | 15 | 850 | 0.10 | 181 | 128 | 0.21 | 13 | 3200 | 0.21 |
| 90 | 88 | 0.21 | 13 | 740 | 0.15 | 131 | 137 | 0.28 | 14 | 3200 | 0.28 |
| 120 | 66 | 0.31 | 10 | 876 | 0.16 | 194 | 165 | 0.27 | 2 | 3200 | 0.27 |
| 180 | 79 | 0.38 | 11 | 957 | 0.21 | 160 | 140 | 0.28 | 3 | 3200 | 0.27 |
| 240 | 74 | 0.49 | 7 | 1044 | 0.21 | 180 | 115 | 0.25 | 3 | 3200 | 0.26 |
| 480 | 79 | 0.67 | 12 | 95 | 0.26 | 12 | 906 | 0.24 | 46 | 3200 | 0.23 |

**Table 6.2.9 Parameters used to obtain multilayer fits to the 30% dPSF2 base layer bilayer samples.**

| Time/ min | $t_1$/Å | $\phi_1$ | $\sigma_1$/Å | $t_2$/Å | $\phi_2$ | $\sigma_2$/Å | $t_3$/Å | $\phi_3$ | $\chi^2$ |
|---|---|---|---|---|---|---|---|---|---|
| 0 | 1111 | 0.00 | 8 | 79 | 0.68 | 5 | 2780 | 0.42 | 4 |
| 5 | 1126 | 0.11 | 84 | 3229 | 0.46 | - | - | - | 8 |
| 10 | 1160 | 0.13 | 130 | 3133 | 0.46 | - | - | - | 14 |
| 60 | 30 | 0.26 | 159 | 1026 | 0.00 | 178 | 3076 | 0.44 | 8 |
| 90 | 43 | 0.38 | 126 | 992 | 0.02 | 172 | 3253 | 0.46 | 6 |
| 120 | 61 | 0.44 | 115 | 1008 | 0.02 | 179 | 3113 | 0.45 | 7 |
| 180 | 60 | 0.56 | 93 | 1059 | 0.10 | 189 | 3200 | 0.46 | 5 |
| 240 | 65 | 0.61 | 73 | 1096 | 0.14 | 167 | 3039 | 0.45 | 6 |
| 480 | 71 | 0.83 | 35 | 798 | 0.45 | 171 | 3383 | 0.43 | 2 |

**Table 6.2.10 Parameters used to obtain multilayer fits to the 50% dPSF2 base layer bilayer samples.**

| Time/ min | $t_1$/Å | $\phi_1$ | $\sigma_1$/Å | $t_2$/Å | $\phi_2$ | $\sigma_2$/Å | $t_3$/Å | $\phi_3$ | $\chi^2$ |
|---|---|---|---|---|---|---|---|---|---|
| 0 | 1056 | 0.0 | 5 | 972 | 1.00 | - | - | - | 10 |
| 5 | 1117 | 0.0 | 88 | 945 | 1.00 | - | - | - | 8 |
| 15 | 93 | 0.20 | 15 | 1329 | 0.20 | 178 | 589 | 1.03 | 16 |
| 60 | 89 | 0.42 | 14 | 1443 | 0.25 | 180 | 497 | 0.90 | 7 |
| 120 | 81 | 0.64 | 15 | 1542 | 0.45 | 212 | 448 | 0.86 | 12 |
| 180 | 84 | 087 | 48 | 386 | 0.20 | 100 | 1600 | 0.69 | 11 |
| 240 | 85 | 0.85 | 48 | 357 | 0.19 | 113 | 1600 | 0.63 | 12 |

**Table 6.2.11 Parameters used to obtain multilayer fits to hPS (1000Å) / dPSF2 (1000Å) bilayer samples.**

| Time/ min | $t_1$/Å | $\phi_1$ | $\sigma_1$/Å | $t_2$/Å | $\phi_2$ | $\sigma_2$/Å | $t_3$/Å | $\phi_3$ | $\chi^2$ |
|---|---|---|---|---|---|---|---|---|---|
| 0 | 821 | 0.0 | 15 | 373 | 1.00 | - | - | - | 7 |
| 5 | 831 | 0.0 | 91 | 362 | 0.95 | - | - | - | 10 |
| 15 | 894 | 0.02 | 137 | 280 | 0.93 | - | - | - | 5 |
| 60 | 77 | 0.42 | 30 | 857 | 0.15 | 199 | 269 | 0.60 | 4 |
| 91 | 80 | 0.53 | 34 | 854 | 0.16 | 199 | 267 | 0.55 | 6 |
| 120 | 93 | 0.70 | 51 | 950 | 0.20 | 256 | 159 | 0.42 | 4 |
| 180 | 104 | 0.69 | 60 | 981 | 0.21 | 165 | 130 | 0.37 | 5 |
| 240 | 103 | 0.77 | 57 | 955 | 0.24 | 137 | 183 | 0.32 | 8 |
| 480 | 93 | 0.82 | 72 | 1024 | 0.23 | 97 | 126 | 0.30 | 6 |
| 2880 | 97 | 0.76 | 74 | 1020 | 0.23 | 69 | 105 | 0.35 | 8 |

**Table 6.2.12 Parameters used to obtain multilayer fits to hPS (850Å) / dPSF2 (400Å) bilayer samples.**

| Time/ min | $t_1$/Å | $\phi_1$ | $\sigma_1$/Å | $t_2$/Å | $\phi_2$ | $\chi^2$ |
|---|---|---|---|---|---|---|
| 0 | 1089 | 0.00 | 4 | 3656 | 0.29 | 7 |
| 5 | 1116 | 0.02 | 80 | 4031 | 0.29 | 13 |
| 15 | 1299 | 0.05 | 153 | 3111 | 0.28 | 9 |
| 60 | 1290 | 0.01 | 179 | 3345 | 0.28 | 7 |
| 120 | 1496 | 0.10 | 240 | 3161 | 0.32 | 2 |
| 240 | 868 | 0.13 | 172 | 3728 | 0.26 | 3 |
| 2880 | 4605 | 0.23 | 5 | - | - | 11 |

**Table 6.2.13 Parameters used to obtain multilayer fits to the dPS/hPS bilayer samples.**

| **Sample** | $\phi_b$ | $\phi_s$ | **exponent** | **decay length/Å** | $\chi^2$ |
|---|---|---|---|---|---|
| 30% dPSF2 | 0.20 | 0.98 | 1.3 | 78 | 4 |
| 50% dPSF2 | 0.37 | 0.99 | 1.3 | 102 | 6 |
| dPSF2 (1000Å) | 0.45 | 1.00 | 2.0 | 120 | 9 |
| dPSF2 (400Å) | 0.23 | 0.73 | 2.0 | 128 | 7 |

**Table 6.2.14 Parameters used to obtain stretched exponential model fits to the fully annealed bilayer samples.**

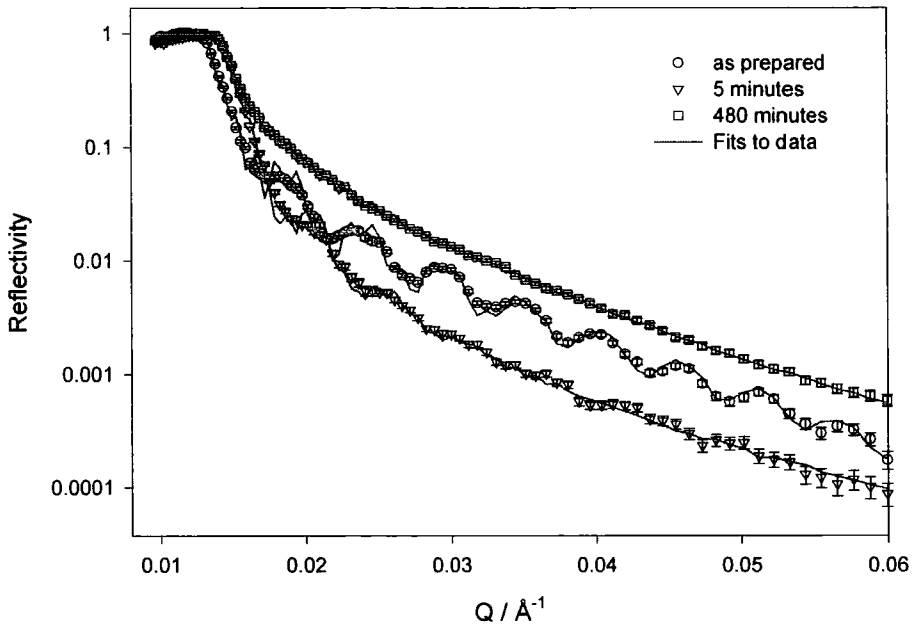


**Figure 6.2.22 Reflectivity profiles showing the fits to the data for the 50% dPSF2 bilayer samples.**

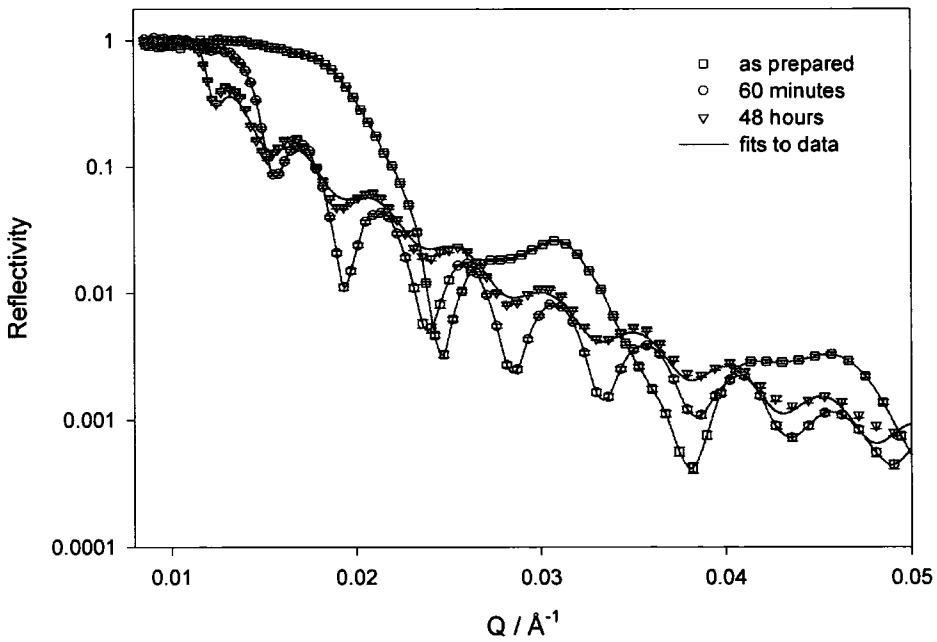


**Figure 6.2.23 Reflectivity profiles showing the fits to the data for hPS (850Å) / dPSF2 (400Å) bilayer samples.**

Figures 6.2.24 to 6.2.27 show some of the volume fraction profiles obtained over time for the bilayer samples. The general trend was that there was initially interfacial broadening and after 60 minutes this was accompanied by a growing

excess at the air surface. In the samples with dPSF2/hPS blends as the base layer the unannealed sample showed an excess at the interface between the base layer and the hPS toplayer. The segregation at the air surface occurred during the sample preparation and was quickly smoothed out once the samples were annealed. The interface between the two layers can be seen to move towards the layer with the functional polymer on annealing, which would be expected if the functional polymer was the more mobile polymer. The profiles shown do not show the full sample thickness as the last layer had a uniform volume fraction so the depth shown was limited to show the area of variation more clearly. However all of the fits were carried out using values for the full sample thickness, though for thick layers (>2000Å) these values were not sensitive to the actual value used.

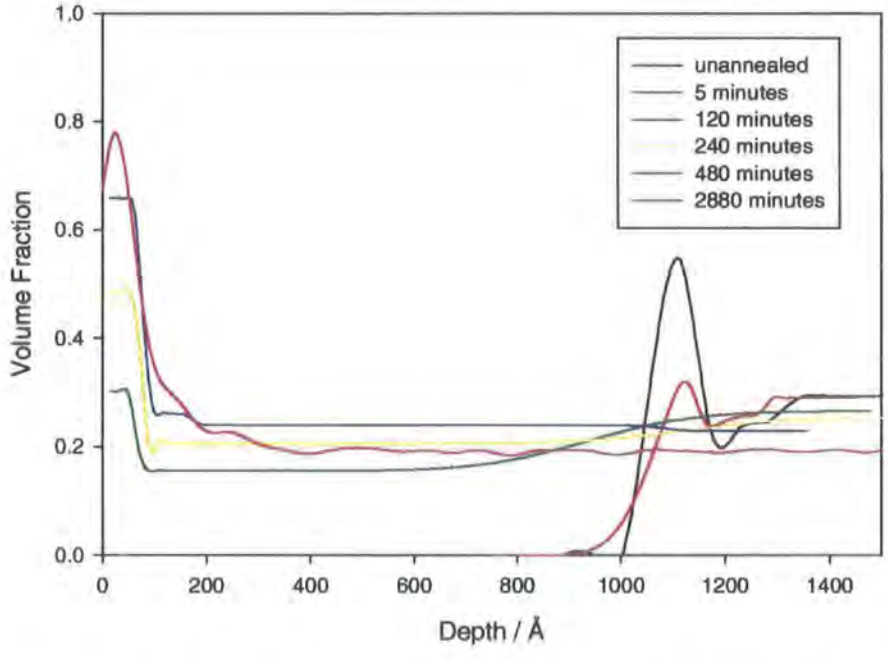


**Figure 6.2.24 Volume fraction profiles for the 30% dPSF2 base layer bilayer samples.**

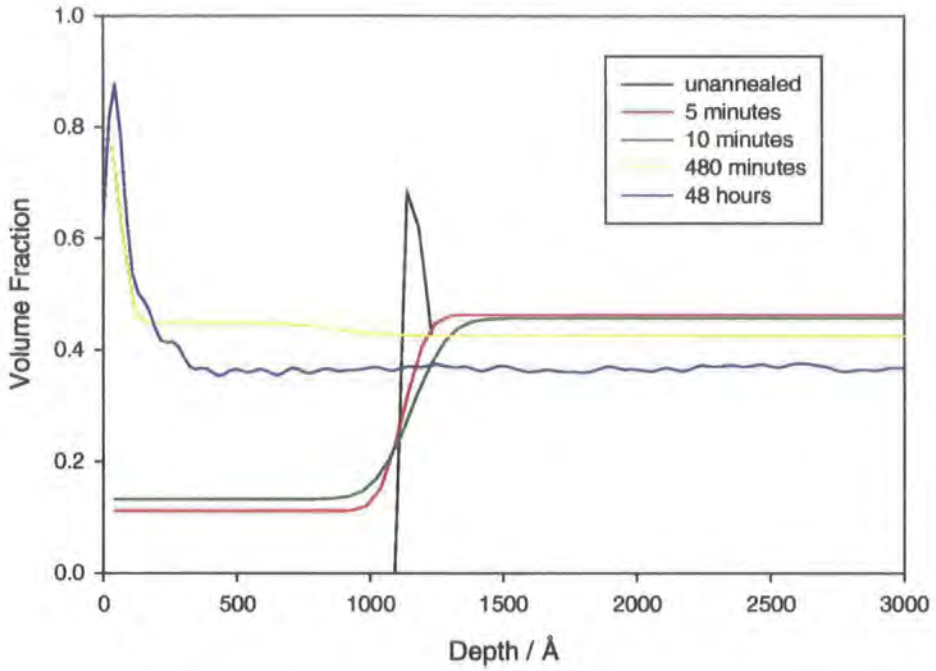


**Figure 6.2.25 Volume fraction profiles for the 50% dPSF2 base layer bilayer samples.**

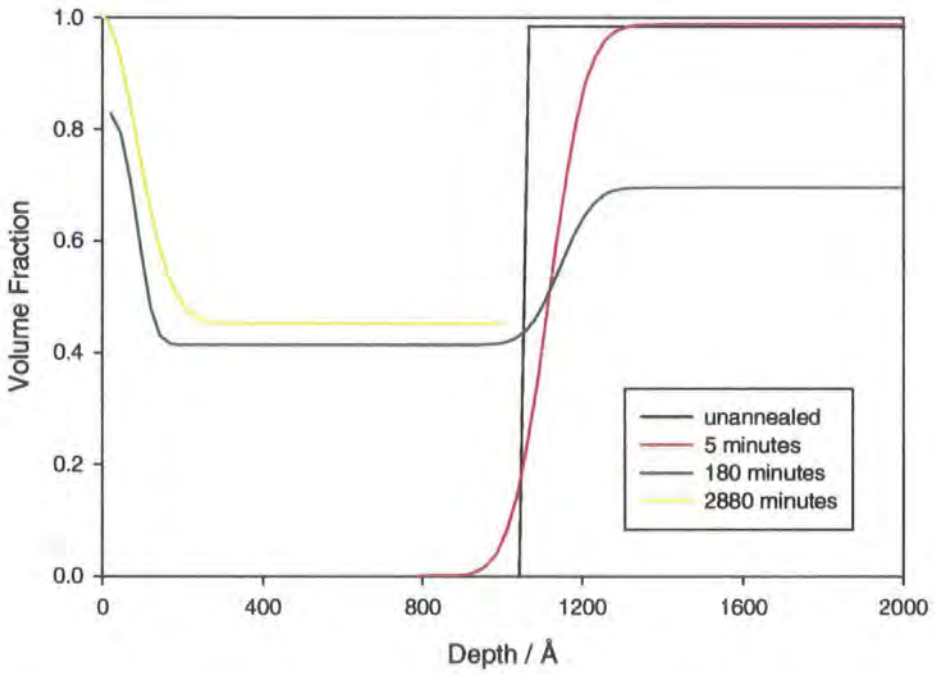


**Figure 6.2.26 Volume fraction profiles for hPS (1000Å) / dPSF2 (1000Å) bilayer samples. Intermediate annealing times had ambiguous fits and the volume fraction profile could not be determined with confidence.**

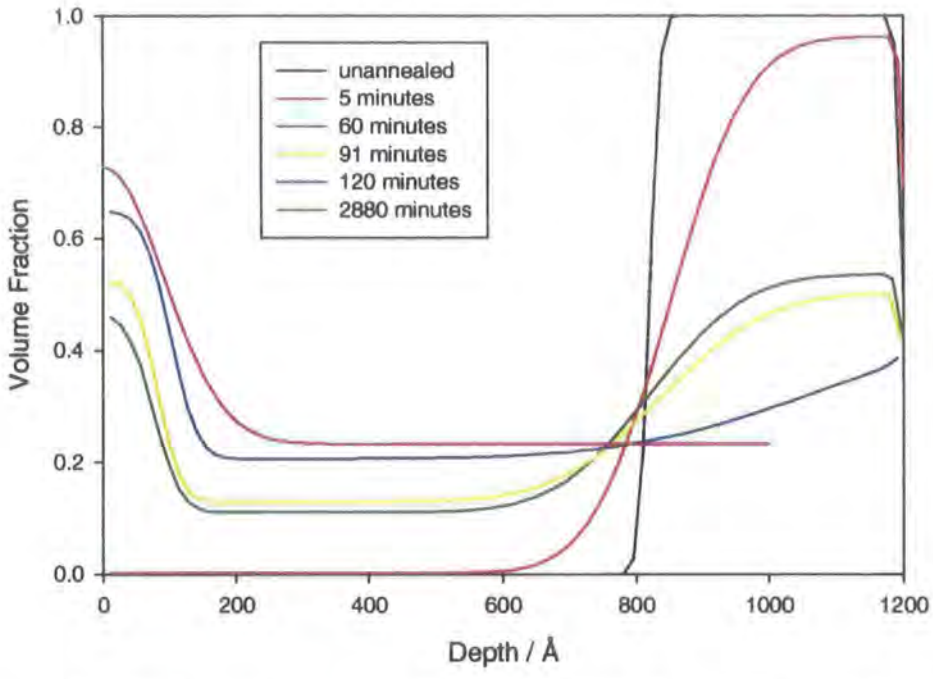


**Figure 6.2.27 Volume fraction profiles for hPS (850Å) / dPSF2 (400Å) bilayer samples.**

Before continuing with the data analysis for the bilayer samples a few points should be raised about the quality and uniqueness of the fits to the data. Figure 6.2.28 shows the reflectivity profile for the hPS/dPSF2 bilayer after annealing for 60 minutes and the lines show three different fits obtained using VOLFMEM. VOLFMEM was used to fit 200 layers over the full sample thickness of 2010Å. For the black line a uniform layer of the average volume fraction was used as the starting point and for the red and green lines the profile shown in yellow in figure 6.2.29 was used as the starting point. Initially the black fit showed the majority of the deuterated material at the surface, a result that would not be expected after such a short annealing time and the volume fraction profile was inverted (i.e. the air surface became the substrate and vice versa). The other fits varied in the amount of Gaussian smoothing used to prevent unrealistic sharp variations in the profiles with 50Å for the red fit and 75Å for the green fit. The resulting profiles show the amount of variation that could be

obtained in the volume fraction profile from a number of acceptable fits to the data. The blue dashed line is the profile that was obtained using the multilayer fitting routine. This was particularly a problem for the symmetrical hPS/dPSF2 samples as shown here, but also for some of the intermediate annealing times for all the samples.

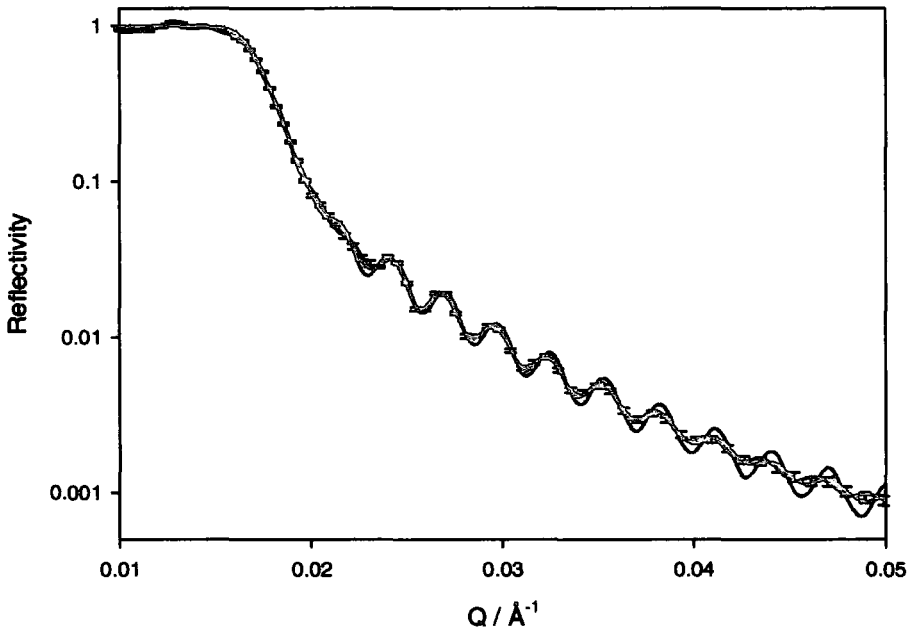


**Figure 6.2.28 Reflectivity profile for hPS (1000Å) / dPSF2 (1000Å) bilayer after annealing for 60 minutes showing VOLFMEM fits as detailed in the text.**

The samples were analysed in a similar manner to that used for the bilayers measured by NRA. The volume fraction profile was integrated to find the surface excess, z* at the air surface. The surface excess at time t was divided by the surface excess at equilibrium and this value was standardised by multiplying by the thickness of the top hPS layer thickness to allow comparison of data obtained from different samples. Tables 6.2.15 to 6.2.17 show the values obtained for the bilayer samples measured. The values obtained were in good agreement with comparable samples measured using NRA.

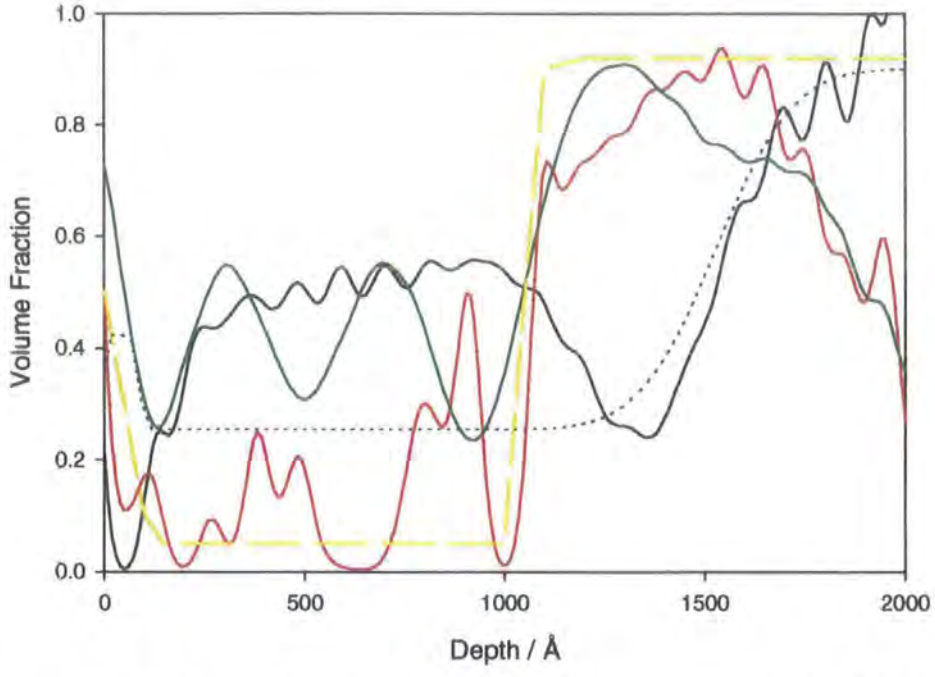


**Figure 6.2.29 Volume fraction profiles obtained using VOLFMEM for hPS (1000Å) / dPSF2 (1000Å) bilayer after annealing for 60 minutes showing (details in the text).**

| Annealing time / minutes | Sqrt time / $s^{-1}$ | Surface excess, z* / Å | $l \times z^*_t / z^*_\infty$ / cm ($\times 10^{-7}$) |
|---|---|---|---|
| 0 | 0 | 0 | 0.0 |
| 60 | 60.0 | 2.7 | 5.0 |
| 90 | 73.5 | 5.3 | 10.0 |
| 120 | 84.9 | 9.8 | 18.5 |
| 180 | 103.9 | 13.6 | 25.7 |
| 240 | 120.0 | 21.0 | 39.6 |
| 480 | 169.7 | 31.8 | 60.0 |
| 2880 | 415.7 | 55.7 | 105.0 |

**Table 6.2.15 Surface excess values and the normalised values for the 30% dPSF2 base layer bilayer samples.**

| Annealing time / minutes | Sqrt time / $s^{-1}$ | Surface excess, z* / Å | $l \times z^*_t / z^*_\infty$ / cm ($\times 10^{-7}$) |
|---|---|---|---|
| 0 | 0 | 0.0 | 0.0 |
| 60 | 60.0 | 7.8 | 15.4 |
| 90 | 73.5 | 15.9 | 31.3 |
| 120 | 84.9 | 25.6 | 50.6 |
| 180 | 103.9 | 28.0 | 55.3 |
| 240 | 120.0 | 30.4 | 60.0 |
| 2880 | 415.7 | 54.7 | 108.0 |

**Table 6.2.16 Surface excess values and the normalised values for the 50% dPSF2 base layer bilayer samples.**

| Annealing time / minutes | Sqrt time / $s^{-1}$ | Surface excess, z* / Å | $l \times z^*_t / z^*_\infty$ / cm ($\times 10^{-7}$) |
|---|---|---|---|
| 0 | 0 | 0.0 | 0.0 |
| 60 | 60.0 | 27.1 | 40.8 |
| 91 | 73.9 | 33.6 | 50.5 |
| 120 | 84.9 | 44.0 | 66.1 |
| 180 | 103.9 | 51.6 | 77.6 |
| 240 | 120.0 | 58.4 | 87.8 |
| 480 | 169.7 | 60.8 | 91.4 |
| 2880 | 415.7 | 56.5 | 85.0 |

**Table 6.2.17 Surface excess values and the normalised values for the hPS (850Å) / dPSF2 (400Å) bilayer samples.**

The calculated values were plotted against the square root of the annealing time (figure 6.2.30). Diffusion coefficients, D, were determined from straight line fits through the data, the slope taken to be equal to $2\sqrt{D}$. For the 30% dPSF2 and pure dPSF2 base layers a single line passed through the data, but for the 50% dPSF2 sample there was a distinct change in the slope at 120 minutes of annealing. This variation in slope was also seen in the bilayer samples studied using NRA. The diffusion coefficients that were calculated are given in table 6.2.18. The comparison

with the values obtained using NRA was good, the values obtained by both methods are shown plotted in figure 6.2.31 as a function of the volume fraction of dPSF2 in the base layer. It appears as if the underlying rate of diffusion is the same for all samples and is of the order of that obtained using the surface excess values for the blended samples. In the samples with 50 or 75% dPSF2 in the base layer there was an increase in the initial rate of diffusion. This could be due to chain ends segregating to the surface during the spinning process for the blended layers and these being correctly aligned to allow diffusion to occur across the interface more rapidly. Again, as for the NRA samples there was an unusual relationship between the surface excess and time as determined from the slope of a log - log plot. For the longer annealing times variation as $t^{1/2}$ was found, but for annealing times up to 120 minutes, slopes of 1.9 and 1.7 were found for the 30% and 50% dPSF2 base layer samples respectively. The increased slope for the blended base layers supports the belief that segregation that had occurred during sample preparation has affected the initial rate of interdiffusion.

| **Sample** | **Slope / cms$^{-1/2}$ ($\times 10^{-8}$)** | **Diffusion Coefficient / cm$^2$s$^{-1}$ ($\times 10^{-16}$)** |
|---|---|---|
| 30% dPSF2 | 5.14 | 6.6 |
| 50% dPSF2 | 14.09 | 49.6 |
| | 2.68 | 1.8 |
| 100% dPSF2 | 7.97 | 15.9 |

**Table 6.2.18 Diffusion coefficients determined from bilayer samples measured using NR.**

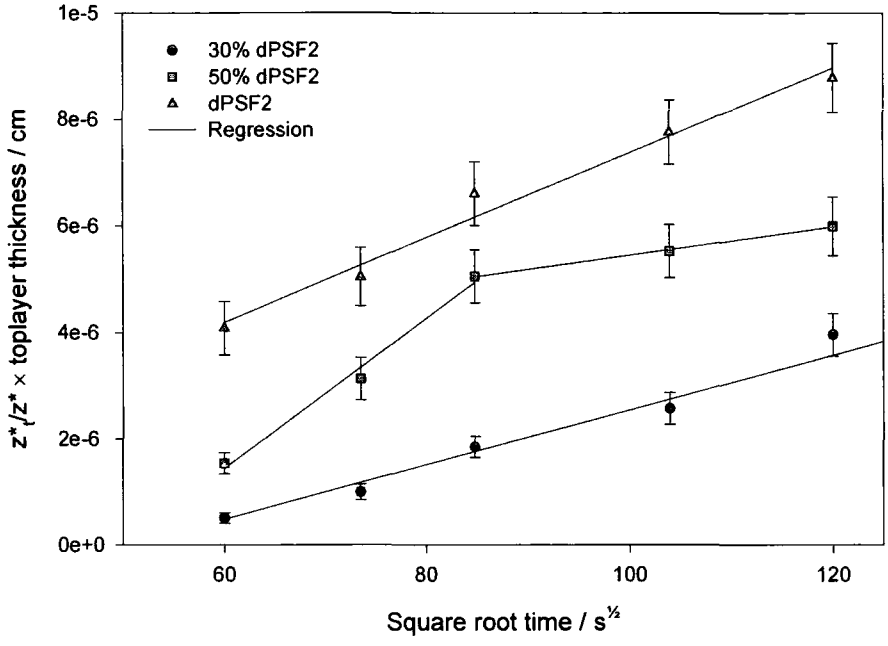


**Figure 6.2.30 Ratio of the surface excess at time t to the equilibrium surface excess multiplied by the hPS layer thickness against the square root of the annealing time for the bilayer samples with dPSF2 in the base layer.**

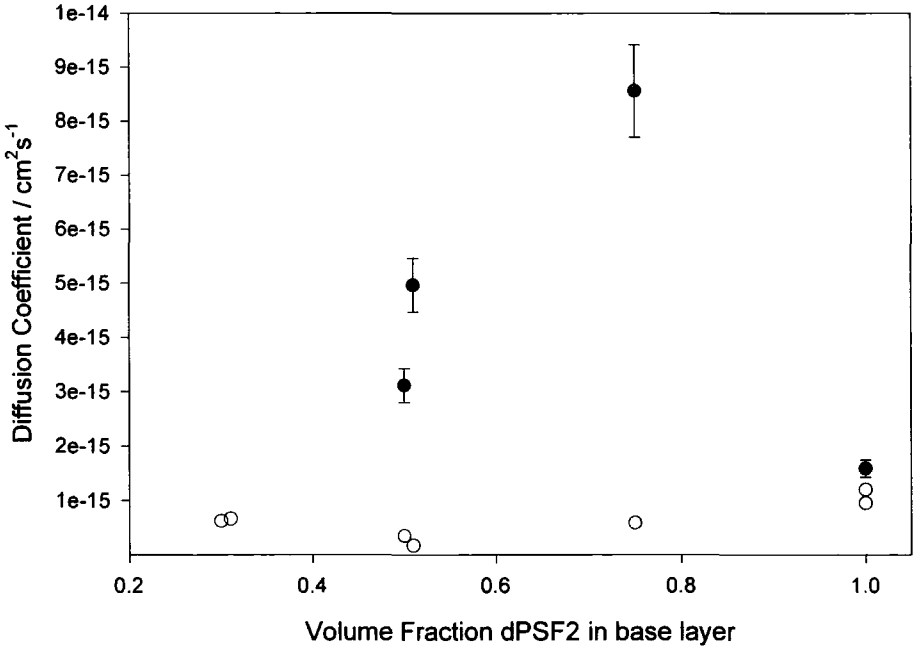


**Figure 6.2.31 Diffusion coefficients obtained from both NR and NRA analysis of bilayer samples as a function of the volume fraction of dPSF2 in the base layer. Filled symbols are the diffusion coefficients determined from measurements from samples annealed between 60 and 90 minutes.**

## 6.3 Discussion

Since the mid 1980's there have been many studies on polymer – polymer interdiffusion and the determination of tracer diffusion coefficients using a variety of polymers and techniques. Much of the early work was on polystyrene and its deuterated analogue using forward recoil spectroscopy (FRES)[8, 13 7, 14, 15], (also referred to as elastic recoil detection); secondary ion mass spectroscopy (SIMS)[11] and the holographic grating technique using photo labelled polystyrene[16]. A good summary of the work on polymer chain dynamics, reptation and interdiffusion is given in the book Polymer Interfaces – Structure and Strength by Wool.

There have been several studies on the kinetics of segregation of one polymer to an interface[5, 6, 15, 17-23]. The majority of these have been the segregation of one polymer to the surface of a blend of itself with another polymer. Jones and Kramer[15] and Geoghegan et al[19, 20] determined diffusion coefficients from the size of the depletion zone that limited the growth of the enrichment layer. Stamm et al[17] and Klein et al[6], as in the blends studied here, observed a depletion layer, but used the growth in the surface excess to determine the diffusion coefficients. However, they did not observe any segregation in the as prepared samples. Clarke's work on deuterated polystyrene with a carboxy end group is the most similar to that studied here except the carboxy group segregated to the substrate interface on annealing and the surface excess values obtained were much greater. Clarke also observed segregation in the as prepared samples studied by neutron reflection, but this was not seen using nuclear reaction analysis[24]. The diffusion coefficients obtained were lower than expected, which, was explained by the formation of dimers increasing the

effective molecular weight. Small angle neutron scattering data obtained on the polymers used here indicated that this did not occur with the fluorinated end groups.

Bucknall et al[21] looked at bilayers of a deuterated diblock polymer (dP(S-b-MMA)) and polymethyl methacrylate, but they only used the growth of the surface excess and did not look at the interface width. Their results indicated that the surface excess was from micelle segregation (cf. brush formation[25]) as opposed to isotopic enrichment. Clarke[5] also carried out some bilayer work, but his functional polymer was grafted to the substrate and as such was studying the rearrangement to equilibrium or some other metastable state. Stamm et al[23] looked at bilayers of PVC on dPMMA using neutron reflection, XPS and SIMS in an experiment most similar to the bilayers studied here. XPS and SIMS were used to confirm the enrichment of dPMMA at the surface and also to show that enrichment occurred in blended samples annealed to equilibrium. The time taken for dPMMA to appear at the surface was used to determine the diffusion coefficients. The volume fraction profiles showed the broadening interface along with surface enrichment, but over the time range studied the two did not appear to merge and neither was used to determine the rate of diffusion. Other work in the literature using bilayers has studied the change in the interface width, but has not been affected by segregation occurring as well.

There was some variation in the diffusion coefficients obtained from the different methods of determination. The lowest values were from the slope of figure 6.1.22, which would suggest that the segregation seen in the unannealed samples did have some affect on the calculation. The values obtained using the surface excess value from the blends were the same as the higher values obtained from the bilayer samples ($\sim 3\times10^{-15}$ $cm^2s^{-1}$), the bilayers at longer annealing times (>120 minutes) had

diffusion coefficients ~$5\times10^{-16}$ $cm^2s^{-1}$. The decrease in diffusion coefficient with time would suggest that the presence of the polymer brush at the surface resists the inclusion of further polymer and impedes the growth of the surface excess.

Comparison of the values of diffusion coefficient obtained here with other values quoted in the literature has been difficult due to the wide range of techniques used and variations in the molecular weights of the polymers and the annealing temperatures used. Green and Kramer[14] determined the tracer diffusion coefficients for dPS diffusing into hPS using FRES at 447K. For molecular weights of 110000 and 915000 values of ~$8\times10^{-13}$ $cm^2s^{-1}$ and ~$1\times10^{-14}$ $cm^2s^{-1}$ were obtained respectively. However, at a constant fractional free volume of 0.042 a diffusion coefficient of ~$5\times10^{-15}$ $cm^2s^{-1}$ was obtained for hPS and dPS of 110000 molecular weight. Whitlow and Wool[11] used SIMS to look at symmetrical dPS-hPS interfaces as a function of molecular weight and temperature. For 111000 molecular weight dPS and 93000 molecular weight hPS diffusion coefficients obtained ranged from $1.993\times10^{-16}$ $cm^2s^{-1}$ at 396.2K to $1.245\times10^{-14}$ $cm^2s^{-1}$ at 413K. The values obtained here were similar, but more closely matched the values quoted for annealing temperatures of 403.4K and 405.4K (i.e. around 6 degrees lower). Guckenbiehl et al[17] looked at blends of 695000 molecular weight dPS and 165000 molecular weight statistical copolymer poly(styrene-co-4-bromostyrene), $PBr_{0.06}S$ at 447K using neutron reflectometry. The value obtained was $4.4\times10^{-16}$ $cm^2s^{-1}$, slower than the values quoted for hPS/dPS at 447K, which was explained by a repulsive interaction between the polymers because of the bromination. Budkowski et al studied a polyisoprene (10000 $M_w$) – polystyrene (100000 $M_w$) diblock copolymer (PIPS) blended with hPS (~50000 $M_w$) using NRA. At 416K a diffusion coefficient of $3.5\times10^{-15}$ $cm^2s^{-1}$ was obtained, around

a factor of 10 less than that obtained at 430K ($2.7\times10^{-14}$ $cm^2s^{-1}$). At 413K, a tracer diffusion coefficient of $1.05\times10^{-15}$ $cm^2s^{-1}$ was obtained from bilayers of 5% PIPS in hPS (330000 $M_w$) on hPS (330000 $M_w$). A control using 5% dPS (90000 $M_w$) gave $2.3\times10^{-15}$ $cm^2s^{-1}$ showing little difference between the functional and non-functional polymer systems. In general the values obtained were of a similar order to those quoted.

For the bilayer samples NRA gave direct profiles but was limited by the resolution and the number of individual samples that it was possible to measure from one silicon wafer. NR had the advantage of being a non-destructive technique so that the same sample could be measured, but in doing this there were errors in the annealing time. These errors arose in the timing of placing the sample in the oven and in removing again giving an error of ±30s, also when the oven door was opened to insert a sample the temperature fell by up to 30 degrees and took ~5minutes to return to 413K. Both of these factors would have a greater effect for the shorter annealing times, but would also have a cumulative effect as the same sample was annealed many times. The NR should have good resolution, but the profiles obtained are limited if the interface is broad which occurred after only a short annealing time.

Although the method of bilayers to determine the rate of diffusion looked to be promising in principle, in practice problems were encountered which reduced its effectiveness. The amount of functional polymer which segregated to the surface was quite small compared to other systems studied such as carboxy terminated polystyrene studied by Clarke. The study of the growth of the segregated layer and / or the increase in the interfacial width between the two layers should both have been good ways to determine diffusion coefficients, however these two effects merged

quite rapidly making the determination of accurate values difficult. A thicker hPS layer might reduce this, but would also reduce the accuracy of the volume fraction profile determined due to the limitations of the techniques used. More surface specific techniques such as XPS or SIMS could be used to measure the increase in the functional polymer at the air surface but would not measure the total amount of segregated polymer at the surface.

This work has shown that the fluorinated end groups will cause segregation to the air polymer interface, but the overall rate of diffusion appears to be no faster than that of the unfunctionalised polymers. Whilst the low surface energy end group causes segregation to the air-polymer interface, the rate limiting step for the diffusion of material is reptation of the polymer chains and tube renewal, which is not affected by the thermodynamics of the end groups. In the bilayer samples with no functional polymer in the top layer initially, the equilibrium structure obtained was the same as for the blended samples of a similar overall composition. The STAR polymer has similar total surface excess values to the linear polymer, but the approach to equilibrium is considerably slower because the polymer has to move by 'arm retraction' and not reptation.

## 6.4 References


1 T. C. B. McLeish and K. P. O'Connor, *Polymer*, 1993, **34**, 2998.

2 F. Brochard-Wyart, A. Ajdari, L. Leibler, M. Rubinstein, and J. L. Viovy, *Macromolecules*, 1994, **27**, 803.

3 A. Sikorski and P. Romiszowski, *Journal of Chemical Physics*, 1996, **104**, 8703.

4 D. G. Walton and A. M. Mayes, *Physical Review E*, 1996, **54**, 2811.

5 C. J. Clarke, R. A. L. Jones, and A. S. Clough, *Polymer*, 1996, **37**, 3813.

6 A. Budkowski, A. Losch, and J. Klein, *Israel Journal of Chemistry*, 1995, **35**, 55.

7 P. F. Green, P. J. Mills, and E. J. Kramer, *Polymer*, 1986, **27**, 1063.

8 P. F. Green and B. L. Doyle, *Physical Review Letters*, 1986, **57**, 2407.

9 K. Kunz and M. Stamm, *Macromolecules*, 1996, **29**, 2548.

10 T. E. Shearmur, A. S. Clough, D. W. Drew, M. G. D. Vandergrinten, and R. A. L. Jones, *Macromolecules*, 1996, **29**, 7269.

11 S. J. Whitlow and R. P. Wool, *Macromolecules*, 1991, **24**, 5926.

12 J. Crank, 'The Mathematics of Diffusion', Oxford, 1956.

13 P. F. Green and B. L. Doyle, *Abstracts of Papers of the American Chemical Society*, 1987, **193**, 182.

14 P. F. Green and E. J. Kramer, *Macromolecules*, 1986, **19**, 1108.

15 R. A. L. Jones and E. J. Kramer, *Philosophical Magazine B-Physics of Condensed Matter Structural Electronic Optical and Magnetic Properties*, 1990, **62**, 129.

16 M. Antonietti, J. Coutandin, and H. Sillescu, *Macromolecules*, 1986, **19**, 793.

17 B. Guckenbiehl, M. Stamm, and T. Springer, *Colloids and Surfaces A: Physiochemical and Engineering Aspects*, 1994, **86**, 311.

18 C. J. Clarke, R. A. L. Jones, J. L. Edwards, A. S. Clough, and J. Penfold, *Polymer*, 1994, **35**, 4065.

19 M. Geoghegan, R. A. L. Jones, D. S. Sivia, J. Penfold, and A. S. Clough, *Physical Review E*, 1996, **53**, 825.

20 M. Geoghegan, T. Nicolai, J. Penfold, and R. A. L. Jones, *Macromolecules*, 1997, **30**, 4220.

21 D. G. Bucknall, J. S. Higgins, J. Penfold, and S. Rostami, *Polymer*, 1993, **34**, 451.

22 C. J. Clarke, *Polymer*, 1996, **37**, 4747.

23 K. Kunze, M. Stamm, M. Hartshorne, and S. Affrossman, *Acta Polymer*, 1996, **47**, 234.

24 C. J. Clarke, personal communication, 1996.

25 K. R. Shull, *Journal of Chemical Physics*, 1991, **94**, 5723.

# CHAPTER 7

## Summary

## 7.1 Comparison between different architectures studied.

In this work the near surface composition profiles of three different functional polymer architectures have been determined when the polymer has been blended with linear polystyrene of the same molecular weight. Figures 7.1 to 7.3 show the volume fraction profiles for these different polymers with a similar bulk volume fraction. At a low value of the bulk volume fraction the H2F polymer showed greater segregation but there was little difference for the other polymers. However, at higher bulk concentrations the MFL polymer gave a greater amount of segregation with the layer stretching more as the bulk concentration increased.

However, the polymers studied were of different molecular weight especially the MFL polymer. If the volume fraction profile was normalised by the radius of gyration ($R_g$) of the functional polymer the profiles obtained for the same bulk volume fraction were essentially the same except for the MFL polymer. This polymer gave relatively less segregation with a much thinner profile at the low volume fractions, but at higher volume fractions the polymer stretched normal to the air polymer interface to be the same as the other architectures. The normalised profiles are shown in figures 7.4 to 7.6. Therefore the architecture of the polymer appears to have had little effect on the extent of surface segregation of functional polymer at relatively high grafting densities. This was a little bit unexpected, the MFL polymer with a large number of functional groups was expected to give a relatively thinner layer which was seen at low volume fractions, the STAR however would be predicted to give a larger segregation. However, the STAR has only one functional group to attach to the surface compared to two or more for the other polymers, also the profiles were normalised by the $R_g$ of the molecule (68Å). This $R_g$ value is of a

similar size to that predicted for the span of the molecule based upon the length of two arms (63Å), but if the $R_g$ of one arm (44.6Å) was used the profile would appear to be relatively larger (shown in figure 7.5). Further experiments using star polymers with arms of different molecular weight and perhaps with only one arm deuterated might help to clarify the situation. The techniques used gave no indication of the amount of functional groups actually at the surface and therefore it would be useful to quantify the amount of fluorine at the surface using XPS, especially if the main interest was in creating a low energy surface.

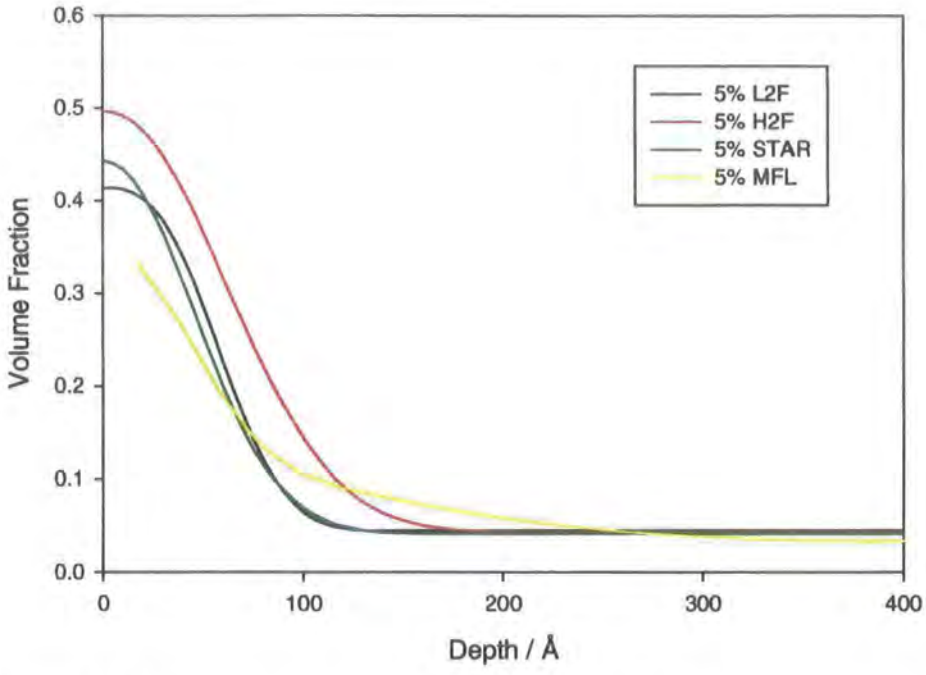


**Figure 7.1 Volume fraction profiles for samples with approximately 4% functional polymer in the bulk.**

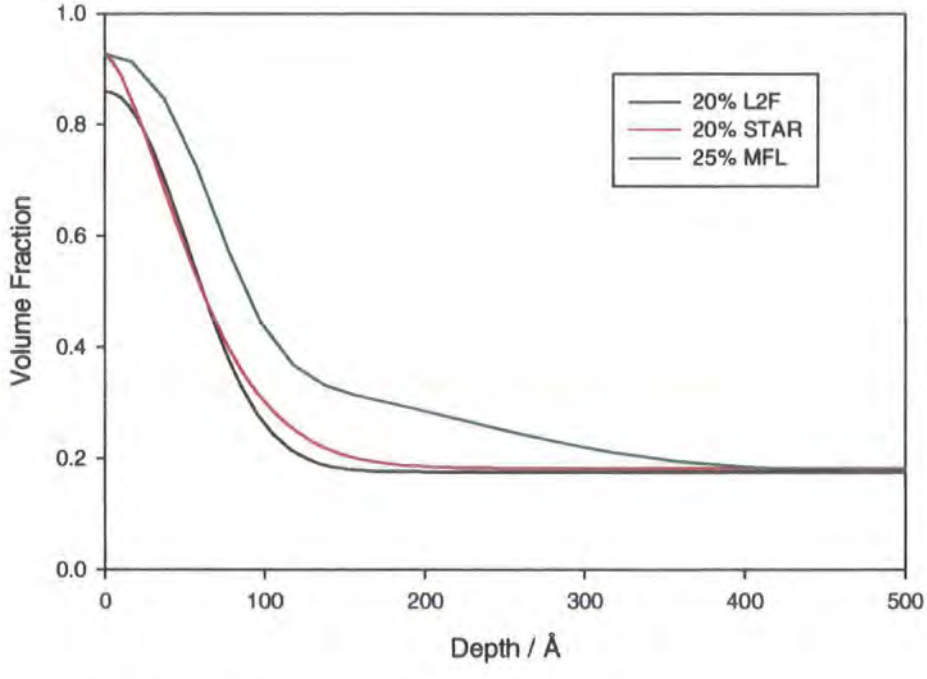


**Figure 7.2 Volume fraction profiles for samples with approximately 18% functional polymer in the bulk.**

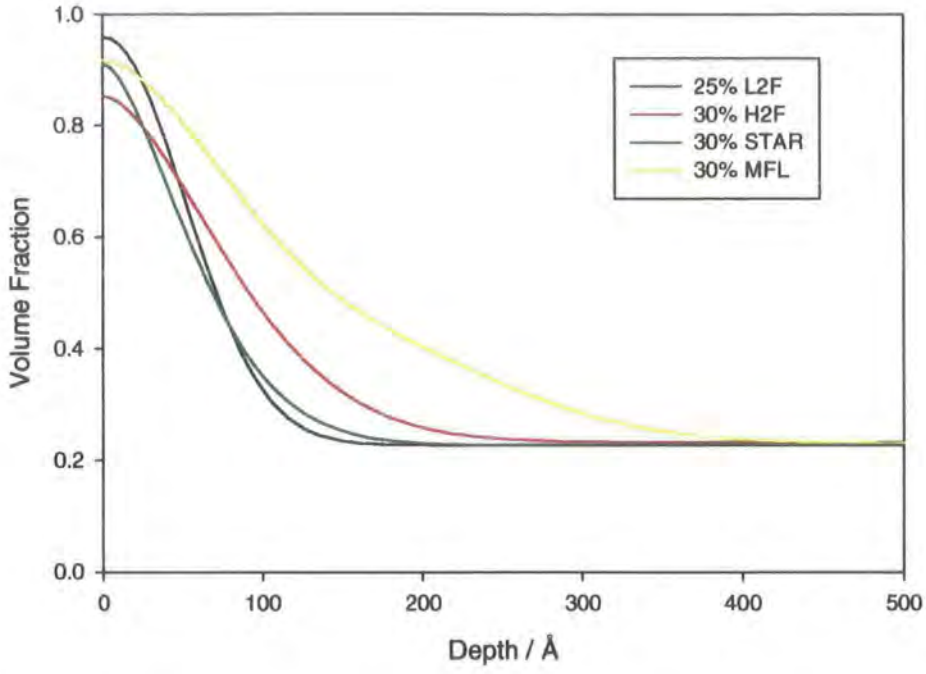


**Figure 7.3 Volume fraction profiles for samples with approximately 23% functional polymer in the bulk.**

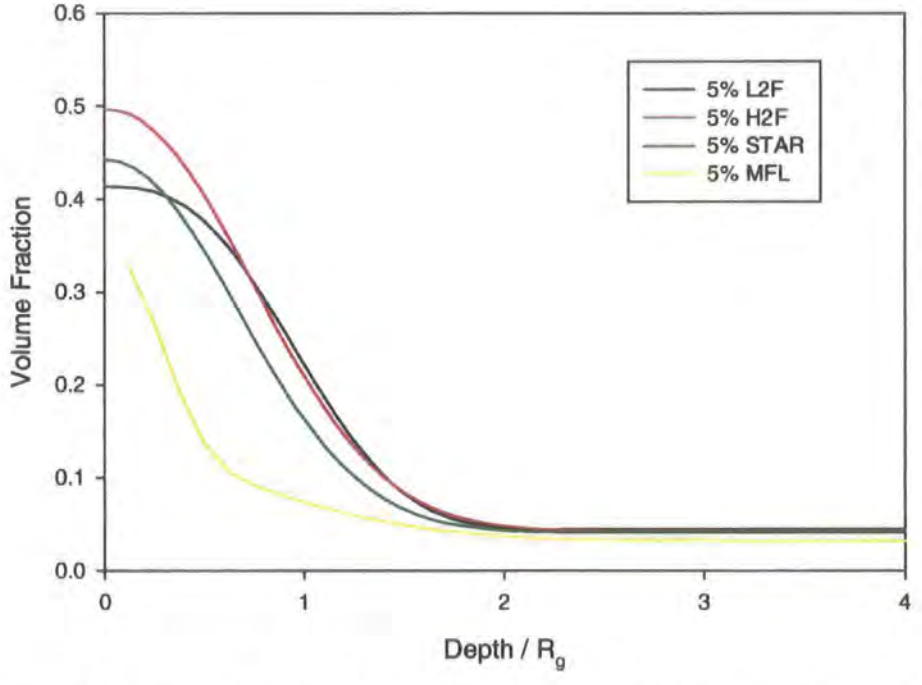


**Figure 7.4 Volume fraction profiles for samples with approximately 4% functional polymer in the bulk normalised by the radius of gyration of the functional polymer.**

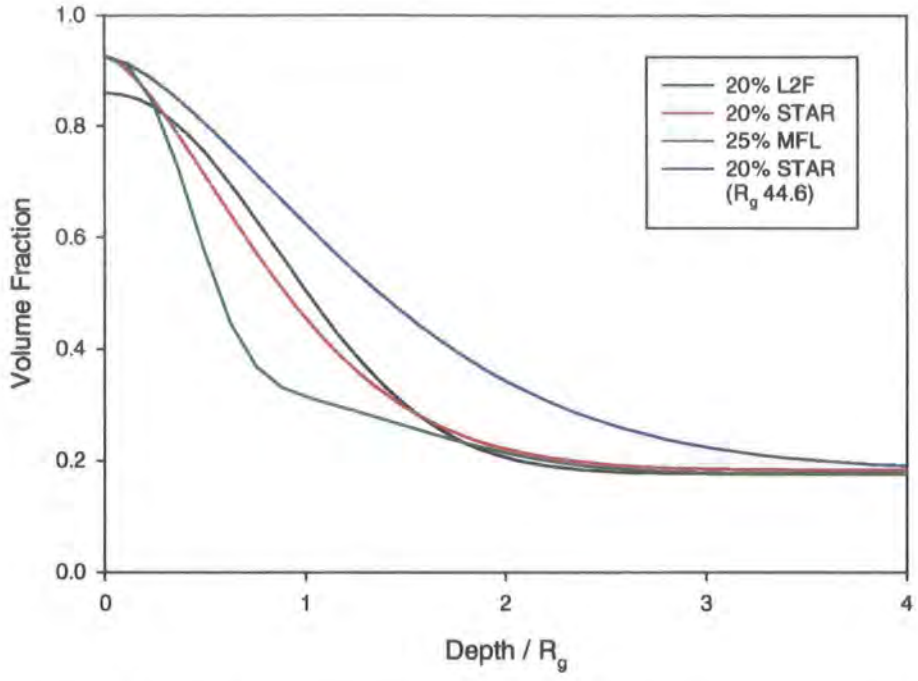


**Figure 7.5 Volume fraction profiles for samples with approximately 18% functional polymer in the bulk normalised by the radius of gyration of the functional polymer. Showing the comparison in the profiles obtained using the $R_g$ of the STAR molecule compared to one arm (44.6Å).**

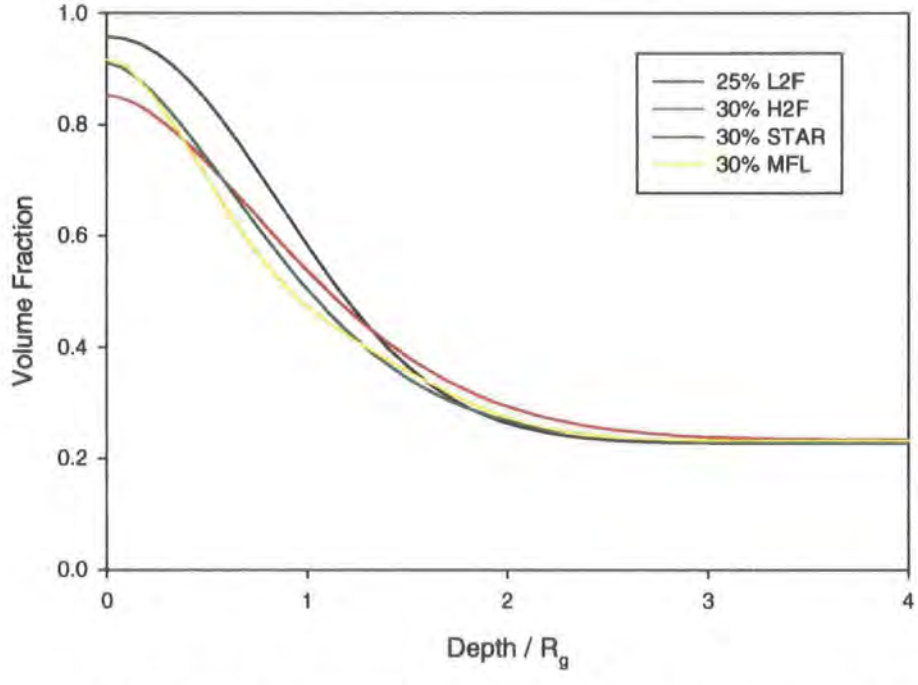


**Figure 7.6 Volume fraction profiles for samples with approximately 23% functional polymer in the bulk normalised by the radius of gyration of the functional polymer.**

The volume fraction profiles obtained were compared with theoretical predictions based upon the 'sticking' energy of the functional group for the surface. For the linear polymers a value of $(\chi_e^b - \chi_e^s) = 4.0$ gave theoretical profiles which matched the experimental data well. For the three armed star polymer a higher value of $(\chi_e^b - \chi_e^s) = 4.5$ gave the best comparison.

A direct comparison with the multiple labelled polymer cannot be made because a different program was used, which accounted for the increased number of functional groups in the chain. However, further study of the multiple labelled polymer would be interesting as the large number of functional groups at the surface increases the areal density of grafted chains allowing different scaling regimes to be studied. It would also be interesting to study the behaviour of the multiple labelled polymer in different molecular weight matrices to see if the behaviour is the same as for the difunctional polymer and carry out kinetics experiments to study the rate of attainment of the equilibrium surface excess values. For linear chains diffusion is based upon reptation, the MFL polymer is linear but there are seven functional groups that are thermodynamically favoured at the surface and these might impede the reptative motion of the chain.

The kinetics experiments showed little difference in the rate of diffusion of functional polymer compared to non-functional polymer with a diffusion coefficient $\sim 2\times10^{-15} cm^2 s^{-1}$. The values obtained were similar to those quoted in the literature for comparable polymer systems. The rate of segregation is dependent upon the kinetics of polymer chain diffusion and not controlled by the thermodynamic benefits of the end group reducing the free energy of the surface. The end group does, however, control the extent of segregation seen at equilibrium. With the bilayer samples initial

rates of diffusion were higher due to the functional groups segregating to the surface during sample preparation allowing interdiffusion to occur more rapidly. It would be useful to study the kinetics when the molecular weight of the top layer polystyrene was varied. Molecular weights around that of the critical entanglement molecular weight (~30000) when constraint release becomes more important than reptation, and into a polymer network where the diffusion is restricted to that of the functional polymer.

Problems were encountered in determining diffusion coefficients due to sample variation and errors in the accuracy of the annealing time and temperature. It would therefore be useful to determine diffusion coefficients in 'real' time. Some work has been carried out using a heated ATR-FTIR crystal, recording spectra at regular intervals until equilibrium is reached. However, the resolution of this technique means that it is not possible to obtain the volume fraction profile. If a high-energy neutron spallation source (such as the European Spallation Source, ESS) is built, this could have high enough flux that reflectivity experiments could be carried out in the melt in real time. However, at the present time this is not possible.

This work has shown that fluorinated functional groups located in a polymer chain will cause segregation to the surface of a film, the extent of segregation was similar for different architectures studied at equilibrium. At equilibrium there is still a substantial amount of functionalised polymer remaining in the bulk. The rate of formation of the segregated layer was that predicted assuming reptative motion of the polymer chains except for the STAR polymer which cannot undergo reptation because of the branched architecture.

# CHAPTER 8

# Appendices

## Glossary of Symbols and Abbreviations Used

| | |
|---|---|
| a | statistical segment length |
| Å | Angstrom ($1\times10^{-10}$m) |
| $\beta$ | free energy of end attachment |
| $\beta$ | exponent in exponential profile |
| $b_I$ | nuclear scattering length of component I |
| $\chi^2$ | normalised $\chi^2$ fit parameter |
| $\chi_e^b$ | bulk interaction contribution to attachment energy |
| $\chi_e^s$ | surface interaction contribution to attachment energy |
| CRISP | neutron reflectometer at RAL |
| D | mutual diffusion coefficient |
| $d_i$ | thickness of the $i^{th}$ layer |
| $d\sigma/d\Omega$ | number of neutrons scattered per unit time into solid angle $d\Omega$ |
| dPS | perdeuterated polystyrene |
| dPSF2 | difunctional end-capped perdeuterated polystyrene |
| FRES | forward recoil spectroscopy |
| FWHM | full width at half maximum peak height of Gaussian distribution |
| hPS | hydrogenous polystyrene |
| $I_o$ | incident neutron intensity |
| $I_R$ | reflected neutron intensity |
| I(Q) | coherent elastic neutron scattering |
| $\underline{k}_1$, $\underline{k}_2$ | neutron wave vectors perpendicular to surface mediums 1 and 2 |
| $k_B$ | Boltzmann constant |
| $\lambda$ | wavelength |

| | |
|---|---|
| $\lambda$ | characteristic decay length of exponential profile |
| L | brush or segregated layer thickness |
| LOQ | small angle neutron scattering instrument at RAL |
| m | monomer mass |
| $m_D$ | mass of perdeuterated polymer |
| $m_H$ | mass of hydrogenous matrix polymer |
| MFL | multiple fluorine labelled perdeuterated polystyrene |
| $M_n$ | number average molecular weight |
| $M_w$ | weight average molecular weight |
| n | refractive index at the boundary between two media |
| $N_A$ | Avogadro's constant |
| $N_A$ | degree of polymerisation of polymer A |
| $N_B$ | degree of polymerisation of polymer B |
| NR | neutron reflectometry |
| NRA | nuclear reaction analysis |
| $\phi_a$ | volume fraction value used in tanh function |
| $\phi_{air}$ | volume fraction at the air/polymer interface |
| $\phi_b$ | bulk volume fraction |
| $\phi_{dep}$ | volume fraction in the depletion layer |
| $\phi_D(z)$ | volume fraction of the deuterated component at depth z |
| $\phi_H(z)$ | volume fraction of the hydrogenous component at depth z |
| $\phi_s$ | surface volume fraction |
| $\phi_{Si}$ | volume fraction at the polymer/silicon interface |
| $\phi(z)$ | volume fraction at depth z |

| | |
|---|---|
| Q | energy released upon nuclear reaction (18.352 MeV) |
| $\underline{Q}$ | scattering vector (momentum transfer) |
| $\rho$ | density of the polymer |
| $\rho_D$ | scattering length density of the deuterated polymer |
| $\rho_H$ | scattering length density of the hydrogenous polymer |
| $\rho_N$ | nuclear scattering length density |
| $\rho_N(z)$ | nuclear scattering length density perpendicular to the surface |
| RAL | Rutherford Appleton Laboratory, Chilton, Didcot, Oxon. |
| $R_g$ | unperturbed radius of gyration |
| $r_{ij}$ | Fresnel coefficient at the ij interface |
| RBS | Rutherford back scattering |
| $R_o$ | reflectivity without surface roughness |
| R(Q) | reflectivity |
| $\sigma$ | areal density of grafted chains at surface |
| $\sigma$ | root mean square gaussian roughness |
| SERS | surface enhanced raman spectroscopy |
| SIMS | secondary ion mass spectroscopy |
| STAR | three-armed perdeuterated polystyrene star polymer |
| SURF | neutron reflectometer at RAL |
| $\theta$ | incident angle |
| $\theta_c$ | critical angle below which total external reflection occurs |
| t | time |
| T | absolute temperature in Kelvin |
| $T_g$ | glass transition temperature |

| | |
|---|---|
| w | width of the overlap region between the brush and the bulk |
| XPS | X-ray photoelectron spectroscopy |
| z | depth perpendicular to sample surface |
| $z^*$ | surface excess |
| $z^*_{air}$ | surface excess at air/polymer interface |
| $z^*_{dep}$ | size of the depletion layer |
| $z_{off}$ | height of the brush used in tanh profile |
| $z^*_{Si}$ | surface excess at polymer/silicon interface |
| $z^*_t$ | surface excess at time t |
| $z^*_\infty$ | surface excess at equilibrium |
| $z^*_{total}$ | surface excess value when there is a depletion layer, determined using $\phi_{dep}$ |

# Publications, Lectures, Conferences and Courses Attended.

## Publications

F. T. Kiff, R. W. Richards, H. L. Thompson, D. G. Bucknall, and J. R. P. Webster,

*Journal de Physique II*, 1997, 1871.

## Lectures.

**UNIVERSITY OF DURHAM - Board of Studies in Chemistry Departmental**

**Colloquia, and other lectures attended.**

1994

| | |
|---|---|
| October 5 | Prof. N.L.Owen, Brigham Young University.<br>Determining Molecular Structure - the INADEQUATE NMR Way. |
| October 19 | Prof. N.Bartlett, University of California.<br>Some Aspects of Ag(II) and Ag(III) Chemistry. |
| November 1 | Dr. J. Brophy, BP Chemicals.<br>Petrochemicals R&D - Dead or Alive |
| November 23 | Dr. J. Williams, University of Loughborough.<br>New Approaches to Asymmetric Catalysis. |
| November 30 | Dr. R. A. L. Jones, Cambridge University.<br>Glass Transition Temperatures in Thin Polymer Films. |

1995

| | |
|---|---|
| February 1 | Dr. T. Cosgrove, Bristol University.<br>Polymers do it at Interfaces. |
| March 1 | Dr. M. Rosseinsky, Oxford University.<br>Fullerene Intercalation Chemistry. |
| March 2 | Prof. E. J. Meijer, Eindhoven University of Technology.<br>Dendrimers and Supramolecular Polymer Chemistry. |

April 26 Prof. M. Schröder, University of Edinburgh.
Redox Active Macrocyclic Complexes: Rings, Stacks and Liquid Crystals.

April 27 Prof. D. J. Cole-Hamilton, University of St. Andrews.
Chemistry on the Nano Scale.

May 5 The Ingold Lecture.
Prof. A. J. Kresge, University of Toronto.
Reactive Intermediates.

May 9 Prof. R. Townsend, Unilever Exploratory Research Council.
Polymers for the Year 2000 - The Challenge Ahead.

May 30 Prof. P. Calvert, University of Arizona.
Freeforming: Chemical Methods for the Processing of Polymers, Ceramics and Composites.

October 25 Dr. D. Martin Davies, University of Northumbria.
Chemical Reactions in Organised Systims; Peracid Reactivity in Surfactant Micelles and Cyclodextrin Hosts.

October 26 Dr. C. J. Ludman, University of Durham.
Explosions.

November 17 Prof. D. Bergbreiter, Texas A&M.
Design of Smart Catalysts, Substrates and Surfaces from Simple Polymers.

November 22 Prof. I. Soutar, Lancaster University.
A Water of Glass? Luminescence Studies of Water Soluble Polymers.

November 23 Dr. P. D. Levy, Kings College, London.
Drug Abuse in Sport.

1996

January 10 Dr. Bill Henderson, Waikato University, New Zealand.
Electrospray Mass Spectometry - a new sporting technique.

January 17 Prof. J. W. Emsley, Southampton University.
Liquid Crystals: More than a Meets the Eye.

January 31 Dr. J. Penfold, Rutherford Appleton Laboratory.
Soft Soap and Surfaces.

March 12 Prof. V. Balzani, University of Bologna.
Supramolecular Photochemistry.

May 28 Prof. W. J. MacKnight, University of Massachusetts, Amherst.
Topological Effects on Blend Miscibility.

August 15 Prof. K. B. Wagener, University of Florida, Gainsville.
Catalyst Selection and Kinetics in ADMET Polymerisation.

October 22 Prof. B. J. Tighe, University of Aston.
Synthetic Polymers for Biomedical Application: Can We Meet Nature's Challenge?

October 23 Prof. H. Ringsdorf, Johannes Gutenberg-Universitat, Mainz, Germany.
Function Based on Organisation.
PERKIN CENTENARY LECTURE

November 12 Prof. R. J. Young, Manchester Materials Centre, UMIST.
New Materials - Fact or Fantasy?

November 20 Prof. J. Earnshaw, Queens College, Belfast.
Surface Light Scattering: Ripples and Relaxation.

December 3 Prof. D. Phillips, Imperial College.
A Little Light Relief.

December 4 Dr. A. C. Barnes, University of Bristol.
Applications of Neutron Spectroscopy and Diffraction to Studies of Disordered Systems.

1997

February 12 Dr. Geert-Jan Boons, University of Birmingham.
New Developments in Carbohydrate Chemistry.

February 26 Dr. Tony Ryan, UMIST.
Making Hairpins from Rings and Chains.

March 11 Dr. A. D. Taylor, ISIS Facility, Rutherford Appleton Laboratory.
Expanding the Frontiers of Neutron Scattering

May 7 Prof. M. Harrington, Caltech, Pasadena, USA.
Polymers Both Enable and Limit the Discovery of Protein Alterations in Studies Ranging from Gene Regulation to Mad Cow Disease.

May 20 Professor Jung-il Jin, President, Korean Chemical Society.
Poly PPV and its Derivatives - Synthesis, Structure and Properties.

June 13 Prof. Dr. Shiro Kobayashi, Kyoto University.
Synthesis of Polyesters via Enzymatic Polymerisation.

June 13 Professor Hyuk Yu, University of Wisconsin, Madison.
Macromolecular Dynamics in Monolayers.

November 26 Prof. R. W. Richards, University of Durham.
A Random Walk in Polymer Science.
Inaugural Lecture

**IRC Lunchtime Seminars on Polymer Science**

1994

October 24 Ezat Khosravi - Synthesis of Tailored Graft Copolymers

November 7 Gilles Widawski - Mesogens, polyenes and electronics

November 21 Mark Taylor - Surface Quasi Elastic Light Scattering

December 5 Lian Hutchings - Making Stars

December 20 Panagiotis Dounis - Tailored Oligomers and Polymers for IT

1995

January 16 Rainer Freudenberger - Polypropellanes

January 30 David Snowdon - Aqueous Romp

February 13 Sîan Davies - Dendrimers

March 13 Richard Towns - Polar polymers

March 27 Nick Haylett - Poly(arylene vinylene)s

May 1 Ian Reynolds - Lauryl methacrylate monolayers

1996

January 22 Ezat Khosravi - Well Defined Graft Co-polymers

February 19 Janette Jones - Shear Flow in Micelles

March 4 Antonio Brunacci - Organisation of Star Diblock Co-polymers at Polymer Interfaces

March 18 Lian Hutchings - Making Stars and More

| | |
|---|---|
| April 22 | Lesley Hamilton - Synthesis and Characterisation of Aliphatic Hyperbranched Polymers. |
| June 17 | Dave Snowden - Living ROMP of Highly Funcionalised Monomers. |
| June 24 | Mark Taylor - Surface Dynamics of Polymer Solutions and Spread Films. |

1997

| | |
|---|---|
| January 20 | Erwin Herzog - Living ROMP of Functionalised Norbornene Derivatives in Aqueous Media. |
| March 24 | Robin Harrison - Hyperbranched Polyimides and Cool Things to do With Them. |
| April 7 | Joanna Megson - The Synthesis and Characterisation of Water Soluble Polymers and Biomimetic Applications. |
| April 21 | Helen Thompson - Surface Organisation of Functionalised Polymer Blends. |
| May 12 | Kate Foster - Thin Aligned Polymer Films at the Substrate/Air Interface: part 1. |
| June 9 | Richard Ainsworth - Synthesis and Characterisation of Molecules Designed to be Surface Active in an Aqueous Environment. |
| June 16 | Mike Watson - New Materials from Trifluoroethene. |
| June 30 | Michael Jeschke - Heterophase Networks Synthesised by Cross-Linking BSB Triblock Copolymers. |
| July 21 | Rob Staples - The 'Tailored' Synthesis of Dendrimer Molecules for Possible Industrial Applications. |
| July 28 | Rusli Daik - Recent Developments in the Synthesis of Electro-luminescent Materials via the McMurry Coupling Reaction. |
| August 11 | Stella Peace - Transesterification in Polyesters. |
| September 1 | Richard Peace - Polymers for LED's. |

**Conferences**

1995

| | |
|---|---|
| 3 - 4 April | UK Neutron Beam and Muon Beam Users' Meeting, Manchester. |
| 10 - 14 July | International Symposium on Olefin Metathesis (ISOM 11), Durham. |
| 27-28 Sept | IRC Industrial Club Seminar, Durham*. |

1996

| | |
|---|---|
| 10 - 12 April | Aspects of Contemporary Polymer Science, Macro Group UK Family Meeting, Manchester*. |
| 12 - 15 May | European Symposium on Polymer Blends, Maastricht. |
| 25 - 29 Aug | 212th ACS National Meeting, Orlando, Florida*. |
| 19 - 20 Sept | UK Neutron and Muon Beam Users Meeting, Rutherford Appleton Laboratory, Oxon*. |
| 18 December | Postgraduate Poster Competition, University of Durham*. |

1997

| | |
|---|---|
| 7 February | Highlights of UK Chemistry Research by Young Chemists, The Royal Society, London‡*. |
| 2 - 4 April | Macro Group UK Spring Meeting '97 for Younger Researchers, Leeds*. |
| 21 April | IRC Lunchtime Seminar‡. |
| 9 July | 3rd Year Graduate Seminar, Durham‡. |
| 14 – 18 July | Polymer Surfaces and Interfaces III, Durham*. |

‡ denotes oral presentation.
* denotes poster presentation.

**Courses**

1995

| | |
|---|---|
| January 10 | IRC Polymer Physics Course, University of Leeds |
| January 12 | IRC Polymer Engineering Introduction Course, University of Bradford |
| March 22 | Reflectivity Training Course, ISIS Facility, Rutherford Appleton Laboratory |

1996

| | |
|---|---|
| August 24 | Interfacial Aspects of Multicomponent Polymeric Materials, PMSE, Orlando, Florida. |